Wisconsin Highway Research Program

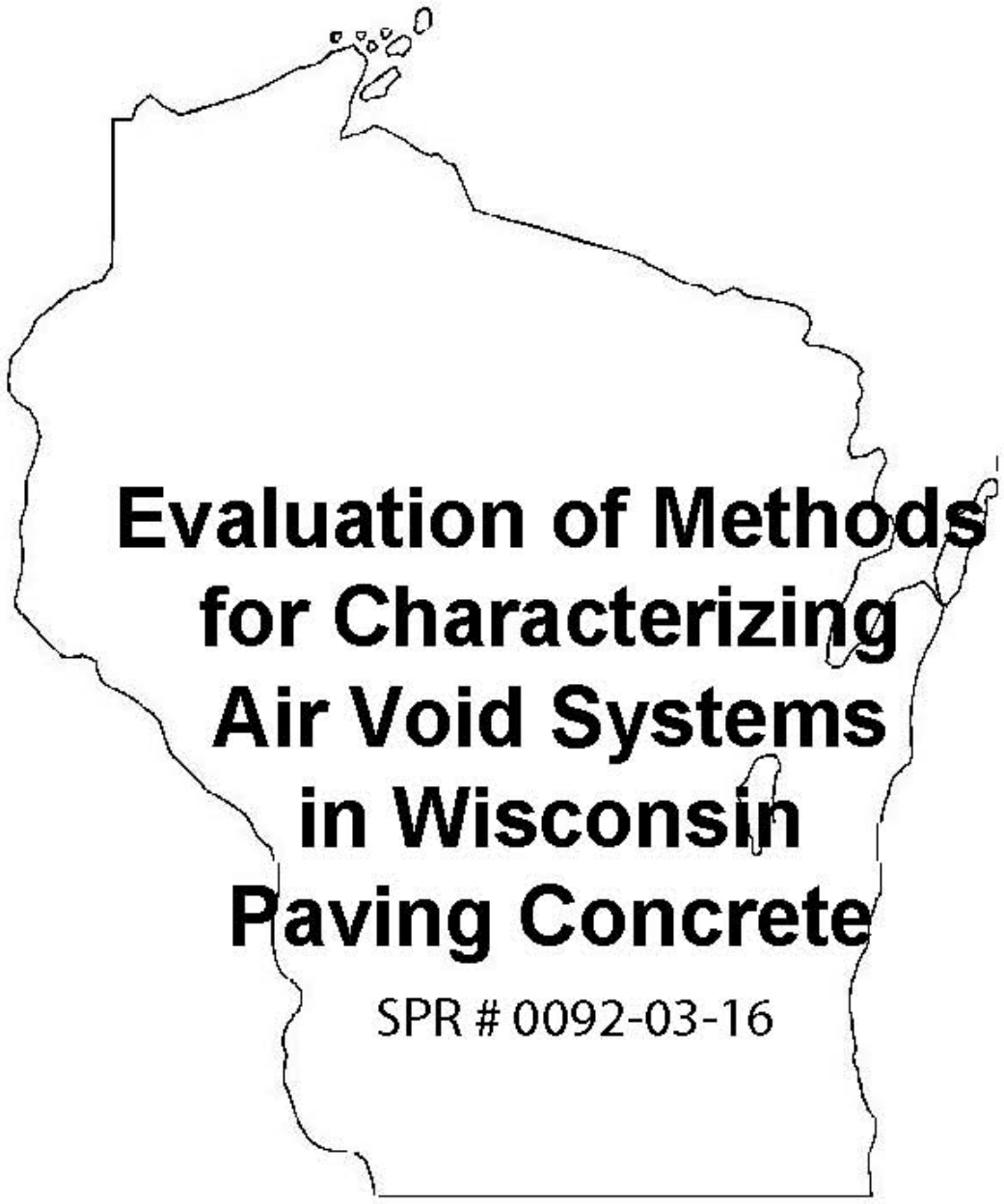

Evaluation of Methods for Characterizing Air Void Systems in Wisconsin Paving Concrete

SPR # 0092-03-16

Lawrence L. Sutter
Michigan Tech Transportation Institute
Michigan Technological University

June 2007

WHRP 07-05

Technical Report Documentation Page

1. Report No. WHRP 07-05	2. Government Accession No	3. Recipient's Catalog No
4. Title and Subtitle Evaluation of Methods for Characterizing Air Void Systems in Wisconsin Paving Concrete		5. Report Date June 2007 6. Performing Organization Code Univ. of Wisconsin - Madison
7. Authors Lawrence L. Sutter		8. Performing Organization Report No.
9. Performing Organization Name and Address School of Technology Michigan Technological University		10. Work Unit No. (TRAIS) 11. Contract or Grant No. WisDOT SPR# 0092-03-16
12. Sponsoring Agency Name and Address Wisconsin Department of Transportation Division of Business Services Research Coordination Section 4802 Sheboygan Ave. Rm 104 Madison, WI 53707		13. Type of Report and Period Covered Final Report, 2003-2006 14. Sponsoring Agency Code

15. Supplementary Notes

16. Abstract

This research investigated primarily two methods of determining the air-void system parameters of hardened concrete. The methods investigated were the use of a flat-bed scanner and the use of a CT x-ray scanner. The flat-bed scanner proved to be an effective means of performing the analysis at a relatively low cost. The CT scanner proved to be technically feasible but not ready for general implementation outside of controlled laboratory conditions. The research also investigated the freeze-thaw performance of Wisconsin paving concrete mixtures prepared with vinsol resin air-entraining admixtures (AEA) and with non-vinsol (synthetic) AEAs. The mixtures prepared with vinsol resin based AEA performed in accordance with what has been historically reported in the literature. The mixtures prepared with synthetic AEAs performed better than the vinsol based AEA when the admixtures were used in low dosages (i.e. low air content). The results indicate that mixtures prepared with synthetic AEA could possibly be prepared with lower target air contents and a satisfactory level of freeze-thaw performance could be expected.

17. Key Words	18. Distribution Statement
Air-void parameters, automated methods, air-entraining admixtures, flat bed scanner, CT scanner	No restriction. This document is available to the public through the National Technical Information Service 5285 Port Royal Road Springfield VA 22161

19. Security Classif.(of this report) Unclassified	19. Security Classif. (of this page) Unclassified	20. No. of Pages	21. Price

Form DOT F 1700.7 (8-72) Reproduction of completed page authorized

Disclaimer

This research was funded through the Wisconsin Highway Research Program by the Wisconsin Department of Transportation and the Federal Highway Administration under Project # 0092-01-06. The contents of this report reflect the views of the authors who are responsible for the facts and the accuracy of the data presented herein. The contents do not necessarily reflect the official views of the Wisconsin Department of Transportation or the Federal Highway Administration at the time of publication.

Table of Contents

Table of Contents

List of Figures

List of Figures

List of Figures

List of Figures

List of Figures

List of Figures

List of Figures

List of Tables

Executive Summary

Introduction

Portland cement concrete (PCC) is an inherently durable material used for constructing roads and bridges. The properties and durability of hardened concrete can vary widely depending upon the relative volumes of cement, sand, aggregate, and water used along with the volumetric content of air. Properly sized and spaced entrained air bubbles have long been known to protect concrete from cyclic freezing and thawing. As a result, air entrained concrete is universally specified for road construction in the upper Midwest (e.g. Wisconsin, Michigan, Minnesota, Iowa).

To construct durable roads, it is necessary to monitor and control the addition of air entraining admixtures (AEAs) used in making concrete. This is generally accomplished by monitoring the total air content of fresh concrete delivered to a job site. The two most common methods used for assessing the air content of fresh concrete are ASTM C 231 *Test Method for Air Content of Freshly Mixed Concrete by the Pressure Method* and ASTM C 173 *Test Method for Air Content of Freshly Mixed Concrete by the Volumetric Method*.

In the past, most air entraining admixtures were derived from naturally occurring vinsol resins. Recently, it is becoming increasingly common that air entrainment is induced using synthetic air entraining admixtures rather than those produced from vinsol resins. It is not well understood how changing this important admixture changes the resulting concrete microstructure.

There are established alternatives to measuring the air content in fresh concrete. The principal alternative is ASTM C 457 *Standard Test Method for Microscopical Determination of Parameters of the Air Void System in Hardened Concrete*, which is performed on polished slabs cut from concrete cores. Although this method is generally viewed as being the most widely accepted characterization of PCC air void systems, inherent difficulties associated with conducting the test in a repeatable manner makes it impractical for use as a routine quality control procedure.

As a result of the known relationship that exists between the air void system parameters (e.g. total air content, spacing factor) and freeze-thaw durability, the true characteristics of the air void system must be known to improve the durability of PCC used for paving in Wisconsin. Such a characterization study must establish the relationship(s) between the measured air content of fresh concrete made with different air entraining agents and the air void system parameters measured in the hardened concrete using the approach described in ASTM C 457. Also, new methods of assessing the air void system parameters in hardened concrete must be developed that reduce operator subjectivity and increase repeatability, providing an additional level of quality control to augment or calibrate measurements performed on fresh concrete. Finally, once procedures for accurately assessing the air void system of PCC are established, best construction practices and materials selection must be employed to ensure that quality concrete pavements are constructed.

Objectives

1. Perform a literature synthesis to document best construction practices and materials selection for producing a consistent, adequate air void system in PCC used in pavement applications. Additionally, the literature review was used to identify if other methods of determining the air-void system parameters, not identified in the original proposal, were available and viable.
2. Examine the relationships between various methods of measuring air content in fresh concrete and measurements of air void system parameters using ASTM C 457 for mixtures made with vinsol resin and synthetic air entraining agents.
3. Evaluate three new emerging technologies that show promise for characterizing the air void system in hardened concrete.
4. Correlate measured air-void system parameters collected using all techniques with freeze-thaw testing data obtained from ASTM C 666.

Approach

The work plan for this study used the following seven tasks to meet the research objectives stated previously:

Task 1: Literature Review
Task 2: Interim Report
Task 3: Preparation of Concrete Mixtures
Task 4: Testing of Fresh Concrete
Task 5: Testing of Hardened Concrete
Task 6: Data Analysis
Task 7: Final Report

Background

The properties and durability of hardened concrete can vary widely depending upon the relative volumes of cement, sand, aggregate, and water used along with the volumetric content of air. Both chemical admixtures and supplementary cementitious materials are used in PCC to improve workability, reduce water requirements, alter set time, or entrain air. Properly sized and spaced entrained air voids have long been known to protect saturated concrete from cyclic freezing and thawing. However, typically only the volume of total air is measured in the field and the more important parameters of spacing factor and specific surface are inferred by empirical relationships. In the past, most AEAs were derived from naturally occurring vinsol resins but a number of so called synthetic AEAs are currently being employed. The empirical relationships developed between the volume of total air measured and other air-void system parameters are based upon the use of vinsol resins AEAs. In the case of synthetic AEAs, there is an issue if the resulting air-void system has a larger volume fraction of smaller air voids with respect to the total air content.

The two most common methods used for assessing the air content of fresh concrete are ASTM C 173 and ASTM C 231. The air content measured by these methods does not ensure the adequacy of the air-void system. It has been observed that the volumetric and pressure tests may not accurately measure the true characteristics of the air-void system of concrete,

especially if a large percentage of the entrained air voids are very small. Although the volume of entrained air in concrete will vary little with small changes in the volume fraction of smaller voids, the spacing factor will decrease and specific surface will increase with increasing numbers of smaller voids.

There are established methods for measuring the characteristics of the air-void system in hardened concrete including total air content, air void spacing factor, and average air void specific surface. The air-void system parameters are measured using an optical microscope and linear traverse or point counting methods as described in ASTM C 457 *Standard Test Method for Microscopical Determination of Parameters of the Air Void System in Hardened Concrete.*

A number of emerging techniques are being developed to allow for easier and more reproducible determination of the air-void system parameters on both hardened and fresh concrete. The first emerging technology is a high-resolution scanner that is able to obtain a true 8 μm resolution, significantly improving the quality of the data. In addition to working with higher resolution digital images, efforts in this study focused on streamlining the technique and simplifying the user interface to create a turnkey analysis tool. The second emerging technology investigated was computed tomography (CT) x-ray scanning. This technique creates a three-dimensional image of the air void system, which could be used to calculate the same parameters described in ASTM C 457. The current focus of the on-going development effort is to achieve 10 μm resolution, and then demonstrate the applicability of this technique to various concrete mixtures.

In the original work plan submitted for this project, it was proposed that a third emerging technique would be evaluated for the analysis of the air content in hardened concrete. This third method was based upon a relatively new instrument called an x-ray microscope. At the start, this approach was the least developed of the three emerging techniques proposed, but potentially offered a number of additional opportunities extending well beyond the analysis of the air-void system. However, research performed as part of this project indicates that sample size limitations, insufficient image resolution, and the analysis time required, makes this test method not viable at this time. Although three techniques were proposed for evaluation, only the results from the flat-bed scanner and the CT scanner are presented in this report.

Experimental

Specimens were prepared in the laboratory using three AEAs with different dosage levels targeting 'high' (9% $^{+}$/- 1.5%), 'optimum' (6% $^{+}$/- 1.5%), and 'low' (3% $^{+}$/- 1.5%) air contents. Two of these AEAs were synthetic while the other was a natural – vinsol resin – type AEA. Half of the mixture designs were based on WisDOT Grade A specifications while the rest were designed according to Grade A-FA specifications using a 30% (by mass) replacement of portland cement with a class C fly ash. Two 4" by 8" cylinders along with two 3" by 3" by 11" prisms were produced from each of the 18 different combinations of AEA, target air content and fly ash replacement.

The materials used to prepare the specimens were selected to best mimic those used in typical WisDOT paving applications. For that reason, materials suppliers who regularly work in the northwestern portion of the state were contacted in the process of obtaining materials.

The concrete mixtures prepared were analyzed to determine air content when the concrete was fresh, and were also analyzed to determine air content using a manual point count method, ASTM C 457 Procedure B. The results are given below in Table A.

Table A. Air content determined by ASTM C 173, ASTM C 231, and ASTM C 457 for mixtures prepared.

Label	Mixture	ASTM C 173 Volumetric Meter (volume %)	ASTM C 231 Pressure Meter (volume %)	ASTM C 457 Hardened Air-Void Analysis (volume %)
A	FA-AE90-L	4.2	4.1	3.8
B	FA-AE90-O	6.7	6.5	5.5
C	FA-AE90-H	8.7	8	10.3
D	AE90-L	3.4	2.8	3.0
E	AE90-O	5.0	4.9	5.2
F	AE90-H	11.4	10.5	10.8
G	FA-MA-L	4.0	3.8	3.5
H	FA-MA-O	7.4	7.2	8.8
I	FA-MA-H	9.7	9.5	7.9
J	MA-L	4.2	3.9	3.2
K	MA-O	5.9	5.6	5.4
L	MA-H	8.2	7.8	8.9
M	FA-VR-L	4.2	3.6	3.5
N	FA-VR-O	4.9	4.5	4.8
O	FA-VR-H	8.9	8.8	7.8
P	VR-L	2.7	2.4	1.8
Q	VR-O	5.4	5.1	4.5
R	VR-H	9.4	9.5	7.4

By performing the manual point count method, other air void system parameters were determined for each mixture that could not be determined for the fresh concrete. These are listed below in Table B. The most important is the spacing factor, which is considered the most important measure of freeze-thaw (F-T) durability. A maximum spacing factor of 0.20 mm (0.08 in) is considered to be necessary for a concrete to be durable. This limit is based on historical practices that determined F-T performance for concrete mixtures with relatively higher water to cement ratios (*w/c*), which relates to a higher strength, and different AEAs (i.e. vinsol resins primarily).

Table B. Results of manual point count according to ASTM C 457.

Label	Mixture	Air Content (volume %)	Spacing Factor (mm)	Paste/Air Ratio	Specific Surface (mm^{-1})	Void Frequency (voids/meter)
A	FA-AE90-L	3.8	0.243	6.46	21.41	200.51
B	FA-AE90-O	5.5	0.114	4.09	35.96	492.31
C	FA-AE90-H	10.3	0.065	2.47	37.90	976.06
D	AE90-L	3.0	0.382	8.51	15.42	113.74
E	AE90-O	5.2	0.163	4.71	27.61	357.99
F	AE90-H	10.8	0.064	2.33	36.21	978.27
G	FA-MA-L	3.5	0.179	5.96	28.07	242.71
H	FA-MA-O	8.8	0.079	2.72	34.39	755.70
I	FA-MA-H	7.9	0.068	3.11	45.87	900.49
J	MA-L	3.2	0.213	8.09	27.12	219.81
K	MA-O	5.4	0.112	4.41	39.08	527.88
L	MA-H	8.9	0.078	3.09	39.60	877.32
M	FA-VR-L	3.5	0.280	6.71	18.94	167.14
N	FA-VR-O	4.8	0.150	5.52	32.34	384.47
O	FA-VR-H	7.8	0.094	2.91	31.08	604.56
P	VR-L	1.8	0.619	15.32	12.37	55.71
Q	VR-O	4.5	0.135	4.82	33.66	375.92
R	VR-H	7.4	0.127	4.17	32.75	607.59

Based upon the spacing factor limit specified above, it was expected that mixtures A, D, J, M, and P would not perform well in ASTM C 666 testing to determine F-T performance.

Problems were encountered producing concrete mixtures with a "high" air content using synthetic AEAs. It was determined that although the hardened air content was increasing as AEA dosage increased (as determined by microscopic analysis), the measured air content in the fresh concrete remained the same. It appears that the conventional tests for air content in fresh concrete are not sensitive to the total air content entrained by means of a synthetic AEA. This insensitivity could lead to batching problems in real concrete production. The problem was solved by use of a water-reducing admixture, which helped attain the desired air contents. In the end, there was good correlation between the various tests for air content in fresh concrete, and these results correlated well with the measured hardened air content.

Results

In the ASTM C 666 testing, all mixtures except mixture P performed well. The better than expected performance of mixtures A, D, J, and M indicate that with modern AEAs and lower *w/c* mixtures, larger spacing factors, or reduced air contents, may provide the necessary level of F-T protection.

With regards to new approaches for determining the hardened air content by automated methods, both the flat bed scanner and the CT scanner showed significant promise. However, the flat bed scanner is clearly the most cost effective and is the nearest to being implemented.

The flat bed scanner method explored here is similar to existing methods that use black ink and white powder to enhance the visibility of air voids. The main distinction is that a flat bed scanner is used to collect the image, as opposed to a microscope in combination with a motorized stage. This offers a low cost approach that does not require a petrographer nor intensive computer applications to implement. The primary research objectives of the flat bed scanner based approach were to develop a streamlined approach to data processing, and to compare manual test results to automated test results to verify performance of this innovative approach.

CT scanners typically produce multiple 2-D x-ray images, each representing cross sections or slices (also known as tomographs) through the specimen. The tomographs may be stacked one on top of one another to create a three-dimensional volume. In a linear array system, tomographic images are generated by projecting a thin-beam of x-rays through one plane of the specimen at many different angles. As x-ray photons pass through a specimen, some are absorbed while transmitted photons are measured by an x-ray detector. By collecting this data over many angles, a cross section representing the attenuation parameter of each element within the slice can be reconstructed by a computer (the reconstruction technique is known as back projection).

Good correlation was found between the air contents determined by the flat bed scanner and manual point counts. Other parameters such as the spacing factor did not correlate as well. These parameters are calculated, not directly measured, and therefore a magnification of errors can occur in the calculation process. The principal problem with the scanner relates to converting the image from a grey scale image to a segmented binary image for analysis. The conversion process relies upon a threshold that distinguishes between pixels that are air and those that are not. When a threshold is set low enough to detect the smallest air voids resolved, the larger air voids are detected with a sensitivity that leads to an increased air void size for the larger air voids, and a commensurate higher air content. Also, small specks in the image can be detected as air voids thereby skewing the measured void frequency and affecting calculations. Advanced image processing can probably address these problems but work is needed.

With the CT scanner, the problem centers on the data set generated, which becomes enormous as sample size increases. Therefore, either a small sample must be analyzed resulting in sampling errors that affect the measured air content and air system parameters, or larger data set must be analyzed requiring very considerable computing resources and very long analysis times. As computing power increases, and other advances are made in this technique, the CT scanning technique will become viable in the future as a method of determining the air void system parameters of hardened and fresh concrete.

Conclusions

- The problems encountered in preparing the necessary concrete mixtures show that it is very possible to overdose a mixture with a synthetic AEA when conventional field air tests indicate a low air content. A vicious cycle could result with failing tests requiring higher dosages of AEA resulting in increasingly reduced quality concrete.
- In some instances, tests for the air content of fresh concrete can underestimate the hardened air content. This may be related to the nature of the air void size distribution produced by a synthetic AEA.
- High correlations were obtained between the results of the three fresh concrete tests (ASTM C 138, ASTM C 173 and ASTM C 231). No particular combination of AEA, air content or fly ash replacement resulted in better or worse correlations between the results.
- Good correlations exist between the results of the fresh concrete tests and the results obtained in performing manual point counts (ASTM C 457) of the hardened concrete specimens prepared from each of the 18 mixtures.
- In ASTM C 666 testing, all mixtures passed with 300 cycles and durability factors greater than 100%, except for mixture P prepared with a low dose of vinsol resin.
- The poor performance of mixture P was consistent with predictions of performance based on the measured spacing factors for each mixture. The good performance of mixtures A, D, J, and M with their marginal spacing factors indicates that the current specification for a maximum spacing factor of 0.200 mm may not be valid for concrete currently produced using a low *w/c* or synthetic AEAs.
- A flatbed scanner was clearly demonstrated to be a viable device for performing ASTM C 457.
- Two types of scanners were compared, a high-resolution flatbed scanner and a conventional office scanner. Both types of scanners were capable of performing ASTM C 457.
- The flatbed scanner method tends to report slightly higher air content values than those determined by manual point counting. Image processing approaches may eliminate this error. In general there was good agreement between the scanner, other automated methods, and manual point counting.
- The degree of correlation with manual results depends on the method used to establish thresholds for segmenting the gray scale image.
- Increased confidence in the automated systems can be achieved by refining the processes involved in the preparation of the sample surface. Improvements in surface preparation quality reduce the quantity of defects analyzed by the automated systems. Therefore, it is easy to appreciate the fact that most researchers dealing with these types of analyses identify the sample preparation as the key factor in obtaining quality results.

- CT scanning is a promising emerging technique for measuring the air-void characteristics of concrete. It has the advantage over traditional techniques in that it can be used to detect air in both fresh and hardened concrete.
- Recent high-resolution micro-CT scanners are capable of detecting air voids below the size that can be detected by optical microscopy. However, a number of difficulties were encountered. Although these drawbacks represent considerable barriers to the wider application of this technique to the measurement of air-void parameters at this time, the technology (both hardware and software) is advancing at a sufficiently rapid rate that many of the problems may be overcome in the near future
- Attention should be given to the current concrete mixture designs used in Wisconsin with regards to air entrainment requirements. With modern chemicals and procedures, it may be possible to reduce air contents without sacrificing durability. Adequate spacing factors seem achievable with 3-4% air by volume, depending upon the AEA used.
- Further development of the flatbed scanner should continue, addressing some of the systematic errors encountered by applying advanced image processing techniques
- The CT scanner is a promising device but is currently not capable of performing ASTM C 457 at a practical level. Further development of software and computing algorithms will result in this technique becoming viable. The ability of this technique to evaluate fresh concrete should be explored in more detail as it may provide a needed alternative for measuring air-void system parameters.

Implementation

Implementation of this research should begin with a close look at the existing mixture designs specified for paving concrete in Wisconsin. A detailed study focusing on the freeze-thaw performance relative to the amount of entrained air should be performed.

Because of the difficulties identified with accurately measuring the air content in fresh concrete when synthetic AEAs are used, QC/QA strategies for paving concrete should include measurement of hardened air content. The automated method detailed in this report, specifically the flat bed scanner approach, is very close to being ready to be implemented. The researchers are currently involved in a FHWA sponsored round robin study using various automated methods and as a result of this work, additional data will be available to help apply advanced image analysis techniques to correct problems still remaining.

The remaining hurdle for implementing ASTM C 457 as a QC/QA tool will be sample preparation. Regardless of whether the air-void system is measured by manual or automated means, scanner or microscope, the preparation of the sample is the single most critical process.

The software developed for using the flat-bed scanner for performing ASTM C 457 is available for download at http://www.cee.mtu.edu/~krpeters/air_voids/.

Chapter 1 – Introduction

1.1 Research Problem Statement

Portland cement concrete (PCC) is an inherently durable material used for constructing roads and bridges. The properties and durability of hardened concrete can vary widely depending upon the relative volumes of cement, sand, aggregate, and water used along with the volumetric content of air. Properly sized and spaced entrained air bubbles have long been known to protect concrete from cyclic freezing and thawing. As a result, air entrained concrete is universally specified for road construction in the upper Midwest (e.g. Wisconsin, Michigan, Minnesota, Iowa). To be effective, a minimum volumetric content of air must be entrained and the bubbles must be within close enough proximity to one another to protect the paste from damage during freezing. Powers developed an expression called the spacing factor that describes, for the majority of the paste, the distance to the nearest air void [Snyder 1998]. Typically, the entrained air bubbles should range in size from 50 to 200 μm [Mehta and Montiero 1993] and the spacing factor should be less than 0.200 mm (0.008 in) to be effective in protecting the hydrated cement paste from F-T damage [ASTM C 457]. However, it is noted that if excessive air is entrained in the concrete, there is a commensurate loss of strength and an increase in permeability, both greatly negatively affecting the durability of the concrete.

To construct durable roads, it is necessary to monitor and control the addition of air entraining admixtures (AEAs) used in making concrete. This is generally accomplished by monitoring the total air content of fresh concrete delivered to a job site. The two most common methods used for assessing the air content of fresh concrete are ASTM C 231 *Test Method for Air Content of Freshly Mixed Concrete by the Pressure Method* and ASTM C 173 *Test Method for Air Content of Freshly Mixed Concrete by the Volumetric Method*. Both methods have been widely applied for many years. It has been observed that these methods may not accurately measure the true volume of air entrained in the fresh concrete, especially if the entrained air bubbles are very small [Roberts 1994].

Typical compounds used as AEAs include salts of wood resins (commonly known as vinsol resins), salts of sulfonated lignin, salts of petroleum acids, alkylbenzene sulfonates, and salts of sulfonated hydrocarbons, among others. In the past, most AEAs were derived from the naturally occurring vinsol resins. It is becoming increasingly common that air entrainment is induced using the synthetic air entraining admixtures, rather than those produced from vinsol resins. It is not well understood how changing this important admixture changes the resulting concrete microstructure. There is some concern that the resulting air void system has a larger volume fraction of smaller air voids with respect to the total air content. If a larger fraction of smaller air voids is coupled with a field test that is insensitive to these smaller air voids, artificially low air readings on the job site may result. Then, the mix plant will adjust to correct for the "low" measured air contents, ultimately producing concrete with an excess air content. This concrete is inherently weaker and more importantly, more permeable, contributing to low durability characteristics.

There are established alternatives to measuring the air content in fresh concrete. The principal alternative is ASTM C 457 *Standard Test Method for Microscopical Determination of Parameters of the Air Void System in Hardened Concrete*, which is performed on polished

slabs cut from concrete cores. The air void system parameters are measured using an optical microscope and linear traverse or point counting methods. The process is tedious and requires a skilled operator to prepare the samples and perform the microscopic analysis. Even experienced operators may end up with different results when evaluating the same concrete depending upon their individual criteria for identifying phases (paste, aggregate, and air) and how they address other factors such as infilling of bubbles with secondary deposits (e.g. ettringite, portlandite). Although this method is generally viewed as being the most widely accepted characterization of PCC air void systems, inherent difficulties associated with conducting the test in a repeatable manner makes it impractical for use as a routine quality control procedure.

As a result of the known relationship that exists between the air void system parameters (e.g. total air content, spacing factor) and F-T durability, the true characteristics of the air void system must be known to improve the durability of PCC used for paving in Wisconsin. Such a characterization study must establish the relationship(s) between the measured air content of fresh concrete made with different air entraining agents and the air void system parameters measured in the hardened concrete using the approach described in ASTM C 457. Also, new methods of assessing the air void system parameters in hardened concrete must be developed that reduce operator subjectivity and increase repeatability, providing an additional level of quality control to augment or calibrate measurements performed on fresh concrete. Finally, once procedures for accurately assessing the air void system of PCC are established, best construction practices and materials selection must be employed to ensure that quality concrete pavements are constructed.

1.2 Research Objectives

1. Perform a literature synthesis to document best construction practices and materials selection for producing a consistent, adequate air void system in PCC used in pavement applications. Additionally, the literature review was used to identify if other methods of determining the air-void system parameters, not identified in the original proposal, were available and viable.
2. Examine the relationships between various methods of measuring air content in fresh concrete and measurements of air void system parameters using ASTM C 457 for mixtures made with vinsol resin and synthetic air entraining agents.
3. Evaluate three new emerging technologies that show promise for characterizing the air void system in hardened concrete.
4. Correlate measured air-void system parameters collected using all techniques with freeze-thaw testing data obtained from ASTM C 666.

1.3 Research Approach

The work plan for this study used the following seven tasks to meet the research objectives stated previously:

Task 1: Literature Review

A review of the relevant literature was initiated at the start of the project. The engineering libraries at both Michigan Tech and the University of New Brunswick have access to extensive on-line databases and subscribe to a large number of journals and conference proceedings related to concrete pavements and materials. The results of the literature review helped develop a better understanding of the air void system characteristics in fresh and hardened concrete, and how it is affected by changes in mixture properties including air entraining admixtures. Additional emphasis was placed on methods used to characterize the air void system in fresh and hardened concrete in order to hone the focus of this study. The literature review was used to draw together information regarding the construction practices and materials selection required to ensure that PCC is produced and placed in Wisconsin having an adequate air void system.

Task 2: Interim Report

Based on the results of the Task 1 Literature Review, an interim report was prepared, summarizing the information obtained and presenting a revised work plan for the remainder of the study. WisDOT reviewed the document and worked with the research team to finalize the interim report. After the process, the project Principal Investigator, Dr. Lawrence Sutter and Co-Investigator, Dr. Thomas Van Dam, P.E. answered any remaining questions and discussed how the project would proceed.

Task 3: Preparation of Concrete Mixtures

An experimental design was developed to create concrete mixtures that are broadly representative of concrete mixtures used in Wisconsin for pavement concrete. Two grades of mixtures were selected for use[1], a Grade A and a Grade A-FA (a fly ash mixture was included because of some of the unique difficulties the presence of fly ash particles can pose to entraining air in concrete and in the analysis of the air void system). The water-to-cementitious ratio was to be held constant at 0.42. The aggregate type and grading was held constant for all mixtures under investigation, although the volume of aggregates per cubic meter (yd^3) was altered slightly to accommodate changes in the volume of paste and air.

Three different air entraining admixtures were used, one being a vinsol resin and the other two were synthetic air entraining admixtures. These were added to the two different mixture designs at three different dosage rates (low, optimum, and high). The full factorial experimental design thus consisted of 18 different concrete mixtures, representing portland cement and fly ash modified mixtures with a range of air entraining admixture types and dosage levels.

[1] These designations were taken from the 1996 WisDOT Standard Specifications. The research team is aware that WisDOT has adopted Performance Based Specifications to provide increased flexibility to contractors, but the designations still reflect representative mixtures used in Wisconsin paving.

The concrete specimens were prepared at Michigan Technological University in accordance with ASTM C 192, *Standard Practice for Making and Curing Concrete Test Specimens in the Laboratory,* using mixture designs, aggregate sources, cement, fly ash, and admixtures approved by WisDOT for use in this project

Task 4: Testing of Fresh Concrete

A number of tests were conducted by Michigan Tech on the fresh concrete prepared in Task 3. In addition to slump and unit weight, both ASTM C 231 *Test Method for Air Content of Freshly Mixed Concrete by the Pressure Method* and ASTM C 173 *Test Method for Air Content of Freshly Mixed Concrete by the Volumetric Method*, were conducted. The results of these tests formed a baseline for comparison between the two common field methods and the results of methods being investigated to assess the air void system parameters for hardened concrete.

In the original work plan submitted for this project, it was suggested that the test equipment known as the air void analyzer (AVA), or the Danish air test, would be evaluated for the analysis of the air content in fresh concrete, contingent upon being able to arrange for use of an AVA. Michigan Tech does not have an AVA and incorporation of this instrument in the project was dependant upon obtaining an instrument on loan, as described in the Interim Report for this project. It was not possible to arrange for use of an AVA during the narrow window of time in which the concrete specimens were being made for this project. Therefore it was not included in the testing of the fresh concrete.

Task 5: Testing of Hardened Concrete

Testing of hardened concrete fell into two categories. The first was F-T testing conducted in accordance with ASTM C 666, *Standard Test Method for Resistance of Concrete to Rapid Freezing and Thawing*. This testing was conducted on two 3 in x 3 in x 11 in (76 mm x 76 mm x 279 mm) prisms from each mixture. Specimens were moist cured for 14-days and then at laboratory ambient conditions for an additional 14-days. The 28-day old specimens were frozen, suspending further hydration, until all specimens for the study were prepared. The 36 prismatic specimens were tested simultaneously for 300 cycles as specified. The dilation was recorded, as was the physical appearance of the beams at the completion of the testing.

The second category of testing to be conducted on hardened concrete was the assessment of the air void system parameters. Two cylindrical specimens were produced from each mixture during batching, and cured alongside the prismatic F-T specimens. After 28-days, the samples were cut into slabs, polished, and microscopically analyzed in accordance with ASTM C 457, *Standard Test Method for Microscopical Determination of Parameters of the Air Void System in Hardened Concrete.* The results of this testing were used as the standard against which all other test results were compared.

After conducting ASTM C 457, the specimens were to be analyzed using three emerging technologies. The first emerging technology is a high-resolution scanner that is able to obtain 8 μm point-to-point resolution, significantly improving the quality of the data over previously available scanners. In addition to working with higher resolution digital images, efforts in this study focused on streamlining the technique and simplifying the user interface to create a turnkey analysis tool. The results presented in this report show that this technology is readily applicable to the analysis of newly placed PCC and the potential for

incorporating this technology into a QC/QA regime is excellent. The second emerging technology investigated was computed tomography (CT) x-ray scanning. This technique creates a three-dimensional image of the air void system, which could be used to calculate the same parameters described in ASTM C 457. The current focus of the on-going development effort is to achieve 10 μm resolution, and then demonstrate the applicability of this technique to a broad range of mixtures. It is envisioned that once the technical feasibility of this approach is demonstrated, that a competitively priced, turnkey system for concrete evaluation could be developed. In the end, although feasible, this technology is not currently ready for field application.

In the case of the flat bed scanner, the specimens analyzed were the same samples that were analyzed by manual point count in accordance with ASTM C 457. Combining this data with that collected on the fresh concrete provided an excellent database for the data analyses conducted in Task 6. The C-T scanner analyzed samples that were cast from the same batches as those analyzed by manual point count and flat-bed scanner. However, they were not the exact same samples.

In the original work plan submitted for this project, it was proposed that a third emerging technique would be evaluated for the analysis of the air content in hardened concrete. This third method was based upon a relatively new instrument called an x-ray microscope. At the start, this approach was the least developed of the three emerging techniques proposed, but potentially offered a number of additional opportunities extending well beyond the analysis of the air-void system. However, research performed as part of this project indicates that sample size limitations, insufficient image resolution, and the analysis time required, makes this test method not viable at this time. Although three techniques were proposed for evaluation, only the results from the flat-bed scanner and the CT scanner are presented in this report.

Task 6: Data Analysis

The data, collected from 18 different concrete mixtures, is a diverse representation of air void structures created by varying dosage levels of three different air entraining admixtures in conventional PCC and that containing a Class C fly ash. At least nine specific types of data were to be collected: the air content of fresh concrete based on the pressure and volumetric methods; hardened air void system parameters from ASTM C 457, the flat-bed scanner technique and the CT x-ray scan technique, and the results of F-T testing including dilation from ASTM C 666. The principal variables to which all others were compared were the air void system parameters determined from ASTM C 457, since this is the most widely accepted test for this purpose.

There were two aspects to the data analysis. The first aspect focused on determining how air void system parameters relate to the observed F-T damage. This aspect of the study was expected to confirm the applicability of the criteria suggested in ASTM C 457 (e.g. spacing factor ≤ 0.200 mm (0.008 in), etc.) commonly used to determine whether a concrete mixture will be resistant to F-T damage. Confirmation is especially relevant since there is some question as to whether the air void system produced with synthetic air entrainers provides the same level of F-T protection as that produced by vinsol resin air entrainers due to differences in the air void size distributions between the two types.

The second aspect of the data analysis was to compare the results of the two viable emerging technologies to those obtained from ASTM C 457. In truth, considerably more data will be gleaned from the emerging technologies than obtained by ASTM C 457, but it is critical that as a minimum, they can be used to obtain similar results.

The results of this task directly addressed Research Objectives 1 through 3, showing the path(s) that must be followed to develop a working approach for field or laboratory air void system quality assurance testing.

Task 7: Final Report

This final draft report details the entire work effort, including the literature review, experimental approach, characteristics of the concrete mixtures, the data collected, the analysis of the data, and an implementation plan to move the results of the research into practice.

Chapter 2 – Literature Review

2.1 Cement Paste Freeze-Thaw Damage in Concrete

When moist concrete is exposed to alternating cycles of freezing and thawing in a saturated state, internal deterioration can result. As this deterioration accumulates, it is referred to as freeze-thaw (F-T) damage. Damage related to freezing and thawing can occur in both the cement paste and aggregate phases of concrete. It has long been recognized [Powers 1945] that damage to the cement paste can occur internally or at the surface. Surface scaling most often occurs in the presence of deicers, which exacerbate the pressures generated through freezing and thawing. In both cases, the basic deterioration mechanism is identical, and the same paste air-void system is expected to protect the paste against damage. Aggregate F-T damage is not considered in this project, being primarily a function of the aggregate porosity, strength, and size.

Paste F-T damage in concrete is considered to be a physical phenomenon arising from excess internal pressures resulting from the freezing action of water. Currently, a consensus on the exact mechanism(s) responsible for these excessive internal pressures does not exist. The most widely accepted theories consider either hydraulic or osmotic pressures (or a combination of the two) to be the primary causes. It is generally agreed that the magnitude of these internal pressures is dependent on the concrete pore structure, moisture content, pore water chemistry, rate of freezing and/or length of the freezing cycle. The temperature at which water will freeze is a function of the size of the pore in which it is contained and the concentration of dissolved species in the water. An excellent review of the literature related to these phenomena is provided by Marchand et al. [1994]. The beneficial role of entrained air voids is a central element in both of the theories.

Powers [1945] first attributed F-T damage to excessive hydraulic pressures resulting from the expansion of ice. It was proposed that as ice gradually forms at discrete sites in a saturated capillary pore system, the resulting 9 percent volume expansion causes the surrounding unfrozen water to be expelled away from the freezing sites. Depending on the nature of the pore system, excessive internal stresses can be generated by hydraulic pressures resulting from resistance to this flow. The pressurized water moving away from the freezing sites can find relief at the air voids, where it will then presumably freeze without causing damage.

Based on experimental results, Powers recognized that the spacing between voids, rather than the total volume of air, was the better measure of resistance to F-T damage. Building on this, he developed equations that provided an average measure of the distance that water within the paste must travel to reach the surface of an air void [Powers 1949]. He proposed the adoption of a void spacing factor (now known as the Powers spacing factor) as the basis of protecting the paste from F-T damage. It is interesting to note that this pioneering work based on the hydraulic pressure theory still forms the primary basis of specifying F-T resistant concrete (ASTM C 457). Nowadays, this theory has been considered invalid by most researchers, including Powers himself, because it cannot account for all the phenomena observed as concrete freezes. For instance, it cannot explain why porous materials can be damaged by freezing and thawing when they are saturated with organic liquids that do not expand upon freezing [Marchand et al. 1994, Pigeon and Pleau 1995, Mindess et al. 2003].

More recent theories [Powers 1975] consider osmotic potential to be the primary cause of excess internal stress. As previously mentioned, the temperature at which water will freeze in concrete is a function of the alkali concentration as well as the pore size in which it is contained. Freezing will only occur when the temperature becomes low enough to allow ice to form at the existing alkali concentration. Because of their relatively large size, air voids are likely initial freezing sites and as the pore water solution freezes, only pure water forms the ice. Thus, the remaining unfrozen liquid at the freezing sites becomes a more concentrated alkaline solution. The less concentrated alkaline solution in the surrounding paste is then drawn to the freezing sites to maintain thermodynamic equilibrium. The driving force for the movement of this solution is a function of the alkali concentration gradient. As the unfrozen solution at the freezing sites is diluted by the infusion of surrounding water, additional ice growth occurs. This progressive ice formation can occur at any solute concentration, including zero and is referred to as ice-accretion [Powers 1956, Powers 1975].

The process of pore water moving from the capillary system to the air voids will continue until one of two possible conditions prevail. If adequate air void space exists, sufficiently distributed throughout the paste, most of the freezable water will eventually diffuse to the freezing sites inside the air voids, eliminating any further fluid flow. This drains the surrounding capillary pore system eliminating the possibility of paste F-T damage. The other possible outcome is that the air-void system is inadequate to accommodate all of the surrounding unfrozen water. If this occurs, osmotic pressures will increase due to the remaining differences in alkali concentrations between the liquid in the air voids and the bulk solution within the capillary pores. Pressures of any kind, whether they are caused by loads, hydraulic forces, or osmotic forces, that approach or exceed the tensile strength of the hardened cement paste will naturally cause damage. In addition, if the rate of temperature drop is too fast to allow all of the water to diffuse to the air voids, damage may occur.

A third and more recent theory was produced by Litvan, who conducted a large number of experiments to study the behavior of porous materials upon freezing (1960-1980). He noticed that during the slow cooling period, a large portion of the evaporable water was lost from the porous samples. The basis of his theory is that because of surface forces, the water in the capillary pores cannot freeze in-situ and thus becomes supercooled [Litvan 1978, Marchand et al. 1994, Pigeon and Pleau 1995].

When the temperature decreases below freezing, the vapor pressure over the bulk of the paste, p, corresponds to the vapor pressure of ice because ice will form on all external faces of the paste. The vapor pressure of the supercooled water, p_{ow} in the capillary pores is greater than that of ice. Therefore, the relative humidity for the supercooled water (p/p_{ow}) will be lower than 100 percent and drying will occur. Water contained in the pores will migrate to, and freeze at, locations where the effect of the surface is not felt. The radius of curvature of the menisci in the capillaries will decrease as the amount of water decreases. Therefore, the vapor pressure of the unfrozen water will be reduced because the free energy of a liquid is less when it has a concave instead of planar surface. Equilibrium will be established when the vapor pressure in the capillary pores equals that of ice. Nevertheless, the difference in vapor pressure between ice and supercooled water is greater at lower temperatures, thus the phenomenon will be more severe in that case [Litvan 1978, Marchand et al. 1994, Pigeon and Pleau 1995].

Litvan attributes the damage of concrete to the following mechanisms: "If a flaw in the solid is surrounded by sound concrete, any water from the undamaged portion will migrate on cooling to the crack, filling it completely; on solidifying it causes the fissure to propagate. On the following cooling portion of the freeze-thaw cycle the crack draws more water and freezing results in further damage. Damage also occurs when the required rate of water expulsion usually necessitated by rapid cooling is so high that it cannot be realized in the paste. In such cases, some of the passageways presumably become blocked by ice and internal pressure is generated" [Litvan 1978, Marchand et al. 1994]. Although there are several indications that some part of the unfrozen water tends to migrate upon freezing, Litvan's assumption that water cannot freeze in situ has been refuted by many experimental investigations [Marchand et al. 1994, Pigeon and Pleau 1995].

Overall, none of the present theories are able to explain the problem of frost action in its entirety. Each theory describes only certain parts of the overall phenomenon, and thus in a way they seem to complement each other. Which mechanism will dominate the action of frost in a particular case will depend on the characteristics of the concrete and on the conditions to which it is exposed. For example, if the ion concentration in the capillaries is low, the hydraulic pressure will be more important, but at high ion concentrations (for example in the presence of deicer salts) it is probably the osmotic pressure that will dominate because the higher the ion concentration the lower the volume of freezable water [Pigeon and Pleau 1995, Fagerlund 1997].

2.2 The Air-Void System

2.2.1 Modern Discovery of Air Entrainment

Modern air entrainment of concrete traces its roots to the northeastern portion of the United States. Exterior concretes placed up until the late 1930's exhibited relatively severe distresses, most notably scaling of the surfaces exposed to the environment, during the harsh climate conditions encountered during the winter months. In the mid 1930's, the Universal Atlas Cement Company recognized that the addition of small amounts of a grease grinding aid into the cement manufacture process produced a cement that resisted this damage by producing entrained air. The resulting concrete showed superior resistance to freezing and thawing cycles than did previously produced concrete.

A set of experiments with the goal of determining other suitable additive materials was devised based upon the observations. Initially, freeze-thaw tests were conducted on laboratory prepared concrete slabs and mortar cube specimens. A variety of additives, such as fish oil stearate, cod oil and vinsol resin, were investigated as potential air entraining admixtures. Specimens were cyclically frozen and thawed to simulate conditions encountered in the field and the results were compared to specimens lacking any additive. The success of mixtures containing the additives in the laboratory tests prompted the Universal Atlas Cement Company to perform a larger scale field test commencing in 1938.

An experimental road was constructed in Hudson, New York with dimensions of 540 feet in length by 18 feet in width. Each 20 foot section of the pavement was designed with a different combination of air-entraining additive (or lack thereof) and cement type. The pavement was allowed to weather for two winter seasons before being cored and analyzed in both the New York State and Portland Cement Association laboratories. The results

confirmed those found in the initial laboratory specimens. The researchers concluded, "…concrete scaling could be prevented by grinding a rosin product into the cement." After observing the results of the Universal Atlas Cement Company study, the state of New York constructed a similar test pavement on Long Island. In the Long Island study, beef tallow was ground into the cement with the goal of entraining air to protect the pavement from freeze thaw damage. Similar successes in increasing durability of the pavement were obtained. After additional work, the researchers concluded that the "…wood rosin product…, vinsol resin, was found to be the best all around scale-preventative material." [Moore 1940, Mindess et al. 2002]

2.2.2 Role of Air Void System

The three frost action mechanisms described earlier all agree that frost damage of concrete results from internal pressures generated by the restrained movement of water, and that a good way to protect the paste is to create a protective network of voids by entraining air in the concrete [Marchand et al. 1994, Pigeon and Pleau 1995, Fagerlund 1997, Mindess et al. 2003]. The present section describes the role played by the air-void system, and the characteristics it needs to have in order to be efficient. The production of the air-void system and the determination of its parameters in hardened cement paste will be described in the next sections.

Air is entrained in concrete to create in the paste a protective network of closely spaced air voids. These voids are approximately spherical in shape and range in diameter from less than 0.00004 to 0.05 inch (< 0.01 to 1.25 mm). According to the hydraulic pressure theory and Litvan's theory, the protective effect of the air voids can be ascribed to the fact that since they are larger than the capillary pores, they will rarely be saturated, and thus provide empty spaces within the paste to which excess water can move and freeze without causing damage. However, according to the osmotic pressure theory of Powers, the role of the air voids is to compete with the capillary pores where ice is forming. Although the air voids are mostly empty, they may have a film solution on their surface that is thick enough to freeze at a temperature near 32 °F (0 °C). The solution will become increasingly concentrated and water will be attracted from the smaller pores where ice forms only at lower temperatures [Litvan 1978, Marchand et al. 1994, Mindess et al. 2003].

Moreover, an indirect effect of air-entrainment is that the tiny voids act like fine aggregates in the cement paste, reducing the interactions between solid aggregates. Therefore, they improve the workability and cohesiveness of the mix, and thus facilitate placing and compaction for a given slump. They also considerably reduce bleeding and segregation during handling and transportation of wet mixes. However, air entrainment introduces additional void space in the paste and thus reduces the strength of the concrete (around 5 percent loss of strength for each 1 percent increase in air-content). This can be offset by taking advantage of the improved workability, to reduce the water-to-cementitious material ratio (*w/cm*) for a desired slump, and so reduce the capillary porosity. Either way, it is recommended that a low *w/cm* should be used for concrete that will be exposed to freezing and thawing [Pigeon and Pleau 1995, Mindess et al. 2003].

2.2.3 Important Parameters of the Air-Void System

In order to obtain an air-void system that has both the volume capacity and the geometric parameters necessary to protect mature saturated cement paste during exposure to freezing and thawing, a lot of small well-distributed air voids are necessary. In other words, the concrete must have an acceptably high air content (A) and a low enough spacing factor ($\overline{L}$) to provide protection (ASTM C 457). The spacing factor is considered the most important factor with regard to frost resistance since it is "the spacing of the air voids which determines the maximum distance that freezable water must travel through the cement paste to reach an escape boundary where ice crystals can grow freely without generating disruptive pressures" [Pigeon and Pleau 1995].

Based upon historical performance, an air content of 2 to 8 percent by volume of concrete provides satisfactory frost protection. The actual required air content depends on many factors including the maximum size of the coarse aggregate. It will be higher for lower maximum size of coarse aggregate, because more paste is required to provide workable concrete in that case. For example, the optimum air content for ¾ inch (19 mm) maximum coarse aggregates size is around 6 percent. However, adequate air content is not directly related to an adequate air-void system. High air contents generally indicate larger void size rather than a smaller spacing factor. In addition, entrapped air voids will be accounted for in the air content even though they don't really have a beneficial effect on the frost resistance of concrete. These voids, which generally have a diameter over 0.04 inch (1 mm) but can reach the size of coarse aggregate particles or larger, result from poor consolidation. They are irregular in shape and usually have an irregular distribution in the concrete. Finally, excessive amounts of air will drastically lower the strength of the concrete and increase its permeability, thus reducing its resistance to stress from freezing [Pigeon and Pleau 1995, St. John 1998, Mindess et al. 2003].

The most widely used maximum value for the spacing factor is 0.008 inches (0.20 mm). However, Pigeon et al. [1995] state that although 0.008 inches (0.20 mm) should normally be considered as a safe design value for concretes exposed to severe weathering in northern climates, the critical spacing factor for deicer salt scaling resistance will depend on the type of cement and the duration and intensity of the freezing cycles. For example, this value can be higher for high performance concretes, since they have a higher tensile stress. Freezing cycles with long freezing periods are also more harmful to concrete than cycles with shorter freezing periods. In practice, for low values of the air-void spacing factor, the performance can be good or bad (because the frost resistance of a given concrete is not just related to its intrinsic characteristics, but also to the conditions that it will be subjected to during freezing), but at high values the performance seems always to be bad, even though there is no clearly defined critical value. In addition, the critical spacing factor is lower in presence of deicer salts [Pigeon and Pleau 1995].

Finally, another parameter that is sometimes used to characterize the air-void system is the specific surface area of the air voids, α, which represents the surface area of the air voids divided by their volume [Pigeon and Pleau 1995]. It is related to the void frequency and reflects the mean size of the voids. In a protective air-void system, α should not be less than 635 $inch^2/inch^3$ (25 mm^2/mm^3) [Mindess et al. 2003].

2.3 Concrete Admixtures

2.3.1 Chemical Admixtures

A number of chemical admixtures can be added during proportioning or mixing to enhance the properties of freshly mixed and/or hardened concrete. Admixtures used in pavement construction in North America include AEAs, water reducers, accelerators, retarders, corrosion inhibitors, supplementary cementitious materials, and alkali-silica reactivity (ASR) inhibitors. An excellent description of these various admixtures can be found in a number of sources [Ansari et al. 2002, ASTM C 457, Cross et al. 2000, ACI 212.32). The following is a brief discussion specifically focused on the impact of AEAs and water reducers on PCC durability.

The standard specification for chemical admixtures used in the United States is presented in ASTM C 494 (AASHTO M 194), which includes the following seven classifications:

Type A - Water-reducing admixtures
Type B - Retarding admixtures
Type C - Accelerating admixtures
Type D - Water-reducing and retarding admixtures
Type E - Water-reducing and accelerating admixtures
Type F - Water-reducing, high range admixtures
Type G - Water-reducing, high range and retarding admixtures

The following text discusses admixtures that are applicable for use in PCC concrete.

2.3.2 Air Entrainers

AEAs are specified and tested under ASTM C 260 and C 233 (AASHTO M 154 and T 157), respectively. AEAs added just prior to, or during, concrete mixing and can be used in place of or in conjunction with air-entraining cement. In addition to protecting hardened cement paste from freeze-thaw attack, AEAs also improve the workability of the fresh concrete, significantly reducing segregation and bleeding.

Most of the air-entraining admixtures contain surface-active agents (surfactants) that concentrate at the air-water interface, and lower the surface tension of the water. Consequently, they reduce the energy required to form the voids and break them down into smaller voids. The natural tendency of small air bubbles in the absence of surfactants is to coalesce to form larger bubbles, because the surface energy (which is equal to the surface tension of the material multiplied by the surface area) of the former is higher, and any system tends towards its lowest value of free energy. However, the surfactants will form an elastic film around the air bubbles that will reduce the risk of coalescence when collisions occur during mixing [Pigeon and Pleau 1995, Mindess et al. 2003]. Indeed, very often, surface-active agents are composed of molecules that have a negatively charged hydrophilic (water-loving) end and a hydrophobic (water-hating) end. These molecules therefore tend to align at the air-water interface with their hydrophilic groups in the water (adsorbed to the cement grains) and the hydrophobic portion in the air, thereby effectively binding the air voids to the cement grains [Pigeon and Pleau 1995, St. John, 1998, Mindess et al. 2003]. This is shown schematically in Figure 2-1 [Ansari et al. 2002].

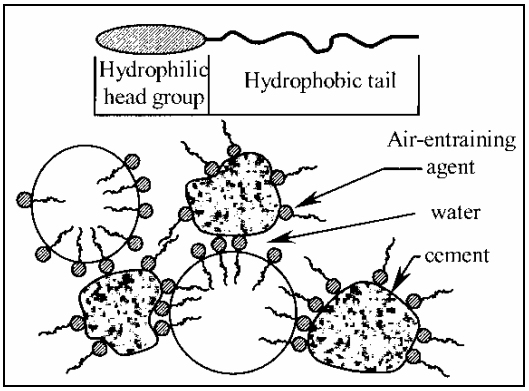

Figure 2-1. Schematic representation of AEA mechanism. [Ansari et al. 2002]

Typical compounds used as AEAs include salts of wood resins (commonly known as vinsol resins), salts of sulfonated lignin, salts of petroleum acids, alkylbenzene sulfonates, and salts of sulfonated hydrocarbons among others. Synthetic admixtures result from the byproducts of producing lubricating oils and kerosene and in general tend to be aromatic sulfonic acids. The water-soluble forms of these chemicals form sulfonic acids, which are neutralized with caustic soda to produce water-soluble sodium sulfate [Ansari et al. 2002].

The dosage rate for AEAs is usually very small, on the order of 0.005 to 0.05 percent active ingredients by weight of cement. They are normally diluted to assist in accurate batching [Cross et al. 2000]. The amount of entrained air required to protect concrete depends on the exposure level and the nominal maximum aggregate size. Recommended air contents for frost-resistant concrete from ACI [ACI 1992] are reproduced in Table 2-1. Concrete pavements subject to deicer application experience severe exposure conditions.

The viscosity of the cement paste is also an extremely important parameter with regards to air entrainment. For stiffer concrete (higher viscosity), more energy is required to stir the mix, but since the movement of all air voids in the paste becomes difficult it also reduces the risk of coalescence of the air voids and helps to keep them in the mix. On the other hand, a more viscous paste usually contains more solid particles (or finer particles) for a given amount of water, so less water will be available for the formation of air voids since all solid surfaces need to be covered with water [Pigeon and Pleau 1995].

Consequently, at a given dose of AEA, lean concretes (more aggregates, less paste) entrain less air than do rich mixes, and low *w/cm* ratio concretes entrain less air than do concretes with high *w/cm* [Pigeon and Pleau 1995]. However, for a given air content, low *w/cm* ratio concretes tend to have a lower spacing factor than high *w/cm* concretes. Since finer particles have a higher specific surface, the air content for a given dosage will also vary inversely with the proportion of fines in the fine aggregate, the addition of finely divided mineral admixtures (e.g. silica fume, fly ash, ground blast furnace slag, natural pozzolans, etc.), and the fineness of the cement. Finally, the amount of air for a given dosage of air entraining agent will also decrease as the temperature increases, because of the loss of slump at higher temperatures [Pigeon and Pleau 1995, Mindess et al. 2003].

Table 2-1. Recommended air contents for frost-resistant concrete [ACI 201.2R].

Nominal maximum aggregate size, in. (mm)		Average air content, percent*	
		Severe exposure†	Moderate exposure‡
⅜	(9.5)	7½	6
½	(12.5)	7	5½
¾	(19.0)	6	5
1	(25)	6	5
1½	(37.5)	5½§	4½§
3	(75)	4½§	3½§
6	(150)	4	3

*A reasonable tolerance for air content in field construction is ± 1½ percent.

†Outdoor exposure in a cold climate where the concrete may be in almost continuous contact with moisture prior to freezing, or where deicing salts are used. Examples are pavements, bridge decks, sidewalks, and water tanks.

‡Outdoor exposure in a cold climate where the concrete will be only occasionally exposed to moisture prior to freezing, and where no deicing salts will be used. Examples are certain exterior walls, beams, girders, and slabs not in direct contact with soil.

§These air contents apply to the whole as for the preceding aggregate sizes. When testing these concretes, however, aggregate larger than 1½ in. (37.5 mm) is removed by handpicking or sieving and the air content is determined on the minus 1½ in. (37.5 mm) fraction of the mixture. (The field tolerance applies to this value.) From this the air content of the whole mixture is computed.

There is conflicting opinion on whether air contents lower than those given in the table should be permitted for high strength (more about 5500 psi) (37.8 MPa) concrete. This committee believes that where supporting experience and experimental data exist for particular combinations of materials, construction practices and exposure, the air contents may be reduced by approximately 1 percent. (For nominal maximum aggregate sizes over 1½ in. (37.5 mm), this reduction applies to the minus 1½ in. (37.5 mm) fraction of the mixture.

2.3.3 Water Reducers

Water reducing admixtures are added to reduce the quantity of mixing water required to produce concrete of a given consistency. This allows for a reduction in the *w/cm* while maintaining a desired slump, and has the beneficial effect of increasing strength and reducing permeability. A reduction in water content by 5 to 10 percent is obtainable using conventional water reducers that are specified under ASTM C 494 Type A. This class of water reducer typically will retard set, so accelerators are often added to offset this effect in PCC mixtures. If it is desired that the water reducer also act as a retarder or accelerator, it can be specified under ASTM C 494 Type D and Type E, respectively. These classes of water reducers are typically composed of lignosulfates, hydroxylated carboxylic acids, or carbohydrates.

The effect of water reducers on the fresh concrete properties varies with the chemical composition of the admixture, the concrete temperature, cement composition and fineness, cement content, and the presence of other admixtures [Whiting and Nagi 1998, Ansari et al. 2002]. The effect on the air void structure is unclear, with some sources reporting an improvement [Ansari et al. 2002] while others reporting possible adverse affect [Peterson et al. 2001b, Whiting and Nagi 1998]. Thus, the fresh and hardened concrete properties of

mixtures containing water reducers should be thoroughly evaluated during design to determine the impact of interactions that may occur.

Type F and Type G high range water reducers, specified under ASTM C 494 (also called superplasticizers) can reduce water content by 12 to 30 percent, but their use in conventional concrete is primarily restricted to applications where "flowing" concrete is desired [Ansari et al. 2002]. One drawback is that voids produced in concrete made with superplasticizers are often large, increasing the spacing factor, and on occasion, instability in the air-void system may occur [Peterson 2001b, Whiting and Nagi 1998].

Water-reducers and superplasticizers usually reduce the amount of air-entraining agent required to obtain a given air content, because they increase the fluidity of the paste and thus tend to enhance the effect of air-entraining agents. However, they do not increase the stabilizing effect, so that this reduction can have a detrimental outcome on the stability of the system, which can result in an increased spacing factor. The use of retarding agents does not seem to have a very significant effect on air entrainment, except that it prolongs the time during which the air-void system can change. Although the system probably doesn't change much after casting since there is no additional energy input [Marchand et al. 1994, Pigeon and Pleau 1995, Mindess et al. 2003].

2.3.4 Supplementary Cementitious Materials – Fly Ash

Supplementary cementitious materials (SCM) are regularly used in PCC construction in North America. Their use provides increased economy, workability and potentially durability to concrete mixtures along with sustainability benefits. Fly ash, ground granulated blast furnace slag and silica fume are three of the major SCMs used in modern PCC construction. Rice husk ash, volcanic ash, natural pozzolans and calcined clays are other examples of SCMs that have also been used in concretes throughout the world. In-depth descriptions of these materials can be found in various sources [Mindess et al. 2003, Kosmatka et al. 2002]. Since this research will utilize concrete mixtures containing fly ash, the following brief discussion on fly ash relates to its impact on the air-void system of PCC.

The standard ASTM specifications for fly ash used in PCC are ASTM C 618 *Standard Specification for Coal Fly Ash and Raw or Calcined Natural Pozzolan for Use as a Mineral Admixture in Concrete* and ASTM C 311 *Standard Test Methods for Sampling and Testing Fly Ash or Natural Pozzolans for Use as a Mineral Admixture in Portland-Cement Concrete*.

Fly ash is produced as a byproduct material from the burning of powdered coal in electric power producing facilities. As the coal is burned in the generating process, noncombustible inorganic portions of the coal are conveyed up the stack with the exhaust gases and are removed from the exhaust stream by electrostatic precipitators. The chemical composition and crystallinity of the removed material can vary widely.

Uniformity in coal fly ash (i.e. fly ash) is desired but difficult to obtain. The pozzolanic and/or cementitious activity of a fly ash is dependent upon the cleanliness and mineralogy of the source coal, and the process producing the fly ash from combustion to silo storage. Fly ash is a heterogeneous mixture of finely divided (i.e. 66% passing 325 mesh), mostly spherical particles, that are each composed of various crystalline and glasseous phases, that occur in wide ranging proportions, and posses varying degrees of pozzolanic and/or cementitious reactivity. Most fly ash used in modern concrete production would have been

considered waste products only decades earlier. Over 250 million tons of fly ash is produced each year in the United States alone [Mindess et al. 2003].

ASTM C 618 divides fly ash into three categories, Class N, Class C, and Class F ashes. Class N ashes are raw or calcined naturally occurring pozzolans. Class C and Class F represent fly ash produced in coal combustion and are the two ash types commonly used in concrete production. These two types of ash have differing chemical and physical properties and require different substitution levels for use in PCC. Class C ash is produced from the burning of lignite coals, which are generally mined west of the Mississippi River while Class F ash is obtained from the burning of bituminous and sub-bituminous coals found further to the east. Class F ash has a higher SiO_2 content and lower CaO content as compared to Class C ash. The composition of Class C ash allows the ash to behave in a cementitious manner while Class F ashes generally are not cementitious.

In either case, the use of fly ash in conjunction with portland cement results in the pozzolanic reaction. In this reaction, shown in equation 2.1, the calcium hydroxide hydration product of hydrated portland cement reacts with the amorphous silica provided from the fly ash to form the more desired calcium silicate hydrate reaction product [Mindess et al. 2003].

$$CH + S + H \rightarrow C\text{-}S\text{-}H \tag{2.1}$$

The reaction given in equation 2.1 uses ceramic notation where CH represents calcium hydroxide, S represents SiO_2, H represents water, and CSH is calcium silicate hydrate. Fly ash is normally used in PCC as a replacement of a portion of the portland cement by mass. Increased mixture economy, workability, and reduced water demand are benefits of using fly ash in addition to the benefit of the pozzolanic reaction, which should result in a long-term increase in strength and a reduction in permeability.

Fly ash chemistry is not a priority in power production since ash is a waste product and not the primary product of the process. Fly ash and other particulate matter are removed from the exhaust stream with the intent of total removal, not selective removal. As a result, materials removed in the electrostatic precipitation include alkali compounds and carbon. A high alkali content is one characteristic of fly ash that may make it unsuitable for use in concrete where long term durability is required (i.e. 30-50 years). Increased carbon contents can cause admixtures such as AEAs to become less effective resulting in less durable concrete that is more likely to fail early in its life. Therefore, it is essential that a fly ash supplier be able to provide a consistent, quality material.

2.4 Other Considerations Regarding the Air-Void System

Significant loss of air content can occur between original mixing and final placement. However, coarse voids are selectively eliminated, and only extended vibration will remove a sufficient number of fine voids to compromise frost resistance [Pigeon and Pleau 1995, St. John 1998, Mindess et al. 2003]. Surface-finishing operations can also influence the air-void system characteristics of the surface layers. Overworking in particular, can increase the value of the air-void spacing factor in the surface layer and thus increase the risk of surface scaling [Marchand et al. 1994, Pigeon and Pleau 1995].

Finally, the air-void system of hardened concrete can also degrade over time if some air voids are filled with secondary deposits. The most common deposit in voids and cracks is

secondary ettringite, which usually forms through the precipitation from solution of dissolved ions from hydrated cement paste. Ettringite is formed during the hydration process from the reaction of tricalcium aluminate (C_3A) with gypsum and water [Mindess et al. 2003]. Over time the incremental deposition of ettringite and other secondary deposits on the walls of the air voids may completely fill the interstitial pore space and air void system, leaving the concrete vulnerable to freeze-thaw deterioration.

It is obvious from this discussion that, considering the large number of parameters that affect the air void production and stability, testing is the only way to verify whether the use of a particular air-entraining admixture in a given mix will yield a system of closely spaced air voids which will stay stable until the concrete has set. In addition, once the dosage of the air-entraining agent required to obtain a correct spacing factor for a given mix is determined, no mix parameter should be changed significantly, because a change may result in a higher spacing factor even if the air content stays constant [Pigeon and Pleau 1995].

2.5 Known Problems with Concrete-Making Admixtures

Although the use of synthetic AEAs in concrete mixtures has become increasingly common over the past two decades, the amount of research performed specifically on such mixtures has been negligible. This is surprising since synthetic AEAs have been suspected to be the cause of material problems in New Jersey, Delaware, South Dakota, Minnesota, Virginia, New York, Michigan and Ohio [Cross et al. 2000]. The literature comparing the performance of natural vinsol resins to synthetically produced AEAs is quite limited. Confounding this problem is the fact that the few studies performed on these mixtures have not resulted in a consensus on the mechanisms of deterioration that have been reported when using synthetic AEAs.

In one study, researchers analyzed data collected from various New Jersey Department of Transportation (NJDOT) construction projects through the 1990's [Ansari et al. 2002]. This investigation demonstrated that concrete mixtures produced with synthetic AEAs resulted in a rather large reduction in compressive strength as compared to mixtures using a vinsol resin based admixture. A decrease of 300-700 psi compressive strength in standard NJDOT concrete mixtures was attributed solely to the substitution of synthetic AEAs for vinsol resin AEAs. Subsequent research to understand this observation was conducted in two phases, the first of which being an initial comparison of specimens produced using two different AEAs. It was found in phase I that the vinsol resin produced a more desirable air-void system than did the synthetic and the larger voids found in the air-void system created by the synthetic were the cause of the decreased compressive strength for those specimens.

The researchers postulated that the larger voids were possibly due to the synthetic AEA that was more effective than vinsol resin at reducing the surface tension at the water/air interface. The results were cautiously viewed as meaningful but incomplete since Phase I was conducted using only one vinsol resin and one synthetic AEA. Thus, phase II research was performed studying AEAs from four producers. Five vinsol resin and four synthetic products were investigated in the study. Strength loss, air-void system parameters and surface tension effects of the varying AEAs were analyzed based on the postulations made after completion of Phase I.

Conclusions arising from this research include that concrete mixtures produced using synthetic AEAs exhibited lower compressive strengths than the mixtures prepared using vinsol resins, mainly due to the creation of larger air voids in the synthetic AEA mixtures [Ansari et al. 2002]. The mechanism appeared to be the synthetic's superior ability to reduce the water surface tension creating a less stable, coarser air-void system. In addition, the severity of the effect of AEA type on concrete durability was brand sensitive. It was stressed that generalizations of concrete durability, based on the use of synthetic AEAs, will lead to erroneous results.

The results of the New Jersey study differ from other research findings from investigations of failures of concrete mixtures produced using synthetic AEAs. These researchers concluded the air voids created were too small, not too large [Cross et al. 2000]. The driving force for this study occurred in 1997 when the South Dakota Department of Transportation (SDDOT) recognized a material problem was at hand. In routine testing of paving, precast and structural concrete work, an unacceptable number of compressive tests were failing.

In the initial SDDOT investigation [Cross et al. 2000], examination of a failed specimen with a scanning electron microscope (SEM) clearly showed a flocculation of air voids attached to the coarse aggregates. The interfacial transition zone (ITZ) in concrete occurs at the interface of the aggregate and the hydrated cement paste (HCP). The ITZ is normally considered the weak link within the concrete structure due to its physical and chemical differences from the bulk HCP. Clustering of air voids at an already weak point within the microstructure only degrades the strength of the concrete. The clustering also provided an excellent location for a shear failure to occur while the concrete was loaded in compression. Thus, a theory was developed that with the synthetic AEA, clustering of air voids at the aggregate face contributed to the test failures.

In subsequent examination, it was found that cylinder tests with low compressive strengths were characterized by fractures mainly through shearing at the ITZ, not through the aggregate itself. These failures left essentially no paste on the surfaces of the aggregate. SEM analysis was able to document the air void clustering at the aggregate interfaces. The researchers noted that the presence of clustering at the aggregate surfaces, in itself, is not a solid explanation for the reduced strength, but compressive strengths will be reduced when the clustering reaches an excessive level. The addition of a water reducing admixtures to the mixture decreased the number of failures but did not provide total mitigation. The research team also concluded that the synthetic AEAs reacted undesirably with low alkali cements, indicating that this reaction seemed to cause the clustering of air voids along aggregate surfaces

SDDOT specified the exclusive use of vinsol resins in its projects during the performance of this research. It was found that this action eliminated abnormal compressive strength failures in paving and structural concrete work. Thus, a recommendation was made to continue the exclusive use of vinsol resin AEAs. They also specified that if a synthetic must be used, it shall be proportioned into the mixture with a vinsol resin AEA making up no less than half of the total AEA dose [Cross et al. 2000].

Other studies have shown variances in the air-void systems created by differing synthetic AEAs. The Portland Cement Association has performed research on the effect of cement alkalinity on the air-void system parameters. This research focused upon cement alkali levels

ranging from 0.21 percent up to 1.20 percent Na_2O equivalents. It was found that AEAs classified as salts of fatty acids produced relatively stable air-void systems regardless of the alkali level of the cement. On the other hand, the sulfonated hydrocarbons and alkylbenzylsulfonate based AEAs were found to produce unstable air-void systems as the alkali level increased. These findings indicate that variability exists within the synthetic AEAs based upon their individual chemistry.

2.6 Existing Methods of Measuring Air Content in Concrete

To construct consistently durable concrete, it is necessary to monitor and control the addition of AEAs used in making concrete. This is generally accomplished by monitoring the total air content of fresh concrete delivered to a job site. The two most common methods used for assessing the air content of fresh concrete are ASTM C 173 and ASTM C 231. Both methods have been widely applied for many years. The air content measured by these methods does not ensure the adequacy of the air-void system, but a well-established, empirical correlation between the volume of properly entrained air and frost resistance exists for air entrained concrete. The complete air-void system in hardened concrete can be assessed microscopically using procedures described in ASTM C 457. The major parameters used to determine the susceptibility of hardened concrete to damage by freezing and thawing under saturated conditions are air content, Powers spacing factor, specific surface, void frequency, and paste-air ratio. ASTM C 457 is the most widely used method for the determining all of these parameters. Emerging techniques exist that can provide ASTM C 457 type information on fresh concrete. However, these are yet to be fully developed and/or accepted. Each of these methods will be discussed in more detail. It should be noted that some mixtures that contain inadequate air-void system parameters exhibit adequate freeze-thaw durability. Such is often the case with mixtures containing water-reducing admixtures.

2.6.1 Measurement of Air Content in Fresh Concrete by ASTM C 138 – Gravemetric Method

ASTM C 138 *Standard Test Method for Density (Unit Weight), Yield, and Air Content (Gravimetric) of Concrete*, is the simplest of all tests for determining the air content of fresh concrete. The measured air content is based upon the difference in unit weight of the air entrained concrete mixture as compared to the same mixture prepared without air entrainment, and is determined using the following equation:

$$A = [\ (T - D) / T\ ] \times 100 \qquad (2.2)$$

In the equation above, A is the volume content of air in the concrete, D is the unit weight of the air entrained concrete (lb/ft^3 or kg/m^3), and T is the theoretical unit weight of the concrete computed on an air-free basis (lb/ft^3 or kg/m^3). As described in ASTM C 138, the theoretical density is a laboratory determination, the value of which is assumed to remain constant for all batches made using identical component ingredients and proportions. The determination of the air content by this approach is subject to possible errors in determining the unit weight of the concrete in both states (i.e. air-free and air entrained). In the case of the air-free unit weight, an average specific gravity for each constituent must be assumed and inherent variations in this value will effect the determined value. Likewise, determining the unit weight of the air entrained concrete is subject to errors in measuring the weight of a known

volume of concrete, and also errors in determining the exact volume of the concrete (e.g. incomplete or overfilling the unit weight container). However, the gravimetric air content does correlate well with the air content as measured by other means and it provides a quick, reliable method of quality control for fresh concrete.

2.6.2 Measurement of Air Content in Fresh Concrete by ASTM C 173 – Volumetric Method

ASTM C 173, known as the volumetric method, measures only the volume of the air voids within the paste fraction of the concrete and ignores the air voids entrapped within the aggregate structure. Thus, this method can be used for all types of aggregates including very porous aggregate particles such as would be found in lightweight concrete mixtures.

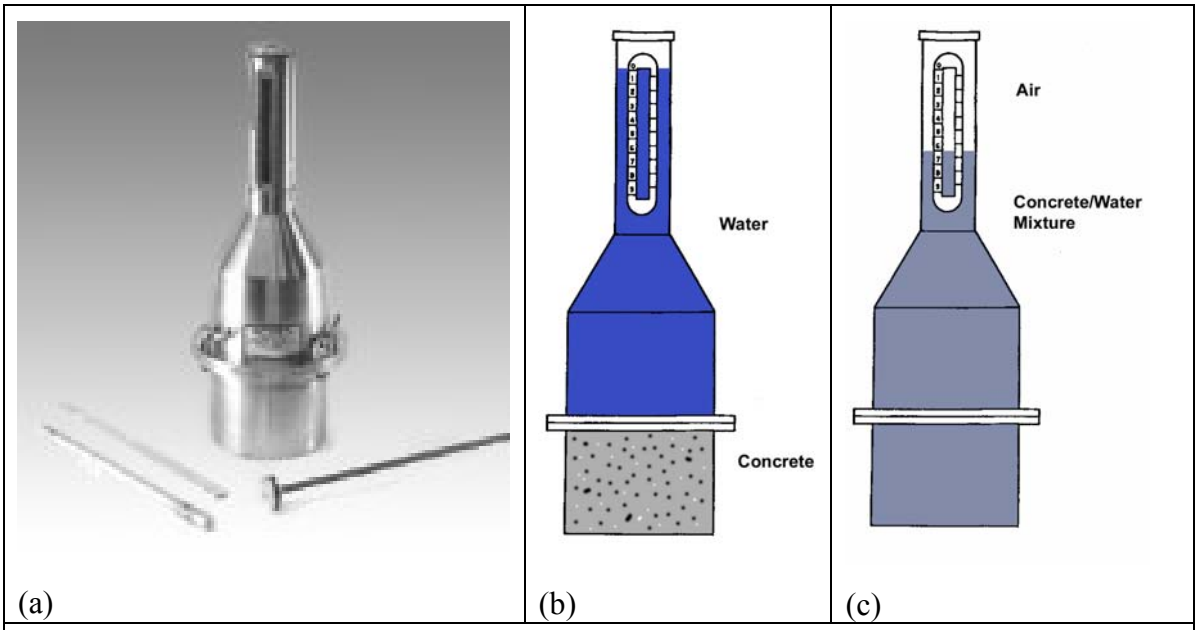

Figure 2-2. (a) A picture of the Roll-o-Meter type air meter (ASTM C 173). (b) A schematic representation of the air meter filled with concrete and water at the start of the test. (c) A schematic representation of the air meter filled with mixed concrete, water, and air at the end of the test. Air collects at the top of the neck as shown.

This method uses an air meter, commonly known as the Roll-o-Meter, consisting of a bowl and a top section as shown in Figure 2-2. The operation of the air meter consists of preparing a known volume of concrete within the bowl portion of the meter. Before the concrete is agitated, the top section of the meter is filled with a combination of water and isopropyl alcohol. The meter is then physically agitated and rolled to sufficiently combine the water/alcohol mixture with the fresh concrete. During this mixing process, the entrapped and entrained air originally within the concrete is "washed" out and allowed to rise to the top of the meter. The volume of air removed from the concrete can then be directly measured.

The relative simplicity in performing the test along with the meter's durability and low maintenance has made the roll-o-meter test an extensively used test within the industry. On

the other hand, the length of time taken to properly perform a single test (upwards of 20 minutes for a single test) in comparison to the pressure meter test (ASTM C 231), along with the large amount of physical energy input by the test technician, makes this a less desirable test to perform.

2.6.3 Measurement of Air Content in Fresh Concrete by ASTM C 231 – Pressure Method

Testing according to ASTM C 231, commonly known as the pressure meter test, is another technique to determine the air content of a fresh concrete sample. This procedure will measure the volume of air within the entire sample including the aggregate pore spaces. Thus, an aggregate correction factor must be used if a mixture contains semi-porous aggregates. This test should not be used for concretes containing lightweight aggregates, air-cooled blast furnace slag, or other high porosity aggregates.

(a)

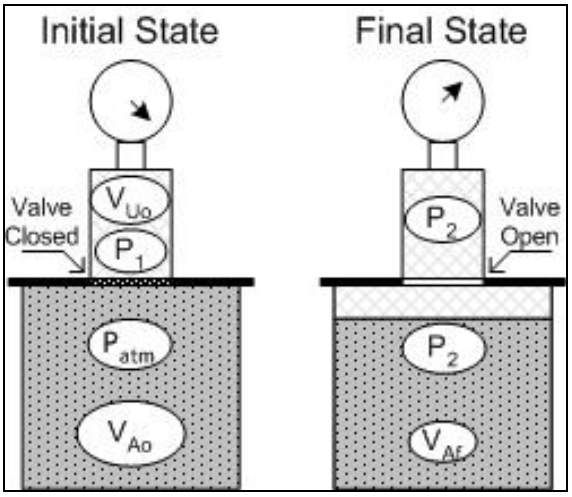

(b)

Figure 2-3. (a) A picture of the type B air meter (ASTM C 231). (b) A schematic representation of the type B air meter. Variables shown in Figure 2.3b are used in equation 2.3.

The testing apparatus, shown in Figure 2-3, consists of a bowl of known volume filled with fresh concrete and a cover section, which is used to seal and pressurize the sample of concrete. The type of pressure meter cover classifies the meter as either a Type A or Type B pressure meter. A Type A meter allows the prepared sample to be slowly pressurized. The more common Type B meter, which was used in this research, allows for a sudden pressurization of the sample.

The prepared sample is pressurized to approximately twice normal atmospheric pressure. A volume decrease in the sample is observed because all the components of concrete except for air are incompressible. Thus, the change in volume can be entirely attributed to the air content of sample. Boyle's law is used to attribute the pressure change to volume change and thus give the percent entrapped and entrained air within the sample.

The lower time of operation and reduced physical exertion required by the pressure meter, as compared to the roll-o-meter, have played a large part in promoting the wide use of the pressure method meter in the field. It is noted that inaccurate measurements will be obtained if care is not taken to ensure proper calibration of the meter's gauge.

2.6.4 Problems with Standard Fresh Concrete Air Tests

It has been observed that the volumetric and pressure tests may not accurately measure the true characteristics of the air-void system of concrete, especially if the entrained air voids are very small [Roberts 1994, Hover 1988, Gay 1982]. Although the volume of entrained air in a concrete will vary little with small changes in the volume fraction of smaller voids, the spacing factor will decrease and specific surface will increase with increasing numbers of smaller voids.

In the case of ASTM C 173, inaccuracies caused by very small entrained voids may occur. Theoretically, all the air within the concrete should be measured since the entire sample is agitated in liquid and the air is allowed to agglomerate at the surface. A concern is that the very small voids washed out of the paste are hindered in the process of rising to the surface by adhering to cement grains or even through attraction to the side of the meter's bowl [Gay 1982]. A more important source of error may be in the timing of the measurements made in the volumetric test. The ASTM C 173 procedure allows for a maximum change of 0.25 percent air within 2 minutes signifying that the air has been sufficiently removed from the sample. Due to buoyancy principles and that the smaller bubbles are being hindered from rising, the smaller bubbles take longer to reach the surface of the liquid than do the larger voids. It has been shown that such small bubbles can continue to accumulate for as long as 20 minutes after agitation of the meter has ceased [Hover 1993]. The error in total measured air content caused by not recording the volume of very small voids may be significant if smaller voids make up a larger volume of the total air within the sample.

Previous research has shown that shortcomings of the pressure meter are accentuated when measuring small air voids in concrete, resulting in a lower measured air content than actually exists [Gay 1982, Hover 1988, Hover 1989]. This variation has been attributed to the relatively higher internal pressures characteristic of small diameter spherical air voids. To fully examine this theory, the principals of the pressure method must be explored in depth.

The pressure meter operates under the assumption that Boyle's Law is applicable to the materials involved in the test. Boyle's law involves the relationship between three properties of a gas in a container. Simply stated, Boyle's law is:

$$PV = kT \tag{2.3}$$

where:
P = pressure within the container
V = total volume of the container
k = constant dependant on units
T = temperature of the container

If the temperature of the container is constant, Boyle's law can be used to relate volume changes of a substance to the pressure change of that substance.

$$P_o V_o = P_f V_f \tag{2.4}$$

where:
P_o = initial pressure
V_o = initial volume
P_f = final pressure
V_f = final volume

Boyle's law, applied to this situation, states that each air void in the sample is under the same internal pressure regardless of the diameter of the individual air void. By using such an assumption, the theoretical mathematics behind the test become quite simple. The test is conducted by filling the bowl in a standardized fashion with a volume of concrete (V_{Co}) at atmospheric pressure (P_{atm}). This volume of concrete contains a volume of total air equal to V_{Ao}. This method assumes that each of the voids in the sample initially has an internal pressure equal to atmospheric pressure. The upper chamber's known volume of air (V_{Uo}) is then compressed to a calibrated pressure (P_1) greater than the atmospheric pressure. The connecting valve between the upper chamber and bowl is then opened and the air pressure between the two volumes stabilizes to a constant value (P_2) within a few seconds. This process causes the pressure in the bowl to increase and compress the air voids within the concrete sample. Since the air voids are taken as the only compressible fraction of the sample, the new volume of the sample (V_{Cf}) will be less than the original sample due to the compression of the air voids in the sample. The described relationships can be written from Boyle's Law as follows:

$$P_1 V_{Uo} + P_{atm} V_{Ao} = P_2 (V_{Uo} + V_{Ao}) \tag{2.5}$$

where:
P_1 = calibrated initial pressure of upper chamber
P_{atm} = initial internal pressure of air voids
P_2 = stabilized pressure for both upper chamber and bowl
V_{Uo} = upper chamber initial air volume
V_{Ao} = initial volume of air voids in concrete sample

Rearranging and solving for the unknown, V_{Ao}, gives:

$$V_{Ao} = [V_{Uo} (P_2 - P_1)] / (P_{atm} - P_2) \tag{2.6}$$

This theory and method are simple enough if the assumptions used in deriving the formula are valid. In the case where a concrete sample contains very small voids, the assumptions may cause significant errors in the final air content meter reading. These errors have been attributed to the fact that the internal pressure of a small void is inversely proportional to the diameter of the individual air void. This geometric factor is not accounted for in the pressure meter calculation. Hover [1988] derived equations based on Boyle's law to model the variation between theoretical and measured air content by the pressure meter. These analyses showed that the meter will read significant errors at normal air contents for voids with diameters of 0.0004 inch (10 μm) or less, if these size voids are present as a large fraction of the total air void volume. For concrete mixtures prepared using vinsol resin AEAs, the small

voids make up a very small percentage of the total air content and the error in pressure meter reading due to the 0.0004 inch (10 μm) and smaller voids is not significant. However, this may not be the case for concrete made with synthetic AEAs.

2.6.5 Automated Methods for Measuring Air-Void System Parameters in Fresh Concrete

A newer technology, which has been under investigation for a number of years, is an alternative method for measuring the air-void system parameters (commonly measured only in hardened concrete), in fresh concrete. The test equipment, known as the air void analyzer (AVA) or the Danish air test, has received mixed reviews [Price 1996, Magura 1996]. The AVA was developed in Europe in the 1990's to meet a demand to be able to accurately and quickly determine the specific surface and spacing characteristics of air-void systems in fresh concrete. Such a tool would allow for mitigation of material problems at the time of placement and would serve as a replacement for having to cure, prepare and microscopically examine specimens to achieve the same results.

The AVA test is performed in approximately 25 minutes on a fresh concrete sample. The sample can be easily collected from the final placement unlike preparation of standard concrete cylinders, which are normally prepared before the concrete is processed through a paving machine or pump. This allows for increased accuracy due to the testing of the final air-void system, which has already experienced any alteration from transport and placement.

The test consists of collecting a 20 cm^3 sample of paste within a syringe type container. The vibratory hand drill, which collects this sample, screens out any particles larger than ¼ inch (6 mm). This sample is injected into a glycerin solution which, when gently mixed, allows for the release of the air voids from the paste. Various size bubbles rise through the glycerin, which separates the bubbles and preserves the original shape and size, then rise through a column of water at different rates, due to buoyancy principals. As the voids reach the surface, a sensitive measuring device records the buoyant force placed upon it by the rising air bubbles. The air-void system size distribution can be calculated since the applied buoyant force changes over time with larger voids rising sooner than smaller voids. The data collection is complete after the voids have been allowed to rise for 25 minutes. The AVA will output the air-void system statistics including air void distribution, specific surface and spacing factor in both tabular and graphic form. The AVA test has gained notice in the past few years and is increasingly being applied in the industry.

2.6.6 Measuring Air Content in Hardened Concrete by ASTM C 457

Concrete can be evaluated for susceptibility to damage by paste F-T damage by following ASTM C 457 procedures to assess the adequacy of the entrained air-void system [Walker 1992]. This test method uses an optical microscope coupled with a movable stage to determine the volumetric fraction of the individual phases in the concrete, including the air voids. From this analysis, the key parameters of the air-void system can be determined including the Powers spacing factor, specific surface, and air content. Turnkey analytical systems to perform ASTM C 457 are not common, but available. Often petrographers purchase the necessary hardware and write the necessary controlling software [Sutter 1998].

The microscopic examination of the air-void system in hardened concrete can take the form of a point count, linear traverse, or an area traverse. All three methods rely on measurements obtained from a polished plane surface of concrete. The general mathematical methods used

to extrapolate measurements obtained from a two-dimensional surface to three-dimensional space are known as stereology [Underwood 1970, Russ 1986]. Hilliard [1968] presents the mathematical derivations for volume fraction relationships based upon measurements in a two-dimensional slice of the volume, as is the case with a polished microscope specimen. For heterogeneous materials like concrete, the fundamental relationship between the volume fraction of a phase and the point, line, or area fraction of the phase is shown below.

$$P_P = L_L = A_A = V_V \tag{2.7}$$

where:
P_P = fraction of total points counted falling in phase of interest
L_L = fraction of total line length traversed falling in phase of interest
A_A = area fraction of phase of interest
V_V = volume fraction of phase of interest

Both methods of volume fraction estimation, point counting and linear traverse, have been applied to air void measurement in concrete. In addition to the total volume of air in hardened concrete, ASTM C 457 details procedures for determining a Powers spacing factor. Powers and Willis [1949] developed two expressions for a spacing factor, both of which require a determination of the total air void specific surface. They demonstrated that the total volume of air voids and their total specific surface could be estimated from the mean air void intercept or chord length obtained from a linear traverse. Assuming all air voids to be spherical and using geometric probability concepts, the total specific surface, α, expressed in terms of the average chord length, $\bar{l}$, was shown to be:

$$\alpha = 4 / \bar{l} \tag{2.8}$$

Powers first spacing factor expression was obtained by simply calculating the volume of cement paste per unit area of air void surface. This is given as:

$$\bar{L} = p / \alpha A \tag{2.9}$$

where:
$\bar{l}$ = average chord length, in units of length
α = total specific surface of the air voids, in consistent units of length^{-1}
$\bar{L}$ = spacing factor, in units of length
p = paste content, in volume percent of concrete
A = total volume of air voids, in volume percent of concrete

His second spacing factor expression is based on a hypothetical system of equal-sized spherical voids uniformly distributed throughout the paste phase. The size of each of these hypothetical voids is determined by setting their specific surface (3/R) equal to the total measured specific surface of the true void system and then solving for the resulting sphere radius, R. By making the total air content of the hypothetical system of voids equal to the measured value of air content, the number of hypothetical voids is then determined. The Powers spacing factor thus obtained is:

$$\bar{L} = 3/\alpha[1.4(1 + p/A)^{1/3} - 1] \quad (2.10)$$

Powers recognized that neither expression for spacing factor provides a true measure of void spacing. Assuming that both expressions overestimate the true average void spacing, he recommended using the smaller spacing factor obtained from the two equations. Equation 2.8 yields a smaller factor for p/A less than 4.33, and Equation 2.9 gives the smaller value when p/A is greater than 4.33.

According to ASTM C 457, for normal strength concrete, entrained air-void systems with a Powers spacing factor of 0.008 inch (0.20 mm) or less will typically provide good F-T protection. This value was empirically established primarily by laboratory F-T testing using ASTM C 666 (AASHTO T 161) [Philleo 1986]. While the Powers spacing factor is not considered a truly definitive measure of F-T protection, it is still used as the standard method of quantifying the distribution of entrained air in concrete. Other measures for characterizing entrained air have been proposed [Walker 1980, Philleo 1983, Attiogbe et al. 1993], but none have been adopted for general use.

2.6.7 Precision of ASTM C 457 Measurements

The precision of the microscopical determination of air-void characteristics may be expected to be subject to the reasonably predictable statistical errors associated with any counting technique, but in addition they will be affected by many other parameters, such as the microscope magnification, the quality of the prepared specimen, the sample size, and the performance of the operator [St. John 1998, Pigeon and Pleau 1995]. Therefore, it is difficult to assess theoretically the precision of this measurement.

However a study done on more than 600 air-entrained concretes [Pleau and Pigeon 1992] indicates that the maximum error associated with the determination of the three most important parameters of the air-void system (air content, specific surface of air voids and air void spacing factor) decreases exponentially with the number of slabs examined. Pleau found that when the minimum requirements of the ASTM C 457 Standard are strictly satisfied for a nominal maximum size aggregate of ¾ inch (19 mm) , the maximum error of the microscopical examination is evaluated at approximately 28, 20 and 16 percent for A, α, $\bar{L}$, respectively. The study also underlines the fact that A is less accurate than α, which is less accurate than $\bar{L}$. This can be explained by the fact that the accuracy increases with the numbers of parameters involved in the computation because one is unlikely to obtain, simultaneously, a large error in all parameters [Pigeon and Pleau 1995].

ASTM C 457 also contains a section on the precision and bias associated with the determination of the air-void system parameters. A study was done on the determinations made on a series of four lapped specimens prepared in one laboratory and then circulated to nine different laboratories. In general, the coefficient of variation found was around 12 percent for the determination of the spacing factor and between 8 and 15 percent for the determination of the air content. The standard underlines that the variability would be higher in actual practice for specimens sampled and prepared from in-place concrete since additional variation due to sample selection and surface preparation in different laboratories would increase the coefficient of variation.

Finally, the air content parameter has to be considered with a grain of salt. As described by St. John et al [1998]: "sources of apparent contradiction between air content findings and actual performance include the type of air voids and the spacing factor". In ASTM C 457, no distinction is made regarding the nature of the air void when recording whether the point is located over an air void, a fly ash particle, an aggregate or cement paste. Therefore, a high air content can be due to the presence of entrapped air voids, glassy spherical shelled fly ash particles, or porous aggregates rather than to multiple entrained air voids, although only the latter will protect the paste against frost action. However, only the entrained air voids are considered when recording the voids intercepting the traverse line, so once again the spacing factor is a better indicator of the adequacy of the air-void system [Pigeon and Pleau 1995, St. John 1998].

2.6.8 Automated Systems for Measuring Air Void System Parameters in Hardened Concrete

Other researchers are developing automated systems for performing this test using convention optical microscopes, coupled with digital cameras and computer aided image analysis, to measure air-void system parameters [Baumgart et al. 2001]. This approach is hampered by the computer's inability to distinguish small air voids from other features in the image, resulting in significant errors in spacing factor and specific surface calculations. Other automated methods have been developed that require darkening the concrete surface with black ink and filling the air voids with a fine white powder such as wollastonite or zinc oxide [Pade et al. 2002]. This latter approach is quick and accurate for new or laboratory concrete but has some limitations for in-service concrete. First, other important information often garnered from a manual ASTM C 457 examination (e.g. aggregate fraction, aggregate type, paste fraction) are not gathered by this method. Second, for concrete that has been in service, infilling of the air voids always occur and such infilling can drastically change the spacing factor and specific surface parameters of the air-void system. Both automated approaches are unable to identify infilling as well as a human operator can and such infilling is not taken into account when determining the air-void system parameters using automated methods.

2.7 Emerging Technologies for Measuring Air Void System Parameters

Research has continued on new methods of characterizing the air-void system parameters of both fresh and hardened concrete with an ultimate goal of making a more reproducible and readily applied method of determining these important material parameters. These new methods are discussed below.

2.7.1 Measurement of Air Void Systems by Flat-Bed Scanner

The first emerging technology for measuring air-void system parameters in hardened concrete uses a high-resolution flat bed scanner to collect a digital image of a polished cross-section through a concrete pavement core. The procedures for the high-resolution flat bed scanner technique have been documented in available publications [Peterson et al. 2001a, 2001b, 2001c, Carlson et al. 2005]. The images obtained from the device used in the published work to date have a maximum point-to-point resolution of 8 μm. Image processing software is used to classify each pixel in the image as cement paste, aggregate, or air void. Once the image has been classified, a standard ASTM C 457 linear traverse or point count can be automatically performed in a few minutes. Multiple analyses of the same specimen can be performed to develop confidence intervals in average values. In addition to the standard ASTM C 457 measurements, other analysis procedures can also be applied. For example, the distance to the nearest air void can be calculated for each pixel classified as cement paste using an accumulated cost surface algorithm. In this novel approach, the presence of aggregate is accounted for in the void-to-void distance calculation, thereby modeling real water flow through the air-void system. The accumulated cost surface algorithm allows pixels classified as aggregate to be treated as obstructions that must be navigated around before reaching the nearest air void. Figure 2-4 shows a classified image obtained from a high-resolution flat bed scanner.

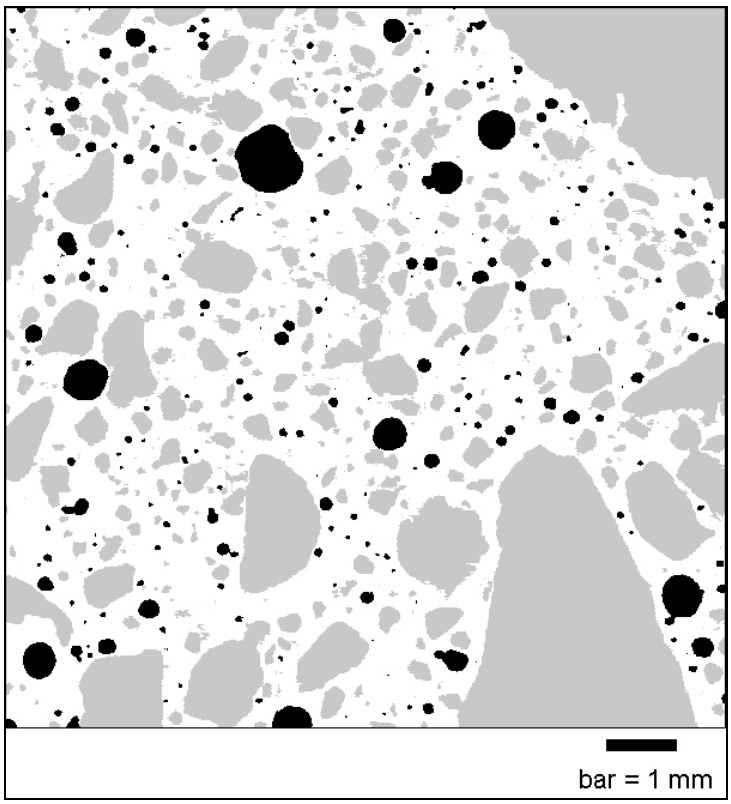

Figure 2-4. Classified image obtained from the high-resolution flat bed scanner. In the image, air voids are black, aggregates are gray, and cement paste is shown as white.

2.7.2 Measurement of Air-Void Systems by CT X-ray Scan

Another emerging technology for measuring the air-void system parameters in hardened concrete involves the application of high-resolution industrial CT x-ray scans to measure air-void system parameters in concrete in three dimensions [Wiese et al. 2000]. The patent pending non-destructive technique uses small diameter samples of fresh or hardened concrete that can be scanned at point-to-point resolutions of up to 10 microns. The resulting data set is a three dimensional representation of the sample showing the spatial distribution of aggregate, paste and air voids. This technique uses the well-established radiographic technique of computed tomography (CT)

CT scanners typically produce multiple two-dimensional x-ray images, each representing cross sections or slices (also known as tomographs) through the specimen. The tomographs may be stacked one on top of another to create a three-dimensional volume. In a linear array system, tomographic images are generated by projecting a thin-beam of x-rays through one plane of the specimen at many different angles. As x-ray photons pass through a specimen, some will be absorbed while transmitted photons are measured by an x-ray detector. By collecting this data over many angles, a cross section representing the attenuation parameter of each element within the slice can be reconstructed by a computer.

In the more innovative volume CT system, the fan beam is extended to a cone beam and thereby collects multiple two-dimensional projections at once. Specialized reconstruction algorithms process the two-dimensional cone-beam projections into a volume that is the equivalent of many simultaneous, contiguous CT slices. The current patent pending system consists of a desktop microfocus industrial CT x-ray scanner that uses cone beam technology. It is connected to a computer workstation that collects and reconstructs the volume. Visualization of the resulting three-dimensional matrix using volume rendering techniques is also done on a computer workstation.

2.8 Summary of Literature Review

The properties and durability of hardened concrete can vary widely depending upon the relative volumes of cement, sand, aggregate, and water used along with the volumetric content of air. Both chemical admixtures and supplementary cementitious materials are used in PCC to improve workability, reduce water requirements, affect set time, or entrain air. Properly sized and spaced entrained air voids have long been known to protect saturated concrete from cyclic freezing and thawing. However, typically only the volume of total air is measured in the field and the more important parameters of spacing factor and specific surface are inferred by empirical relationships. In the past, most AEAs were derived from naturally occurring vinsol resins but a number of synthetic AEAs are currently being employed. The empirical relationships developed between the volume of total air measured and other air-void system parameters are based upon the use of vinsol resins AEAs. In the case of synthetic AEAs, there is an issue if the resulting air-void system has a larger volume fraction of smaller air voids with respect to the total air content.

There are established methods for measuring the characteristics of the air-void system in hardened concrete including total air content, air void spacing factor, and average air void specific surface. The air-void system parameters are measured using an optical microscope and linear traverse or point counting methods.

The two most common methods used for assessing the air content of fresh concrete are ASTM C 173 and ASTM C 231. The air content measured by these methods does not ensure the adequacy of the air-void system. It has been observed that the volumetric and pressure tests may not accurately measure the true characteristics of the air-void system of concrete, especially if a large percentage of the entrained air voids are very small. Although the volume of entrained air in concrete will vary little with small changes in the volume fraction of smaller voids, the spacing factor will decrease and specific surface will increase with increasing numbers of smaller voids.

A number of emerging techniques are being developed to allow for easier and more reproducible determination of the air-void system parameters on both hardened and fresh concrete. The first emerging technology for measuring air-void system parameters in hardened concrete uses a high-resolution flat bed scanner to collect a digital image of a polished cross-section through a concrete pavement core. Image processing software is used to classify each pixel in the image as cement paste, aggregate, or air void. Another emerging technology for measuring the air-void system parameters in hardened concrete involves the application of high-resolution industrial CT x-ray scans to measure air-void system parameters in concrete in three dimensions. The resulting data set is a three dimensional representation of the sample showing the spatial distribution of aggregate, paste and air

voids. The final emerging technique is the air void analyzer (AVA) or the Danish air test that is performed on fresh concrete. The air-void system size distribution can be calculated since the applied buoyant force changes over time with larger voids rising sooner than smaller voids. The AVA will output the air-void system statistics including air void distribution, specific surface and spacing factor in both tabular and graphic form.

Chapter 3 – Test Specimen Preparation

3.1 Concrete Mixture Preparation

3.1.1 Mixture Design

Preparation of the 18 PCC mixtures specified in this study began with a mixture design process. The process was initiated by consulting WisDOT specifications (found at www.dot.wisconsin.gov) on PCC (section 501 of the standard specifications manual). Section 501.3.2.2, and its accompanying table, presented the master limits of components for various WisDOT grades of concrete including the grades A and A-FA concrete used on this project. The research proposal called for a constant *w/cm* of 0.42. For Grade A Concrete with a cement content of 565 pounds per cubic yard (6.0 bag mix), this equated to 238 pounds of water per cubic yard (lb/cy). The aggregate content is specified to have a maximum total weight of 3,120 lb/cy. The fine aggregate as a percent of total aggregate weight has a permissible range of 30 to 40 percent by weight.

3.1.1.1 Initial Mixture Design Determination

The initial mixture design used a fine aggregate content ranging from 40 to 45 percent. To determine the exact weights of coarse and fine aggregate to be used, the volumes of the cement, water and target air content were calculated using each component's specific gravity. The coarse and fine aggregate contents were then calculated to ensure the yield of the mixture design was 1 cubic yard. The proper dosage of air entrainment to use in each mixture design was determined after experimentation with trial mixtures. Factors considered in determining the air dosage were target air content, fly ash content and target slump. The mixture designs for the A-FA grade concrete were done in a similar manner except the cementitious material consisted of 395 pounds of cement and 170 pounds of class C ash. These mixture designs were then scaled down to the necessary batch sizes in order to complete the tests and produce the specimens necessary for this project.

3.1.1.2 Collection of Materials

Necessary constituent materials were collected as the initial mixture designs were being completed. One boundary condition of the research was to utilize materials comparable to those used in typical WisDOT paving mixtures. To accomplish this, an established aggregate producer[2] used extensively in the northern portion of the state was used as the source. Both coarse and fine aggregates were obtained from this source. Section 501.2.5.3.4 of the WisDOT specifications indicates the gradation requirements of the fine aggregate to be used in the concrete mixtures. Table 3-1 presents the WisDOT specification along with a gradation of the fine aggregate used in the preparation of the mixtures.

[2] Coons Aggregate Supply, a division of Wissota Sand and Gravel Company

Table 3-1. Fine aggregate gradation. Values presented are in percent passing the specified sieve by weight. Fineness modulus (FM) of this aggregate is 2.90

Sieve Size	3/8 inch (9.5 mm)	No.4 (4.75 mm)	No.16 (1.18 mm)	No.50 (300 µm)	No.100 (150 µm)
WisDOT Specification	100	90-100	45-85	5-30	0-10
Source Gradation	100	100	61	22	6

Similarly, section 501.2.5.4.4 presents the gradation requirements for the coarse aggregates. Table 3-2 presents the gradations required by WisDOT's specifications along with the gradation of the coarse aggregate used in the sample preparation. The coarse aggregate to be used is typically referred to as a ¾ inch top size aggregate and falls under the category of a "No.1" aggregate as characterized in Table 3-2.

Table 3-2. Coarse aggregate gradation. Values presented are in percent passing the specified sieve by weight. Size No. according to AASHTO M 43

Sieve Size	Size No.1	Size No.2	Source Gradation
2 inch (50 mm)	-	100	-
1 ½ inch (37.5 mm)	-	90-100	-
1 inch (25.0 mm)	100	20-55	100
¾ inch (19.0 mm)	90-100	0-15	98
⅜ inch (9.5 mm)	20-50	0-5	35
No.4 (4.75 mm)	0-10	-	2
No.8 (2.36 mm)	0-5	-	0

The aggregate producer ensured that these aggregates met ASTM C 33, *Specification for Concrete Aggregates,* standards for deleterious substances and physical properties.

The portland cement required in WisDOT grade A and A-FA is a Type II cement. As specified in ASTM C 150*, Specification for Portland Cement*, Type II cement provides moderate sulfate attack resistance and reduced heat liberation during hydration. Cement for this project was produced at Lafarge Corporation's Alpena, Michigan plant and is certified as meeting the ASTM C 150 requirements for both Type I and Type II portland cement. Thus, it is commonly marketed and referred to as Type I/II cement. The cement was obtained from Lafarge Corporation in the standard 94lb bagged packaging. The quantity of cement obtained was a full pallet of forty bags to ensure the cement used throughout the sample preparations would be consistent. A mill certification of the chemical composition of the cement was provided by Lafarge Corporation, including alkali equivalent content, Blaine Fineness and simplified Bogue calculation results as presented in Table 3-3.

Table 3-3. Portland Cement Composition

Compound/Characteristic	Ceramic Notation	Chemical Formula	Weight Percent
Silicon Dioxide	S	SiO_2	20.7
Aluminum Dioxide	A	Al_2O_3	4.7
Iron Oxide	F	Fe_2O_3	2.6
Calcium Oxide	C	CaO	65.6
Magnesium Oxide	M	MgO	2.3
Sulfur Trioxide	$\overline{S}$	SO_3	2.6
Tri-Calcium Silicate	C_3S	$3CaO•SiO_2$	67.03
Di-Calcium Silicate	C_2S	$2CaO•SiO_2$	8.78
Tri-Calcium Aluminate	C_3A	$3CaO•Al_2O_3$	8.06
Tetra-Calcium Alumino Ferrate	C_4AF	$4CaO•Al_2O_3•Fe_2O_3$	7.91
Total Alkali	-	Na_2O	0.49
Blaine specific surface (m^2/kg)	-	-	363

Fly ash is used in some mixtures for this research since it is known that the air-void system of PCC can be adversely affected by the introduction of fly ash into the concrete mixture. The class C fly ash was obtained in bulk from Enduracon Technologies of St. Paul, Minnesota. The fly ash was produced at North Shore Mining Company in Silver Bay, Minnesota as a byproduct of operating a coal-fired power generating plant in its taconite pellet production process. The fly ash product used, marketed as "Poz NS", met ASTM C 618.

Water used was obtained from the City of Houghton municipal water supply. The water used in preparing the mixtures meets ASTM C 94, *Specification for Ready-Mixed Concrete*.

The AEAs used in this research were obtained from Master Builders Corporation of Cleveland, OH. Two synthetics and one natural AEA were obtained in bulk quantities of 3 gallons each. The first synthetic AEA is marketed as "AE-90". This chemical is classified as an anionic surfactant. The other synthetic AEA is marketed as "Micro Air" and is classified as a surfactant mixture, aqueous solution. The natural AEA is called "VR-Standard". This is a vinsol resin based AEA which is a saponified natural wood resin.

3.1.1.3 Final Mixture Design Determination

Once all the component materials were gathered and the initial mixture designs were completed, trial batches were prepared. After mixing three trial batches, the following observations were made. The workability of the mixtures was very poor, with the slump values averaging about ½ inch. Although the air content was in the target range, concern existed regarding the quality of the test specimens produced since the low slump mixtures were very difficult to properly consolidate. To improve the workability of the mixtures, two options were discussed. The first option was to increase the paste content of the mixture by increasing the cement content of the mixture design from 6.0 bags to 6.5 bags per cubic yard of concrete. The second option was to use the 6.0 bag mixture with a 0.44 *w/cm* along with a water-reducing admixture to increase the workability to the desired level. Trial mixtures representing each option were prepared. Both trial mixtures achieved a desirable slump while

retaining the target air content values. Ultimately, after discussion with WisDOT representatives, the decision was made that a cement content of greater than 6.0 bags was undesirable. In addition, since WisDOT regularly uses water-reducing admixtures in concrete mixtures, the second option was chosen.

To mitigate the chance of unwanted interactions between the air entraining and water reducing admixtures, a product from the same admixture producer was selected. The Master Builders mid-range water-reducing admixture "Polyheed 997" was chosen and obtained after consulting with WisDOT engineers. This admixture was delivered in a similar container, volume and fashion as the AEAs to Michigan Tech.

Once the workability of the trial mixtures was found to be satisfactory, the dosages of AEAs to be used needed to be determined. In initial mixtures, the synthetic AEA "Micro Air" was used. This admixture worked well for the previously mentioned trial mixtures when targeting an air content of 6 percent +/- 1.5 percent, but mixtures aimed at entraining a high amount of air (i.e. 9 percent) could not be produced.[3] To try to meet the high air requirement, the dosage of the synthetic AEA was increased from a slightly high dose (~ 2.0 fluid oz/100# cementitious material) to an extremely high dosage (~ 26 fluid oz/100# cementitious material). Eleven mixtures were produced with Micro Air dosages within this range. Three utilized an 18 percent fly ash replacement of cement while the other eight varied only in the AEA dosage. Only one of the eleven mixtures produced a measured volume of air within the 9 percent +/-1.5 percent range (dosage of 20 fluid oz/100#) as measured by ASTM C 231, ASTM C 173, and ASTM C 138. However, a cylinder produced from one of the eleven mixtures was cured for 28 days, lapped and polished for ASTM C 457 analysis. Microscopic analysis revealed entrained air within the sample in the form of an agglomeration of very small air voids around the aggregate particles of the sample. Example micrographs illustrating these types of air voids are shown in Figures 3-1 thru 3-4. For this specimen, a hardened air content of 7.8 percent was measured. That is compared to 5.5, 5.9, and 4.3 percent as measured by ASTM C 231, ASTM C 173, and ASTM C 138, respectively. The fresh concrete tests seemed to underestimate the hardened air content for high doses of synthetic AEAs.

The problems encountered in preparing these mixtures show that it is very possible to overdose a mixture with AEA when conventional field air tests indicate a low air content. A vicious cycle could result with failing tests requiring higher dosages of AEA resulting in increasingly reduced quality concrete.

[3] Air content was measured using methods ASTM C 173 and ASTM C 231.

Table 3-4. Air Dose Trial Mix Results. MA represents Micro-Air, VR vinsol resin. Sample T-3M (20) was also analyzed microscopically and found to have a hardened air content of 7.8%.

Mixture ID	AEA Type	Fly Ash	Unit Weight (lb/ft^3)	ASTM C 231	ASTM C 173	ASTM C 138	Air Entrainer Dose (fl.oz/100 #)
				(volume %)			
T 1	MA	NO	148.84	5.6	5.3	4.6	7.4
T 2	MA	NO	149.16	5.0	5.2	4.4	3.7
T 3	MA	NO	148.52	5.6	6.2	4.3	11.1
T 4	MA	Yes	148.24	6.1	6.3	4.2	9.6
T 5	MA	Yes	151.04	4.3	4.7	2.7	2.0
T 6	MA	Yes	143.56	8.0	8.3	7.0	20.0
T 2R	MA	NO	154.64	3.1	4.2	0.9	7.4
T 3R (16)	MA	NO	150.08	5.0	4.9	3.3	14.9
T 3 (20)	MA	NO	148.72	5.7	5.6	4.2	18.6
T 3M (20)	*MA*	*NO*	*148.48*	*5.5*	*5.9*	*4.3*	*18.6*
T (28)	MA	NO	146.36	6.8	6.5	5.7	26.0
T No Air	None	NO	156.68	1.6	2.3	0.0	0.0
T (20)	VR	NO	134.04	13.5	14.0	13.6	18.6

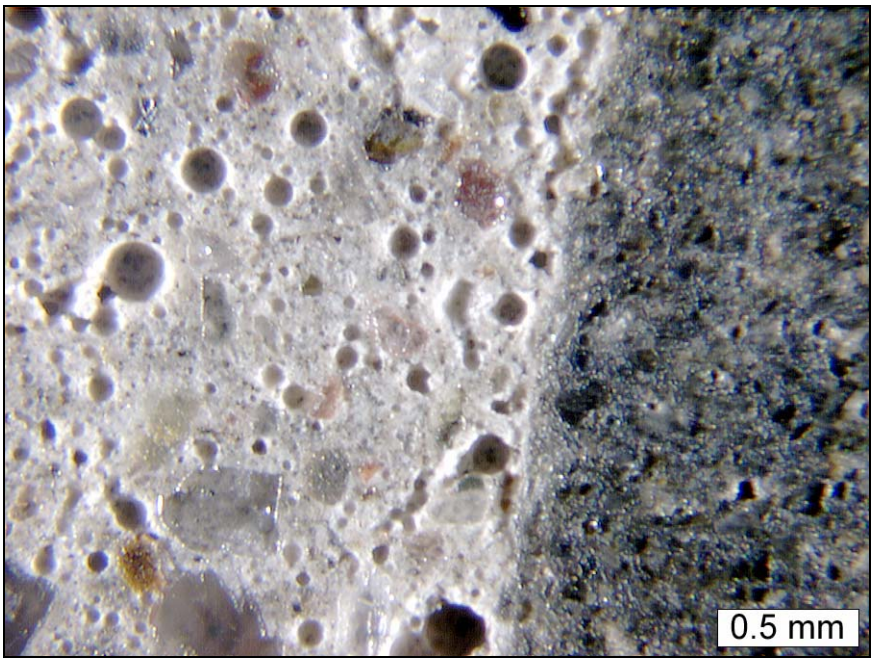

Figure 3-1. Air voids coalescing at the aggregate surface in trial batches prepared in the laboratory.

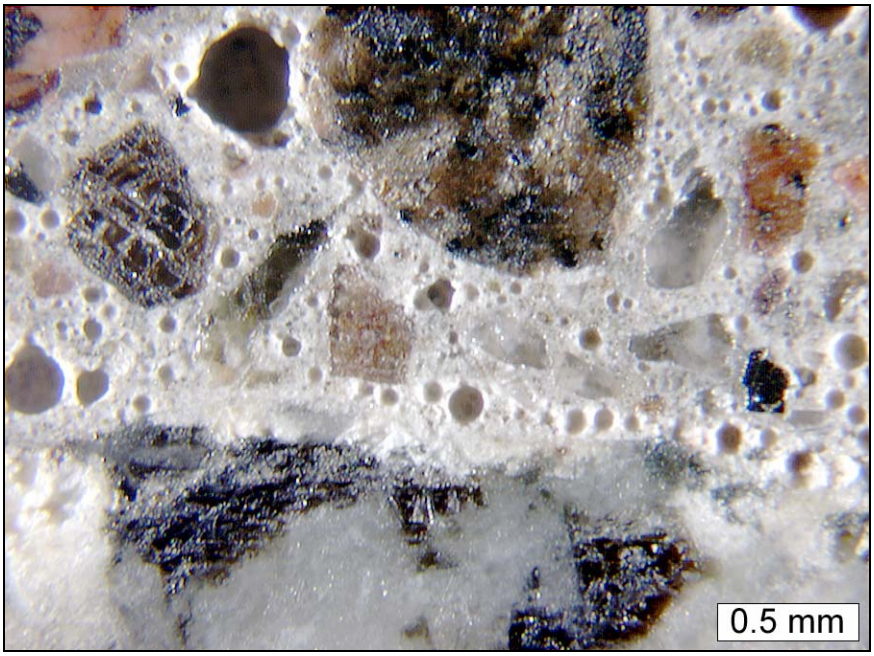

Figure 3-2. Air voids coalescing at the aggregate surface in trial batches prepared in the laboratory.

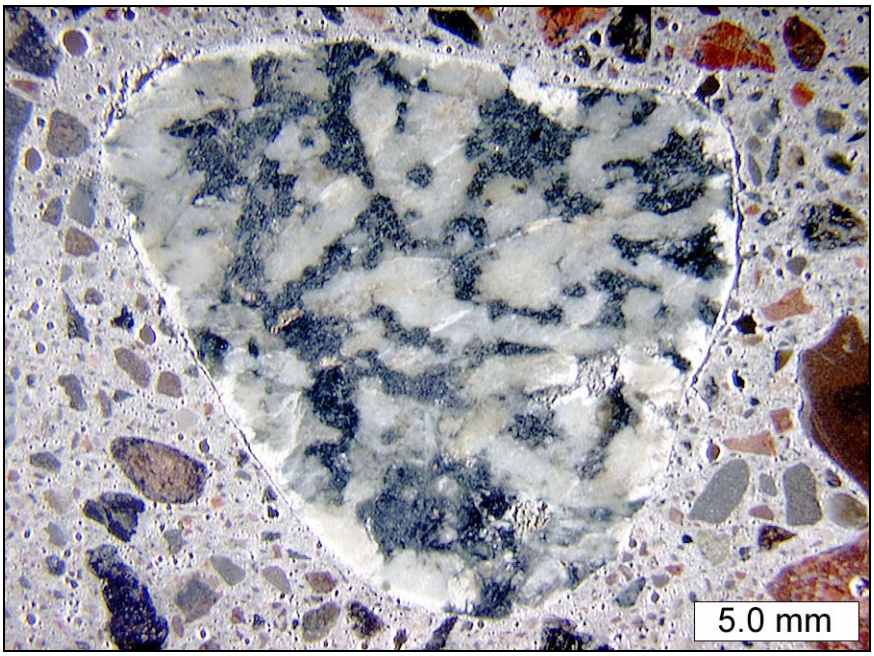

Figure 3-3. Air voids coalescing at the aggregate surface in trial batches prepared in the laboratory.

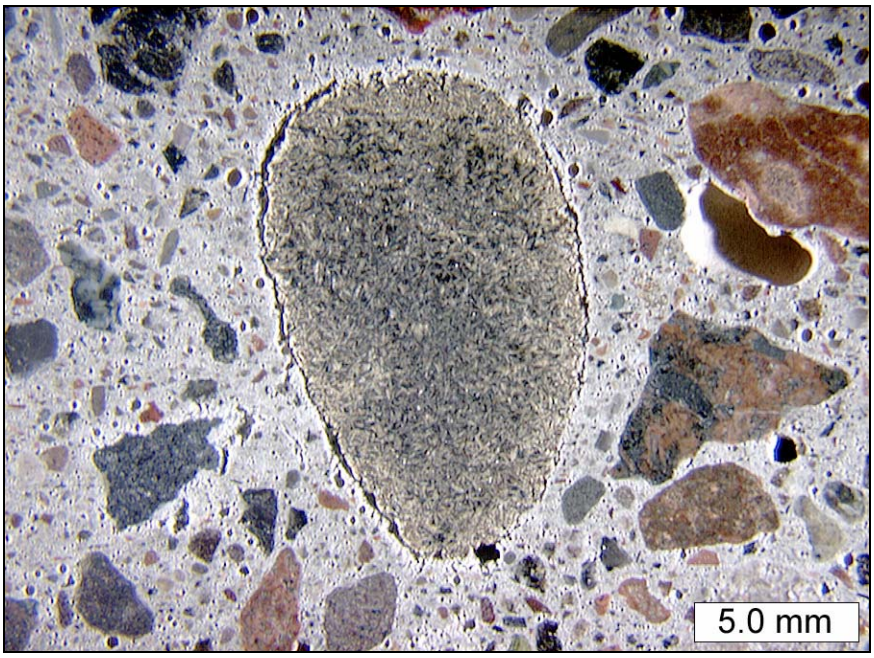

Figure 3-4. Air voids coalescing at the aggregate surface in trial batches prepared in the laboratory.

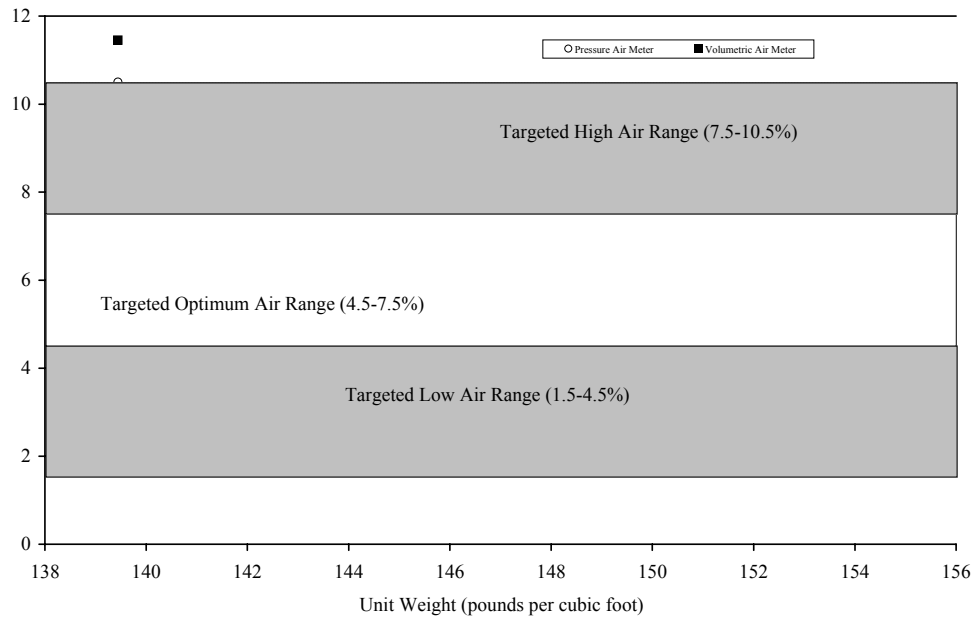

Figure 3-5. Unit weight, pressure and volumetric air content for trial mixtures showing a consistent relationship between measured air content and unit weight.

Strength tests were not conducted on these specimens, but the photomicrographs show that the ITZ shear resistance is definitely compromised by the presence of the agglomerations. It is also interesting to note that both the pressure and volumetric air tests resulted in similar results although the prepared hardened sample showed otherwise. These results may be explained by the previously mentioned problems with fresh concrete air tests (Roberts, 1994, Hover, 1988, Gay, 1982, Hover, 1993). Other results from the eleven mixtures were that the measured unit weights correlated with the results from the pressure and volumetric air tests. These results are summarized in Table 3-4 and Figure 3-5. It would be expected that the unit weight of the mixtures would accurately reflect the actual air content of the mixtures, but in this case, the unit weight correlated well with the performed air tests.

After reviewing the data along with the prepared cylinder, it was decided to produce a mixture without any AEA addition. This mixture resulted in an air content of less than 2.5 percent air, confirming that the original synthetic AEA mixture was entraining air. Next, a vinsol resin based AEA was used to obtain a high air content. A high dosage of vinsol resin AEA, similar to the high dosages of Micro Air, produced very high test results (~ 13.5 percent air) in the same mixture where the Micro Air resulted in only 5.5-5.9 percent air. The Micro Air dosage was reduced along with an increased water reducer dosage to increase workability and thus more entrained air. By making these adjustments, along with further trial and error, the desired air contents were obtained with all of the AEAs.

A set of trial mixtures produced with a cement content of 564 pounds per cubic yard (6.0 bags), 0.44 *w/cm* and utilizing the water-reducing admixture performed within reasonable limits. Thus, the initial mixture designs were adjusted to incorporate these characteristics into them. Although there were to be eighteen different sets of samples produced, only six different final mixture designs were necessary. This was because each of those six mixtures

would be prepared with three different AEAs. The six different mixtures included three with fly ash and three without fly ash. Each set of three mixtures had target air ranges of 3, 6 and 9 percent, +/- 1.5 percent (low, optimum and high air contents). To properly design these mixtures, the specific gravities of the components were needed. These were determined and are presented in Table 3-5.

Table 3-5. Material specific gravities used for mixture design

Material	Type I/II Cement	Class C Fly ash	Coarse Aggregate	Fine Aggregate	Water
Specific Gravity	3.15	2.58	2.72	2.72	1.00

The final mixtures were proportioned following the guidelines from section 501 of the WisDOT specifications. For the grade A mixtures, the cement content used was 565 pounds per cubic yard. At a *w/cm* of 0.44, this allows 248 pounds of water per cubic yard. The coarse and fine aggregate quantities were determined after calculating the volumes occupied by the cement and water along with the target volume of entrained and entrapped air voids. The allowed weight of total aggregate is 3120 pounds per cubic yard for grade A concrete. As with the initial mixture designs, the final mixture designs have a fine aggregate content of 41 to 46 percent. The variations in fine aggregate content between mixtures are due to the adjustment in volume to account for the various targeted air void volumes.

Grade A-FA mixtures were similarly proportioned. A thirty percent replacement of the cement by weight was used to calculate the weight of fly ash used in the mixture. Resulting was a cement content of 395 pounds per cubic yard and a fly ash content of 170 pounds per cubic yard. Total cementitious material and water content by weight are the same in both the grade A and A-FA mixtures, but due to differing specific gravities between portland cement and class C fly ash, the fine aggregate proportion was adjusted to ensure the proper yield of the mixture.

It was expected that some trial and error would be necessary to determine the proper dosages of AEA needed to obtain the required air contents. Dosage rates of 0.5-1.0 fluid ounces per 100 pounds of cementitious material were chosen as starting points in the process. Master Builders recommended a dosage range of 3 to 15 fluid ounces of the water-reducing admixture per 100 pounds of cementitious material. A constant dosage of 3.6 fluid ounces of water reducing admixture per 100 pounds of cementitious material (26.8 ml) was selected and used for these mixtures. This low dosage was selected to ensure proper workability with the least chance of introducing interactions between the two chemical admixtures. In addition, this dosage was kept constant for all mixtures to ensure the only variation in the mixtures was due to the air entraining chemical and necessary yield adjustments.

The tests to be performed, number of samples to be made, and a reasonable factor of safety were considered in determining the volume of concrete to be made for each batch. The research proposal stated that the tests to be performed include pressure and volumetric air (ASTM C 231 and C173), , ASTM C 143, *Test Method for Slump of Portland Cement Concrete*, ASTM C 1064, *Test Method for Temperature of Freshly Mixed Portland Cement Concrete*, ASTM C 138, *Test Method for Unit Weight, Yield, and Air Content (Gravimetric) of Concrete*. Specimens to be prepared included two 4” by 8” standard cylinders and two 3”

by 3" by 11" standard prisms. As a factor of safety, an additional 25 percent of the needed volume to perform the tests and prepare the samples was added. This computed to sample batches of 1.19 cubic feet of concrete. The mixture designs were then proportioned down from 27 cubic feet to the sample size of 1.19 cubic feet. Tables 3-6 thru 3-11 present the six final mixture designs in both cubic yard (27 cubic feet) and 1.19 cubic feet proportions.

Table 3-6. "Grade A" – Optimum air content mixture design. The final batch size was 1.19 cubic feet. Batch weights are provided on a per cubic yard and per 1.19 cubic foot basis.

Material	Specific Gravity	Volume (volume %)	Weight (lbs/yd^3)	Weight ($lbs/1.19ft^3$)
Cement	3.15	10.6	565	24.83
Fly Ash	2.58	-	-	-
Water	1.00	14.8	249	10.92
Coarse Aggregate	2.72	38.2	1750	76.94
Fine Aggregate	2.72	30.4	1394	61.30
Air Content	-	6.0	1.62	0.071

Table 3-7. "Grade A-FA" – Optimum air content mixture design. The final batch size was 1.19 cubic feet. Batch weights are provided on a per cubic yard and per 1.19 cubic foot basis.

Material	Specific Gravity	Volume (volume %)	Weight (lbs/yd^3)	Weight ($lbs/1.19ft^3$)
Cement	3.15	7.4	395	17.37
Fly Ash	2.58	3.9	170	7.47
Water	1.00	14.8	249	10.92
Coarse Aggregate	2.72	38.2	1750	76.94
Fine Aggregate	2.72	29.7	1361	59.85
Air Content	-	6.0	1.62	0.071

Table 3-8. "Grade A" – Low air content mixture design. The final batch size was 1.19 cubic feet. Batch weights are provided on a per cubic yard and per 1.19 cubic foot basis.

Material	Specific Gravity	Volume (volume %)	Weight (lbs/yd^3)	Weight ($lbs/1.19ft^3$)
Cement	3.15	10.6	565	24.83
Fly Ash	2.58	-	-	-
Water	1.00	14.8	249	10.92
Coarse Aggregate	2.72	38.2	1750	76.94
Fine Aggregate	2.72	33.4	1531	67.35
Air Content	-	3.0	0.81	0.036

Table 3-9. "Grade A-FA" – Low air content mixture design. The final batch size was 1.19 cubic feet. Batch weights are provided on a per cubic yard and per 1.19 cubic foot basis.

Material	Specific Gravity	Volume (volume %)	Weight (lbs/yd^3)	Weight ($lbs/1.19ft^3$)
Cement	3.15	7.4	395	17.37
Fly Ash	2.58	3.9	170	7.47
Water	1.00	14.8	249	10.92
Coarse Aggregate	2.72	38.2	1750	76.94
Fine Aggregate	2.72	32.7	1499	65.89
Air Content	-	3.0	0.81	0.036

Table 3-10. "Grade A" – High air content mixture design. The final batch size was 1.19 cubic feet. Batch weights are provided on a per cubic yard and per 1.19 cubic foot basis.

Material	Specific Gravity	Volume (volume %)	Weight (lbs/yd^3)	Weight ($lbs/1.19ft^3$)
Cement	3.15	10.6	565	24.83
Fly Ash	2.58	-	-	-
Water	1.00	14.8	249	10.92
Coarse Aggregate	2.72	38.2	1750	76.94
Fine Aggregate	2.72	27.4	1256	55.26
Air Content	-	9.0	2.43	0.107

Table 3-11. "Grade A-FA" – High air content mixture design. The final batch size was 1.19 cubic feet. Batch weights are provided on a per cubic yard and per 1.19 cubic foot basis.

Material	Specific Gravity	Volume (volume %)	Weight (lbs/yd^3)	Weight ($lbs/1.19ft^3$)
Cement	3.15	7.4	395	17.37
Fly Ash	2.58	3.9	170	7.47
Water	1.00	14.8	249	10.92
Coarse Aggregate	2.72	38.2	1750	76.94
Fine Aggregate	2.72	26.7	1224	53.80
Air Content	-	9.0	2.43	0.107

3.1.2 Aggregate Preparation/Mixture Water Adjustments

The absorption and moisture contents of the aggregates to be used must be known to determine how much the available mixture water value needs to be adjusted. Absorption values for the aggregates used in this research are 1.2 percent for the coarse aggregate and 1.5 percent for the fine aggregate. The aggregates were prepared 24 hours in advance to ensure the targeted *w/cm* ratio was met. An amount of fine aggregate greater than what would be necessary for the following day's mixtures was obtained from the bulk source. A process of sprinkling with water and thorough mixing moistened the aggregate uniformly. A representative sample (~ 3 to 4 pounds) was taken once a moisture content of approximately 2.0 to 3.0 percent was reached. This sample was dried in an oven for 24 hours at 230 °F (110 °C) to determine the actual moisture content of the material. The remaining moistened fine aggregate was stored in sealed containers until the following day when the concrete was mixed. On the day before mixing, the coarse aggregate was prepared. The moisture content of the bulk stockpile was estimated. A representative amount of coarse aggregate (**C**) was obtained based upon the coarse aggregate value from the mixture design (**A**) and estimated stockpile moisture content (**B**).

$$C = \frac{-A}{\left(\frac{B}{100} - 1\right)} \tag{3.1}$$

That amount of coarse aggregate (**C**) was submerged for 24 hours to ensure that the aggregate would be saturated when used the following day in the mixture. A representative sample of the stockpile was taken (~ 10 to 12 pounds) and dried in the same manner as the fine aggregate to determine the actual moisture content. After 24 hours had passed, the samples were removed from the oven and the actual moisture contents of the materials were calculated. In addition, at that time, the free water was allowed to drain from the coarse aggregates.

After draining, the saturated weight of the coarse aggregate (**H**) was determined. The actual moisture content of the aggregate (**R**) was used to determine the dry weight of the coarse aggregate (**S**) and approximated the value from the mixture design (**A**).

$$S = C - \frac{C \times R}{100} \approx A \tag{3.2}$$

The saturated surface dry weight of the coarse aggregate (**U**) was found using the dry weight of the aggregate (**S**) along with the known absorption of 1.2 percent.

$$U = \frac{1.2 \times S}{100} + S \tag{3.3}$$

The difference between the saturated surface dry weight of the aggregate (**U**) and the initial weight of the aggregate before submerging (**C**) was the weight of water absorbed by the aggregate over the 24 hour period (**V**). Finally, the amount of free water in the coarse aggregate (**W**) that must be subtracted from the mixture design water was calculated.

$$W = H - U - V \tag{3.4}$$

The final preparation of the fine aggregate began by calculating the weight of moist aggregate needed for the concrete batch (**h**). This was accomplished using the calculated moisture content (**f**) and the mixture design weight (**g**) of the fine aggregate.

$$h = \frac{-g}{\frac{f}{100}} - 1 \tag{3.5}$$

The resulting weight (**h**) of fine aggregate is to be used in the mixture and was retrieved from the sealed buckets prepared the previous day. The saturated surface dry weight of the fine aggregate (**k**) was found using the known absorption of 1.5 percent and the mixture design proportion (**g**).

$$k = \frac{1.5 \times g}{100} + g \tag{3.6}$$

Finally, the free water in the fine aggregate (**m**) that must be subtracted from the mixture design water was calculated.

$$m = h - k \tag{3.7}$$

The actual water to be added to the mixture (**Y**) can be calculated after determining the mix water corrections (**W**, **m**) and knowing the mixture design water requirement (**Z**).

$$Y = Z - W - m \tag{3.8}$$

3.1.3 Mixing Procedure

The mixture design amount of cement and, if necessary, fly ash were weighed out in preparation of mixing. The water reducing admixture dosage was measured with a graduated cylinder and the AEA dosage with a pipette. The AEA was added and distributed throughout the mix water. The water-reducing admixture was added to the mix water after the AEA was sufficiently distributed.

The inside of the mixer was coated with a mortar mixture before mixing the actual batch of concrete. The purpose of this was to ensure that the *w/cm* and mortar content of the actual batch of concrete to be tested was not compromised through the loss of mortar and/or water to coating a dry mixer. This process called buttering was accomplished by dampening the inside surfaces of the mixer and adding approximately two pounds of cement and four pounds of sand of the same source used in the research. The mixer was rotated and the mortar was allowed to cover the inside surfaces. The excess mortar was removed and discarded.

The mixer was prepared for the actual batch of concrete after the mortar batch was removed. The components were then added to the mixer in the following order: coarse aggregate, fine aggregate, cement, fly ash (if necessary) and water. Mixing lasted for three minutes, beginning once all the mix water was in the mixer. At that time, the mixer was stopped and allowed to sit idle for two minutes. Finally, the batch of concrete was mixed for two more minutes and then discharged from the mixer into a dampened steel tray.

3.1.4 Fresh Concrete Testing

Testing was performed by a certified ACI concrete field testing technician. Testing of the fresh concrete included performing the volumetric and pressure air tests (ASTM C 173 and ASTM C 231) along with slump (ASTM C 143), temperature (ASTM C 1064) and unit weight (ASTM C 138). Throughout the testing of the various mixtures, the same technicians operated the volumetric and pressure meters. This was necessary to ensure the most consistent results possible. Testing began immediately after the concrete was discharged from the mixer. The unit weight of the concrete was found using the weight of the concrete needed to fill the ¼ cubic foot volume bowl of the pressure meter. Test results were recorded and concrete used in the testing was discarded as to ensure it was not used in specimen preparation.

3.1.4.1 Fresh Concrete Testing Results

Mixtures were designated to facilitate discussion of the results. For example, mixture “FA-MA-L” contains fly ash (FA) and a low (L) dosage of the Micro Air (MA) air entraining agent. As another example, mixture “VR-O” contains no fly ash and an optimum (O) dosage of the VR-Standard (VR) AEA. The notations are shown in Table 3-12.

Table 3-12. Mixture shorthand notations used in this research

Component	*Shorthand*
Fly Ash	FA
Micro Air	MA
AE-90	AE90
VR-Standard	VR
High Air	H
Optimum Air	O
Low Air	L

Table 3-13. Final air entrainment dosages used for all mixtures.

Mixture	ml	fl. oz. per 100 lbs	Mixture	ml	fl. oz. per 100 lbs	Mixture	ml	fl. oz. per 100 lbs
FA-AE90-L	2.0	0.27	FA-MA-L	5.5	0.27	FA-VR-L	3.0	0.27
FA-AE90-O	4.5	0.61	FA-MA-O	9.0	1.23	FA-VR-O	4.5	0.61
FA-AE90-H	7.0	0.95	FA-MA-H	18.0	2.45	FA-VR-H	10.5	1.43
AE90-L	0.7	0.10	MA-L	3.3	0.45	VR-L	0.3	0.04
AE90-O	3.5	0.48	MA-O	7.0	0.95	VR-O	3.0	0.41
AE90-H	9.5	1.29	MA-H	16.0	2.18	VR-H	12.0	1.63

The final dosages of the AEAs to be used were determined by trial and error adjustments. The dosage rates came out to be 0.10-1.29 fl.oz/100 lbs cement for the AE-90, 0.45-2.45 fl.oz/100 lbs cement for the MA and 0.04-1.63 fl.oz/100 lbs cement for the VR. As expected, in all cases, more AEA was required to obtain greater air contents. In almost every case, the volume of AEA used was higher for a mixture with FA than its counterpart without any FA replacement. Table 3-13 presents the dosages of the AEAs used in preparation of the final mixtures in both total milliliters added and the equivalent fluid ounces per 100 pounds of cementitious material.

As stated previously, the pressure and volumetric air tests were performed along with slump, unit weight and temperature. The results of all these tests are tabulated in Table 3-14.

Table 3-14. Fresh Concrete Testing Results

Label	Mixture	Slump (inches)	Temp (°F)	Unit Weight (lb/ft^3)	Air Content ASTM C 231 (volume %)	Air Content ASTM C 173 (volume %)
A	FA-AE90-L	2.25	64	151.44	4.1	4.2
B	FA-AE90-O	3.75	64	146.96	6.5	6.7
C	FA-AE90-H	5.75	64	144.32	8.0	8.7
D	AE90-L	0.75	77	154.60	2.8	3.4
E	AE90-O	2.00	66	150.16	4.9	5.0
F	AE90-H	4.50	74	139.44	10.5	11.4
G	FA-MA-L	1.00	69	153.36	3.8	4.0
H	FA-MA-O	6.75	64	146.12	7.2	7.4
I	FA-MA-H	5.50	65	141.52	9.5	9.7
J	MA-L	0.50	73	152.04	3.9	4.2
K	MA-O	1.75	74	148.48	5.6	5.9
L	MA-H	2.75	75	144.88	7.8	8.2
M	FA-VR-L	2.50	67	151.88	3.6	4.2
N	FA-VR-O	4.00	66	150.92	4.5	4.9
O	FA-VR-H	7.00	68	143.24	8.8	8.9
P	VR-L	1.75	70	153.08	2.4	2.7
Q	VR-O	2.50	65	149.84	5.1	5.4
R	VR-H	3.50	66	141.04	9.5	9.4

3.1.5 Specimen Preparation/Curing Process

Two 4” by 8” standard cylinders and two 3” by 3” by 11” standard prisms were prepared from each batch of concrete according to ASTM C 192, *Standard Practice for Making and Curing Concrete Test Specimens in the Laboratory*. These specimens were placed in a moist cure room after preparation. The specimens were removed from their forms after the specified 24-hour curing period. They were then returned to the moist curing room for an additional 13 days to give a total of 14 days of moist curing. The samples were then removed from the moist cure room and allowed to cure at laboratory ambient conditions for an additional 14 days. The 28-day-old specimens were moved to a refrigeration unit kept at a constant 40 °F (~ 4.5 °C) in order to suspend the hydration process. This was done to ensure that all specimens would be at the same state of hydration no matter when they were actually prepared.

3.2 Hardened Concrete Air Void Analysis by ASTM C 457

3.2.1 Initial Sample Preparation Process

A slab of approximately 4” x 8” x ¾” (100 x 200 x 20 mm) was cut perpendicular to the finished surface of the cured cylinders using a kerosene-cooled diamond blade saw. One face of the slab was polished on a flat lapping wheel. A series of abrasive magnetic platens were used with water as the coolant/cleansing medium. The slab was polished using successively

finer grit abrasive down to, and including, 200 grit. Between each grit size, short blasts of compressed air along with a water rinse were applied to ensure polishing residuals did not accumulate in the voids. A solution of 5:1 by volume acetone and fingernail hardener was applied to the partially polished surface to stabilize the voids with the goal of obtaining the sharpest void edges possible [Dewey and Darwin 1991]. This solution was brushed on to the dried surface in two coats applied perpendicular to each other. Once the fingernail hardener had set, lap wheel polishing continued with 325, 500 and finally 600 grit adhesive-backed silicon carbide paper. Finally, the polished surface was bathed in acetone for one minute to remove the remaining fingernail hardener. To complete the initial surface preparation, twelve ½ in x ¼ in (6 mm x 3 mm) x 200 micron thick hologram stickers were applied to the perimeter of the polished surface. These stickers were used to protect the glass surface of the flat-bed scanners and also as location standards. The location standards facilitated alignment and comparison of data collected during the standard motorized stage point count, the high-resolution flat-bed scanner image analysis, and the conventional office flat-bed scanner image analysis.

3.2.2 ASTM C 457 Manual Point Count

Reference values for the air void systems of each of the specimens needed to be known to determine the accuracy of the flat-bed scanner based analyses. In this study, the methods described in ASTM C 457 Procedure B (modified point count method) [ASTM 2005] were used as the standard to which the scanner based analyses were compared. A stereo microscope, video camera, and motorized stage were used to perform the manual modified point count. These components were connected to a computer and operated with the assistance of a macro. The macro was written for NIH Image which is an image analysis program developed by the United States National Institutes of Health available for download on the web (www.scioncorp.com) [Sutter 1998]. Along with performing the modified point count, the macro allowed for the x,y coordinates and corresponding concrete phase (hydrated cement paste, aggregate or air void) of each of the 1,388 stops in the point count to be recorded. These coordinates and observed phases were used to perform an accuracy assessment between the images collected by the scanners and the data recorded by the operator performing the motorized stage point count.

3.2.3 Comparison of ASTM C 173, ASTM C 231, and ASTM C 457 Results

Presented in Table 3-15, for all mixtures prepared, are the results of the hardened air-void analysis determined by ASTM C 457 Procedure B. Figures 3-7 and 3-8 present the ASTM C 173 and ASTM C 231 results plotted against the hardened air content as measured by ASTM C 457. Table 3-16 compares the air content determined by volumetric meter, pressure meter, and manual point count.

Table 3-15. Results of manual point count according to ASTM C 457.

Label	Mixture	Air Content (volume %)	Spacing Factor (mm)	Paste/Air Ratio	Specific Surface (mm^{-1})	Void Frequency (voids/meter)
A	FA-AE90-L	3.8	0.243	6.46	21.41	200.51
B	FA-AE90-O	5.5	0.114	4.09	35.96	492.31
C	FA-AE90-H	10.3	0.065	2.47	37.90	976.06
D	AE90-L	3.0	0.382	8.51	15.42	113.74
E	AE90-O	5.2	0.163	4.71	27.61	357.99
F	AE90-H	10.8	0.064	2.33	36.21	978.27
G	FA-MA-L	3.5	0.179	5.96	28.07	242.71
H	FA-MA-O	8.8	0.079	2.72	34.39	755.70
I	FA-MA-H	7.9	0.068	3.11	45.87	900.49
J	MA-L	3.2	0.213	8.09	27.12	219.81
K	MA-O	5.4	0.112	4.41	39.08	527.88
L	MA-H	8.9	0.078	3.09	39.60	877.32
M	FA-VR-L	3.5	0.280	6.71	18.94	167.14
N	FA-VR-O	4.8	0.150	5.52	32.34	384.47
O	FA-VR-H	7.8	0.094	2.91	31.08	604.56
P	VR-L	1.8	0.619	15.32	12.37	55.71
Q	VR-O	4.5	0.135	4.82	33.66	375.92
R	VR-H	7.4	0.127	4.17	32.75	607.59

Table 3-16. Air content determined by ASTM C 173, ASTM C 231 and ASTM C 457, for mixtures prepared.

Label	Mixture	ASTM C 173 Volumetric Meter	ASTM C 231 Pressure Meter	ASTM C 457 Hardened Air-Void Analysis
A	FA-AE90-L	4.2	4.1	3.8
B	FA-AE90-O	6.7	6.5	5.5
C	FA-AE90-H	8.7	8	10.3
D	AE90-L	3.4	2.8	3.0
E	AE90-O	5.0	4.9	5.2
F	AE90-H	11.4	10.5	10.8
G	FA-MA-L	4.0	3.8	3.5
H	FA-MA-O	7.4	7.2	8.8
I	FA-MA-H	9.7	9.5	7.9
J	MA-L	4.2	3.9	3.2
K	MA-O	5.9	5.6	5.4
L	MA-H	8.2	7.8	8.9
M	FA-VR-L	4.2	3.6	3.5
N	FA-VR-O	4.9	4.5	4.8
O	FA-VR-H	8.9	8.8	7.8
P	VR-L	2.7	2.4	1.8
Q	VR-O	5.4	5.1	4.5
R	VR-H	9.4	9.5	7.4

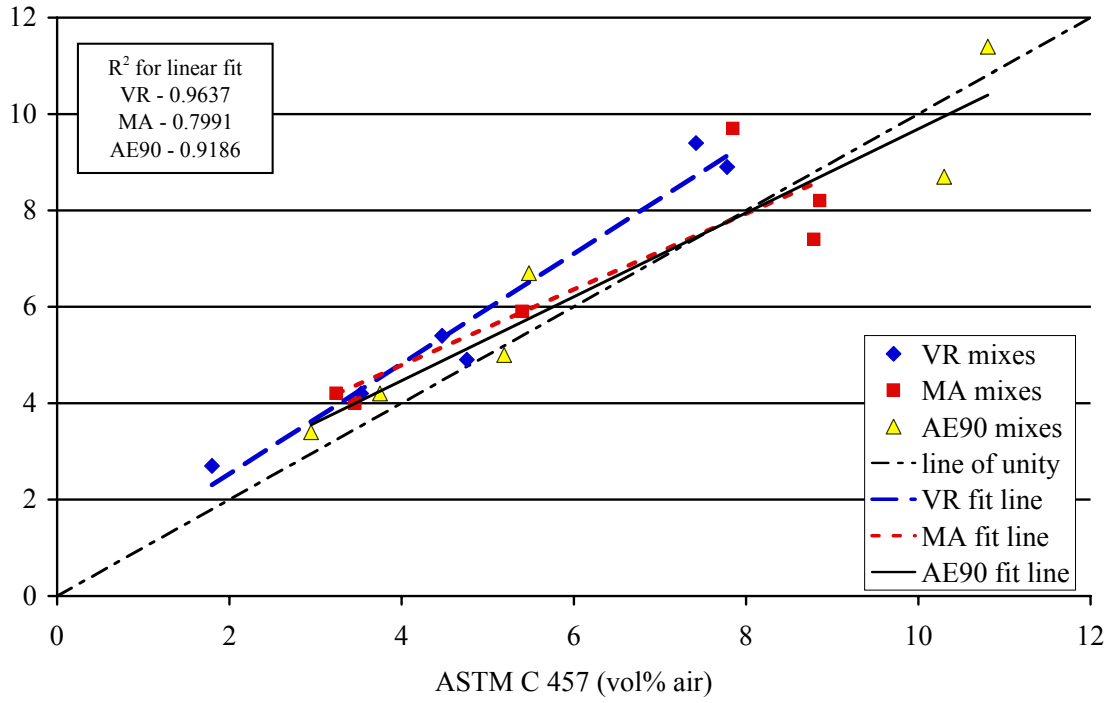

Figure 3-6. Results of ASTM C 173 tests plotted against the results of ASTM C 457 both performed on the same concrete mixtures.

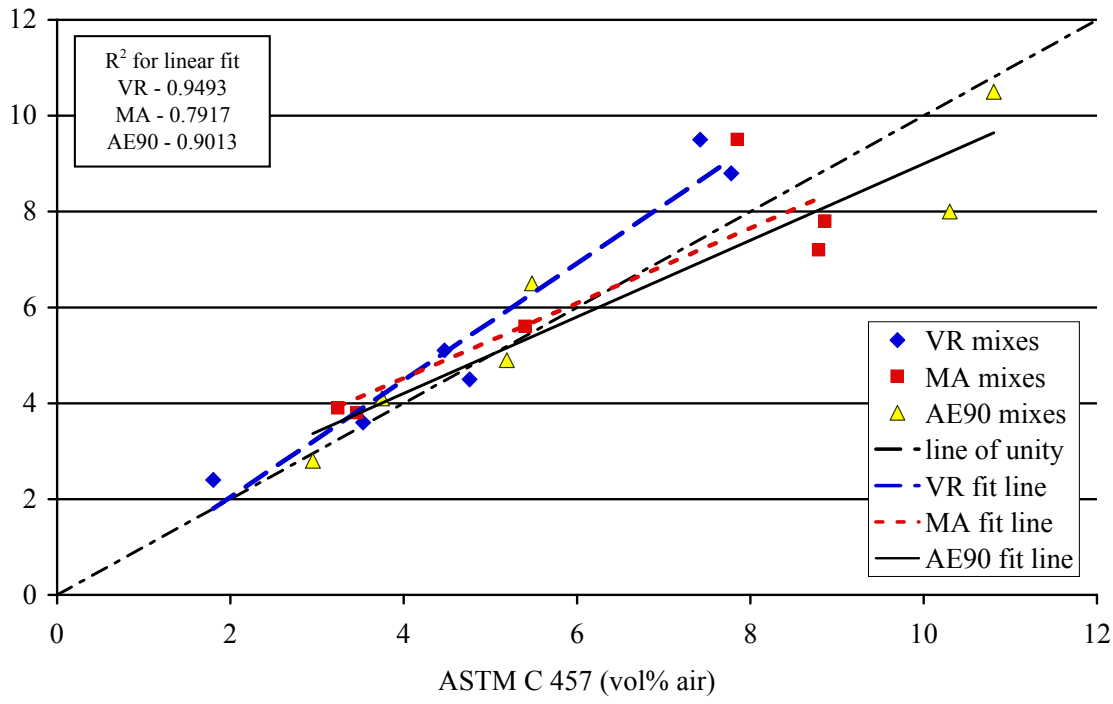

Figure 3-7. Results of ASTM C 231 tests plotted against the results of ASTM C 457 both performed on the same concrete mixtures.

Chapter 4 – Results of ASTM C 666 Freeze-Thaw Testing

4.1 Freeze-Thaw Tests

4.1.1 Experimental Details

A total of 36 concrete prisms 3in x 3in x 11in (75 x 75 x 275 mm) and 18 concrete cylinders 4in diameter x 8 in long (100 diameter x 200 mm long) were tested. The samples represented 18 concrete mixes (i.e. two specimens per mix) and were labeled A through R. Stainless-steel studs were cast into the ends of the specimens providing a gage length of 10in (250 mm).

The concrete prisms were tested in accordance with ASTM C 666 Standard Test Method for Resistance of Concrete to Rapid Freezing and Thawing – Procedure A. Since ASTM C 666 requires full saturation prior to first freezing, the specimens were immersed in saturated limewater for 48 hours prior to test (see Clause 8.1 for conditioning beam samples sawn from hardened concrete). Following the 48-hour soaking period, the concrete prisms were tested to determine the initial mass, length and fundamental transverse frequency. The prisms were then placed into a test chamber, which cycled the concrete temperature (as determined by a thermocouple placed in the center of a dummy specimen) from 40 ^{o}F to 0 ^{o}F (4.4 ^{o}C to -17.8 ^{o}C). The prisms were exposed to a total of 300 freeze-thaw cycles and were removed approximately every 30 cycles to determine mass, length and fundamental transverse frequency. The fundamental transverse frequency was used to calculate the durability factor, *DF*, using the following equation:

$$DF = PN/M \tag{4.1}$$

where P is the relative dynamic modulus after N cycles and M is the specified number of cycles at which the exposure is to be terminated (usually, as in the current study, M = 300 cycles). The relative dynamic modulus, P, is calculated from the following equation:

$$P_c = (n_1^2/n^2) \times 100 \tag{4.2}$$

Where P_c is the relative dynamic modulus after c cycles of freezing and thawing, n and n_1 are the fundamental transverse frequencies after 0 and c cycles, respectively.

4.1.2 Test Results

The durability factors, *DF*, and changes in mass and length after freeze-thaw testing are shown in Table 4-1. With the exception of specimens P2 and P3, the durability factor (*DF*) has been calculated using the relative dynamic modulus of elasticity (P) after 300 freeze-thaw cycles (i.e. $N = M = 300$). For specimens P2 and P3, the relative dynamic modulus after 90 cycles was used (i.e. $N = 90$) as the relative dynamic modulus of elasticity was observed to have fallen below 50% at this time (i.e. $P < 50\%$) - see Clause 8.3 and Note 5 in ASTM C 666.

Table 4-1. Results after 300 Cycles of Freezing and Thawing – ASTM C 666 Proc. A. For specimens P2 and P3, the relative dynamic modulus after 90 cycles was used (i.e. *N = 90*).

Sample #	Durability Factor (%)	Mass Change (%)	Length Change (%)
A2	111	-1.3	-0.010
A3	107	-1.0	-0.024
B2	107	-0.2	-0.011
B3	108	-0.5	-0.015
C2	106	-0.2	-0.004
C3	107	0.0	0.008
D2	105	-0.7	0.036
D3	99	-0.7	0.029
E2	108	-0.2	0.000
E3	106	-0.1	-0.002
F2	105	0.0	0.004
F3	103	0.1	0.071
G2	106	-0.2	-0.001
G3	105	-0.5	-0.006
H2	109	-0.5	-0.001
H3	110	0.0	0.000
I2	113	-0.6	0.042
I3	115	-0.2	0.018
J2	110	-0.6	0.018
J3	109	-0.6	0.017
K2	107	0.1	0.019
K3	107	0.1	0.022
L2	108	0.3	0.024
L3	110	0.2	0.026
M2	111	-0.9	0.031
M3	111	-0.9	0.023
N2	100	-1.9	0.031
N3	109	-1.2	0.026
O2	111	0.2	0.025
O3	110	0.1	0.023
P2*	10	0.0	0.376
P3*	15	0.3	0.300
Q2	107	-0.3	0.024
Q3	109	-0.8	0.022
R2	101	-0.1	0.019
R3	103	0.0	0.018

The mass and length changes shown relate to changes after 90 cycles for specimens P2 and P3, and after 300 cycles for all other specimens. All test specimens (including P2 and P3) remained in the freeze-thaw chamber for the 300-cycle period.

With the exception of specimens P2 and P3, all specimens achieved a durability factor of greater than or equal to 99%. There is no universally accepted limit regarding what value of the durability factor constitutes acceptable performance in this test. However, a value of $DF \geq 80\%$ is most commonly used.[4] Mix P clearly fails such a limit with an average durability factor of 13%. The change in frequency and change in relative dynamic modulus with time for mix P are shown in Figures 4-1 and 4-2, respectively.

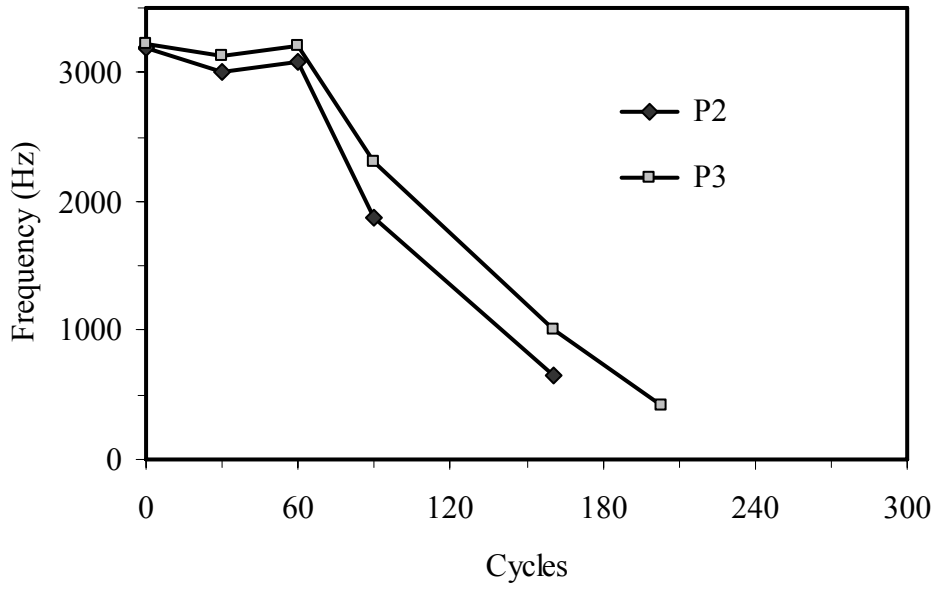

Figure 4-1. Change in Fundamental Transverse Frequency for Mix P

[4] For example, ASTM C 494 Standard Specification for Chemical Admixtures for Concrete requires a minimum durability factor of 80% for admixtures to be used in concrete subjected to freezing and thawing.

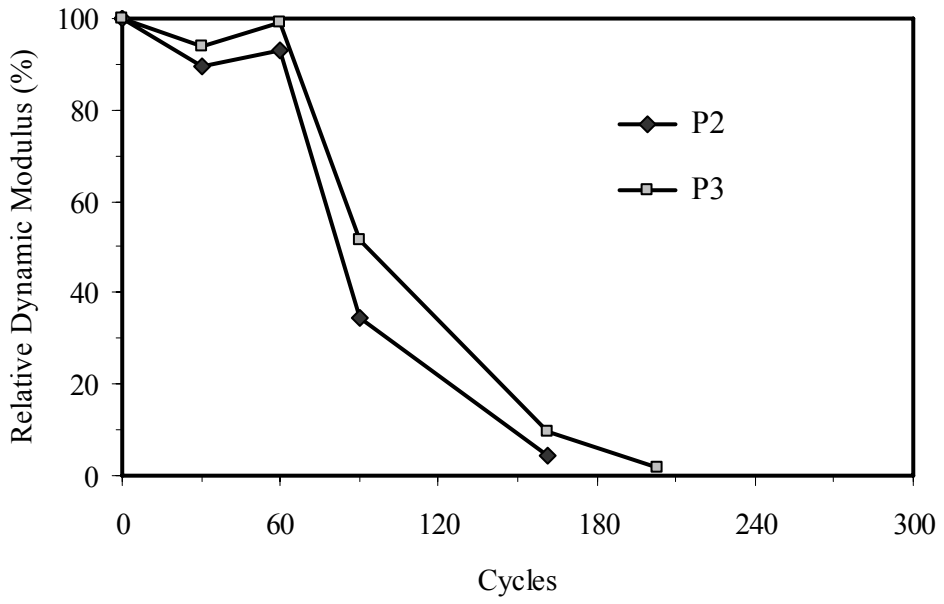

Figure 4-2. Change in Relative Dynamic Modulus for Mix P

Figures 4-3 and 4-4 show, respectively, the changes in mass and length for mix P. Mix P was the only mix that showed significant expansion and mass loss during testing. The values reported in Table 4-1 for mix P are those calculated after 90 cycles, i.e. after the relative dynamic modulus decreased by more than 50%. At this point the mass loss was relatively small, but significant loss of mass occurred beyond this point as the cumulative number of freeze-thaw cycles increased.

Figure 4-5 shows photographs of P2 and P3 after 300 cycles of freezing and thawing. Significant deterioration of the concrete occurred between 90 and 300 cycles resulting in loss of material from the corners. Surface scaling of the struck (i.e. hand finished) surface of the prisms was also observed. Beyond minor surface scaling, none of the other specimens tested showed any visual signs of deterioration.

The results from the freeze-thaw tests performed are reasonably consistent with performance predicted from the literature. Figures 4-6 and 4-7 show the effects of air content and spacing factor on the Durability Factor of concretes tested in accordance with ASTM C 666. The Figures are reproduced from Newlon and Mitchell (1994) who used data from Cordon (1966) and from Neville (1995) using data from the U.S. Bureau of Reclamation (1956). Figures 4-8 and 4-9 show data obtained superimposed on the published data.

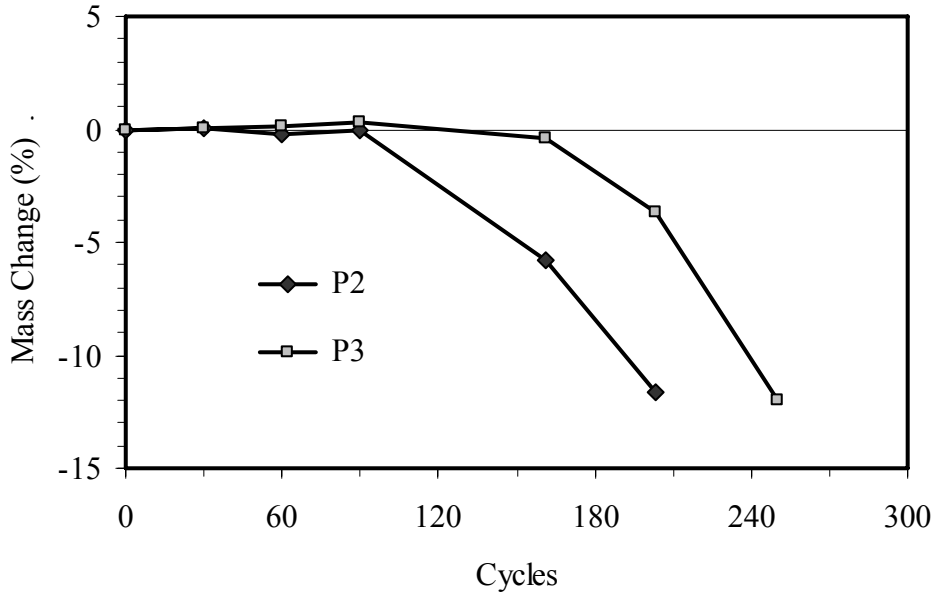

Figure 4-3. Change in Mass for Mix P

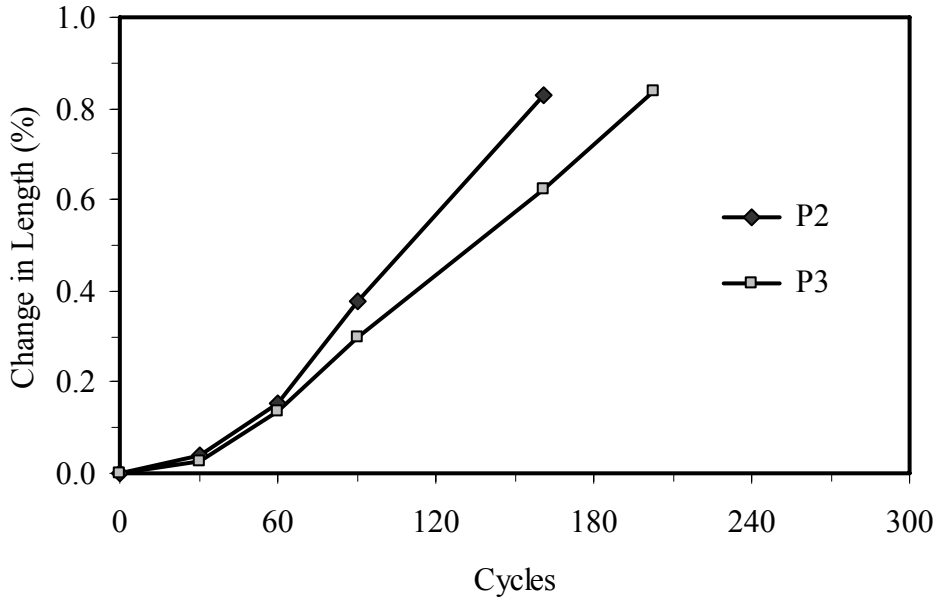

Figure 4-4. Change in Length for Mix P

(a)

(b)

Figure 4-5. Photographs of Formed (a) and Struck (b) Faces of Test Specimen from Mix P Following 300 Cycles of Freezing and Thawing

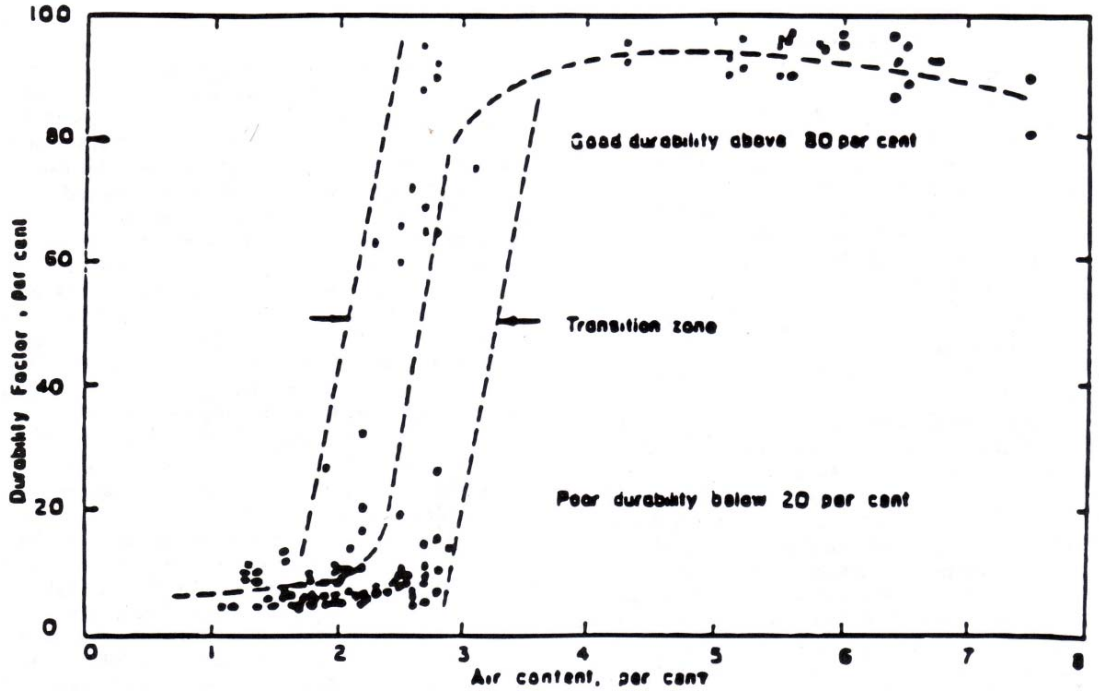

Figure 4-6. Effect of Air Content on the Durability Factor (Newlon & Mitchell, 1994)

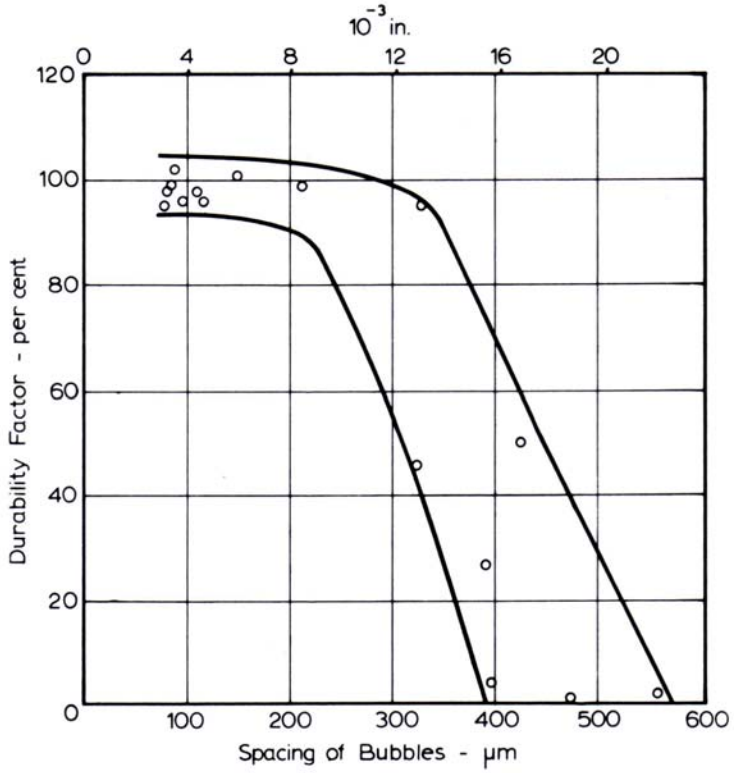

Figure 4-7. Effect of Spacing Factor on the Durability Factor (Neville, 1995 from USBR, 1956)

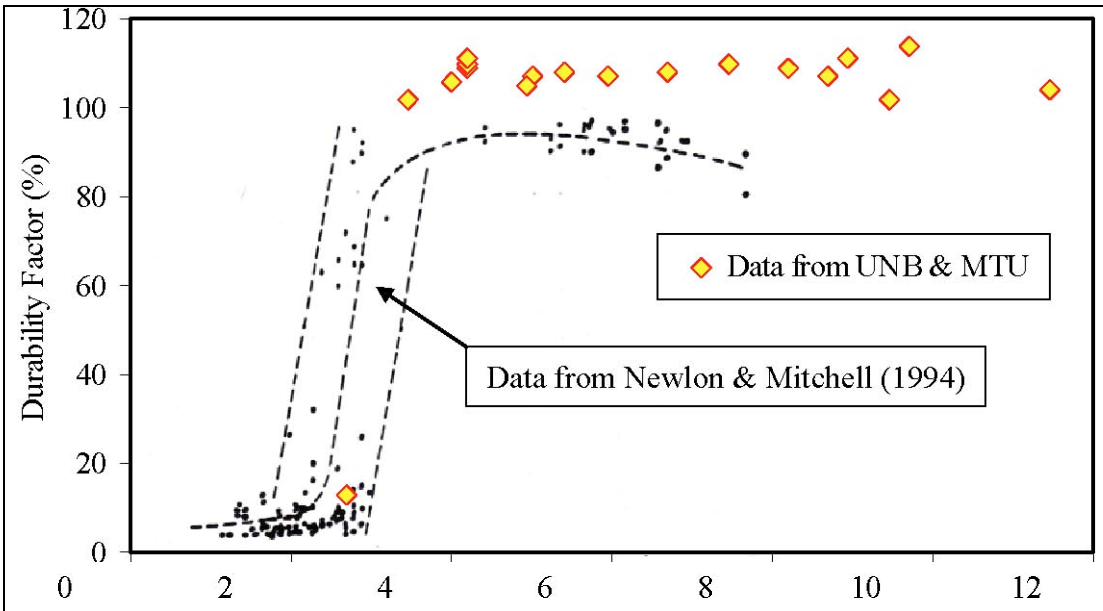

Figure 4-8. Comparison with published data of measured durability factor versus air content

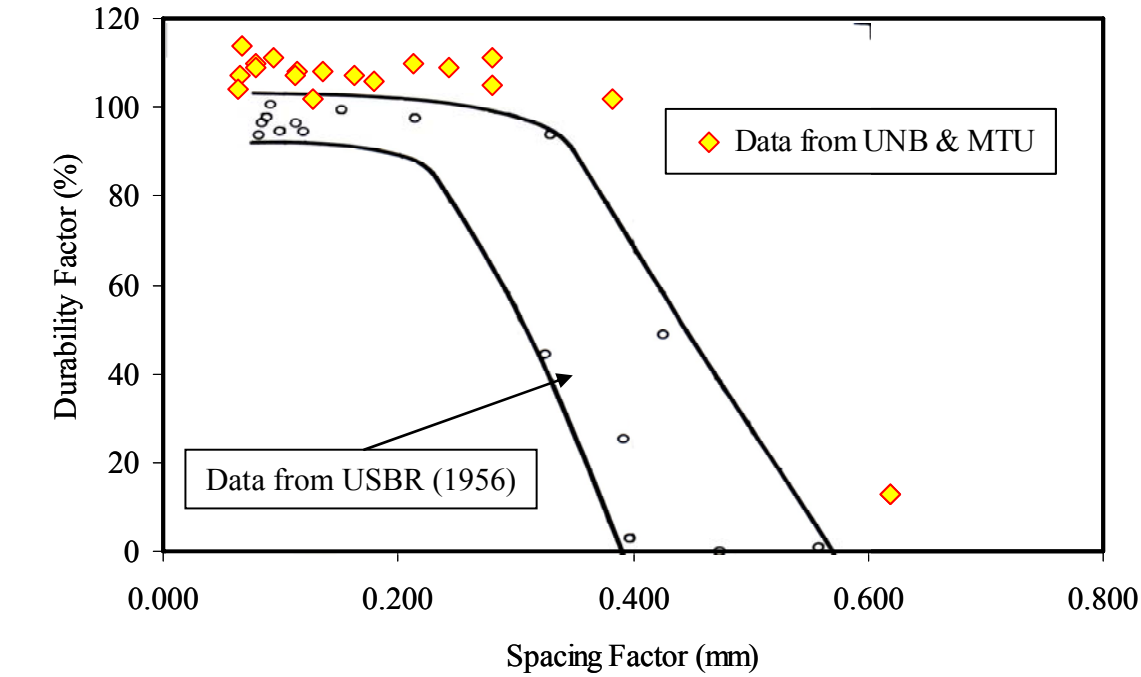

Figure 4-9. Comparison with published data of measured durability factor versus spacing factor

Chapter 5 – Air Void Analysis by Emerging Technologies

5.1 Automated Flat Bed Scanner Method

5.1.1 Introduction

As discussed in Chapter 2, there are several available methods of air void characterization. The flat bed scanner method explored here is similar to existing methods that use black ink and white powder to enhance the visibility of air voids. The main distinction is that a flat bed scanner is used to collect the image, as opposed to a microscope in combination with a motorized stage. This offers a low cost approach that does not require a petrographer nor intensive computer applications to implement. The primary research objective of this project was to develop a streamlined approach to, and verify the performance of, a flat bed scanner based approach to performing ASTM C 457.

As discussed in Chapter 3, manual point counts were performed on the 18 slabs cut and polished to represent the 18 different mixes. During the manual counts, the x,y stage coordinates from each stop in the point count, along with the phase identified at each stop, were recorded. In addition, the x,y stage coordinates of prismatic stickers placed along the perimeters of the slabs were also recorded. These stickers were used as reference points to align the scanned images to the same coordinate system as the motorized stage in order to compare points identified by the manual operator to corresponding pixels in the scanned and threshold images. This accuracy assessment approach is key to verifying performance of any automated system and is typically omitted by others developing such systems.

5.1.2 Sample Preparation

5.1.2.1 Sample Lapping

Four by eight inch standard test cylinders were prepared from each of the eighteen mix designs. Slabs of approximately 4 in x 8 in x 3/4in (100 mm x 200 mm x 20 mm) were cut perpendicular to the finished surfaces of the cylinders using a diamond blade. Then, one face on each of the slabs was polished using hand-pressure on a lapping wheel. A series of diamond abrasive grit magnetic backed platens were used with water as the coolant/cleansing medium. The slabs were polished using successively smaller diamond grit abrasive, starting at 60 grit and ending at 500 grit. Between each grit size, short blasts of compressed air along with a water rinse were applied to ensure polishing residuals did not accumulate in the voids. Next, to stabilize the voids with the goal of obtaining the sharpest void edges possible, a solution of 5:1 by volume acetone and fingernail hardener was applied to the partially polished surfaces. This solution was brushed on to the dried surfaces in two coats applied perpendicular to each other. Once the fingernail hardener had set, lap wheel polishing continued with 600 grit adhesive backed silicon carbide paper. Finally, the polished surfaces were bathed in acetone for one minute to remove the remaining fingernail hardener. To complete the initial surface preparation, twelve small prismatic stickers were applied to the perimeter of the polished surface. These stickers served three purposes. The first purpose of the stickers was to prevent the polished surfaces from resting directly on the glass plate of the flat-bed scanner, thereby avoiding scratches on the glass plate. Second, as is discussed in detail later, the highly reflective stickers performed as bright "end points" in the scanned images to ensure that image brightness was uniform from sample to sample. And third, the

center points of the stickers were used as reference points to correlate the scanned images to a motorized stage coordinate system developed during the manual point counts performed on the slabs.

5.1.2.2 Polished Surface Contrast Enhancement Procedure

The specimens were contrast-enhanced, or colored black and white, once the manual modified point counts were completed. The steps and materials used to obtain a contrast-enhanced image vary for the different laboratories that perform such analyses, but the desired results are the same [Gudmundsson and Christensen 1978, Dewey and Darwin 1991, Pade et al. 2002, Peterson et al. 2002, Zhang et al. 2005]. The goal of the contrast enhancement was to produce a surface where the voids in the concrete were filled with a white medium while the remaining phases (cement paste and aggregate) were colored black. Ideally, this contrast enhancement allows the image processing routine to clearly distinguish between voids and non-voids. The steps used in this study were as follows:

1. A $^{5}/_{8}$ x $^{5}/_{16}$ in (16 x 8 mm) black permanent marker was used to apply the initial coat of ink to the surface. The ink was applied in overlapping parallel lines across the sample being careful to avoid marking the prismatic stickers.
2. The same marker was used to apply a second coat of ink. This coat was applied in the same overlapping fashion but perpendicular to the initial coat.
3. The ink on the sample was allowed to dry sufficiently to ensure it would not be removed or smudged in the following steps.
4. The surface was covered with a thin layer (~ $^{1}/_{8}$ in) of 2 micron wollastonite powder (NYCO Minerals Inc., NYAD 1250 wollastonite).
5. The flat portion of a glass slide was used to press the white powder into the voids in the sample.
6. A razor blade edge was gently passed across the surface to remove the bulk of the excess wollastonite powder.
7. Finally, a very slightly oiled index finger was gently passed across the surface to remove the remaining residual wollastonite powder.

The contrast enhancement quality was checked using a stereo microscope ensuring the voids were sufficiently permeated and residual wollastonite was removed. It should be mentioned that the specimen preparation (lapping, grinding and polishing) is much more important to the final quality of the contrast-enhanced surface than the contrast enhancing itself. A poorly polished specimen can have scratches, pits or torn portions of the cement paste. These imperfections will accept the wollastonite in the same manner as the air voids. Having some imperfections in the sample due to preparation is inevitable, but the goal should be to minimize as best as possible the frequency of these surface defects in order to ensure the most representative analysis.

5.1.3 Data Collection

Each slab was scanned with both a CreoScitex EverSmart Pro II flat bed scanner (advertised 3,175 x 8,000 dpi maximum optical resolution) and a Hewlett-Packard 8200 ScanJet flat bed scanner (advertised 4,800 x 4,800 dpi maximum optical resolution). The images were collected in 8-bit grayscale mode at a pixel resolution of 8 x 8 micrometers. The lid on each scanner was left open during scanning, and the scanning was performed in a dark room (no

overhead lighting). When selecting the region to be scanned on each sample, care was taken to include the prismatic stickers, as well as some of the blank space outside the perimeters of the polished slabs. As mentioned previously, the highly reflective prismatic stickers provided consistent bright end points from sample to sample. Similarly, the blank spaces outside the perimeters of the polished slabs provided uniform dark end points from sample to sample. Figure 5-1 compares the image quality attained by the two scanners.

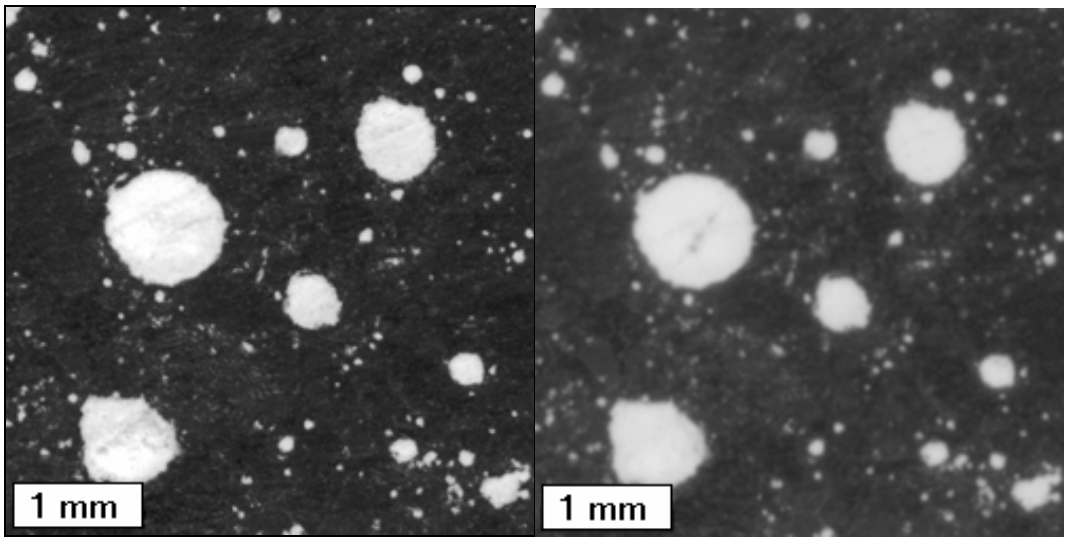

Figure 5-1. Image from high resolution scanner (left) and image from office scanner (right).

5.1.3.3 Automated Flat-Bed Scanner Analysis Script Development

The heart of the flat bed scanner approach is a computer script developed to calculate the standard air void system parameters from ASTM C 457 using the images collected from any flat bed scanner. This script was written in the Visual Basic Script language, which has the capability of controlling multiple Microsoft Windows applications within a single script program. This script was programmed to utilize Adobe Photoshop CS, Microsoft Excel and Microsoft Word in performing a modified point count upon the image and to output a report file. The steps performed by the script, and a brief discussion of each, are as follows:

1. *The operator enters identifying information about the specimen.*

This information includes the specimen's identification, source, technician's name and other miscellaneous information to be presented in the output report.

2. *In determining the paste content of the sample, the operator may, with the assistance of the program, either perform a manual point count on a digital image of the surface, enter the mixture batch weights, or enter a known paste content for the concrete specimen.*

In order to estimate how the entrained air voids are distributed in the concrete, the volume percent of the hardened cement paste must be known. For example, when computing the spacing factor, a higher paste percentage will yield a higher spacing factor value, keeping the air content constant. This is an important step in being able to perform this analysis. The ASTM C 457 calculations require knowledge of the volume of paste in the sample. In a

standard point count, the operator simply keeps track of what percentage of stops fall upon the paste. In a linear traverse, the percentage of the traverse line passing over the paste is recorded. These methods are not viable when analyzing the contrast-enhanced specimen since the black portion of the specimen masks both the aggregate and paste phases of the concrete. Therefore, the script allows three ways for the paste content of the sample to be input. First, an image of the polished surface of the sample can be collected by the flat-bed scanner before the contrast enhancing procedure. The program allows the operator to perform a quick point count upon this image to determine the percent paste in the sample. A second method of determining paste content with this script is by using the theoretical amount of paste that should be in the sample based on the batch weights of the concrete. The specific gravities of the materials must be known to perform the volumetric calculations, and may be obtained from the material supplier. Typing in batch weight and specific gravity information can be tedious, so as an alternative, a single number, the aggregate to paste volume ratio, can be typed in directly, and the paste volume computed. The calculated paste volume in most cases will be sufficiently close to the actual value. Finally, if the volume of paste is already known or is being assumed, the operator may enter the paste content directly into the program. It has been suggested that the air void system parameters are not sensitive to slight variations in the reported paste volume [Pade et al. 2002].

3. *The grayscale image is opened in Adobe Photoshop and the desired portion of the specimen to be analyzed is selected by cropping out the undesired portions.*

This step prompts the operator to select a square shaped area that avoids the portions of the image that may be undesirable for analysis such as the prismatic stickers.

4. *The operator selects a threshold value for the grayscale image.*

The threshold step, along with proper sample preparation, is one of the most important steps in performing C 457 on a contrast-enhanced image. The scanned grayscale image of the sample consists of many pixels, each with its own grayscale intensity falling in the 0 - 255 range between pure black and pure white.

To compare the air void system of specimens against each other, a consistent threshold value must be used. It is believed that this threshold value needs to be determined on a laboratory to laboratory basis, since each laboratory will have different sample preparation techniques, different flat-bed scanners, and different environments (particularly lighting) in which their flat-bed scanners will be operating.
The importance of selecting a threshold for an ASTM C 457 analysis is that it becomes the dividing line between what is and is not classified as air. Figure 5-2 depicts a series of images adjusted with increasing threshold values. The amount of ‘air’, or white pixels, in the image decreases as the threshold value is increased.

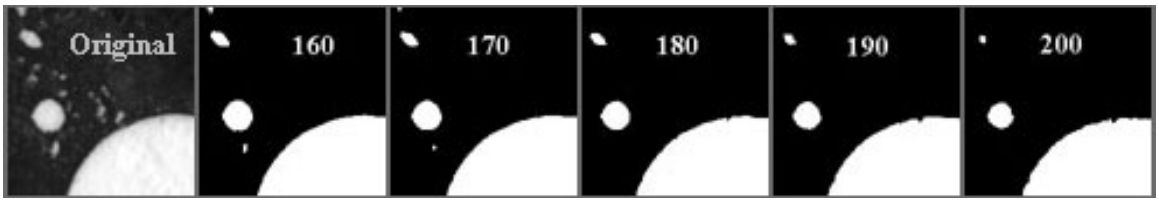

Figure 5-2. Example threshold value comparison

The program allows the operator to view 400 pixel by 400 pixel portions of the flat-bed scanner collected grayscale images while selecting the desired threshold value. Figure 5-3 displays an example side by side layout of a grayscale image and the corresponding binary image that the operator is allowed to observe during the selection of the threshold value.

Many other automated methods employ further processing to eliminate non-entrained air features mistakenly identified as air through such methods as erosion/dilation, shape factors, and other digital processing filters. The method described here relies solely on the threshold level.

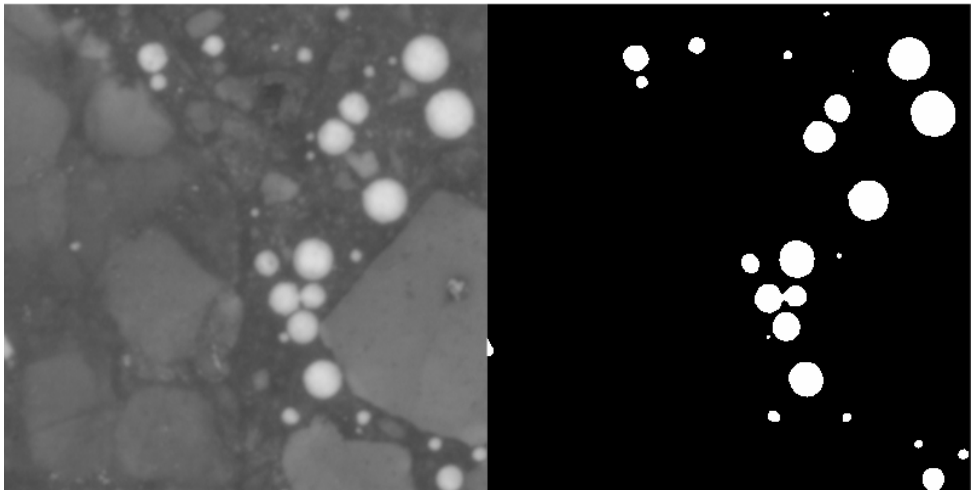

Figure 5-3. Example threshold selection display (grayscale on left, binary on right)

5. *The operator is given the opportunity to mask internal voids within aggregate particles using the image software tools.*

The aggregates used in portland cement concrete mixtures are extremely variable. Their hardness, chemistry and angularity are all characteristics that are important to concrete, but the amount of internal voids are very important in such analyses. A plane section of concrete will intersect a great number of individual aggregate particles. Depending on the source of the aggregate, a number of these particles will have interior macroscopic voids. The operator of a manual motorized stage point count or traverse ignores the voids within the aggregate by inspection. However, during black and white contrast enhancement of the sample, the voids in the aggregate will become filled along with the voids in the cement paste, and a simple threshold will not differentiate between the two types of voids. Therefore, the operator is prompted to use the Adobe Photoshop tools to mask the voids in aggregate to avoid allowing the script to count these pixels as 'air'. Figure 5-4 displays an example of an aggregate particle before and after the masking operation. The masking step can, in cases of concretes composed entirely of porous aggregates, take up to an hour or longer to perform. For this study, in which a partially crushed natural gravel was used, the masking operation took approximately five to ten minutes per image to perform. An alternate method of effectively masking the aggregate voids is by marking the voids with a black marker prior to scanning.

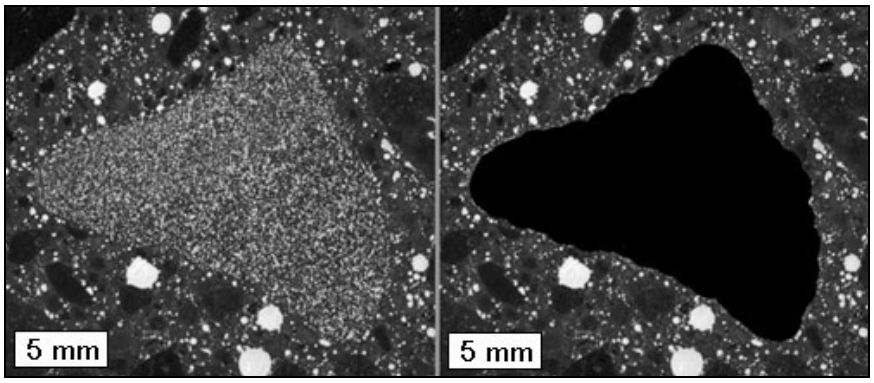

Figure 5-4. Masking of internal air voids in an aggregate particle

6. *The specific regions of the image to be analyzed per ASTM C 457 are selected.*

Based upon the size of the aggregate used in the mixture, ASTM C 457 requires a minimum number of points to be counted, a minimum length of line to be traversed, and a minimum area to be covered when performing a modified point count. The script selects and removes the required strips of pixels from the full image and creates a new composite image of these points as shown in Figure 5-5. The composite image contains fewer pixels than the scanned image and is thus analyzed more quickly while still meeting ASTM requirements.

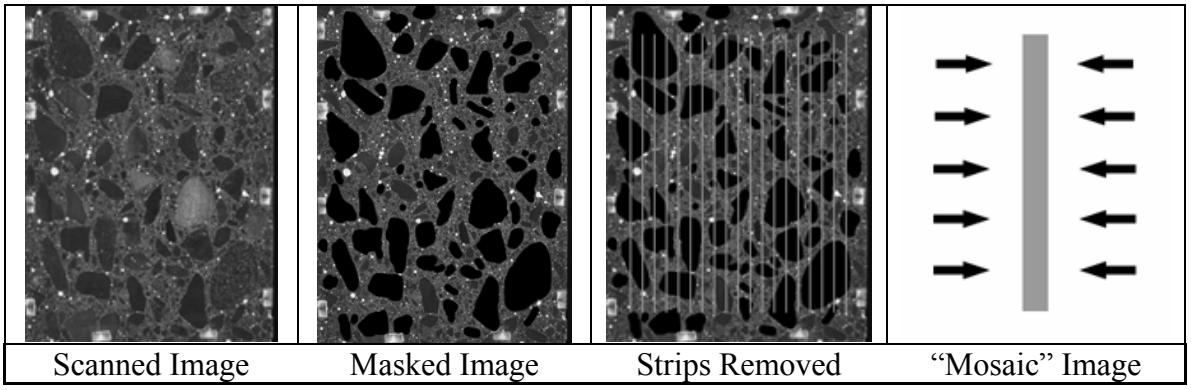

Figure 5-5. Steps in creation of composite image by script

7. *The selected threshold value is applied to the composite image to convert the image to binary format.*

The pixels in the image are converted from the 256 grayscale values collected by the flat-bed scanner to binary values per the selected threshold value. Figure 5-6 shows an example of sixteen pixels with varying pixel intensities being converted to a binary image.

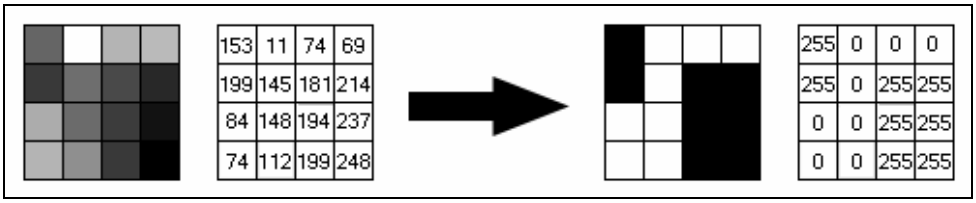

Figure 5-6. Example threshold conversion from scanned to binary pixel intensities

8. *The binary image is analyzed per ASTM C 457 using a spreadsheet as the analysis tool.*

As in Figure 5-7, the binary image is exported from the imaging software to a spreadsheet in such a fashion that each of the cells in the spreadsheet corresponds to a single pixel from the image.

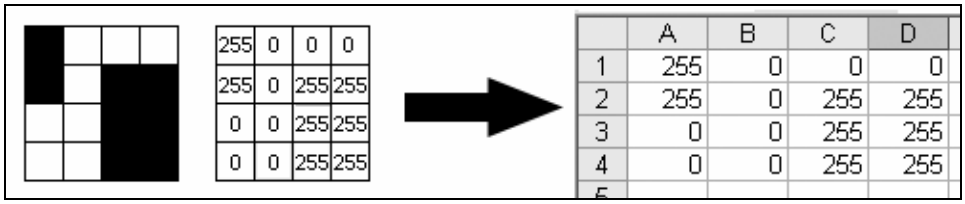

Figure 5-7. Example binary pixel export to spreadsheet import

The modified point count is then performed upon the cells to determine the parameters of the air void system. Each cell is considered to be a stop in the point count portion of the test and is counted as either air (for cells = 0) or not air (for cells = 255). Dividing the total count of cells classified as air by the total number of cells gives the volume percent air in the sample. Each of the columns in the spreadsheet is considered to determine the number of voids intersected for the modified point count. The quantity of the intercepted voids is obtained along with the length of each void, or chord, intercepted.

Figure 5-8 depicts an example of this portion of the analysis. If a count was performed on these pixels alone, the sample would have an air content of 56.25% (9 out of the 16 pixels are white). This example also has three intercepted voids with lengths of 8, 16 and 48 microns.

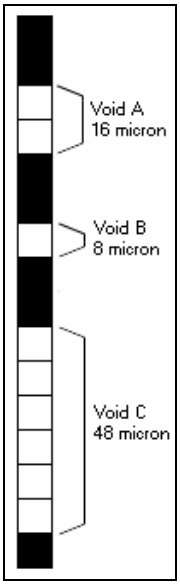

Figure 5-8. Void intercepts

9. *The script allows the user to analyze the image multiple times in different locations.*

The script requires a minimum of two analyses, that is, a minimum of two sets of traverse lines. The second set of traverse lines is always oriented 90 degrees with respect to the first set. This is accomplished, as shown in Figure 5-9, by rotating the image 90 degrees between analyses. For this reason, the script always requires that an even number of analyses is specified. The script allows for multiple analyses (greater than 2) by simply shifting the position of the traverse lines between pairs, as shown in Figure 5-10. The purpose of rotating the image is to account for any preferred orientation of the voids based on the concrete's original placement procedures.

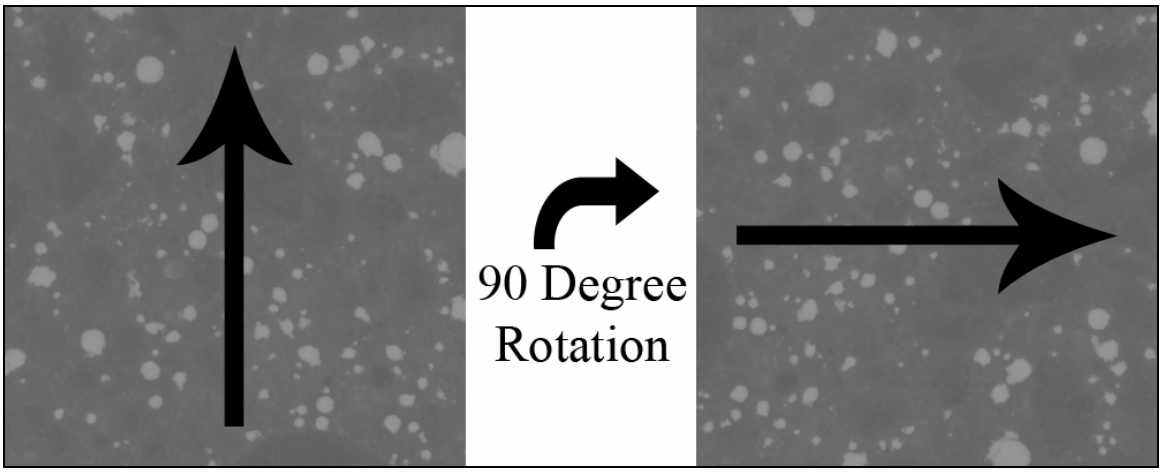

Figure 5-9. Image orientation rotation

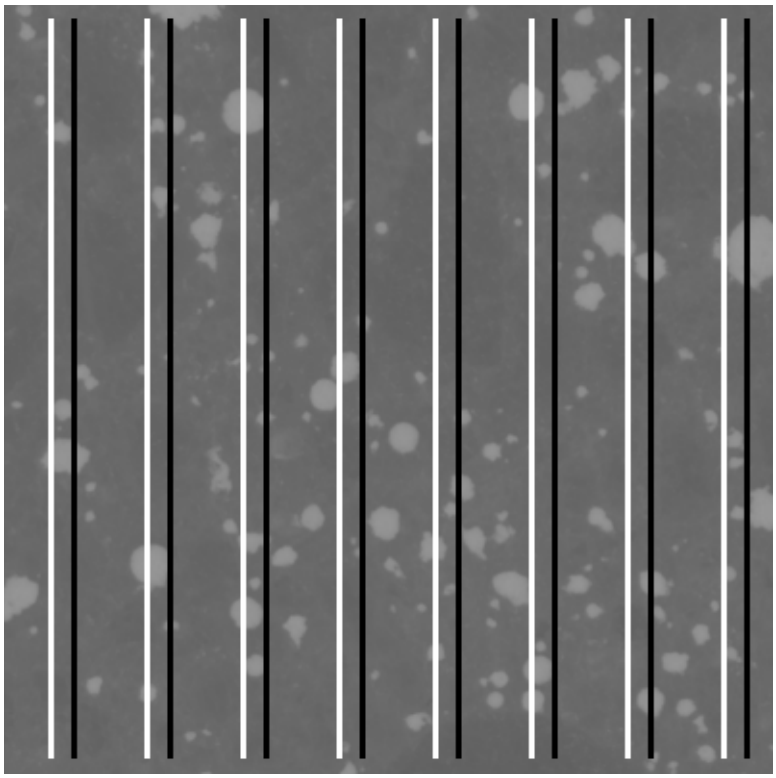

Figure 5-10. Traverse line shift during multiple analyses

Once all the data are collected, the calculations for void frequency, paste to air ratio, average chord length, specific surface and spacing factor are performed. In addition, collecting and averaging the lengths of all the intersected air voids from the individual analyses allows easy plotting of the air void chord length distribution.

10. Results are presented in report format with the aid of word processing software.

5.1.4 Manual ASTM C 457 Test Results versus Flat Bed Scanner Test Results

The automated script was performed on each of the 18 samples. The resulting air void system parameters were compared to the parameters calculated during the manual point count. Figures 5-11 through 5-14 depict linear regressions of the parameters obtained from the manual point counts to those calculated by the automated script analyses. Threshold values were selected at 180 and 160 for the high-resolution and office scanners respectively. Thresholds were established by visual inspection. Volume percent paste inputs were based on mix design criteria for the automated runs, and based on point count data for the manual runs. The volume percent air plots from both scanners show general agreement with the manual point count results, sometimes over predicting or under predicting the volume percent air. However, more alarming, results from both scanners consistently reported *lower* spacing factor values when the manual point counts indicated spacing factors in excess of the recommended upper limit of 0.2 mm.

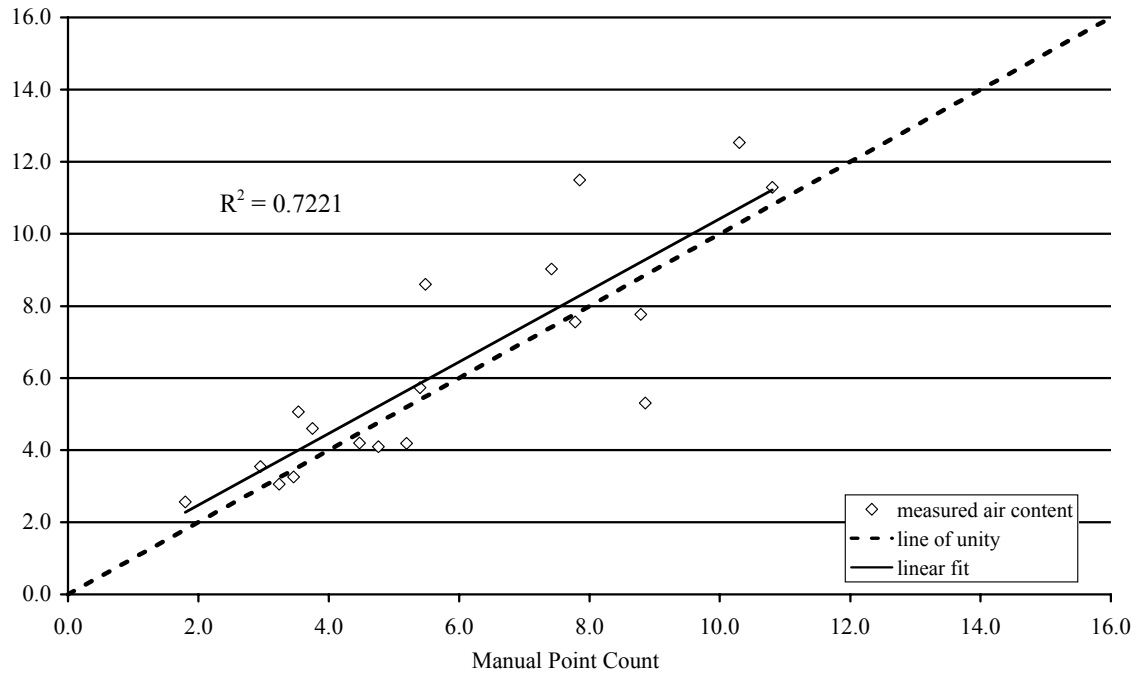

Figure 5-11. CreoScitex EverSmart Pro II flat bed scanner parameter regression for air content.

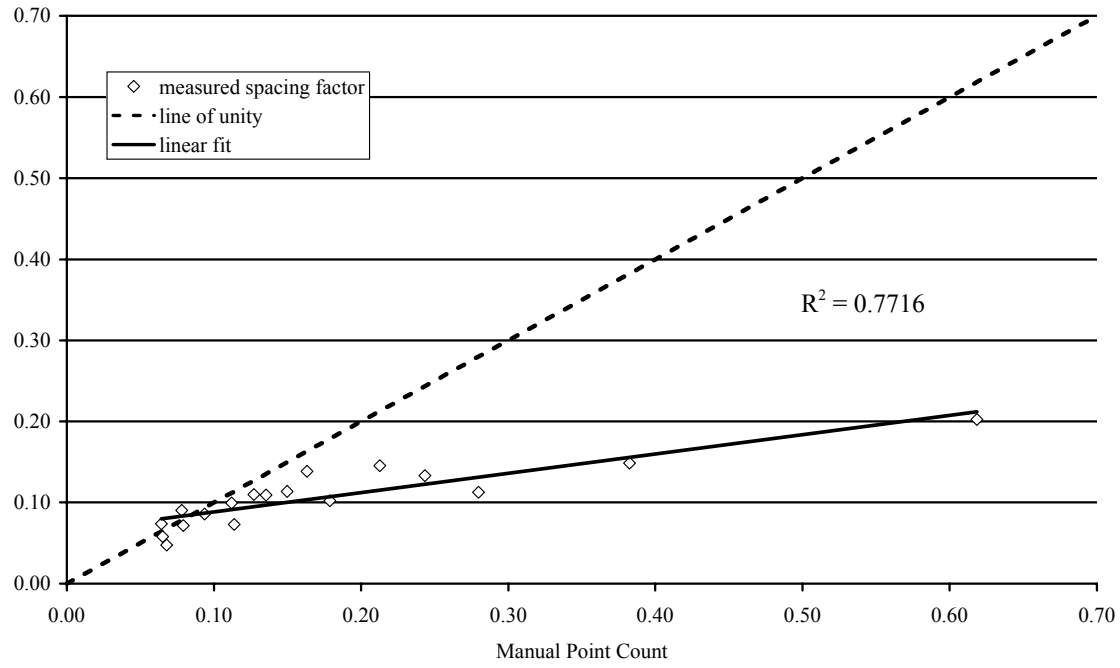

Figure 5-12. CreoScitex EverSmart Pro II flat bed scanner parameter regression for spacing factor.

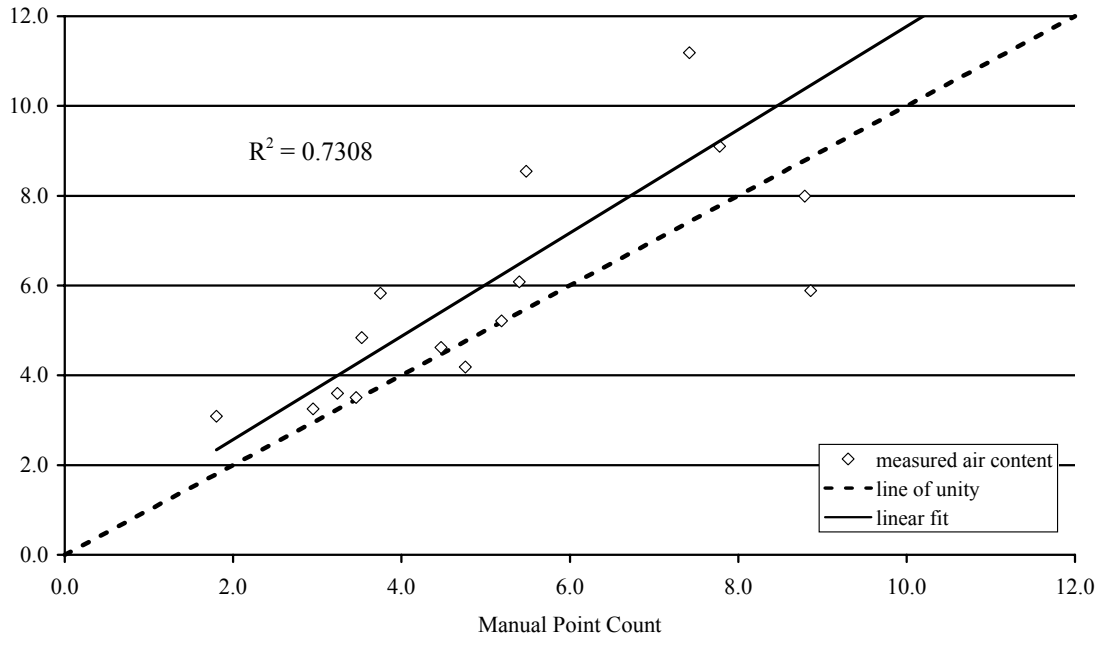

Figure 5-13. Hewlett-Packard 8200 ScanJet flat bed scanner parameter regression for air content.

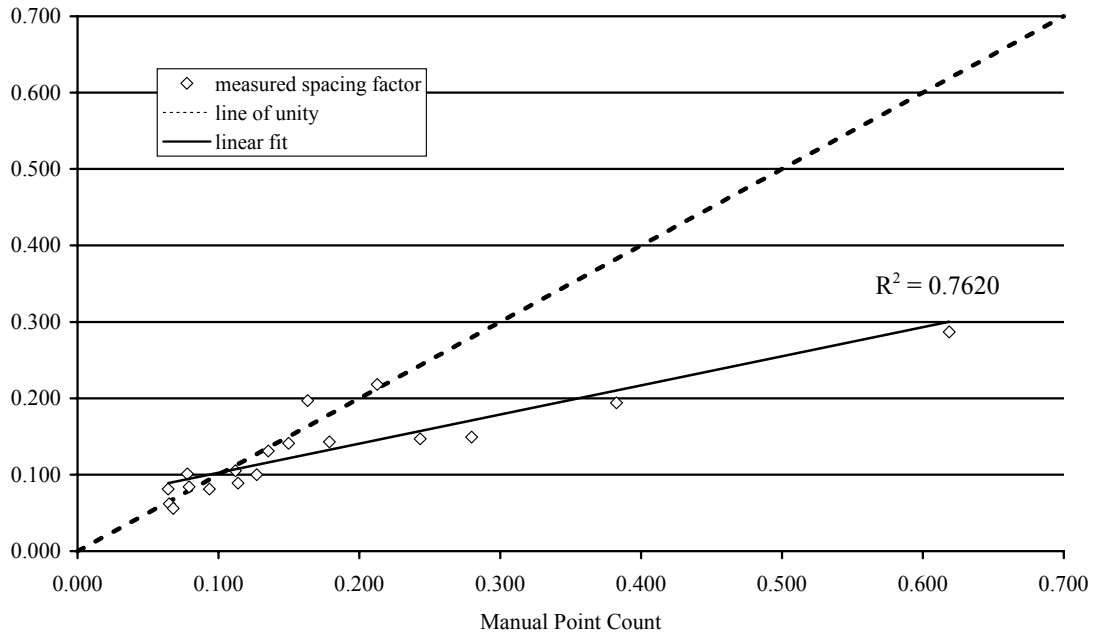

Figure 5-14. Hewlett-Packard 8200 ScanJet flat bed scanner parameter regression for spacing factor.

To investigate, an accuracy assessment was performed using the stage coordinates collected during the manual point count. A total of 1,388 points were counted on each of the 18 slabs, for a total of 24,984 points. According to the manual point counts, 1,582 of these points were recorded as air, while the remaining 23,402 points were recorded as non-air. As shown in Table 5-1, The corresponding pixels from the threshold images collected with the high resolution flat-bed scanner misclassified 320 of the manually recorded air points as non-air (20% of the 1,582) and misclassified 2,109 of the manually recorded non-air points as air (9% of the 23,402).

Table 5-1. Summary of high resolution scanner accuracy assessment.

High Resolution Flat bed Scanner	Manual Point Count		
		Air Stops	*Non-air Stops*
	Air Pixels	1,262	2,109
	Non-air Pixels	320	21,293
Agreement between all pixels/stops			22,555/24,984 (90.28%)

Table 5-2. Summary of Hewlett-Packard 8200 ScanJet flat bed scanner accuracy assessment.

Office Flat bed Scanner	Manual Point Count		
		Air Stops	*Non-air Stops*
	Air Pixels	1,289	2,300
	Non-air Pixels	293	21,102
Agreement between all pixels/stops			22,391/24,984 (89.62%)

The accuracy assessment of the high resolution scanner images revealed that the misclassification of non-air points as air effectively doubled the amount of air as compared to the manual point counts. Overall, there was 6.3% air according to the manual point counts versus 13.5% air according to the corresponding pixels in the scanner images. As shown in Table 5-2, a similar trend was found in the accuracy assessment from the office flat bed scanner images. The misclassification of non-air pixels as air contributed to erroneously low spacing factors reported for the low air content mixes by the flat bed scanner method. A quick optical review of the black and white treated slabs with the stereo microscope indicated that insufficiently smooth surfaces in the hardened cement paste had retained enough white powder to be misinterpreted as air voids in the threshold images.

5.1.5 High Resolution Scanner Versus Office Scanner

Although the automated test results did not correlate well with the manual test results, the automated test results did correlate well with each other, as shown in Figures 5-15 and 5-16. As a result of the accuracy assessment, it was determined that the sample preparation used originally was not sufficient and more careful preparation must be employed.

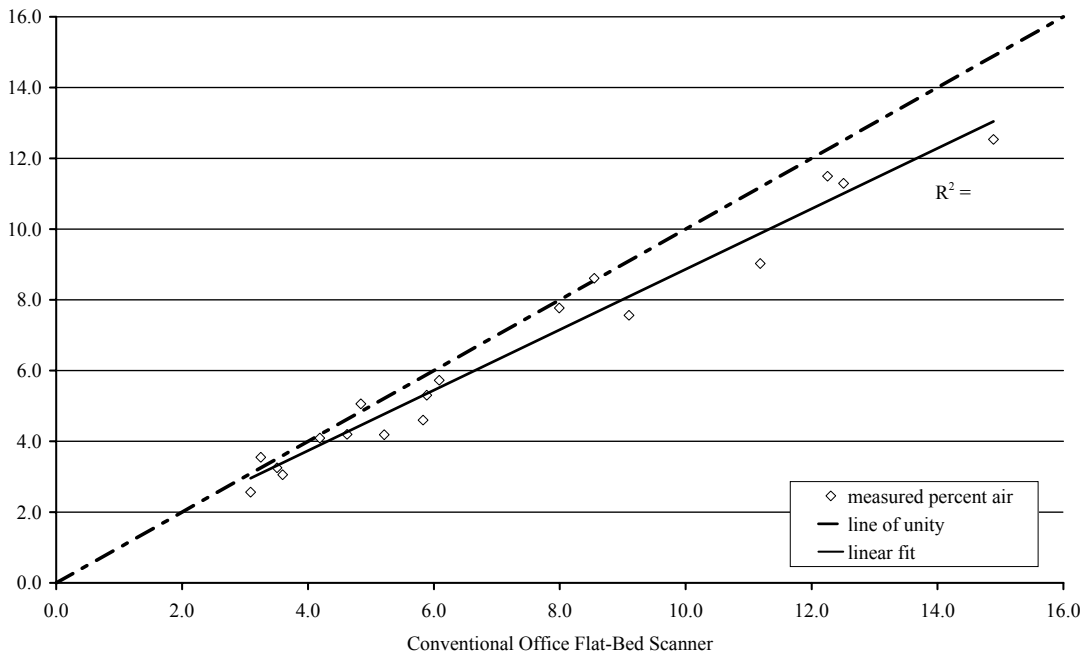

Figure 5-15. Correlation between scanners – volume % air.

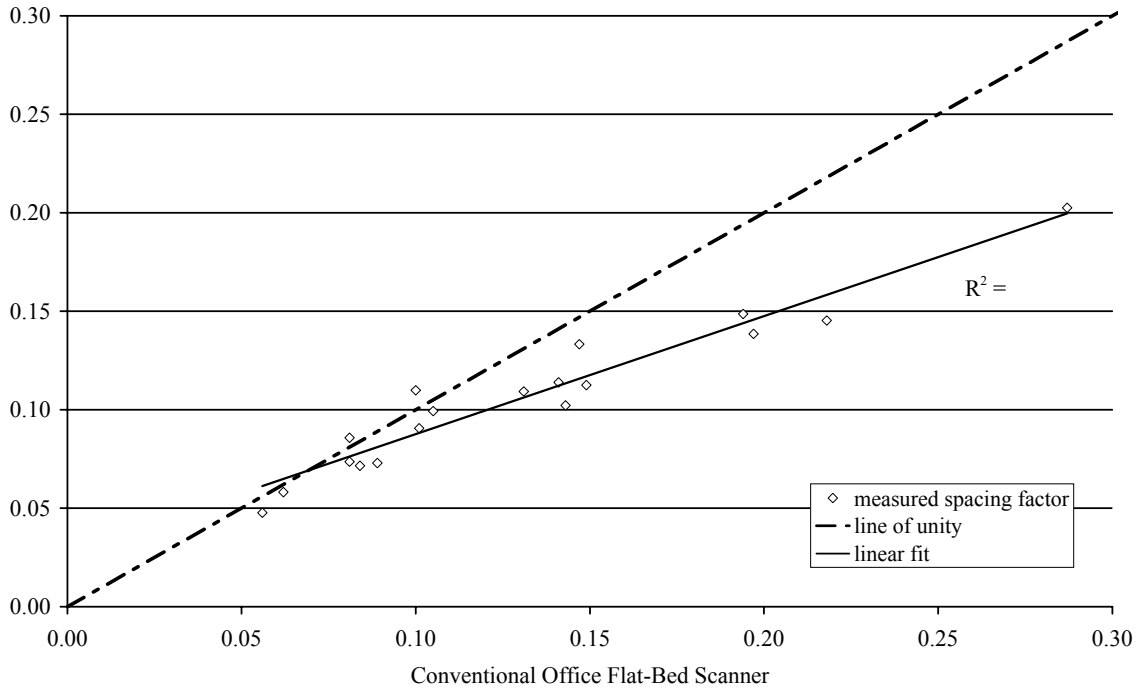

Figure 5-16. Correlation between scanners – air void spacing factor.

5.1.6 Scanner Method to RapidAir Comparison

One of the most widely used automated system is available from the independent firm Concrete Experts International (CXI) of Copenhagen Denmark. The CXI system is marketed and commonly known as the 'RapidAir 457' automatic air void analysis system. This system performs air void analyses with the aid of a grayscale camera attached to a computer controlled motorized control stage as shown in Figure 5-17.

Figure 5-17. Concrete Experts International's RapidAir 457 system

The RapidAir system analyzes a lapped, polished and contrast enhanced concrete specimen according to either the ASTM C 457 or EU 480-11 standard for hardened concrete air void analysis. The RapidAir system has recently been tested by seven European and American laboratories in a round robin format. The round robin tests administered by CXI involved sending three fully contrast enhanced specimens to the independent laboratories equipped with RapidAir systems for analysis. Results of the round robin analysis of the different specimens showed a high correlation in the air void system parameters on a laboratory to laboratory basis [Jakobsen 2005].

Nine of the eighteen specimens prepared for this report were analyzed with the RapidAir 457 automated analysis system. The contrast-enhanced surfaces of the specimens, which were originally analyzed via the flat-bed scanner method, were also analyzed with the RapidAir system without being re-prepared. The only alteration to the contrast-enhanced surface necessary was the manual masking of the voids in the aggregate particles. In the flat-bed scanner method, the voids found within the aggregate particles were masked digitally after the image was collected by the flat-bed scanner. In preparation for the RapidAir system, the voids needed to be manually masked by painting over the porous aggregate particles that had taken in the wollastonite powder meant for the entrained air voids. This painting was accomplished in approximately five minutes per sample using a fine, felt tipped black marking pen under the aid of stereo microscope magnification. The specimen was then analyzed by the RapidAir system according to ASTM C 457 in approximately 12 minutes. Tables 5-3 and 5-4 present the results of the RapidAir analyses along with the corresponding results from the conventional office flat-bed scanner analyses for the same nine samples.

Table 5-3. Summary of RapidAir results: void frequency and spacing factor

Mixture ID	*Freq. (per/mm)*		*Spacing (mm)*	
	*Scanner**	*RapidAir*	*Scanner**	*RapidAir*
FA-VR-H	0.697	0.826	0.081	0.076
MA-L	0.227	0.280	0.218	0.177
VR-L	0.162	0.197	0.287	0.226
AE90-O	0.297	0.356	0.197	0.160
VR-O	0.372	0.458	0.149	0.137
FA-MA-L	0.305	0.350	0.143	0.142
AE90-L	0.236	0.296	0.194	0.180
FA-AE90-H	1.023	1.196	0.062	0.052
FA-MA-O	0.709	0.829	0.084	0.075

*Hewlett-Packard 8200 ScanJet

Table 5-4. Summary of RapidAir results: air volume and specific surface

Mixture ID	*Air (% vol.)*		*Sp. Surface (mm^{-1})*	
	*Scanner**	*RapidAir*	*Scanner**	*RapidAir*
FA-VR-H	9.10	10.53	30.65	31.36
MA-L	3.60	3.77	25.24	29.73
VR-L	3.09	3.07	21.01	25.61
AE90-O	5.21	4.86	22.79	29.26
VR-O	4.84	5.80	30.75	31.55
FA-MA-L	3.51	3.78	34.76	37.04
AE90-L	3.25	4.29	29.05	27.62
FA-AE90-H	14.89	16.10	27.48	29.71
FA-MA-O	7.99	8.79	35.49	37.73

*Hewlett-Packard 8200 ScanJet

The resulting parameters obtained by both the RapidAir and flat-bed scanner analyses included percent volume air, air void frequency, Powers spacing factor and specific surface area. Figures 5-18 through 5-21 compare the data presented in Tables 5-3 and 5-4.

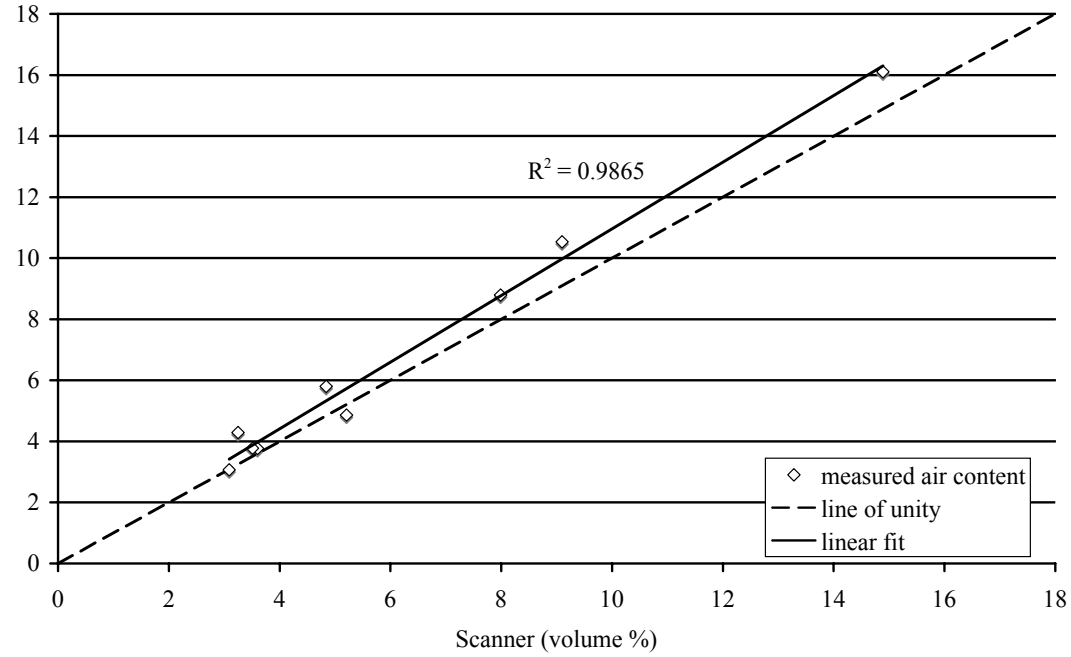

Figure 5-18. RapidAir to conventional flat-bed scanner air content comparison.

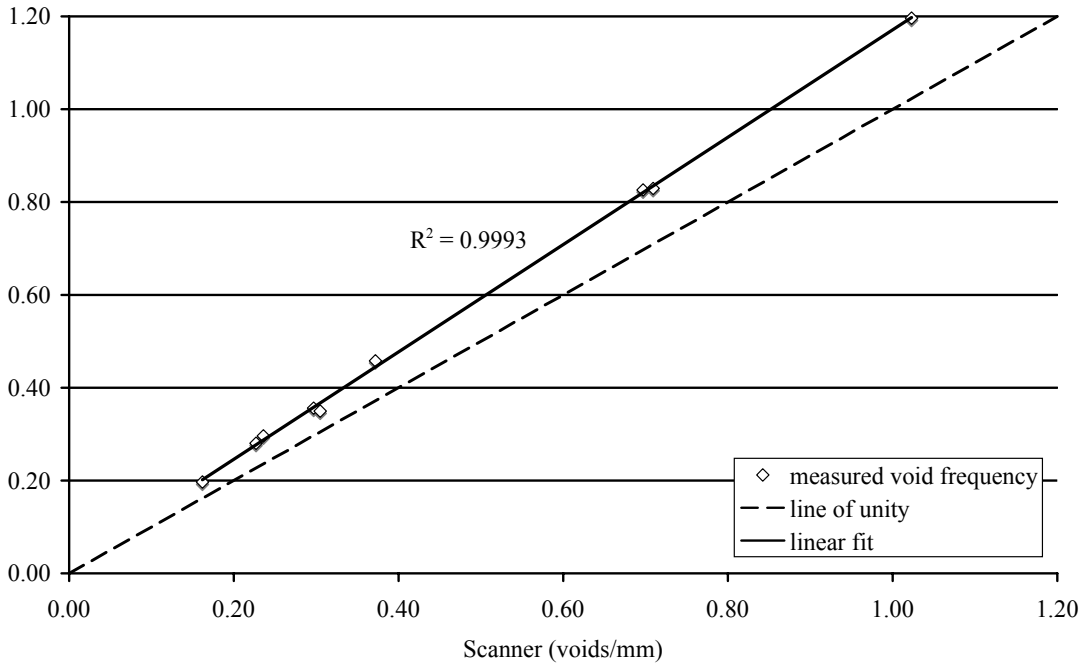

Figure 5-19. RapidAir to conventional flat-bed scanner void frequency comparison

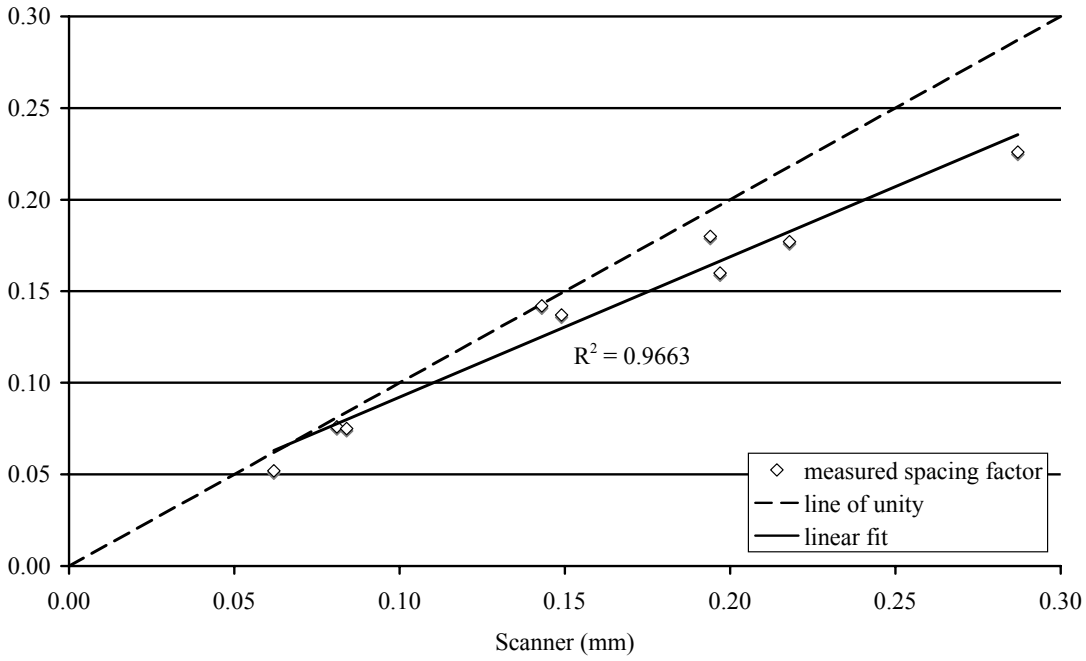

Figure 5-20. RapidAir to conventional flat-bed scanner spacing factor comparison

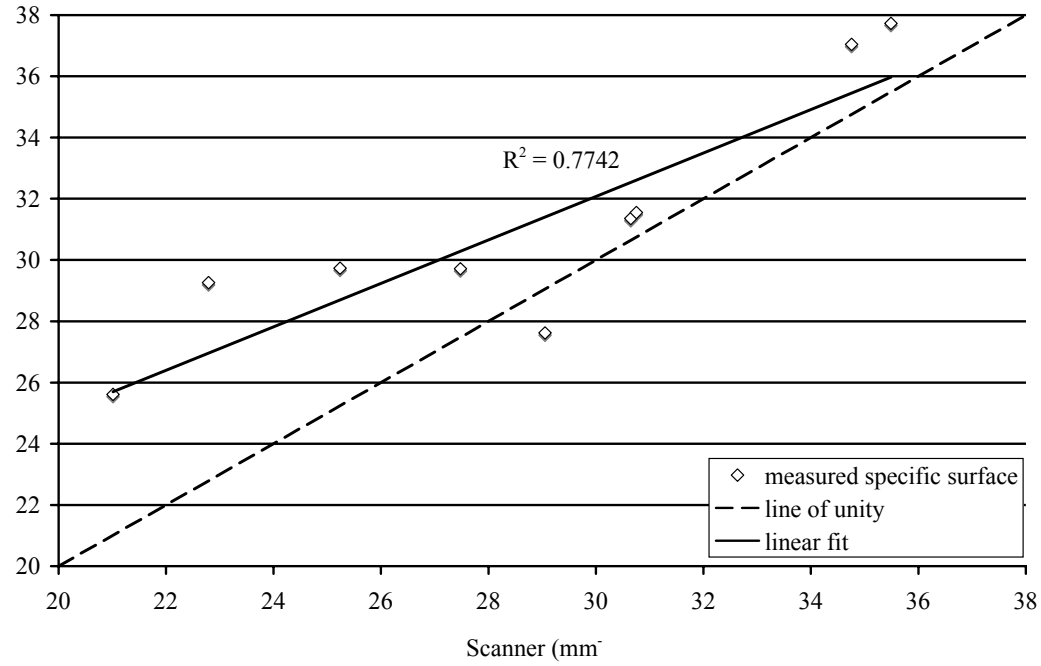

Figure 5-21. RapidAir to conventional flat-bed scanner specific surface comparison

It should be noted that the data collected from the RapidAir system correlated highly with that from the flat-bed scanner, but the points did not necessarily lie upon a line of unity. In the case of the percent air, the equation of the best fit line showed that the RapidAir results reported a slightly higher air content than did the flat-bed scanning method. The RapidAir system similarly reported higher values for the void frequency. Due to the slightly higher void frequency values, the RapidAir system reported a slightly lower spacing factor than did the flat-bed scanning method. Finally, the specific surface area, which is sensitive to variation in both the void frequency and air content, had the worst correlation of the four parameters. A correlation existed between the specific surface area data points, but it was weaker than the correlations of the other three aforementioned parameters.

5.1.7 Sample Preparation Revisited

The previous polishing method of hand pressure on a water-cooled rotating lap with successively finer magnetic backed diamond embedded platens and finished with 600 grit adhesive-backed silicon carbide paper was abandoned in favor of a more automated approach with a grooved cast iron rotating lap equipped with guide yokes and retaining rings. The new lapping equipment used was a 12" diameter LapMaster, which was capable of simultaneously lapping three 4 x 3" slabs. The flatness of the platen was monitored daily and kept within 1/10,000 inch (2.5 micrometers).

The following modified sample preparation method was employed:

- Two 4 x 3"slabs were cut from each of the 18 slabs. The existing black and white treated surfaces were removed using hand pressure on a water-cooled rotating lap with a 60 grit diamond embedded magnetic backed platen.
- The ground surfaces were cleaned with a gentle pressurized water spray (compressed air blown through running tap water) and lapped 24 minutes with an 800 grit silicon carbide water slurry on the LapMaster.
- The lapped surfaces were cleaned with a gentle pressurized water spray, alternating with a short ultrasonic water bath.
- The slabs were dried in a 50 degree Celsius oven followed by application of a 5:1 by volume solution of acetone and fingernail hardener. The solution was brushed on to the lapped surface in two coats.
- After setting, the slabs were briefly polished using hand pressure on a water-cooled rotating lap with a 600 grit adhesive backed silicon carbide paper, followed with the same cleaning regimen as before.
- Prismatic stickers were placed along the perimeters of the slabs.

Ten of the 4 x 3" slabs were re-examined. Nine of the slabs were chosen to represent all of the ordinary portland cement mixes, while only one of the slabs was chosen from the fly ash mixes: the low dosage vinsol resin.

5.1.8 Manual Modified Point Count Revisited

New manual modified point counts were performed on the ten 4 x 3" re-prepared surfaces. For expediency, each manual modified point count consisted of approximately half of the required points to satisfy ASTM C 457. In addition to recording the stage coordinates and

phase at each stop, a 640 x 480 pixel (2.612 x 1.959 mm) image was recorded at each stop for visual comparison with the flat bed scanner images.

5.1.9 Scanning and Analyzing the Samples

The slabs were scanned with the high resolution CreoScitex EverSmart Pro II flat bed scanner (advertised 3,175 x 8,000 dpi maximum optical resolution) but a different office desktop scanner was used, a Microtek ScanMaker s400 (advertised 4,800 x 9,600 dpi maximum optical resolution). The images were collected in 8-bit grayscale mode at a pixel resolution of 8 x 8 micrometers. The lid on each scanner was left open during scanning, and the scanning was performed in a dark room (no overhead lighting). When selecting the region to be scanned on each sample, care was taken to include the prismatic stickers, as well as some of the blank space outside the perimeters of the polished slabs. As mentioned previously, the highly reflective prismatic stickers provided consistent bright end points from sample to sample. Similarly, the blank space outside the perimeters of the polished slabs provided a uniform dark end point from sample to sample. When running the automated script, a mix design value, the aggregate to paste volume ratio, was entered for each sample, and the volume percent paste computed by the script.

5.1.10 Threshold Determination and Accuracy Assessment Revisited

There are many different digital image processing methods available to segment or classify images. Excellent summaries of some of the most common procedures can be found in image processing textbooks, such as those by Russ, 1994, and Gonzales and Woods, 2002. The simplest method, and the method used here, was to apply a threshold. Pixels brighter than the chosen threshold were classified as air, and the remaining pixels were classified as non-air. Whatever method is chosen, the question always remains of how effective, or accurate, is the result. For air voids in concrete, as is the case in many situations, the results can only be compared to those obtained by a human operator.

Two basic approaches were used to assess the quality of the threshold-based classification method. The first approach involved direct comparison between the air void parameters obtained by the manual operator and the air void parameters obtained by the automated procedure by linear regression and by departure from unity. The second approach involved accuracy assessment procedures outlined by Congalton and Green, 1999. In the second approach, grids of points on the samples were identified as being air or non-air by a human operator during the manual modified point counts. The same grids were located on the threshold digital images, the identities of the points were compared, and the results presented in error matrices such as those previously shown in Tables 5-1 and 5-2. In both approaches, the threshold levels were stepped between 0 and 255, and the accuracy parameters monitored.

5.1.10.1 Maximum R square threshold determination method

Figures 5-22 through 5-27 plot changes in the R square values for the correlations between the manual and automated air void parameters at each threshold step. For each of the air void parameters, the R square values achieved maxima at specific threshold values. However, the maxima did not all occur at the same threshold value, which complicated the issue of which threshold value should be chosen to maximize the correlation between the manual and automated procedure. During the automated procedure, only two measurements were actually

made of the air void system: the total number of air void pixels and the total number of air void intercepts. From these two measurements, the air content and void frequency were calculated respectively. Specific surface and average air void chord length were calculated (as outlined in ASTM C 457) using both the air content and void frequency values. Paste volume was not directly measured, but was provided as an input value, and was used to compute the paste/air ratio. The only remaining air void parameter, the spacing factor (depending on which ASTM C 457 equation was used), was derived using air content, void frequency, and paste volume values. Hence, to evaluate the performance of the automated procedure, the only air void parameters that were considered were the air content and the void frequency. Figure 5-28 plots an average of normalized R square values computed using the air content and void frequency. To construct the plot, the maximum R square values depicted in Figures 5-22 and 5-23 were normalized to a value of one and the remaining values adjusted accordingly. Next, an average was taken of the normalized R square values and plotted for each threshold level. As shown in Figure 5-28, maxima occurred at a threshold level of 180 for the high-resolution scanner and at a threshold level of 185 for the office desktop scanner.

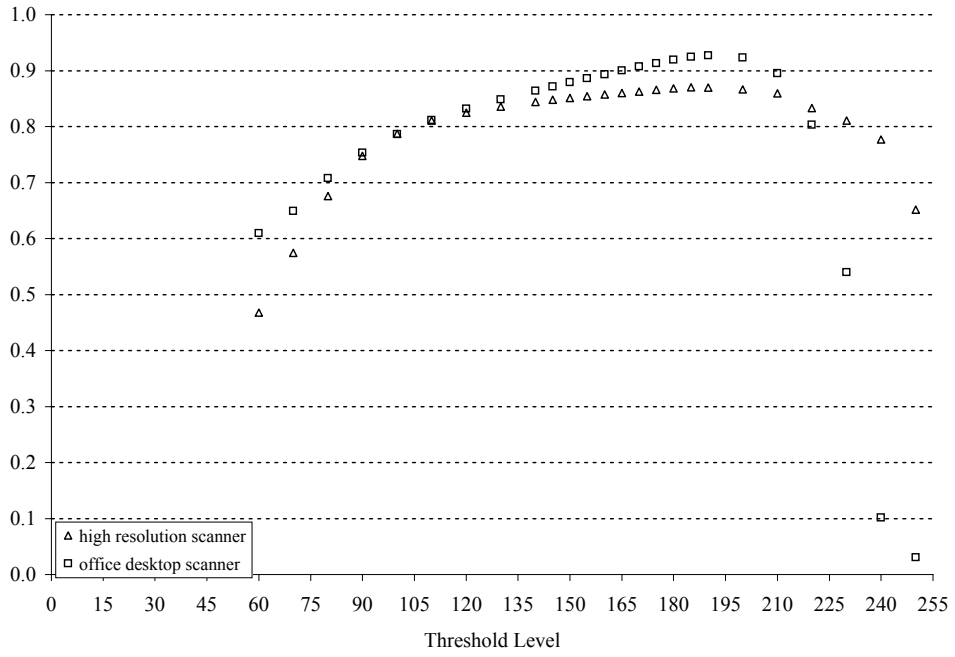

Figure 5-22: Change in R square values for correlation between manual procedure air content values and automatic procedure air content values versus threshold level.

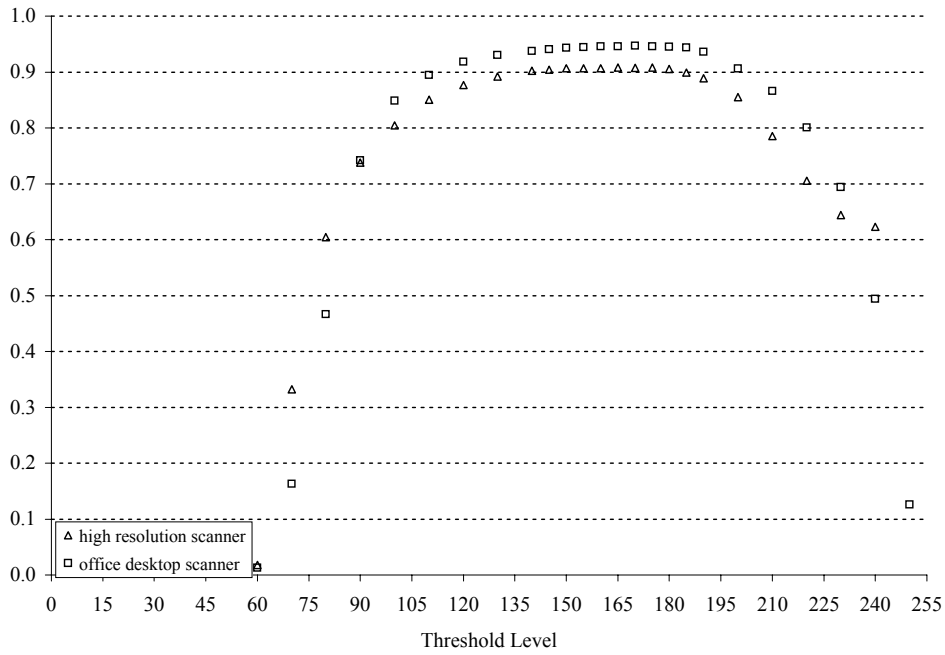

Figure 5-23: Change in R square values for correlation between manual procedure void frequency values and automatic procedure void frequency values versus threshold level.

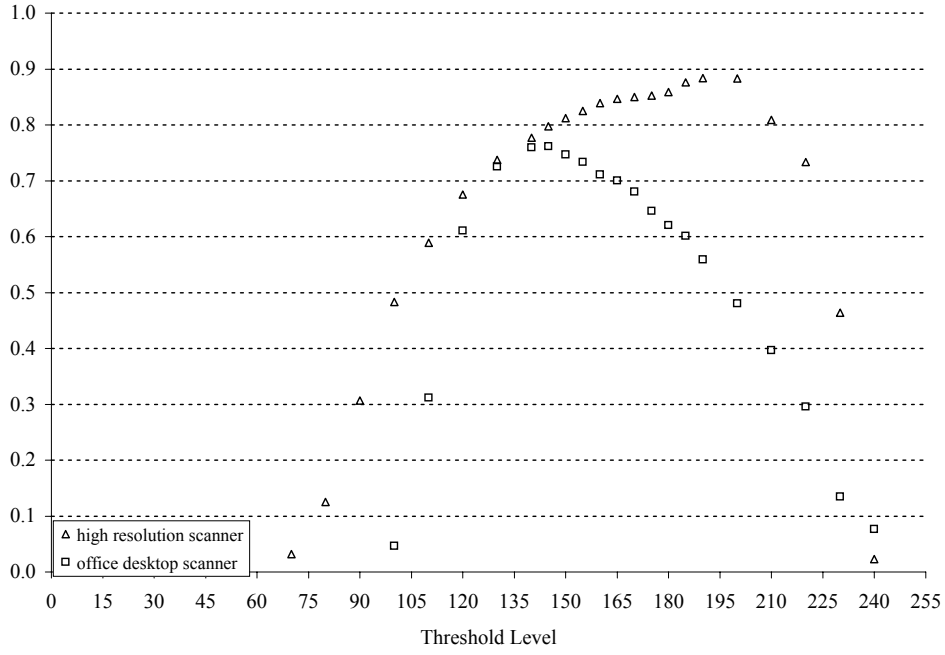

Figure 5-24: Change in R square values for correlation between manual procedure spacing factor values and automatic procedure spacing factor values versus threshold level.

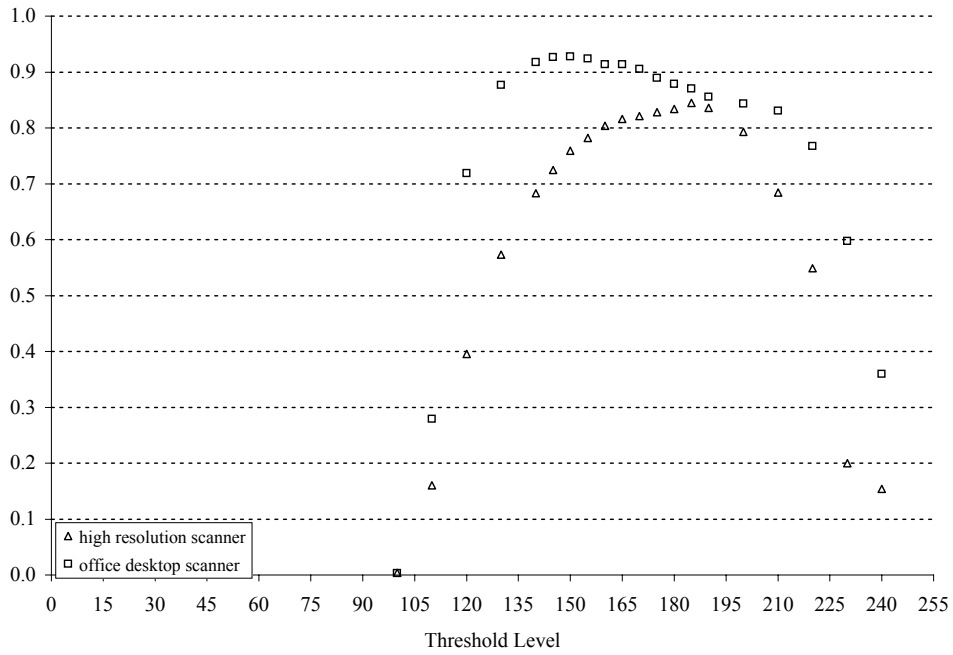

Figure 5-25: Change in R square values for correlation between manual procedure average chord length values and automatic procedure average chord length values versus threshold level.

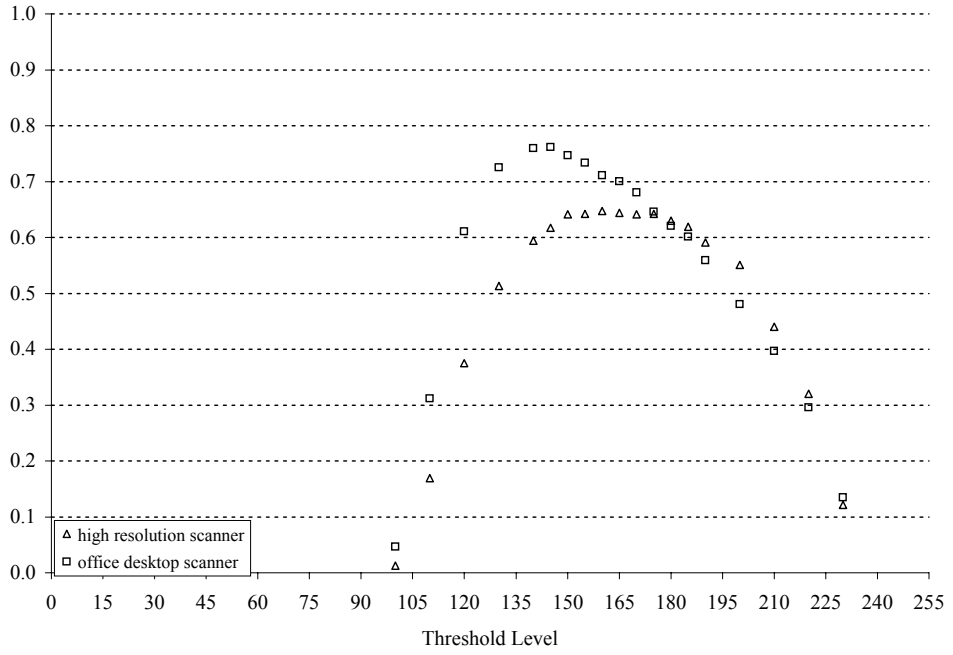

Figure 5-26: Change in R square values for correlation between manual procedure specific surface values and automatic procedure specific surface values versus threshold level.

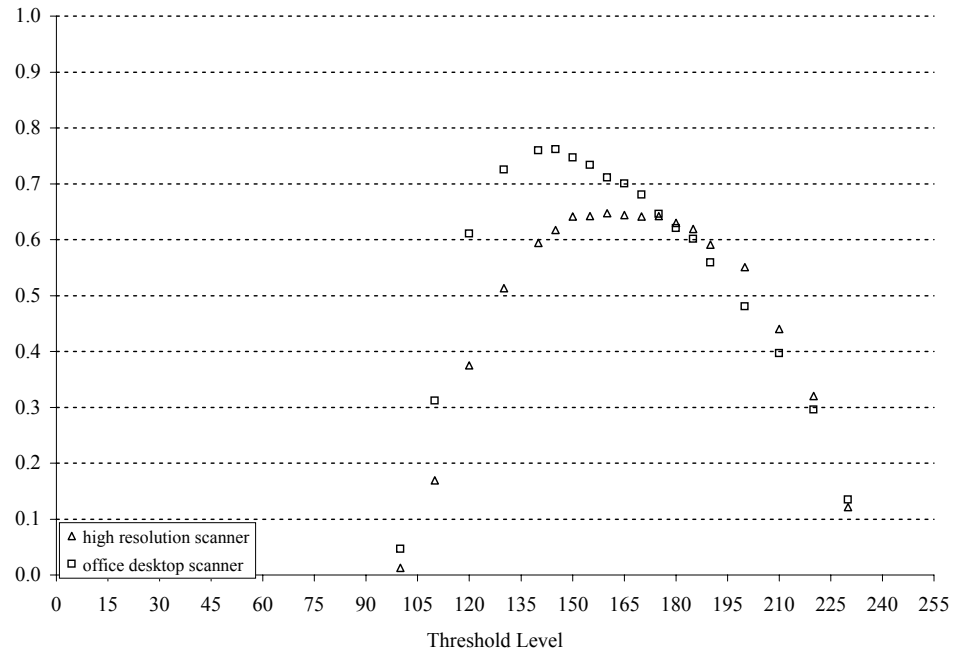

Figure 5-27: Change in R square values for correlation between manual procedure paste to air ratio values and automatic procedure paste to air ratio values versus threshold level.

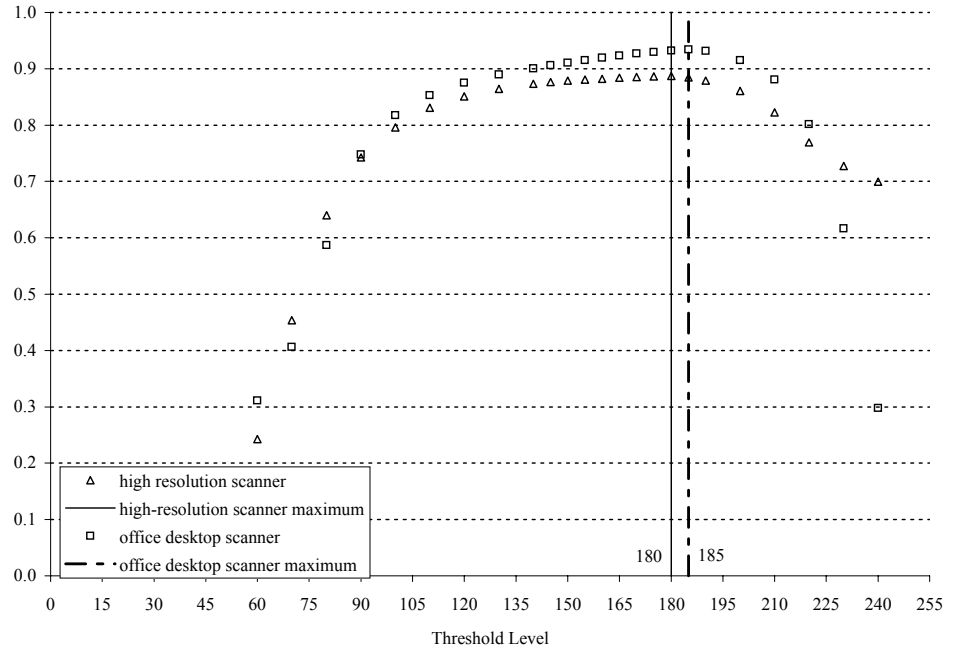

Figure 5-28: Plot to show maxima in average of normalized R square values from correlations between air content and air void frequency values from manual procedure and automatic procedures versus threshold level.

5.1.10.2 Minimum deviation from unity threshold determination method

The previously described threshold determination method involved maximizing the correlation between the manual and automated procedures. However, a high degree of correlation does not guarantee that the two procedures will provide similar results when analyzing the same specimens. Ideally, a plot comparing results from the two methods should lie on or near the line of unity. Figures 5-29 through 5-34 plot changes in the departure from unity for each air void parameter versus threshold level. To construct the plots, the absolute difference between unity and each data point was calculated, and the result divided by each point's x-axis value (the automated procedure value) to yield a percent deviation from unity. The average percent deviation from unity was then calculated using all of the points for each air void parameter. Figure 5-35 plots an average of the air content and void frequency deviation values versus threshold level. As shown in Figure 5-35, minima occurred at a threshold level of 160 for the high-resolution scanner, and at a threshold level of 145 for the office desktop scanner.

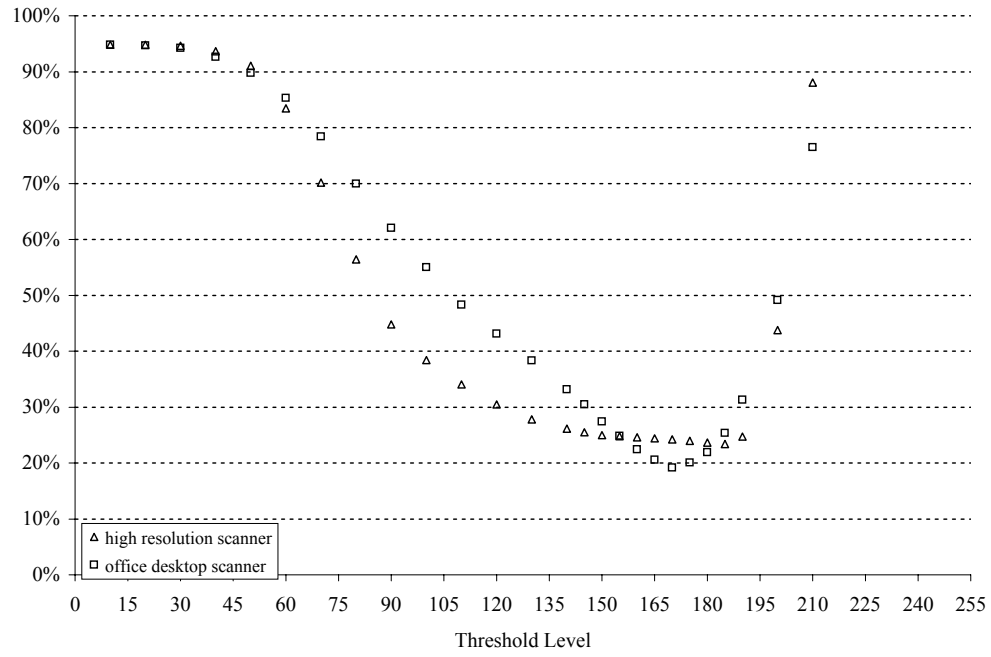

Figure 5-29: Change in average deviation from unity in relationship between manual procedure air content values and automatic procedure air content values versus threshold.

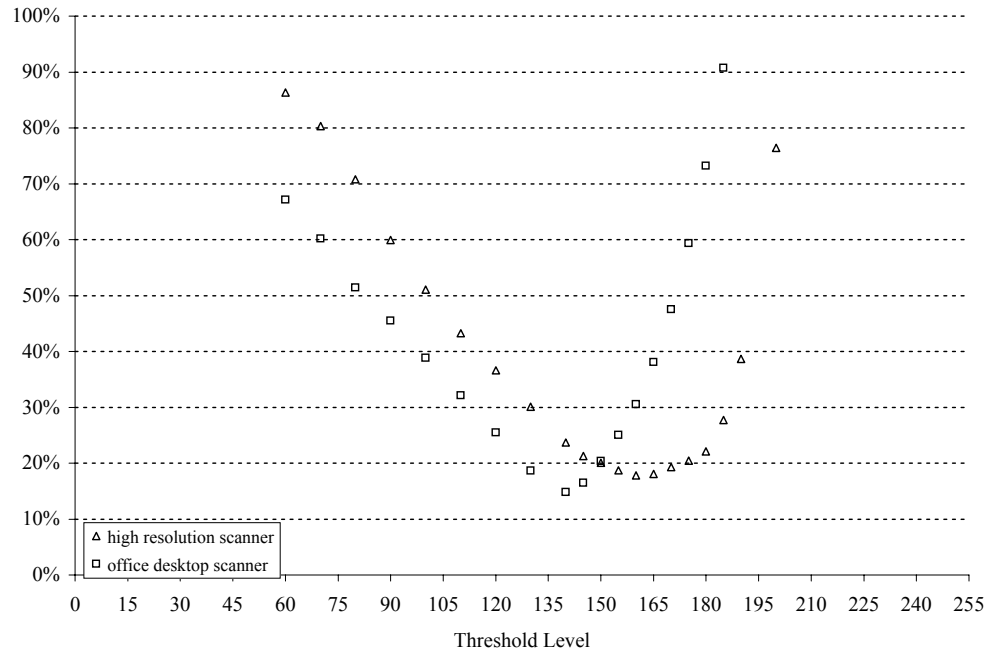

Figure 5-30: Change in average deviation from unity in relationship between manual procedure void frequency values and automatic procedure void frequency values versus threshold

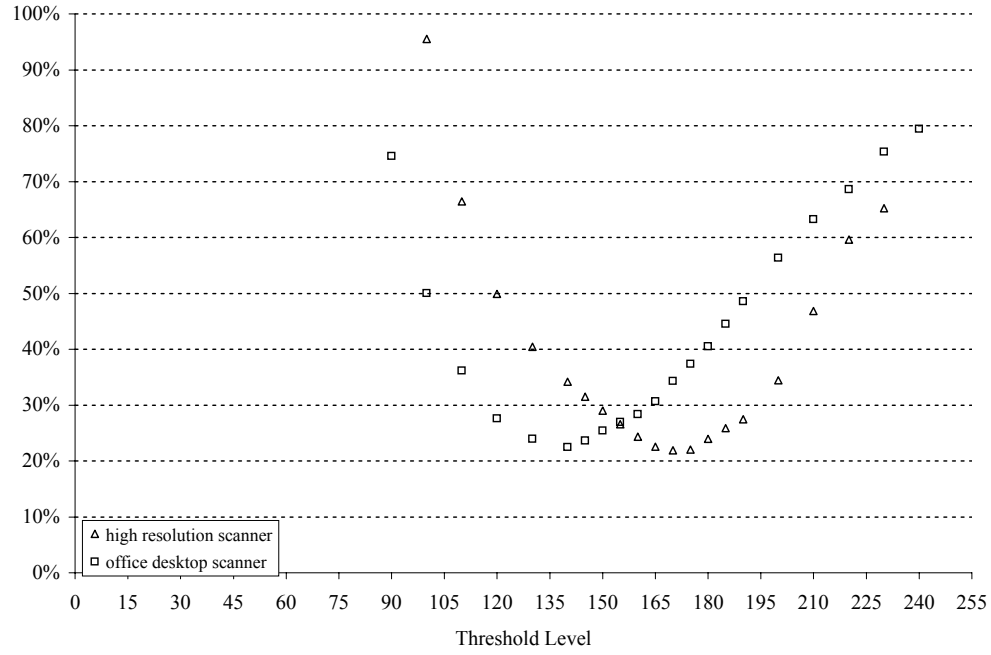

Figure 5-31: Change in average deviation from unity in relationship between manual procedure spacing factor values and automatic procedure spacing factor values versus threshold.

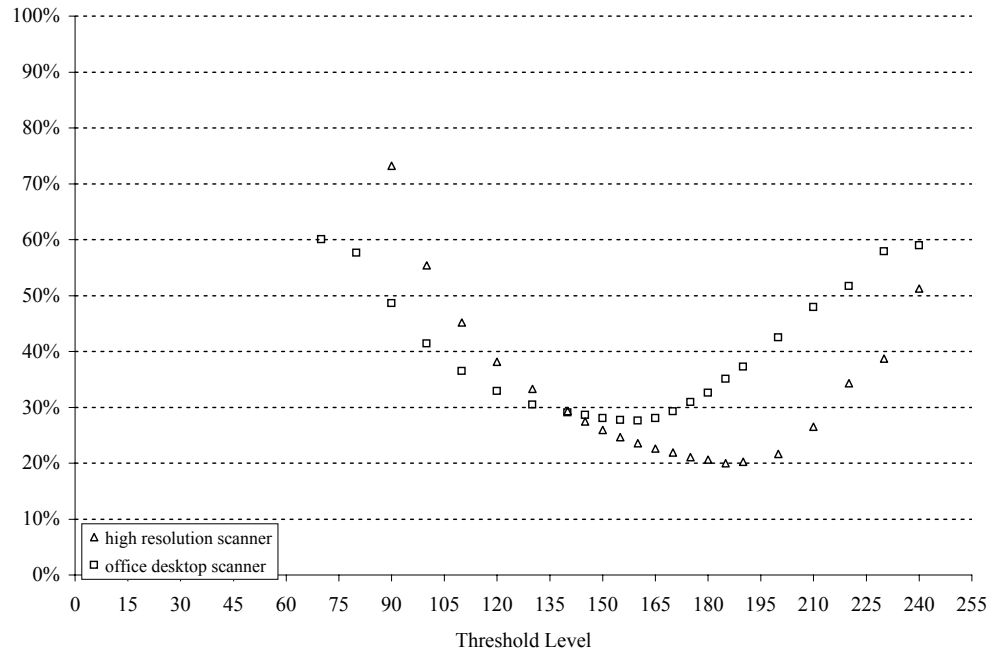

Figure 5-32: Change in average deviation from unity in relationship between manual procedure average chord length values and automatic procedure average chord length values versus threshold.

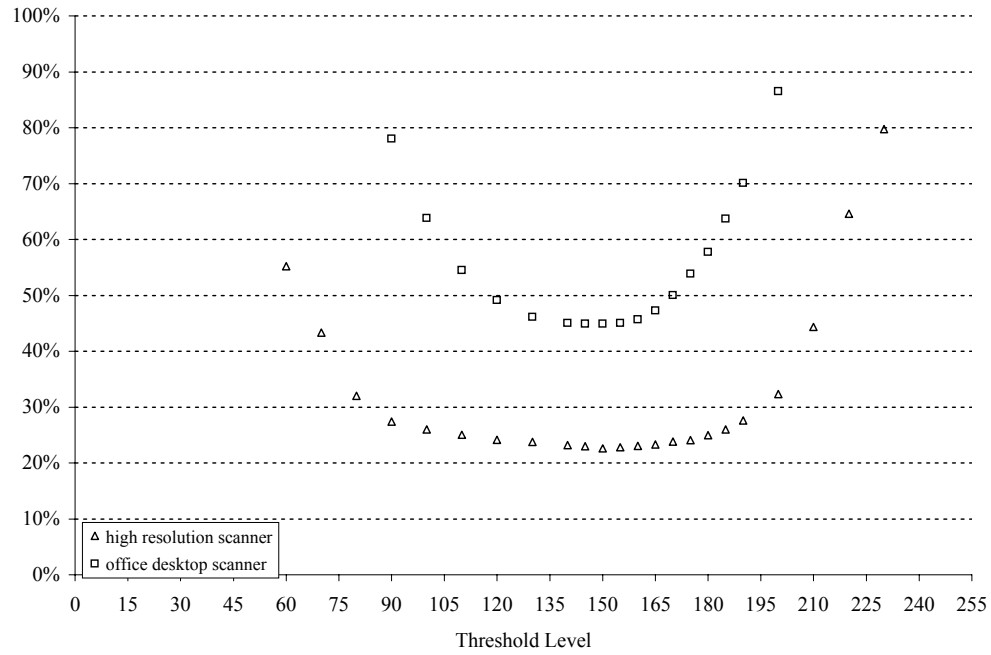

Figure 5-33: Change in average deviation from unity in relationship between manual procedure specific surface values and automatic procedure specific surface values versus threshold.

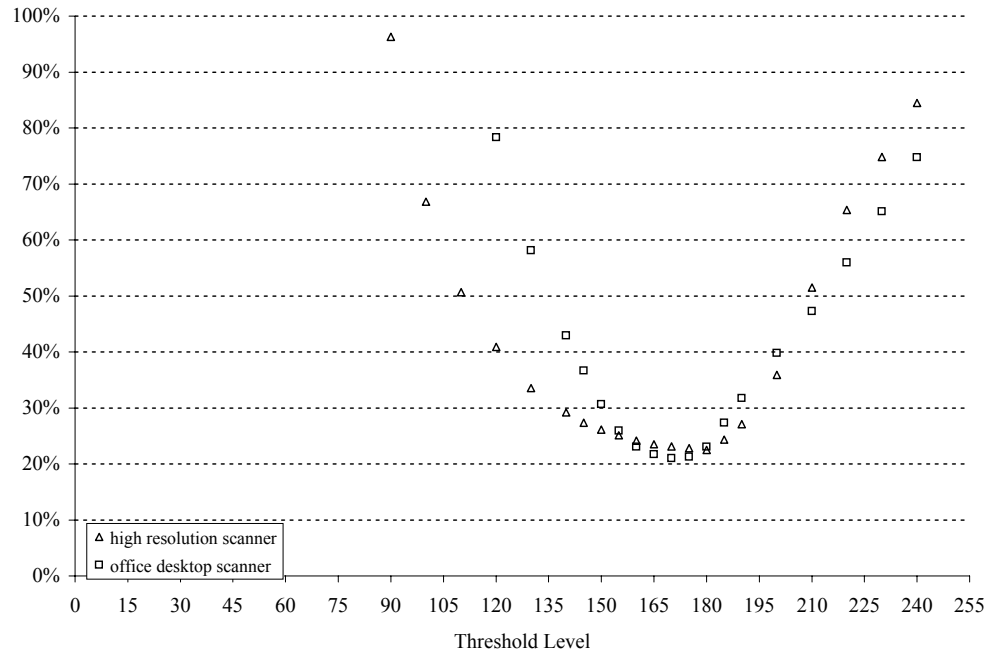

Figure 5-34: Change in average deviation from unity in relationship between manual procedure paste to air ratio values and automatic procedure paste to air ratio values versus threshold.

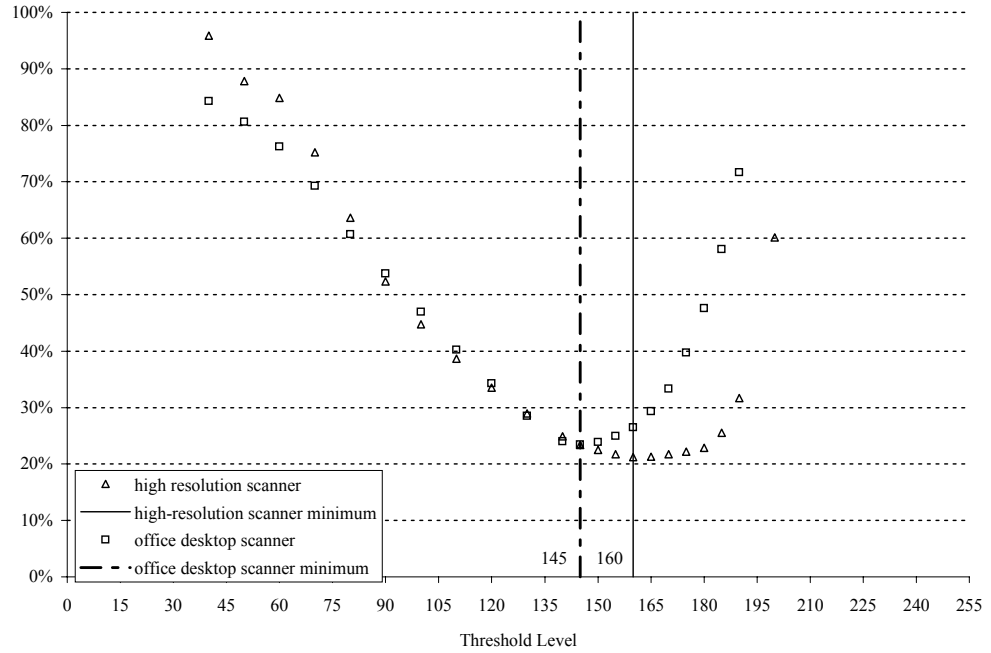

Figure 5-35: Plot to show minima in average of percent deviation from unity in relationship between air content and air void frequency values from manual procedure and automatic procedures versus threshold level.

5.1.10.3 Maximum Kappa statistic threshold determination method

The application of the Kappa statistic to problems of threshold determination has been addressed by Fung and LeDrew, 1988, and a similar approach was applied here. To compute the Kappa statistic values, it was first necessary to construct error matrices at each threshold step. The use of error matrices to perform accuracy assessments on digital images has been outlined in a text book by Congalton and Green, 1999. Basically, an error matrix compares information collected from locations on a sample to information collected from the same locations on a digital image. Since manual modified point counts were performed on the samples, a convenient choice for locations were the motorized stage coordinates from each stop. To help align the digital images to the same coordinate system, eight prismatic mosaic stickers were placed along the perimeters of each of the polished slabs, as shown in Figure 5-36. The motorized stage coordinates of the centers of the stickers were recorded, and the pixel locations of the centers of the corresponding stickers were found in the digital images. The data sets of stage coordinates and pixel locations were used to align the scanner images to the stage coordinate system using standard geometric correction procedures as outlined by Jensen, 1996. A first order polynomial interpolation was used to align the images, and a nearest neighbor interpolation was used to assign pixel intensities in the aligned images.

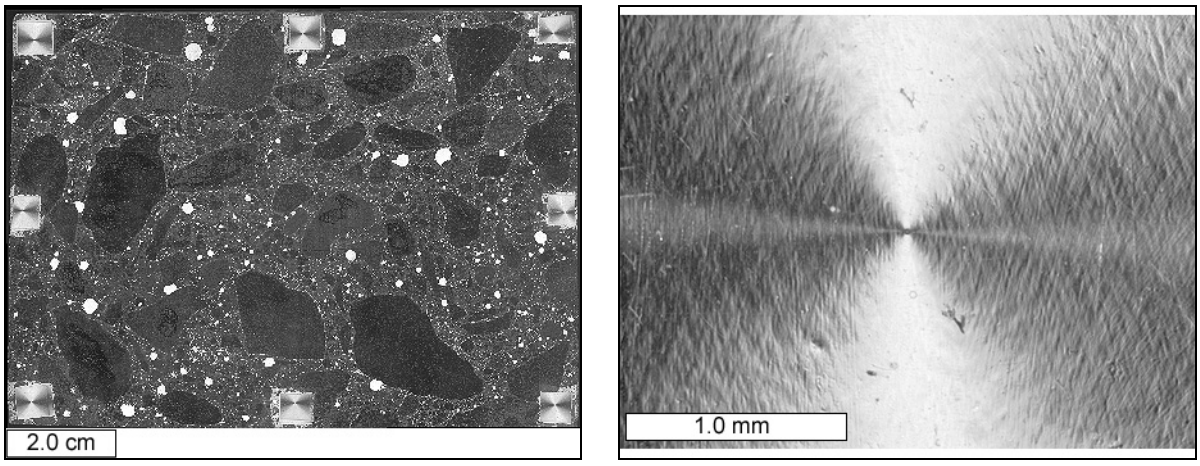

Figure 5-36: Scanned image from sample VRFA to show placement of prismatic stickers (left) and stereo microscope image to show detail of prismatic sticker (right).

The root mean square error (RMS error), a measure of distortion in the aligned images, was an average of 2.2 pixels (18 micrometers) with a standard deviation of 1.0 pixels (8 micrometers) for the ten images from the high-resolution scanner, and an average of 2.1 pixels (17 micrometers), with a standard deviation of 0.7 pixels (6 micrometers), for the ten images from the office desktop scanner. Once the images were aligned to the coordinate system, the identities of the coordinates from the manual point count (air or non-air), were compared to the identities of the corresponding pixels in the scanner images. The results of the comparisons were summarized in error matrices, shown in Tables 5-5 and 5-6.

Table 5-5. Summary of high resolution scanner accuracy assessment at threshold of 160.

High Resolution Flat bed Scanner	Manual Point Count		
		Air Stops	Non-air Stops
	Air Pixels	239	97
	Non-air Pixels	123	6,561
Agreement between all pixels/stops			6,800/7,020 (96.87%)

Table 5-6. Summary of office desktop scanner accuracy assessment at threshold of 145.

Office Desktop Flat bed Scanner	Manual Point Count		
		Air Stops	Non-air Stops
	Air Pixels	242	113
	Non-air Pixels	120	6,545
Agreement between all pixels/stops			6,787/7,020 (96.68%)

The Kappa statistic is a measure of the overall agreement between the manual and automated locations minus the chance agreement between the manual and automated locations. The Kappa statistic was developed by Cohen,1960, and first applied to digital image accuracy assessment by Congalton, 1983. Table 5-7 shows a mathematic representation of an error matrix (after Congalton and Green 1999). Formula 5-1 shows how the Kappa statistic is calculated using the error matrix.

Table 5-7. Mathematical representation of the error matrix (after Congalton and Green, 1999).

	j = columns (reference data)				row total
i = rows (classification data)		1	2	k	n_{i+}
	1	n_{11}	n_{12}	n_{1k}	n_{1+}
	2	n_{21}	n_{22}	n_{2k}	n_{2+}
	k	n_{k1}	n_{k2}	n_{kk}	n_{k+}
column total	n_{+j}	n_{+1}	n_{+2}	n_{+k}	n

$$\hat{K} = \frac{n\sum_{i=1}^{k} n_{ii} - \sum_{i=1}^{k} n_{i+}n_{+i}}{n^2 - \sum_{i=1}^{k} n_{i+}n_{+i}} \quad \text{where } n_{i+} = \sum_{j=1}^{k} n_{ij} \text{ and } n_{+i} = \sum_{i=1}^{k} n_{ij} \tag{5-1}$$

The Kappa statistic can be a number between -1 and 1. A value of 1 corresponds to perfect agreement. The Kappa statistic can be more informative than other accuracy indices, such as overall agreement (the proportion of correctly identified locations). For air measurement, overall agreement can be quite misleading as an accuracy index, particularly for low air content samples. For example, consider a sample that was manually point counted and found to be 2% air by volume. If the threshold was set at the upper limit of 255 during the

automated analysis of the same sample, the entire image would be classified as non-air. In such a situation, the overall agreement with the manual point count would be 98%, which sounds very good, but is in fact a useless result. Figure 5-37 plots changes in the Kappa statistic versus threshold level. As shown in Figure 5-37, maxima occurred at a threshold level of 155 for the high-resolution scanner and at a threshold level of 140 for the office desktop scanner.

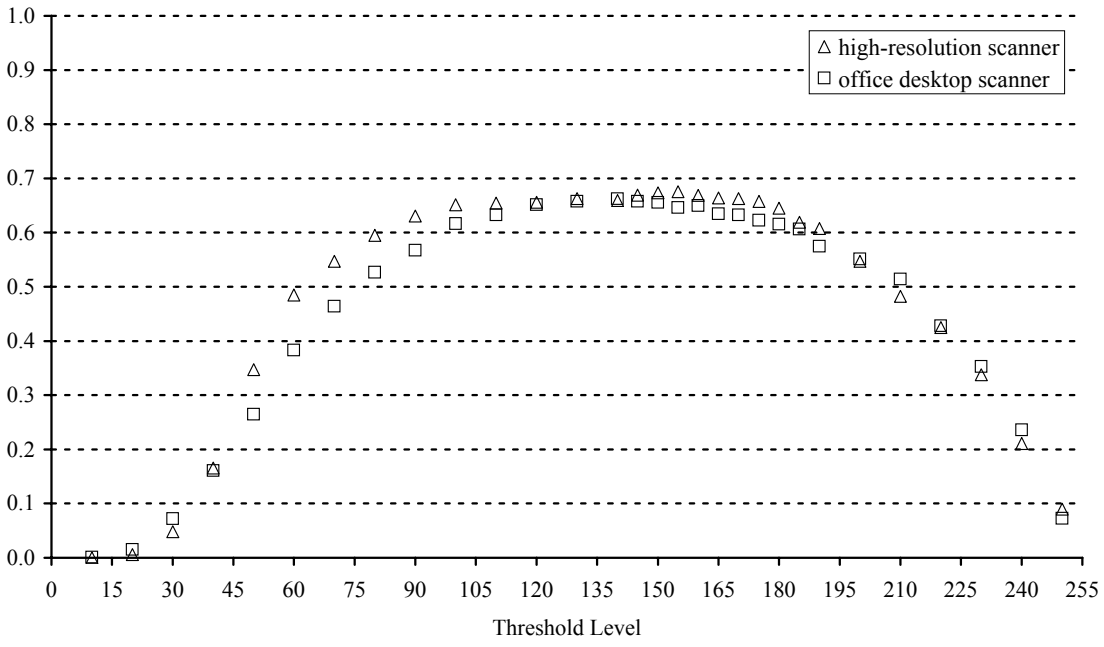

Figure 5-37: Plot to show maxima in Kappa statistic for accuracy assessment between locations from manual procedure and corresponding pixels in automatic procedure versus threshold level.

5.1.10.4 Error cross-over threshold determination method

Two error matrix derived accuracy parameters have already been introduced, the Kappa statistic and overall agreement. Two other error matrix derived parameters, errors of omission and commission, were used to develop the fourth and final threshold determination method. Formulas 5-2 and 5-3 show the formulas for the errors of omission and commission respectively.

$$\text{error of omission } = \frac{n_{+i} - n_{ii}}{n_{+i}} \tag{5-2}$$

$$\text{error of commission } = \frac{n_{i+} - n_{ii}}{n_{i+}} \tag{5-3}$$

Errors of omission occurred when the automated procedure failed to identify an air void. Errors of commission occurred when the automated procedure mistakenly identified non-air as air. Figure 5-38 plots changes in the errors of omission and commission versus threshold

level. The point on the plot where the two errors cross is the point where the two types of mistakes, omission and commission, effectively cancel each other out. The error cross-over point for the high-resolution scanner occurred at a threshold level of 150, and the error cross-over point for the office desktop scanner occurred at a threshold level of 145.

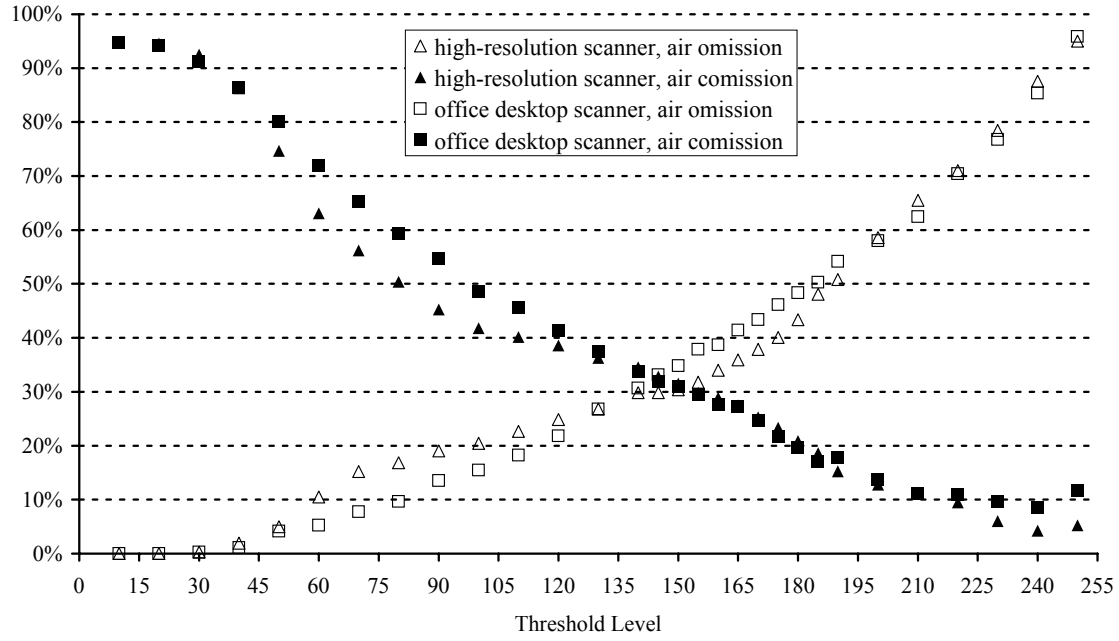

Figure 5-38: Plot to show air omission error and air commission error cross-over points for accuracy assessment between locations from manual procedure and corresponding pixels in automatic procedure versus threshold level.

5.1.11 Comparison of threshold determination methods

Figures 5-39 through 5-44 compare the air void parameters obtained using the optimum threshold values from the maximum R square method to the air void parameters from the manual point count. Figures 5-45 through 5-50 compare air void parameters obtained using the optimum threshold values from the minimum deviation from unity method. Figures 5-51 through 5-56 compare air void parameters obtained using the optimum threshold values from the maximum Kappa statistic method. Figures 5-57 through 5-62 compare air void parameters obtained using the optimum threshold values from the error cross-over method. Tables 5-8 and 5-9 list all of the air void parameters resulting from the different threshold determination methods. Figures 5-63 through 5-68 compare linear best fit lines for the air void parameters from the four methods.

Table 5-8. Comparison of air content and void frequency values from different threshold determination methods.

			High Resolution Scanner				Office Desktop Scanner			
			Threshold Determination Method				Threshold Determination Method			
Air Void Parameters	Sample ID	Manual Modified Point Count	Max R^2 180	Min Deviation from Unity 160	Max Kappa 155	Error Cross-Over 150	Max R^2 185	Min Deviation from Unity 145	Max Kappa 140	Error Cross-Over 145
Air Content (vol %)	AE-H	11.5	12.9	14.6	15.0	17.1	9.1	17.1	18.2	17.1
	MA-H	5.4	7.4	8.5	8.8	10.0	5.4	10.0	10.7	10.0
	VR-H	10.0	8.3	9.4	9.6	11.6	7.4	11.6	12.2	11.6
	AE-O	5.7	4.4	5.0	5.2	6.0	4.1	6.0	6.3	6.0
	MA-O	3.9	4.7	5.5	5.6	5.6	2.7	5.6	5.9	5.6
	VR-O	3.9	4.4	5.1	5.2	5.7	3.5	5.7	6.1	5.7
	AE-L	4.1	2.5	2.8	2.8	3.2	2.4	3.2	3.3	3.2
	MA-L	1.9	2.2	2.6	2.6	3.0	1.9	3.0	3.1	3.0
	VR-L	2.1	1.6	1.8	1.8	3.2	2.5	3.2	3.3	3.2
	VRFA-L	3.1	3.4	3.9	4.1	5.5	3.6	5.5	5.8	5.5
Void Frequency (voids/m)	AE-H	1197	1464	1681	1728	1282	731	1282	1334	1282
	MA-H	864	853	1033	1072	828	406	828	878	828
	VR-H	998	749	880	912	783	488	783	815	783
	AE-O	442	305	382	399	392	224	392	414	392
	MA-O	490	526	650	678	490	214	490	525	490
	VR-O	422	349	435	455	398	196	398	421	398
	AE-L	163	123	160	168	147	80	147	159	147
	MA-L	262	178	228	239	206	107	206	221	206
	VR-L	87	90	118	127	141	89	141	149	141
	VRFA-L	250	286	377	403	366	184	366	401	366

Table 5-9. Comparison of spacing factor and average chord length values from different threshold determination methods.

			High Resolution Scanner				Office Desktop Scanner			
			Threshold Determination Method				Threshold Determination Method			
Air Void Parameters	Sample ID	Manual Modified Point Count	Max R^2 180	Min Deviation from Unity 160	Max Kappa 155	Error Cross-Over 150	Max R^2 185	Min Deviation from Unity 145	Max Kappa 140	Error Cross-Over 145
Spacing Factor (mm)	AE-H	0.068	0.049	0.042	0.040	0.053	0.102	0.053	0.050	0.053
	MA-H	0.073	0.086	0.070	0.067	0.086	0.161	0.086	0.080	0.086
	VR-H	0.062	0.095	0.080	0.077	0.088	0.147	0.088	0.084	0.088
	AE-O	0.136	0.189	0.162	0.158	0.174	0.249	0.174	0.168	0.174
	MA-O	0.104	0.118	0.103	0.101	0.138	0.216	0.138	0.134	0.138
	VR-O	0.114	0.169	0.146	0.141	0.170	0.267	0.170	0.165	0.170
	AE-L	0.327	0.354	0.287	0.274	0.334	0.530	0.334	0.316	0.334
	MA-L	0.131	0.232	0.195	0.188	0.235	0.356	0.235	0.226	0.235
	VR-L	0.460	0.374	0.303	0.285	0.345	0.478	0.345	0.333	0.345
	VRFA-L	0.171	0.180	0.149	0.142	0.182	0.289	0.182	0.171	0.182
Average Chord Length (mm)	AE-H	0.096	0.088	0.087	0.087	0.133	0.125	0.133	0.137	0.133
	MA-H	0.063	0.086	0.082	0.082	0.121	0.133	0.121	0.122	0.121
	VR-H	0.100	0.111	0.107	0.106	0.148	0.151	0.148	0.149	0.148
	AE-O	0.129	0.143	0.131	0.129	0.154	0.182	0.154	0.152	0.154
	MA-O	0.079	0.089	0.084	0.083	0.113	0.127	0.113	0.113	0.113
	VR-O	0.091	0.127	0.117	0.115	0.145	0.180	0.145	0.144	0.145
	AE-L	0.254	0.207	0.175	0.169	0.217	0.303	0.217	0.208	0.217
	MA-L	0.071	0.125	0.112	0.109	0.145	0.181	0.145	0.142	0.145
	VR-L	0.245	0.180	0.152	0.145	0.225	0.278	0.225	0.220	0.225
	VRFA-L	0.125	0.117	0.104	0.101	0.150	0.193	0.150	0.145	0.150

Table 5-10. Comparison of specific surface and paste to air ratio values from different threshold determination methods.

			High Resolution Scanner				Office Desktop Scanner			
			Threshold Determination Method				Threshold Determination Method			
Air Void Parameters	Sample ID	Manual Modified Point Count	Max R^2 180	Min Deviation from Unity 160	Max Kappa 155	Error Cross-Over 150	Max R^2 185	Min Deviation from Unity 145	Max Kappa 140	Error Cross-Over 145
Specific Surface (mm^{-1})	AE-H	41.5	45.4	46.1	46.1	30.0	32.0	30.0	29.3	30.0
	MA-H	63.9	46.4	48.5	48.8	33.1	30.1	33.1	32.9	33.1
	VR-H	40.0	36.0	37.4	37.9	27.0	26.5	27.0	26.8	27.0
	AE-O	31.0	28.0	30.5	31.0	26.1	22.0	26.1	26.4	26.1
	MA-O	50.9	45.0	47.7	48.1	35.3	31.5	35.3	35.3	35.3
	VR-O	43.9	31.6	34.1	34.8	27.7	22.2	27.7	27.8	27.7
	AE-L	15.7	19.4	22.9	23.7	18.5	13.2	18.5	19.2	18.5
	MA-L	56.7	31.9	35.7	36.5	27.6	22.1	27.6	28.1	27.6
	VR-L	16.3	22.2	26.3	27.7	17.8	14.4	17.8	18.2	17.8
	VRFA-L	31.9	34.1	38.5	39.8	26.7	20.7	26.7	27.6	26.7
Paste to Air Ratio	AE-H	2.8	2.2	1.9	1.9	1.6	3.3	1.6	1.5	1.6
	MA-H	5.1	4.0	3.4	3.3	2.8	5.5	2.8	2.6	2.8
	VR-H	2.5	3.4	3.0	2.9	2.4	3.9	2.4	2.2	2.4
	AE-O	4.2	6.7	5.8	5.6	4.8	7.2	4.8	4.6	4.8
	MA-O	6.8	6.7	5.7	5.5	5.6	11.8	5.6	5.2	5.6
	VR-O	6.0	6.8	5.9	5.7	5.2	8.6	5.2	4.9	5.2
	AE-L	6.3	11.9	10.8	10.6	9.4	12.5	9.4	9.1	9.4
	MA-L	14.3	14.2	12.4	12.0	10.5	16.3	10.5	10.0	10.5
	VR-L	14.7	18.5	16.7	16.4	9.3	12.0	9.3	9.0	9.3
	VRFA-L	7.2	9.3	8.0	7.7	5.6	8.8	5.6	5.3	5.6

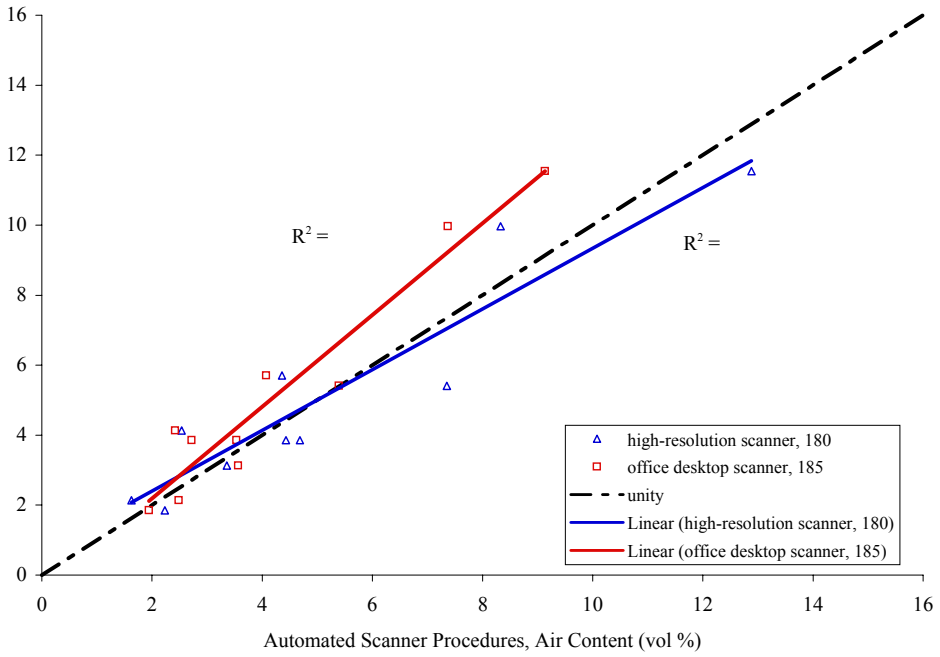

Figure 5-39: Plot to show correlation in air content values from manual and automatic procedures using optimum threshold as determined by maximum R square method.

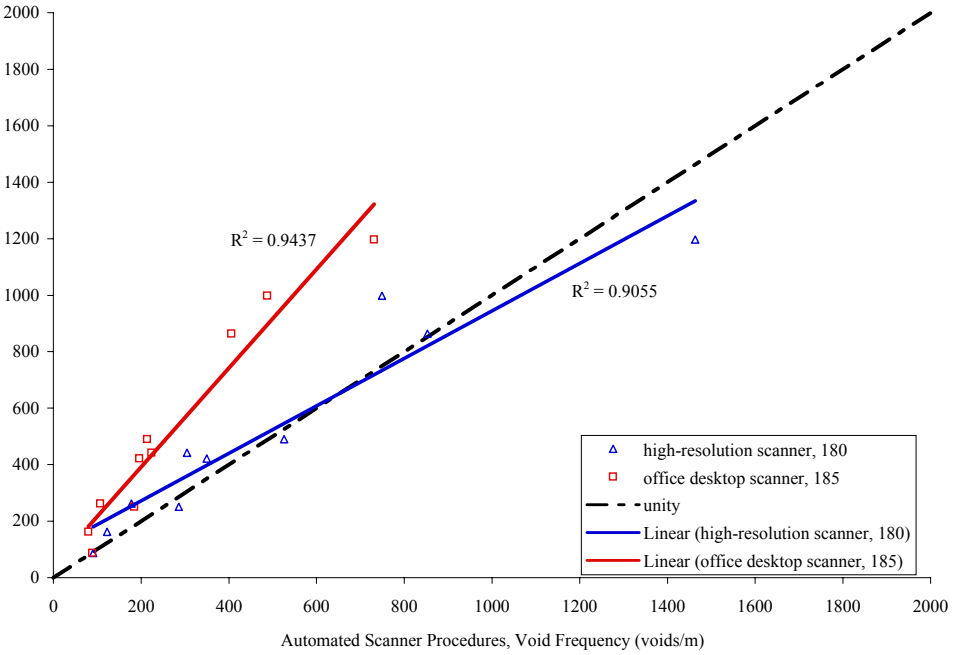

Figure 5-40: Plot to show correlation in void frequency values from manual and automatic procedures using optimum threshold as determined by maximum R square method.

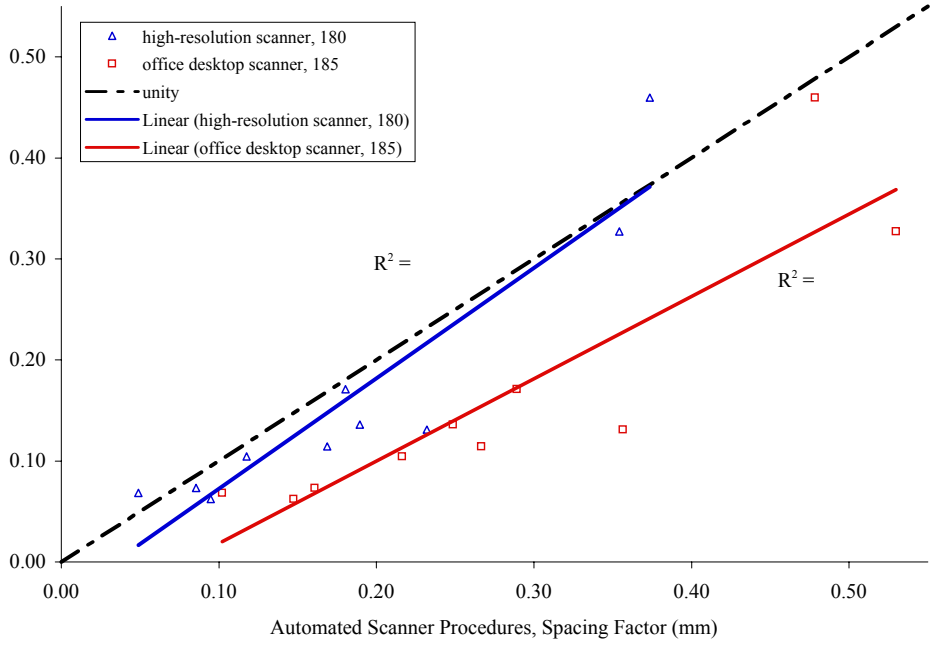

Figure 5-41: Plot to show correlation in spacing factor values from manual and automatic procedures using optimum threshold as determined by maximum R square method.

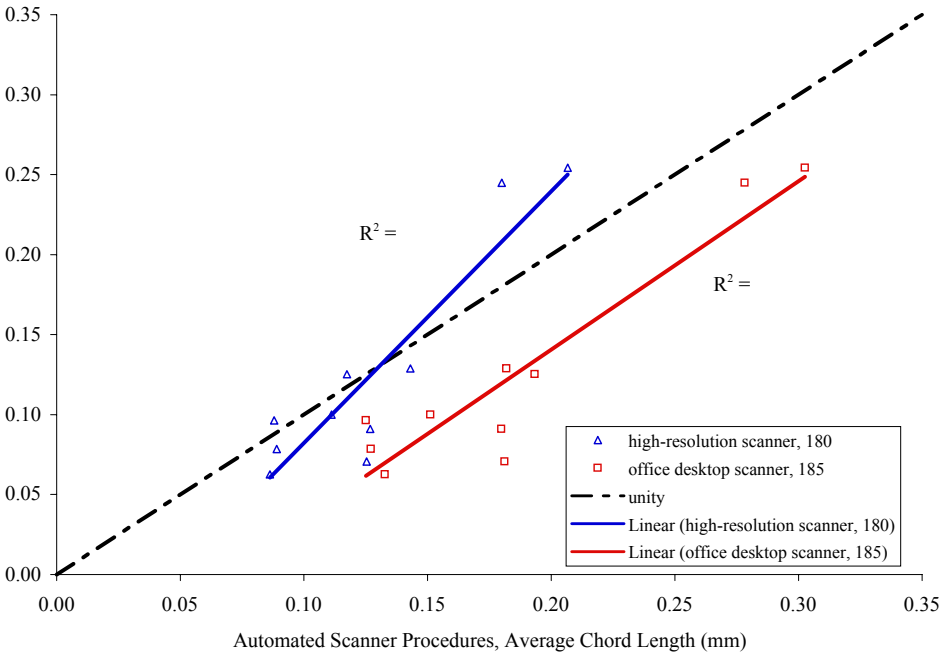

Figure 5-42: Plot to show correlation in average chord length values from manual and automatic procedures using optimum threshold as determined by maximum R square method.

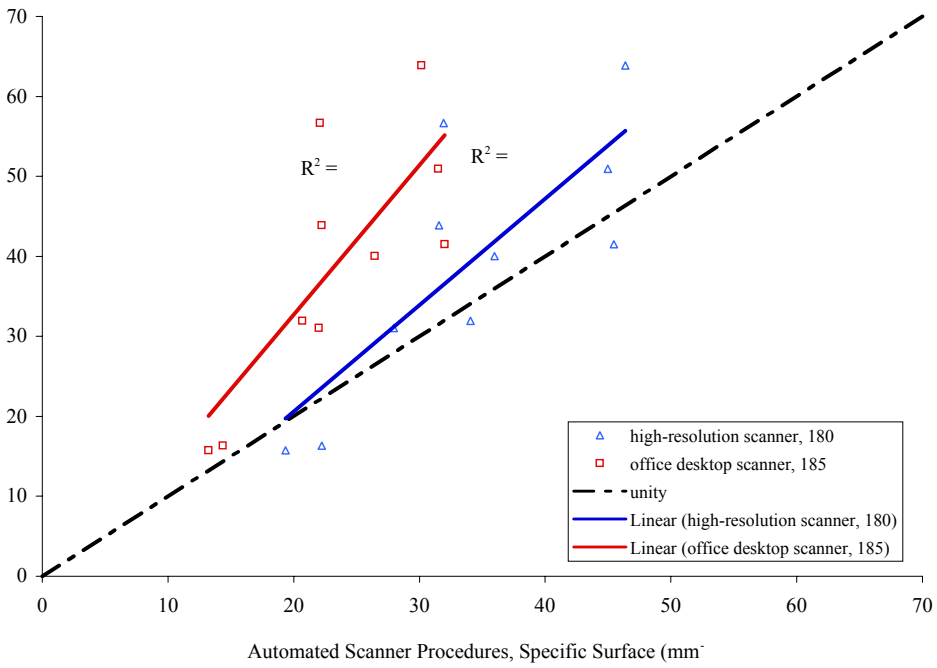

Figure 5-43: Plot to show correlation in specific surface values from manual and automatic procedures using optimum threshold as determined by maximum R square method.

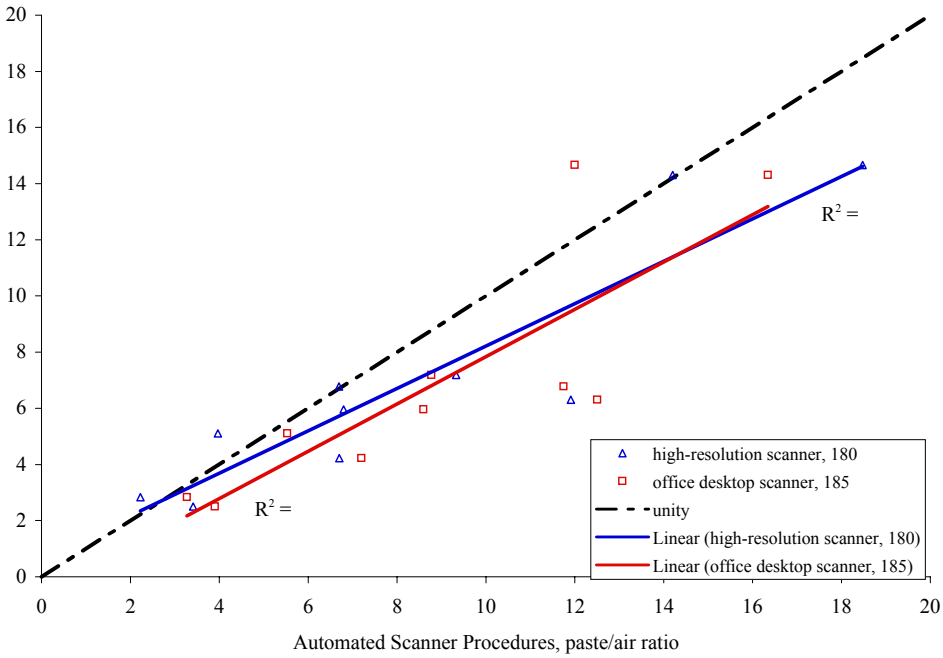

Figure 5-44: Plot to show correlation in paste to air ratio from manual and automatic procedures using optimum threshold as determined by maximum R square method.

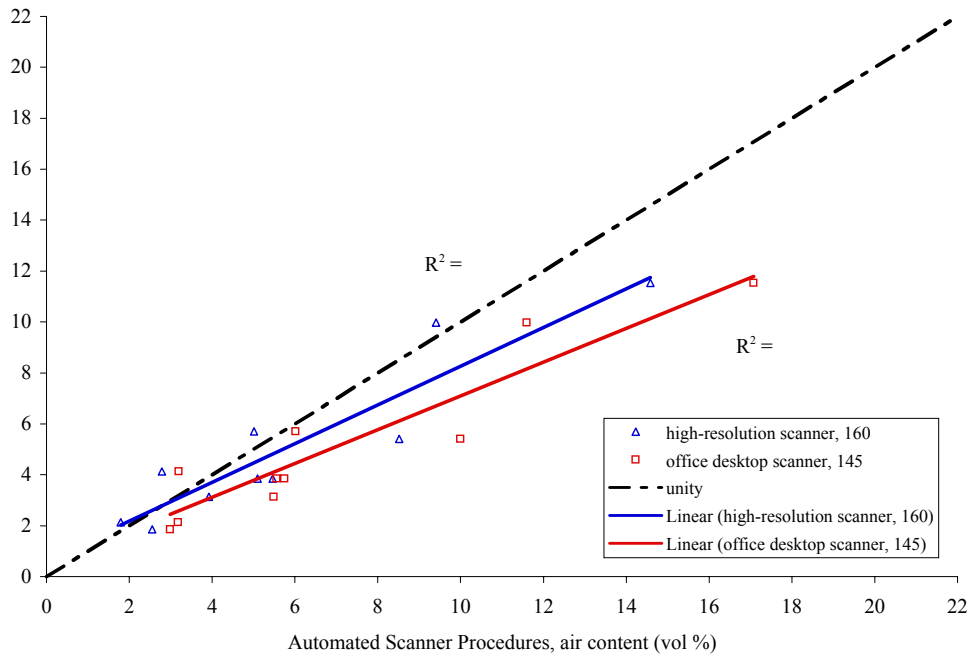

Figure 5-45: Plot to show correlation in air content values from manual and automatic procedures using optimum threshold as determined by minimum deviation from unity method.

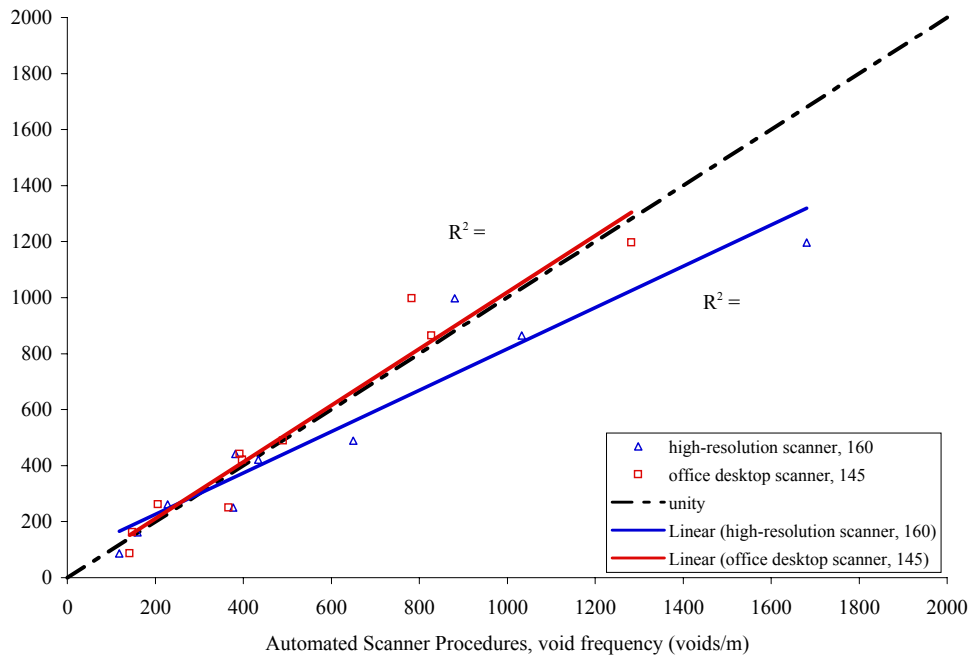

Figure 5-46: Plot to show correlation in void frequency values from manual and automatic procedures using optimum threshold as determined by minimum deviation from unity method.

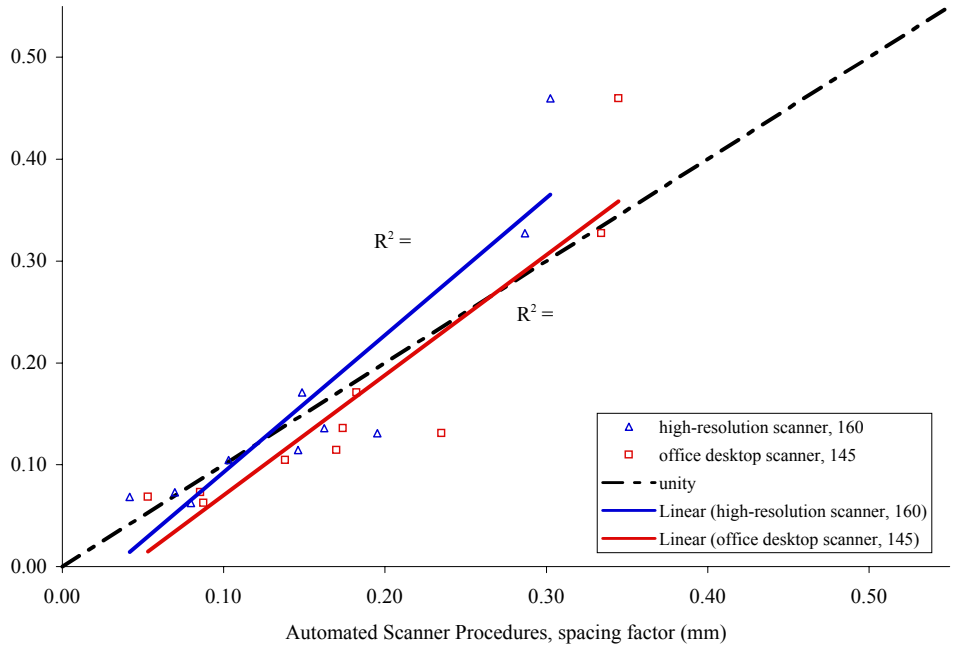

Figure 5-47: Plot to show correlation in spacing factor values from manual and automatic procedures using optimum threshold as determined by minimum deviation from unity method.

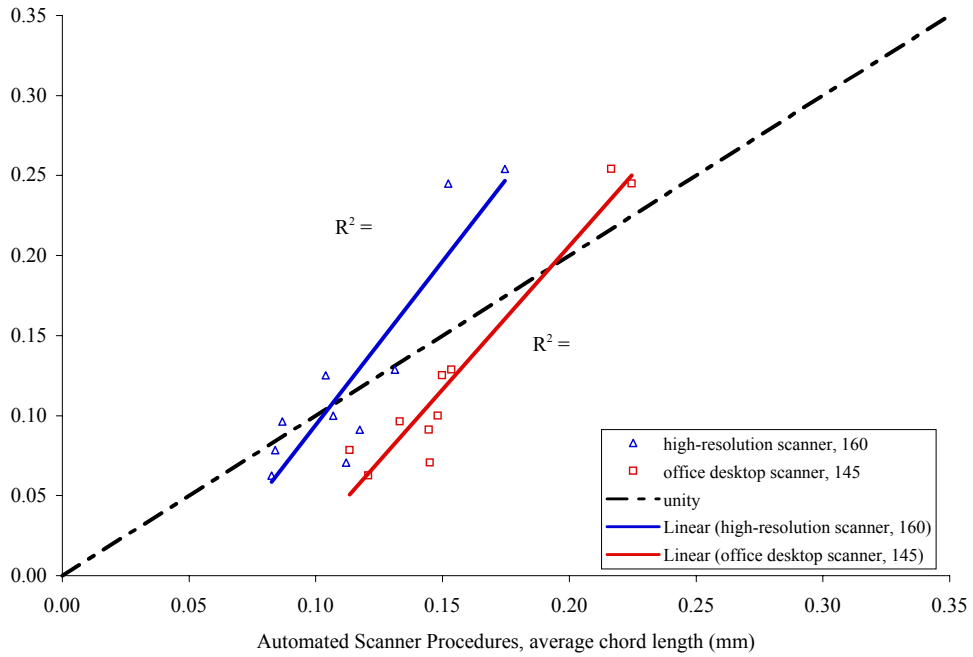

Figure 5-48: Plot to show correlation in average chord length values from manual and automatic procedures using optimum threshold as determined by minimum deviation from unity method.

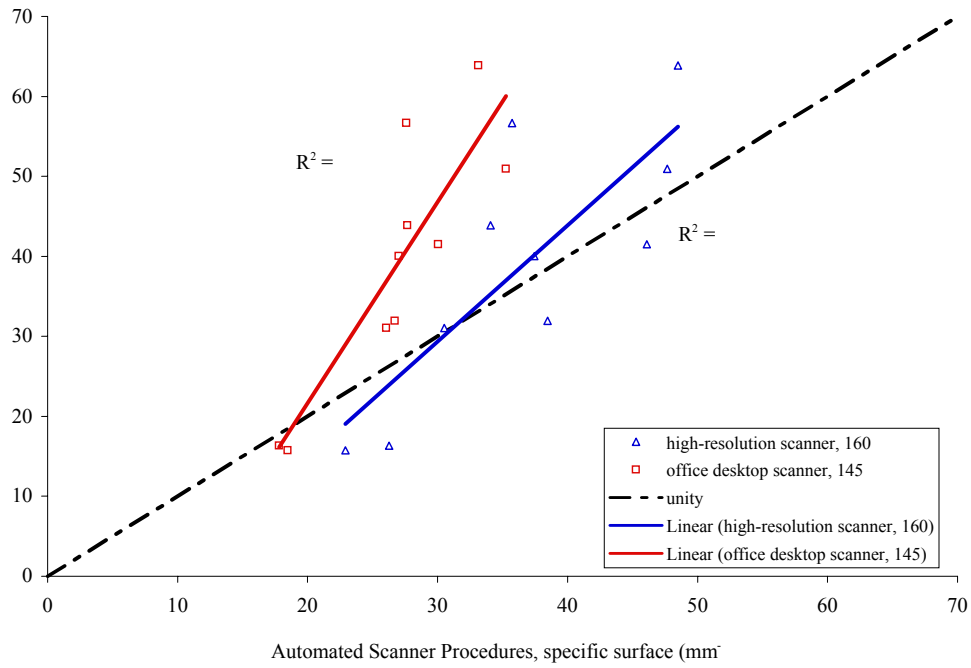

Figure 5-49: Plot to show correlation in specific surface values from manual and automatic procedures using optimum threshold as determined by minimum deviation from unity method.

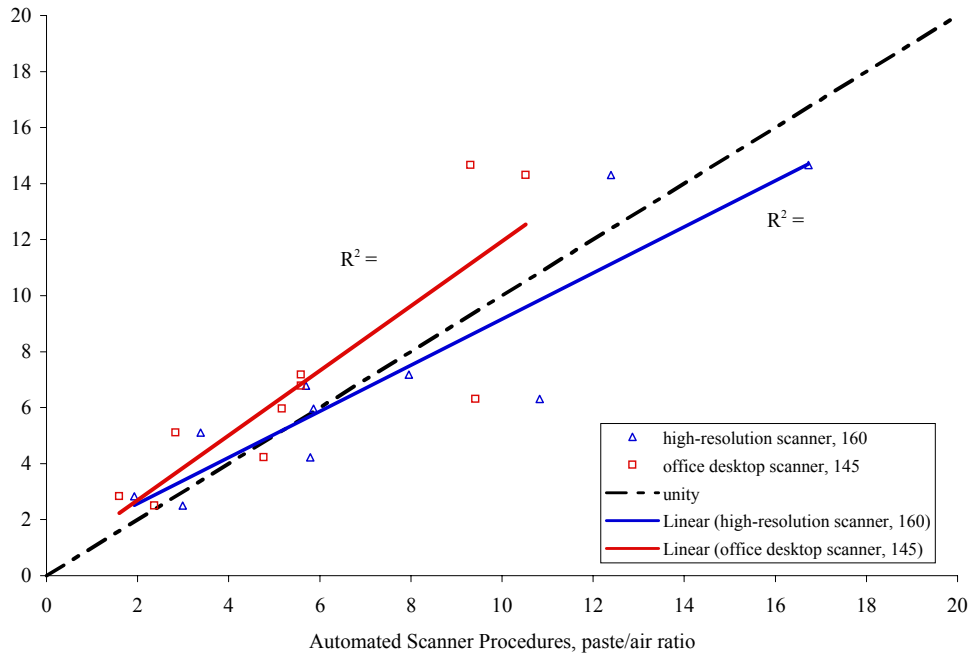

Figure 5-50: Plot to show correlation in paste to air ratio values from manual and automatic procedures using optimum threshold as determined by minimum deviation from unity method.

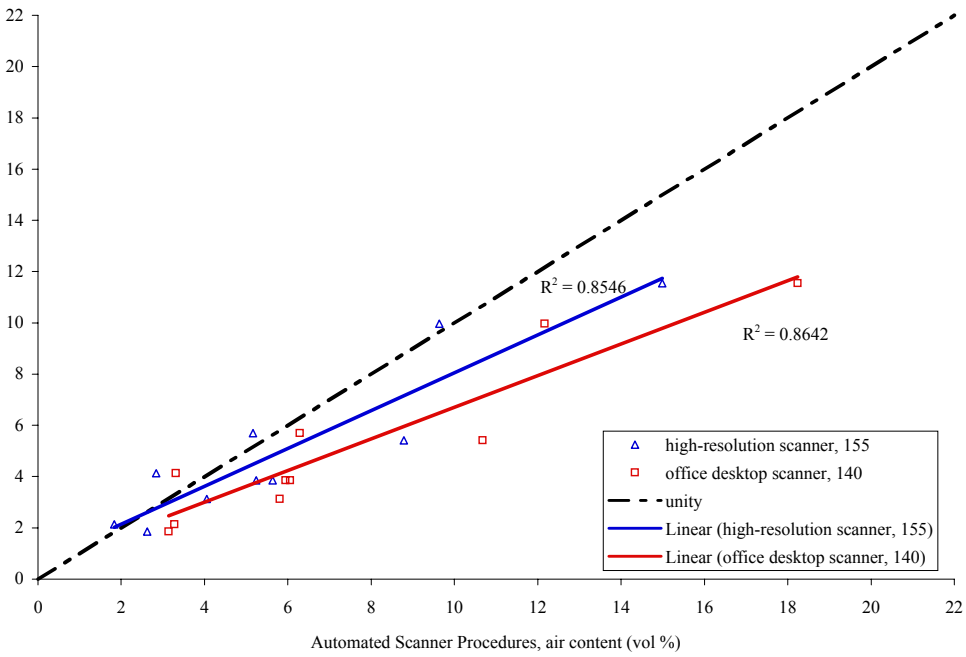

Figure 5-51: Plot to show correlation in air content values from manual and automatic procedures using optimum threshold as determined by maximum Kappa statistic method.

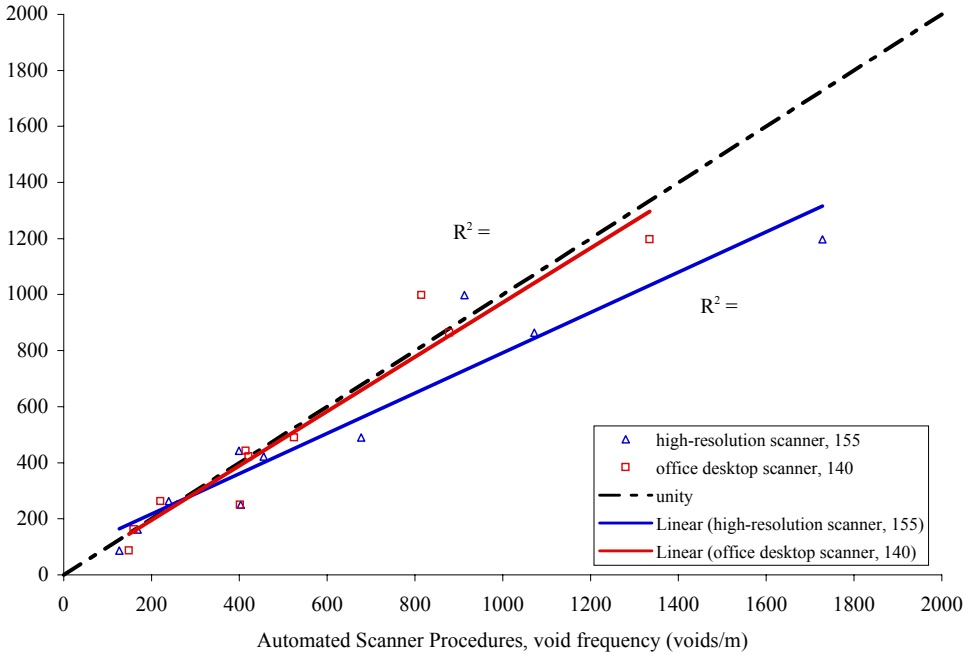

Figure 5-52: Plot to show correlation in void frequency values from manual and automatic procedures using optimum threshold as determined by maximum Kappa statistic method.

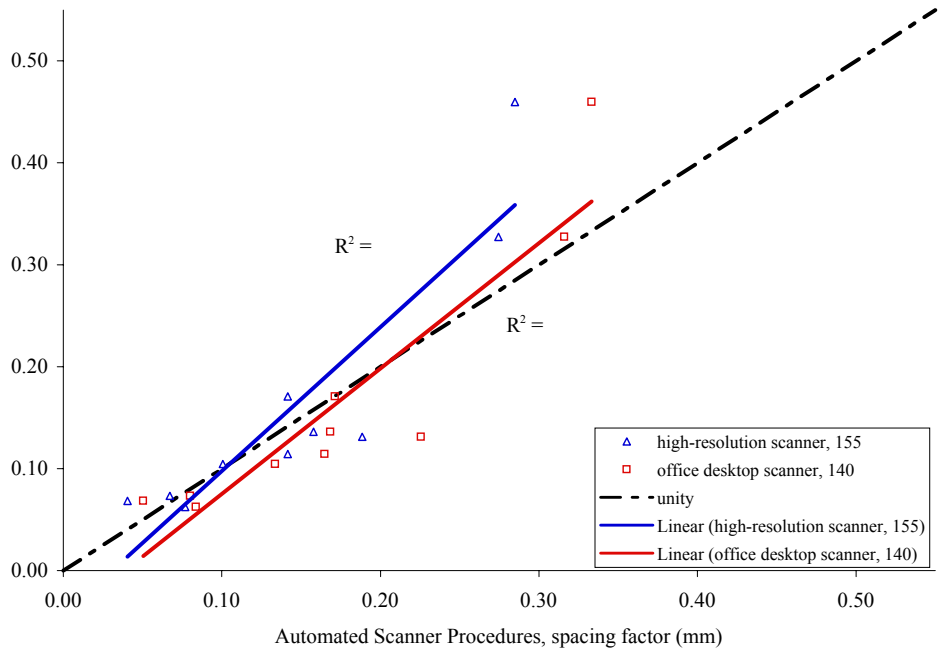

Figure 5-53: Plot to show correlation in spacing factor values from manual and automatic procedures using spacing factor as determined by maximum Kappa statistic method.

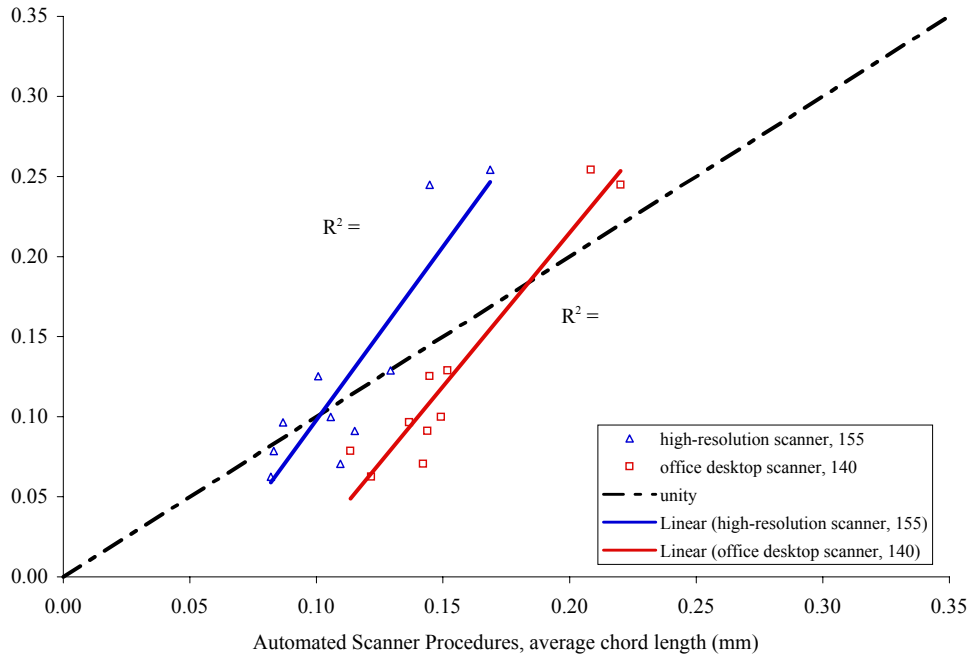

Figure 5-54: Plot to show correlation in average chord length values from manual and automatic procedures using optimum threshold as determined by maximum Kappa statistic method.

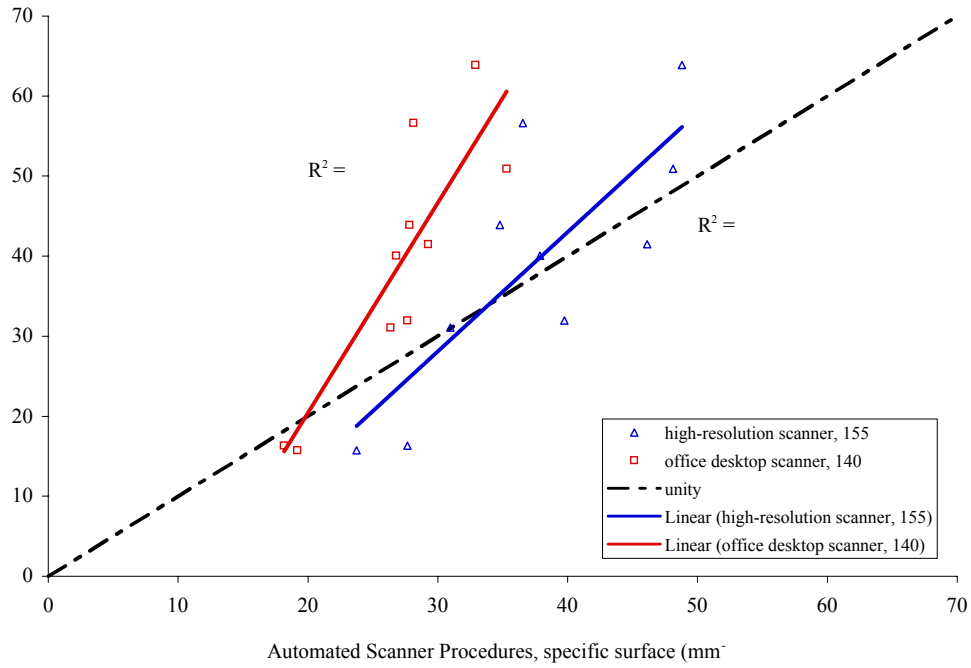

Figure 5-55: Plot to show correlation in specific surface values from manual and automatic procedures using optimum threshold as determined by maximum Kappa statistic method.

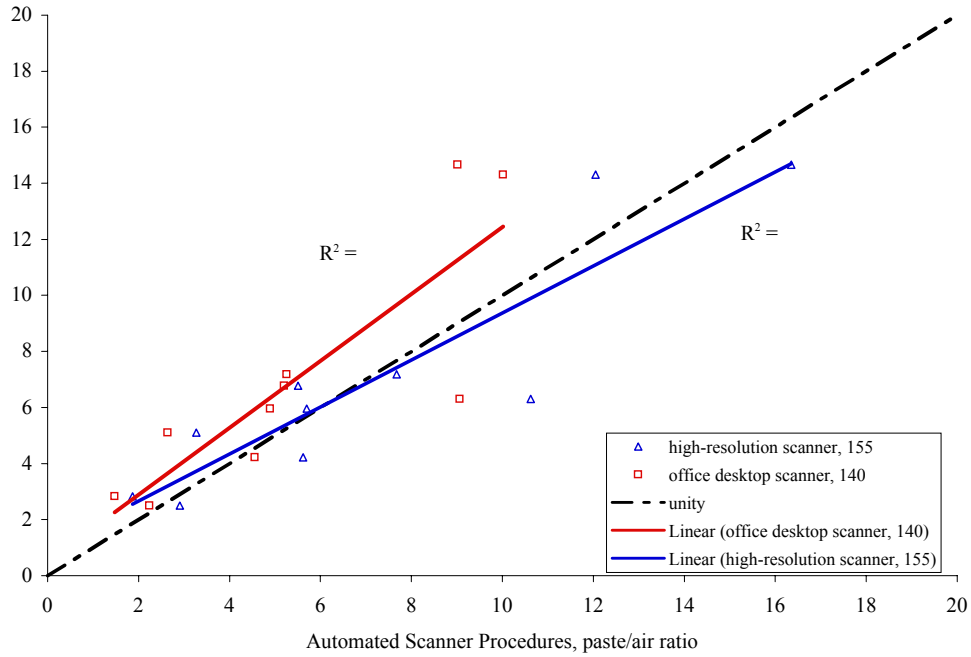

Figure 5-56: Plot to show correlation in paste to air values from manual and automatic procedures using optimum threshold as determined by maximum Kappa statistic method.

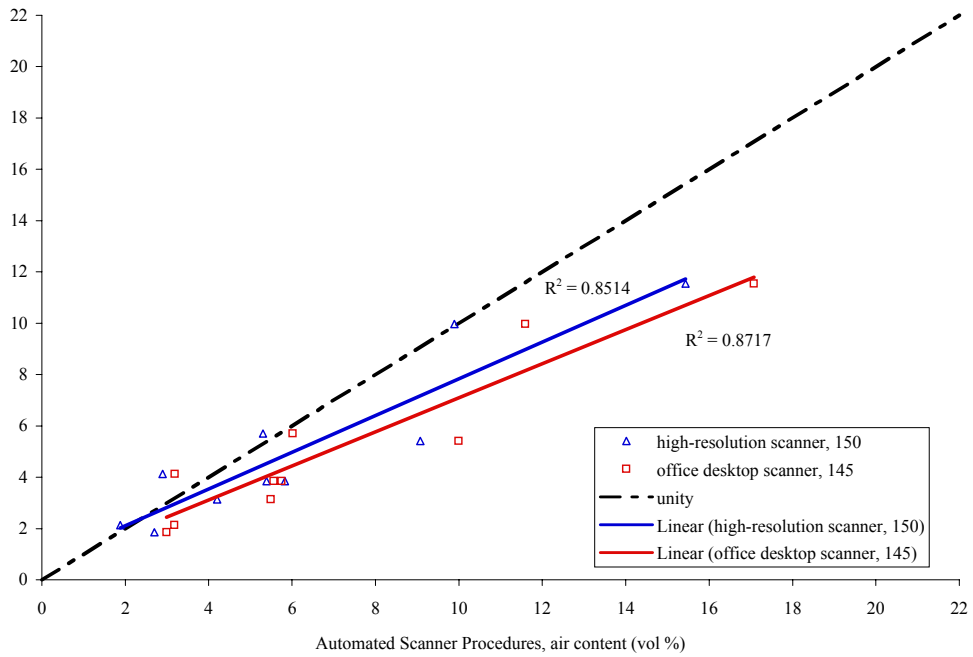

Figure 5-57: Plot to show correlation in air content values from manual and automatic procedures using optimum threshold as determined by error cross-over method.

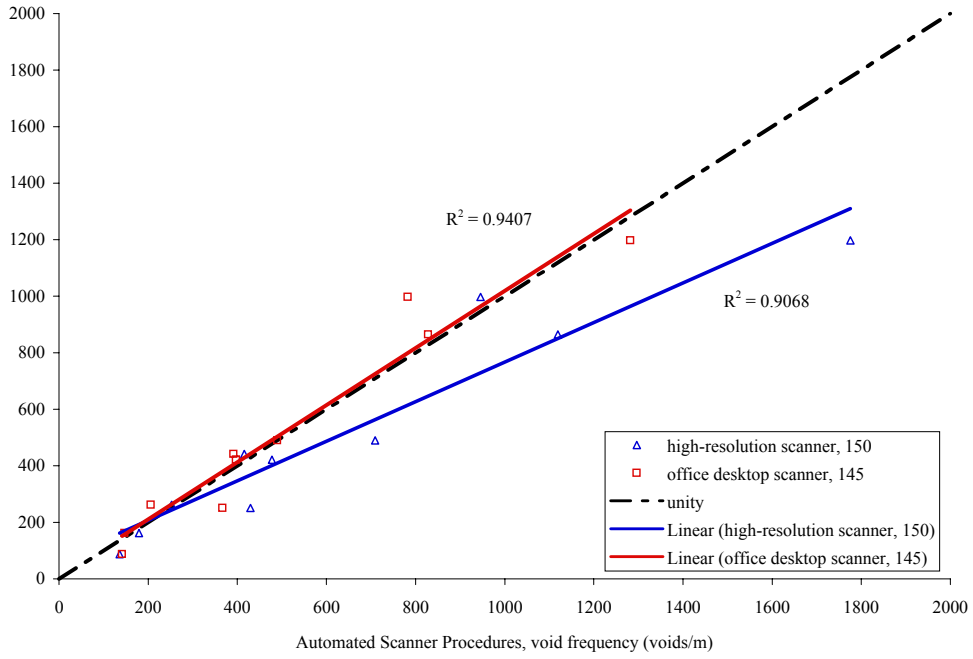

Figure 5-58: Plot to show correlation in void frequency values from manual and automatic procedures using optimum threshold as determined by error cross-over method.

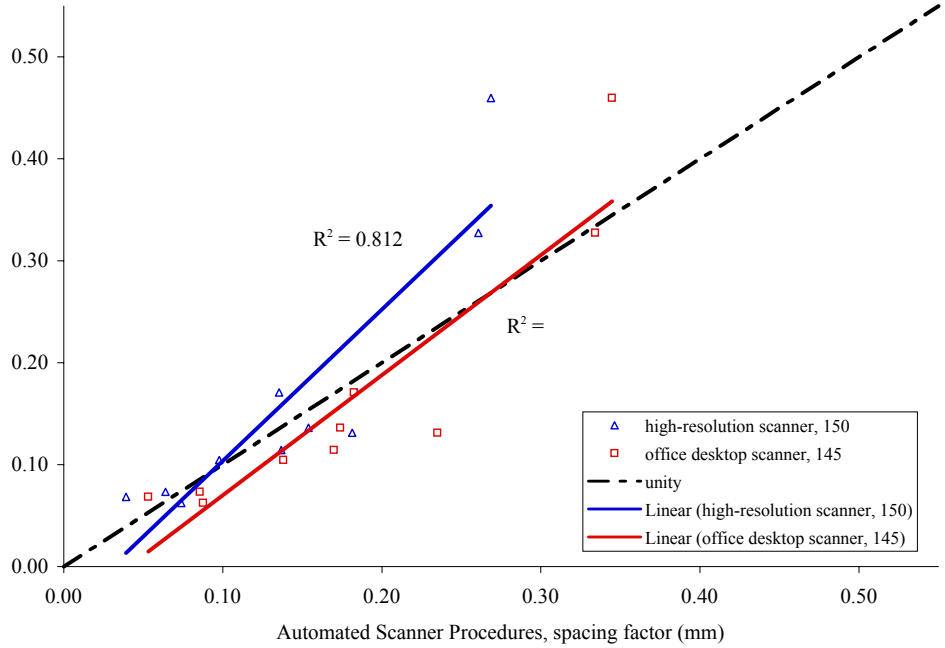

Figure 5-59: Plot to show correlation in spacing factor values from manual and automatic procedures using optimum threshold as determined by error cross-over method.

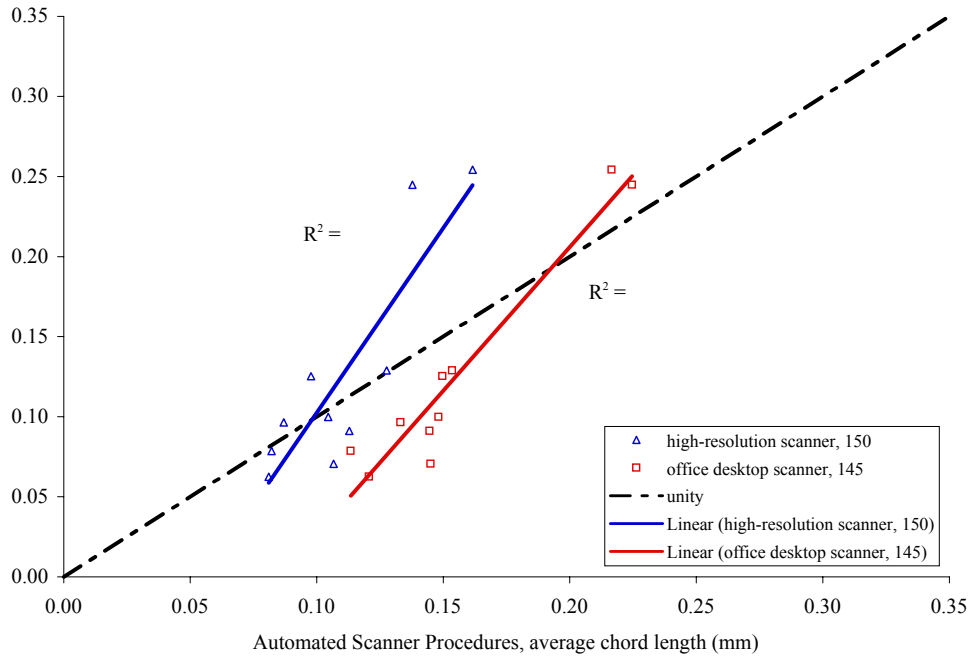

Figure 5-60: Plot to show correlation in average chord length values from manual and automatic procedures using optimum threshold as determined by error cross-over method.

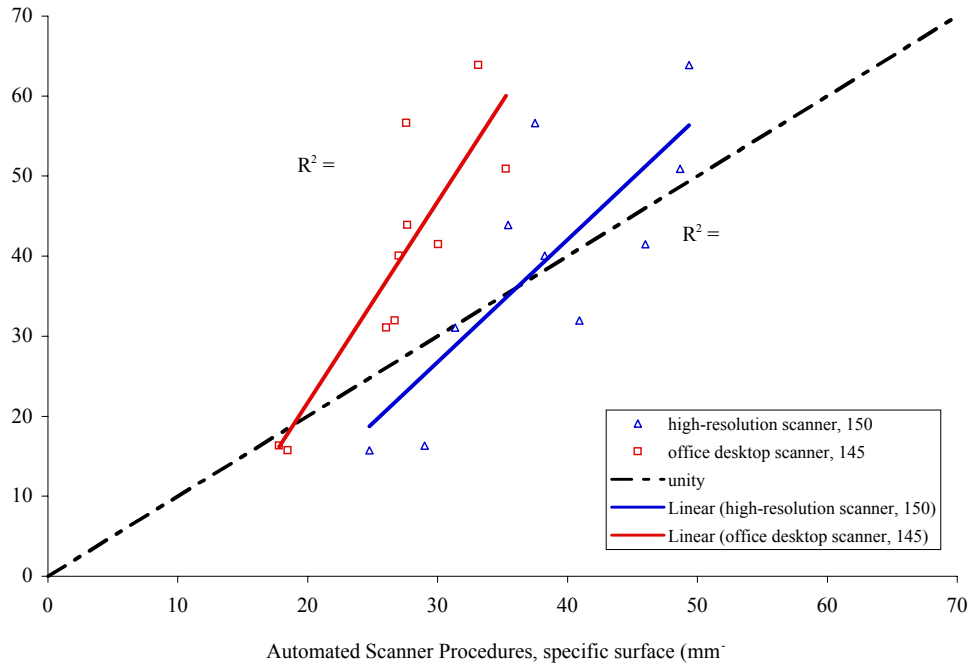

Figure 5-61: Plot to show correlation in specific surface values from manual and automatic procedures using optimum threshold as determined by error cross-over method.

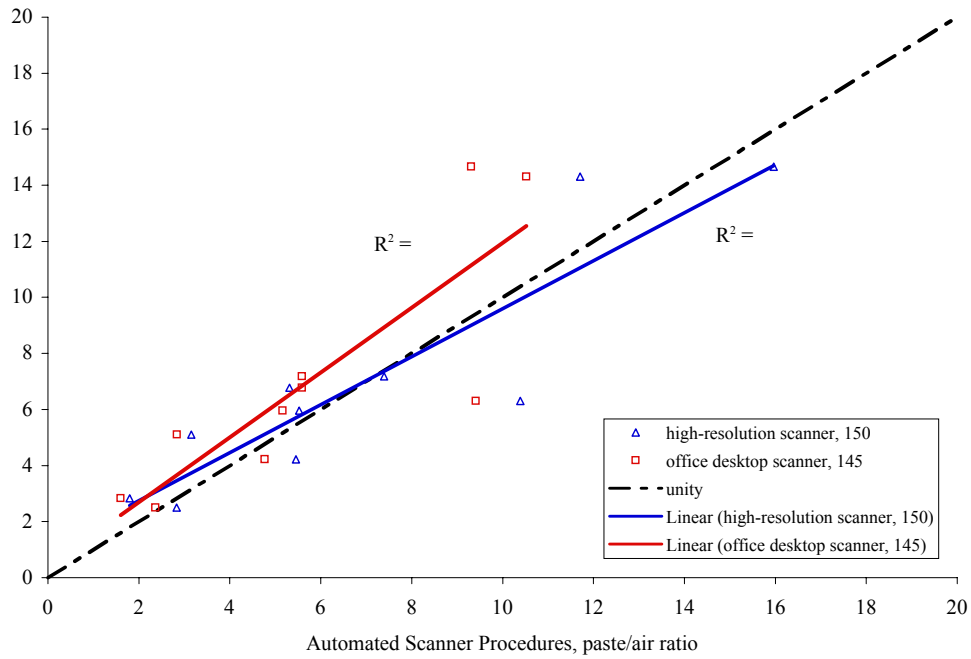

Figure 5-62: Plot to show correlation in paste to air ratio values from manual and automatic procedures using optimum threshold as determined by error cross-over method.

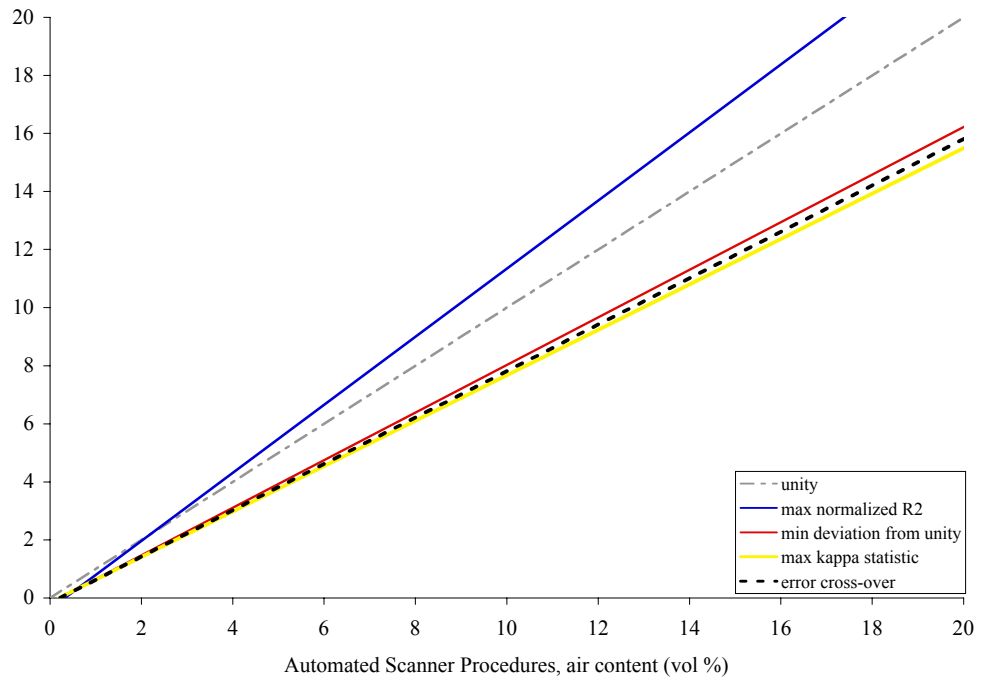

Figure 5-63: Plot to show linear best fit lines for correlation in air content values from manual and automatic procedures using the four different threshold optimization methods.

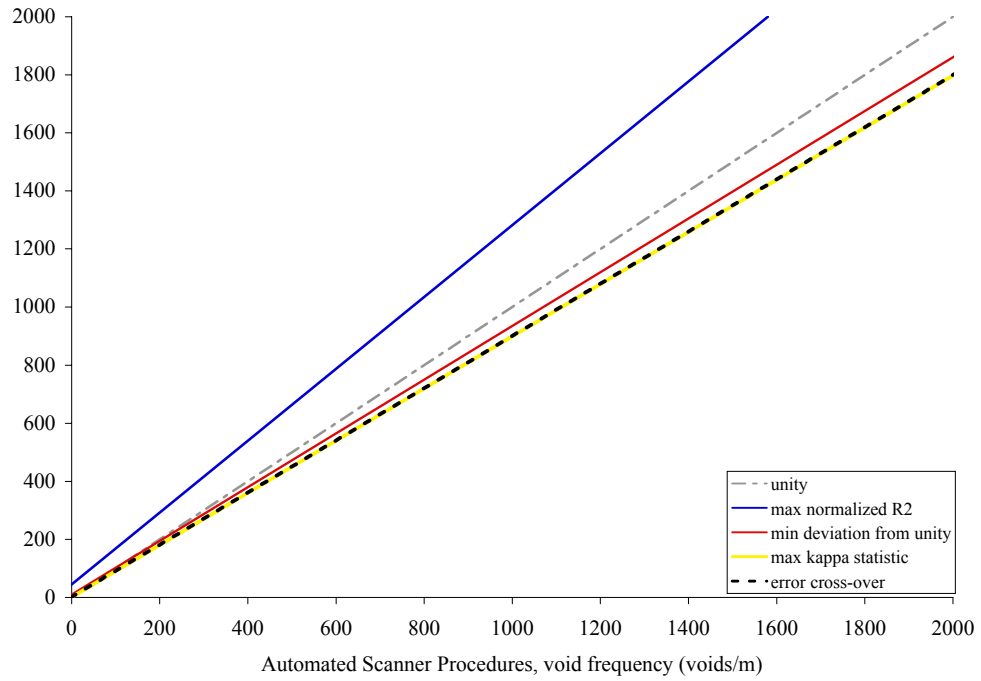

Figure 5-64: Plot to show linear best fit lines for correlation in void frequency values from manual and automatic procedures using the four different threshold optimization methods.

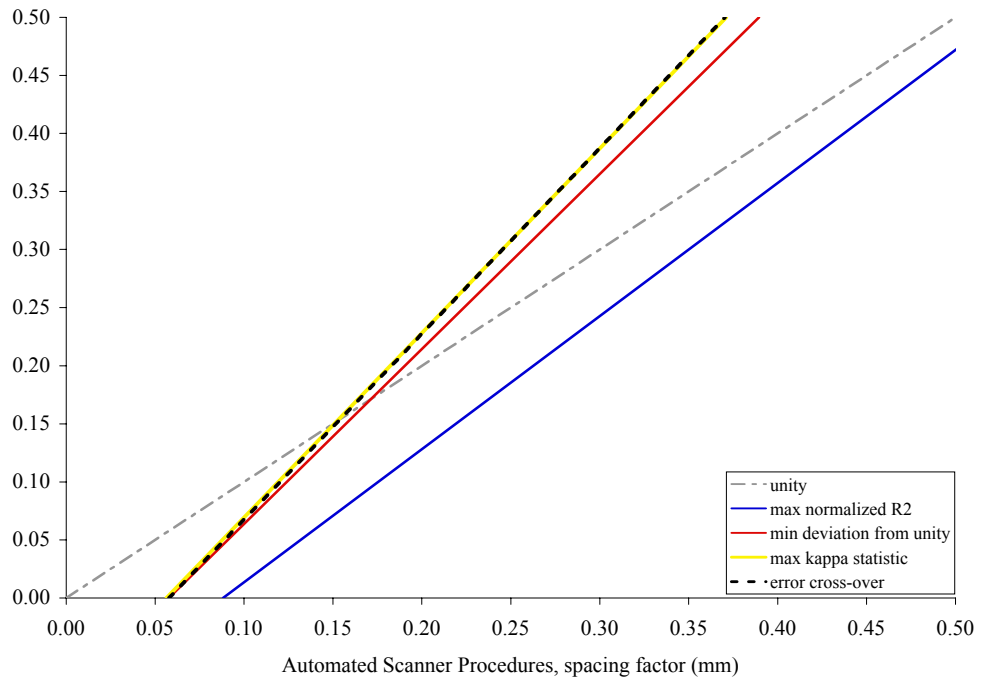

Figure 5-65: Plot to show linear best fit lines for correlation in spacing factor values from manual and automatic procedures using the four different threshold optimization methods.

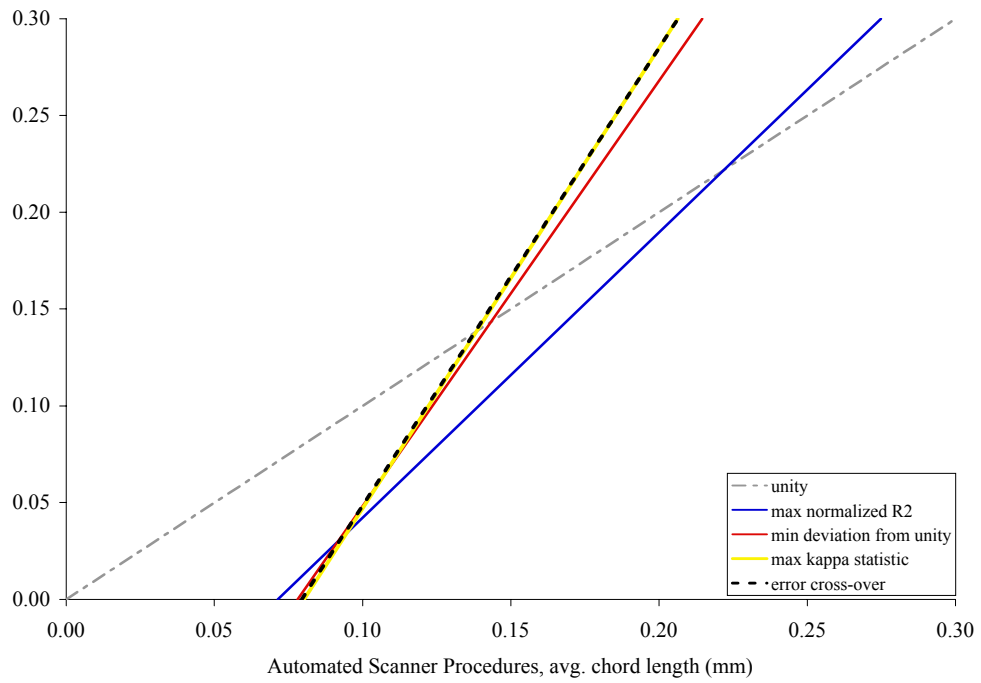

Figure 5-66: Plot to show linear best fit lines for correlation in average chord length values from manual and automatic procedures using the four different threshold optimization methods.

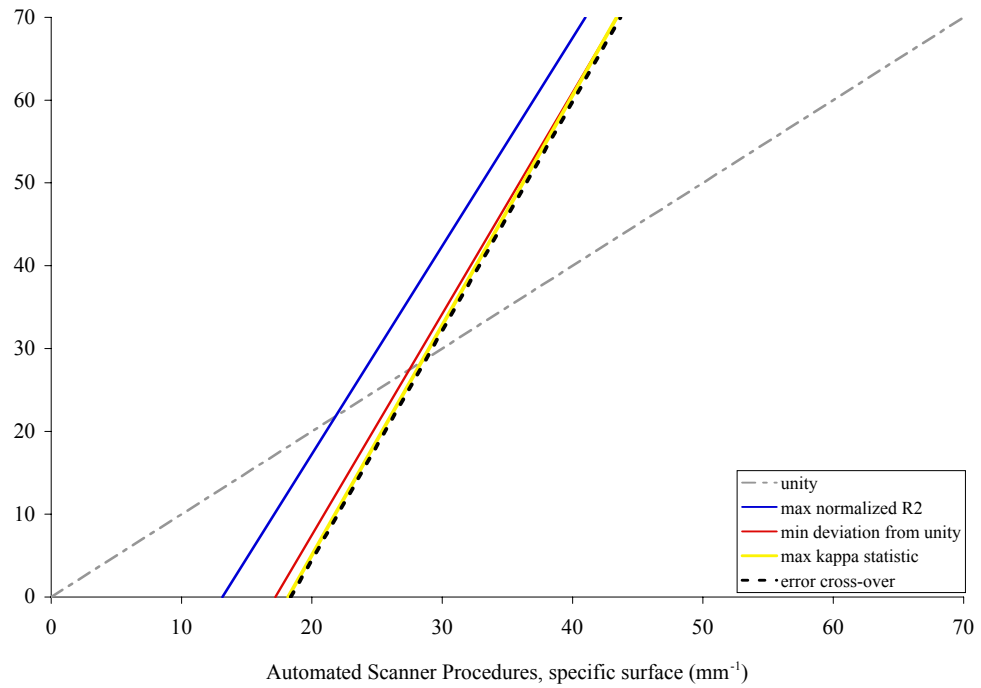

Figure 5-67: Plot to show linear best fit lines for correlation in specific surface values from manual and automatic procedures using the four different threshold optimization methods.

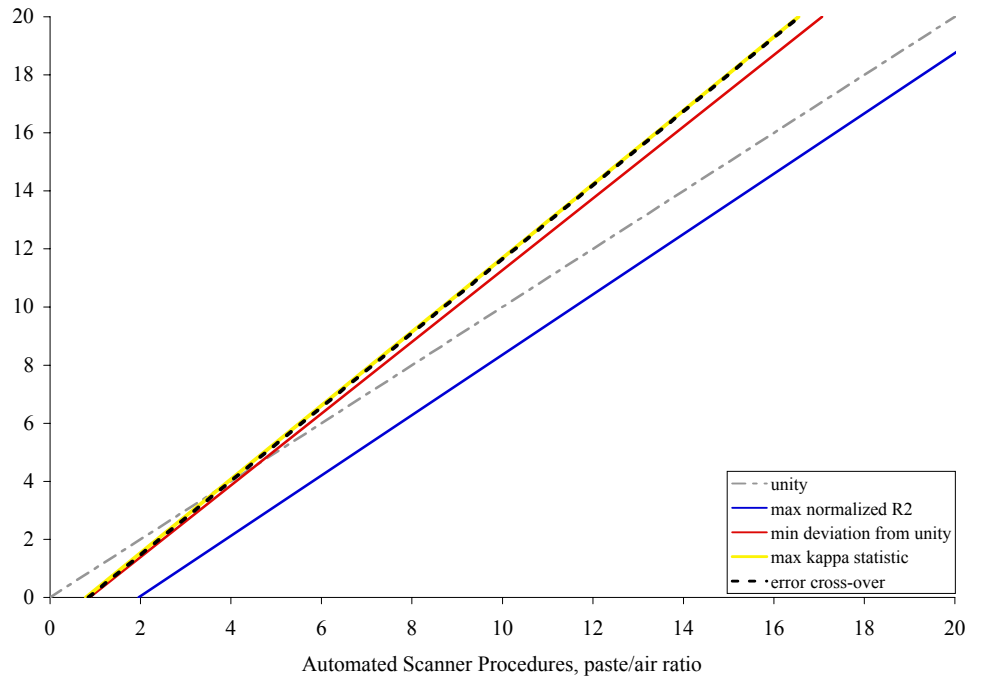

Figure 5-68: Plot to show linear best fit lines for correlation in paste to air ratio values from manual and automatic procedures using the four different threshold optimization methods.

Table 5-11. Comparison of air void parameter results using threshold level set according to minimum deviation from unity method with results from manual modified point count.

		Sample ID									
Air Void Parameters	Method	AE-H	MA-H	VR-H	AE-O	MA-O	VR-O	AE-L	MA-L	VR-L	VRFA-L
Air Content (vol %)	High Resolution Scanner	14.6	8.5	9.4	5.0	5.5	5.1	2.8	2.6	1.8	3.9
	Office Desktop Scanner	17.1	10.0	11.6	6.0	5.6	5.7	3.2	3.0	3.2	5.5
	Manual	11.5	5.4	10.0	5.7	3.9	3.9	4.1	1.9	2.1	3.1
Void Frequency (voids/m)	High Resolution Scanner	1681	1033	880	382	650	435	160	228	118	377
	Office Desktop Scanner	1282	828	783	392	490	398	147	206	141	366
	Manual	1197	864	998	442	490	422	163	262	87	250
Spacing Factor (mm)	High Resolution Scanner	0.042	0.070	0.080	0.162	0.103	0.146	0.287	0.195	0.303	0.149
	Office Desktop Scanner	0.053	0.086	0.088	0.174	0.138	0.170	0.334	0.235	0.345	0.182
	Manual	0.068	0.073	0.062	0.136	0.104	0.114	0.327	0.131	0.460	0.171
Average Chord Length (mm)	High Resolution Scanner	0.087	0.082	0.107	0.131	0.084	0.117	0.175	0.112	0.152	0.104
	Office Desktop Scanner	0.133	0.121	0.148	0.154	0.113	0.145	0.217	0.145	0.225	0.150
	Manual	0.096	0.063	0.100	0.129	0.079	0.091	0.254	0.071	0.245	0.125
Specific Surface (mm^{-1})	High Resolution Scanner	46.1	48.5	37.4	30.5	47.7	34.1	22.9	35.7	26.3	38.5
	Office Desktop Scanner	30.0	33.1	27.0	26.1	35.3	27.7	18.5	27.6	17.8	26.7
	Manual	41.5	63.9	40.0	31.0	50.9	43.9	15.7	56.7	16.3	31.9
Paste to Air Ratio	High Resolution Scanner	1.9	3.4	3.0	5.8	5.7	5.9	10.8	12.4	16.7	8.0
	Office Desktop Scanner	1.6	2.8	2.4	4.8	5.6	5.2	9.4	10.5	9.3	5.6
	Manual	2.8	5.1	2.5	4.2	6.8	6.0	6.3	14.3	14.7	7.2

5.1.12 Visual assessment of scanned images

Appendix A contains a series of micrographs collected from the stereo-microscope during the manual modified point counts. These are compared with corresponding areas collected by the two scanners, both before and after minimum deviation from unity threshold application for the ten samples.

There was an improvement in the overall accuracy with the more rigorous sample preparation as compared to the initial sample preparation (97% versus 90%). Most important, the misclassification of non air points as air was greatly reduced with better sample preparation (4% versus 9%). This improvement is reflected in the improved spacing factor and void frequency correlations between the manual and automated methods. Further improvements might be made through implementation of digital filtering, but it is easy to appreciate the fact that most researchers dealing with these types of analyses identify the sample preparation as the key factor in obtaining quality results. Careful examination of the image comparisons in Figures A-1 through A-50 show that even more care could be taken during sample preparation, particularly in the darkening of voids in aggregates, and during the wiping away of excess powder (many of the larger voids exhibit dark smudges due to contamination of the white powder with the black pigment).

5.2 High Resolution CT Scanner Air Void System Analysis

Samples of the concrete specimens produced were analyzed using a Micro-CT Scanner. Computer tomography (CT) is a well established radiographic technique that has been used for medical diagnosis for decades and higher-energy industrial scanners are finding increasing applications outside of medicine. One of the main advantages of CT is that it can image a single planar cross-sectional slice of a specimen without interference from other cross sections. This is in contrast to conventional radiography, which represents all planes through the specimen.

CT scanners typically produce multiple 2-D x-ray images, each representing cross sections or slices (also known as tomographs) through the specimen. The tomographs may be stacked one on top of one another to create a three-dimensional volume. In a linear array system, tomographic images are generated by projecting a thin-beam of x-rays through one plane of the specimen at many different angles. As x-ray photons pass through a specimen, some are absorbed while transmitted photons are measured by an x-ray detector. By collecting this data over many angles, a cross section representing the attenuation parameter of each element within the slice can be reconstructed by a computer (the reconstruction technique is known as back projection). A schematic showing the principal of CT measurements and reconstruction is shown in Figure 5-69.

In the more innovative volume CT system, the fan beam is extended to a cone beam and thereby collects 2-D projections at once. Specialized reconstruction algorithms process the 2-D cone-beam projections into a volume that is the equivalent of many simultaneous, contiguous CT slices. Figure 5-70 shows the main components of fan-beam and cone-beam CT scanners.

Preliminary studies (Weise et al, 2000) indicated that CT scanning was a promising tool for evaluating air-void parameters and other features of concrete but, at the time, the technique

was limited by its resolution as only air voids larger than 40 microns could be detected. Micro-CT scanners available today claim resolutions of 10 microns or less.

Small core samples from specimens P1, Q1, and R1 (100 x 200 mm cylinders accompanying the freeze-thaw prisms produced) were extracted by drilling and analyzed using the Micro-CT. The samples from specimen Q1 were used in a preliminary evaluation of the new CT. Images from sample Q1 are shown below in Figure 5-71 .

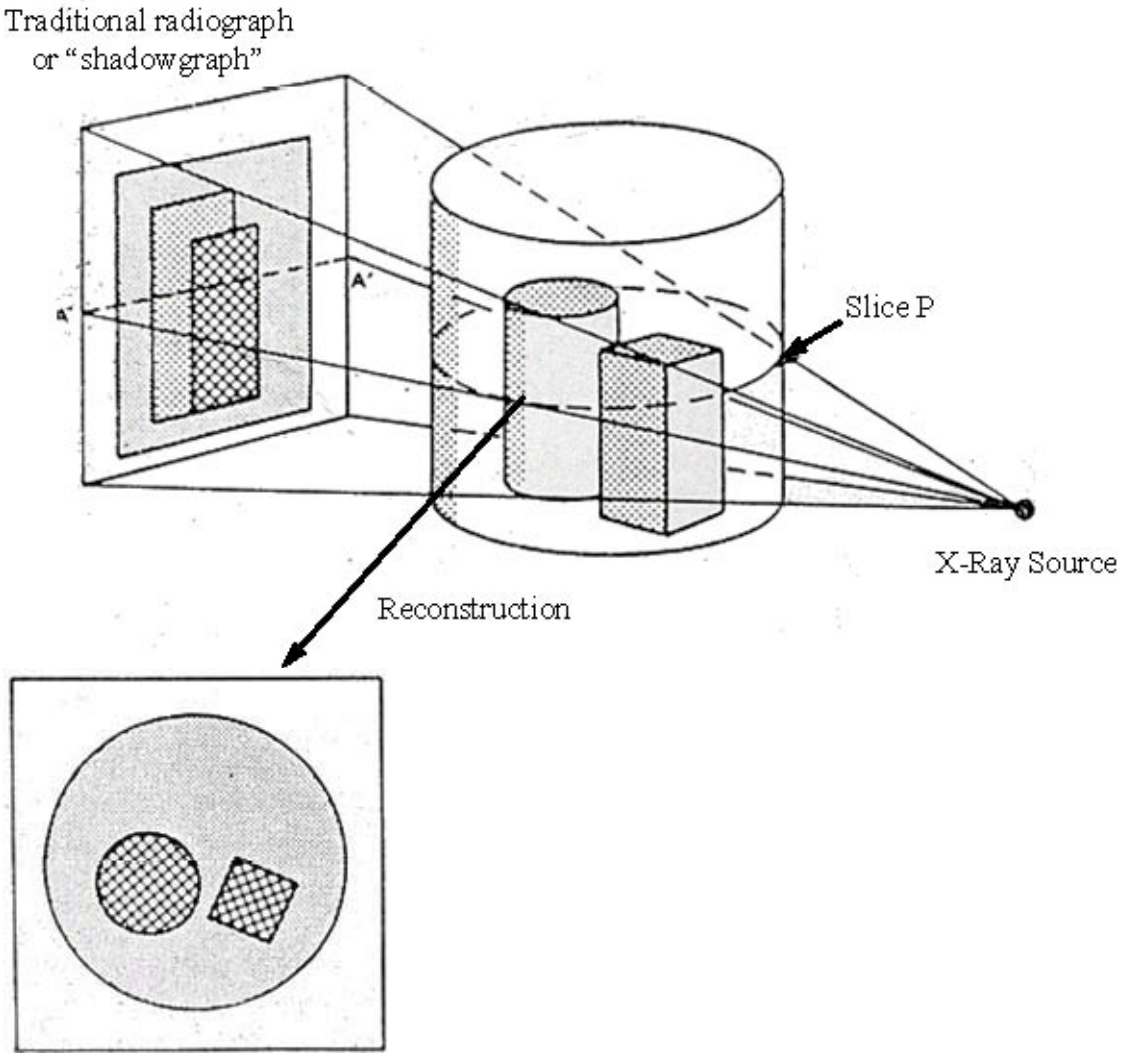

Figure 5-69. Schematic showing principal of computer tomography (CT) and comparison with traditional radiography (Source of original Figures unknown).

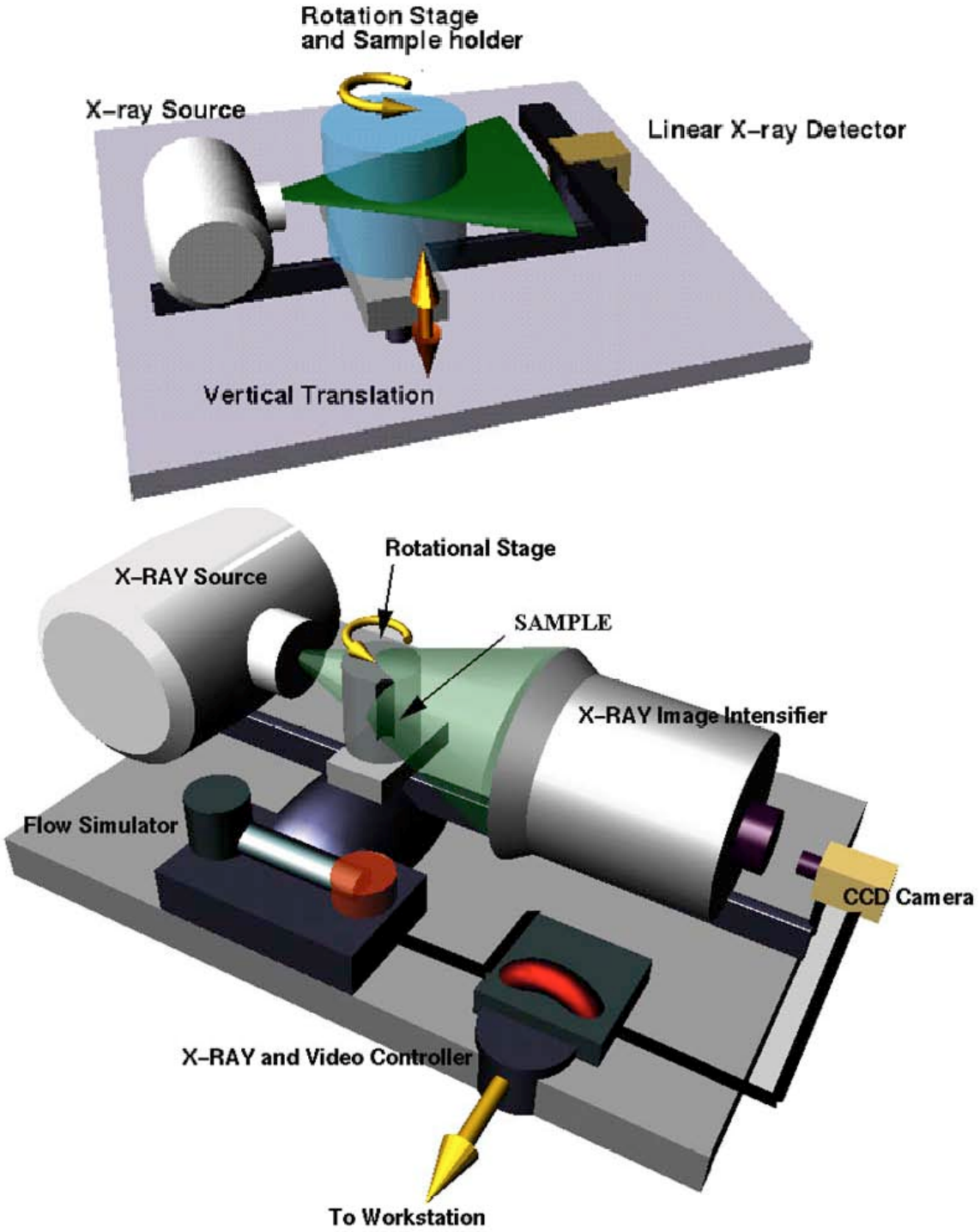

Figure 5-70. Comparison of fan-beam CT (top) and cone-beam CT (bottom) (Source of original Figures unknown).

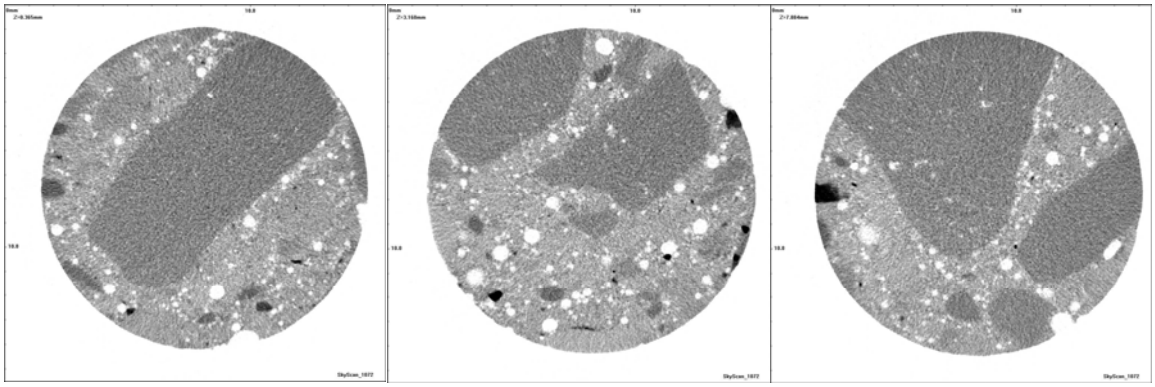

Figure 5-71. Two-dimensional slices through concrete samples Q1.

This report includes data from the analysis of samples taken from specimens P1 and R1. Mix P was selected as it was the only mix that failed to perform adequately in the ASTM C 666 freeze-thaw test and it also had unsatisfactory air-void parameters. Mix R was selected as it is from the same mix series as mix P, but contains a higher dose of vinsol resin air-entraining agent, has a satisfactory air-void system and performed well in freeze-thaw testing.

Ten core samples approximately 10 mm diameter x 28 mm long were cut from each of the specimens labeled P1 and R1. The size of the sample was limited by the sample holder of the Micro-CT scanner, hence a large number of samples were used per mix in attempt to ensure that a represented volume of concrete was tested. Each sample was scanned using a Skyscan® 1072 high-resolution desk-top Micro-CT system. The samples were rotated through 180° in increments of 0.45° and an x-ray image was taken at each step (i.e. 400 scans per sample). The resulting data were then reconstructed into a series of approximately 900 horizontal, circular slices using a resolution (pixel size) of 13 microns. The output for each slice is a bitmap in which each 13-microns pixel is assigned a gray level from 0 (black) to 255 (white). The value of the gray level is a related to the attenuation coefficient of material represented by the pixel. Generally the amount that x-rays are attenuated is related to the electron density and, to a lesser extent, the atomic number of the material through which the x-ray passes. Dense materials will result in low level-level values (i.e. dark shades) and voids will result in high level-level values (i.e. near white). In principal this should make air voids easy to detect because of the large density contrast between the voids and solid phases of concrete.

Figure 5-72 shows results of a CT scan of sample R1. The rectangular image on the left shows one of the 400 radiographs (shadowgraph). The dark gray area dominating the central portion of the sample is a coarse aggregate particle. The circular image on the right is one of the 900 CT slices reconstructed for this sample. The large aggregate particle is clearly discernible in the center of the slice as are other aggregate particles and air voids.

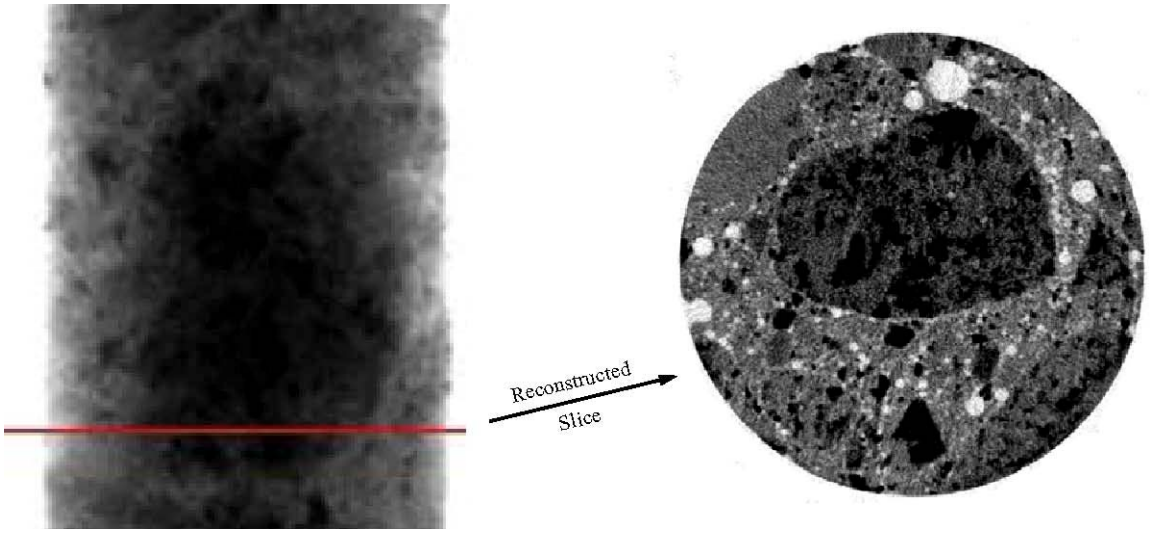

Figure 5-72. Example of CT scanning (sample R1)

Features within a selected range of level-level values can be selected using image analysis software. Figure 5-73 shows a slice through sample R1 (slice R10897). Areas of interest have been selected using three different threshold values, these being 140 to 255, 170 to 255 and 210 to 255. The selected areas have been shaded black in these images. The total cross-sectional area and the area of the selected features can be calculated by the software and used to determine relative proportion of the selected area. For the case in Figure 5-73 the selected areas represent 15.4%, 8.7% and 4.6%, respectively, when the lower thresholds are set at gray levels of 140, 170 and 210.

Three-dimensional images of selected objects can also be produced by "stacking" contiguous slices together. Figure 5-74 shows three-dimensional images of samples P1 and R1 using threshold values of 181 to 255. There are clearly few lower-density objects (e.g. air voids) in P1 although it appears that the objects present are, to some extent, larger than those observed in R1. The location of the large aggregate particle in R1 can be discerned as no voids are detected in that location.

Ten samples from mix R (R1 to R10) and mix (P1 to P10) were scanned and reconstructed and the resulting data were analyzed using Skyscan CT-Analyzer and CT-Volume software. A gray level threshold of 181-255 was used to detect low-density objects. The selection of the threshold values was somewhat arbitrary at this stage. Selected data from the analysis are presented in Table 5-12.

Noteworthy, CT scanning is a promising emerging technique for measuring the air-void characteristics of fresh concrete as shown in Figure 5-75.

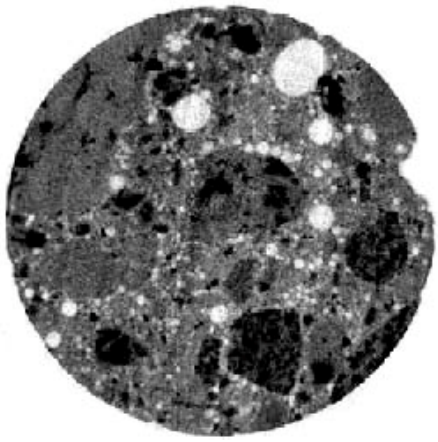

CT image slice R10897

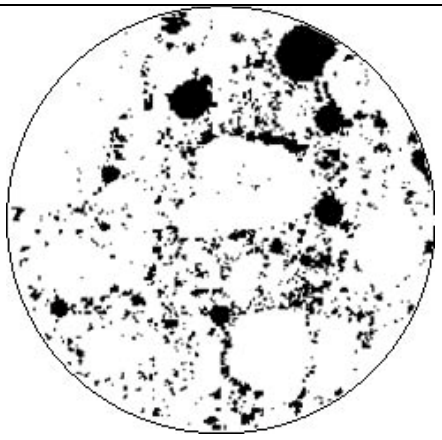

CT image slice R10897
Threshold: 140 – 255
Measured Air Content: 15.4%

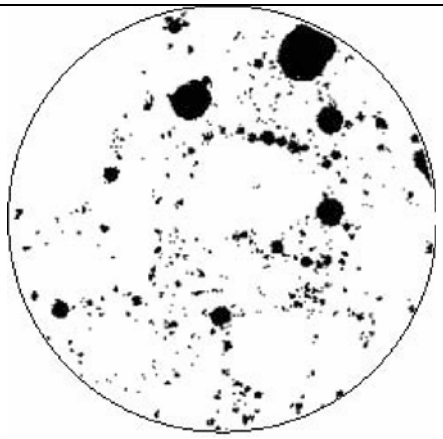

CT image slice R10897
Threshold: 170 – 255
Measured Air Content: 8.7%

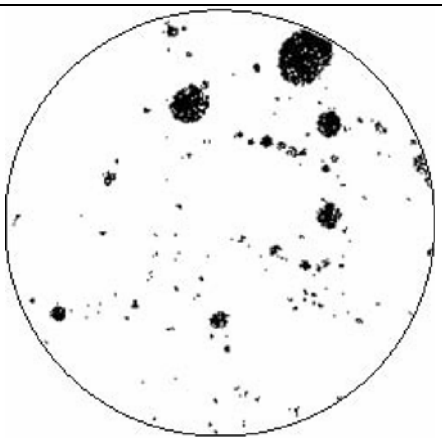

CT image slice R10897
Threshold: 210 – 255
Measured Air Content: 4.6%

Figure 5-73. Selecting area of interest using different grayscale levels.

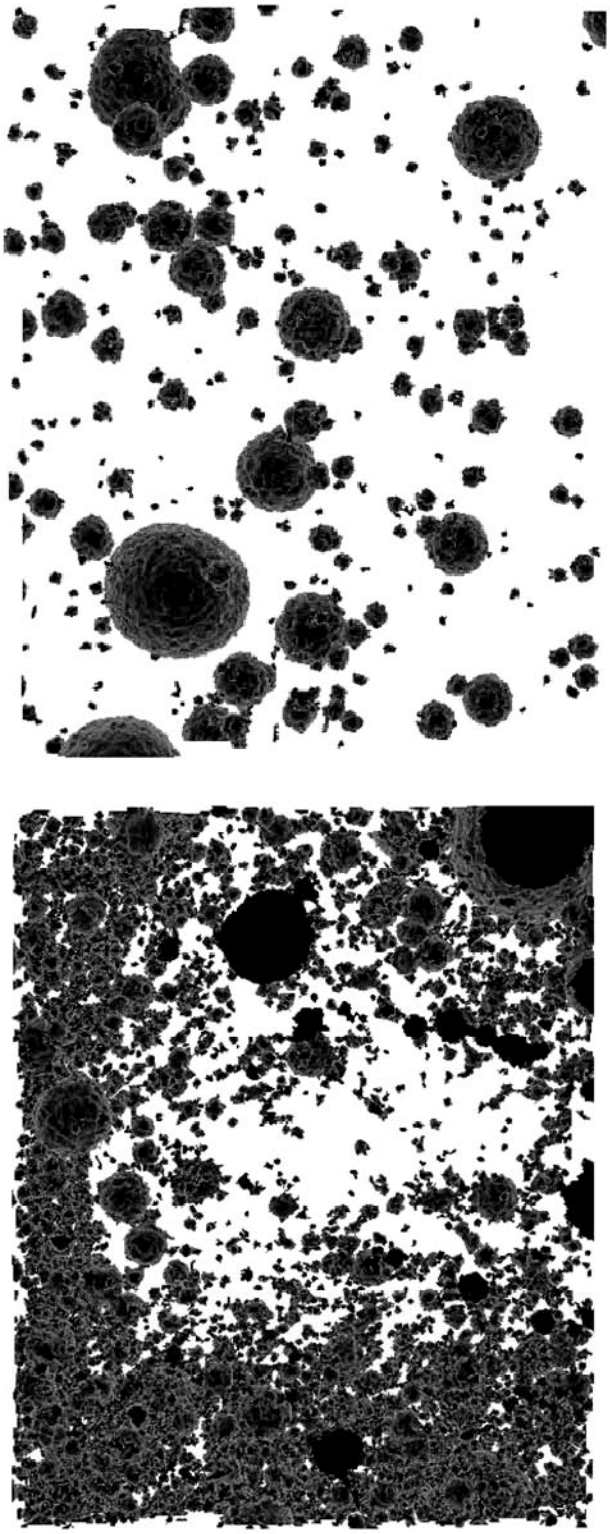

Figure 5-74. Three-dimensional image of air voids in P1 (top) and R1 (bottom)

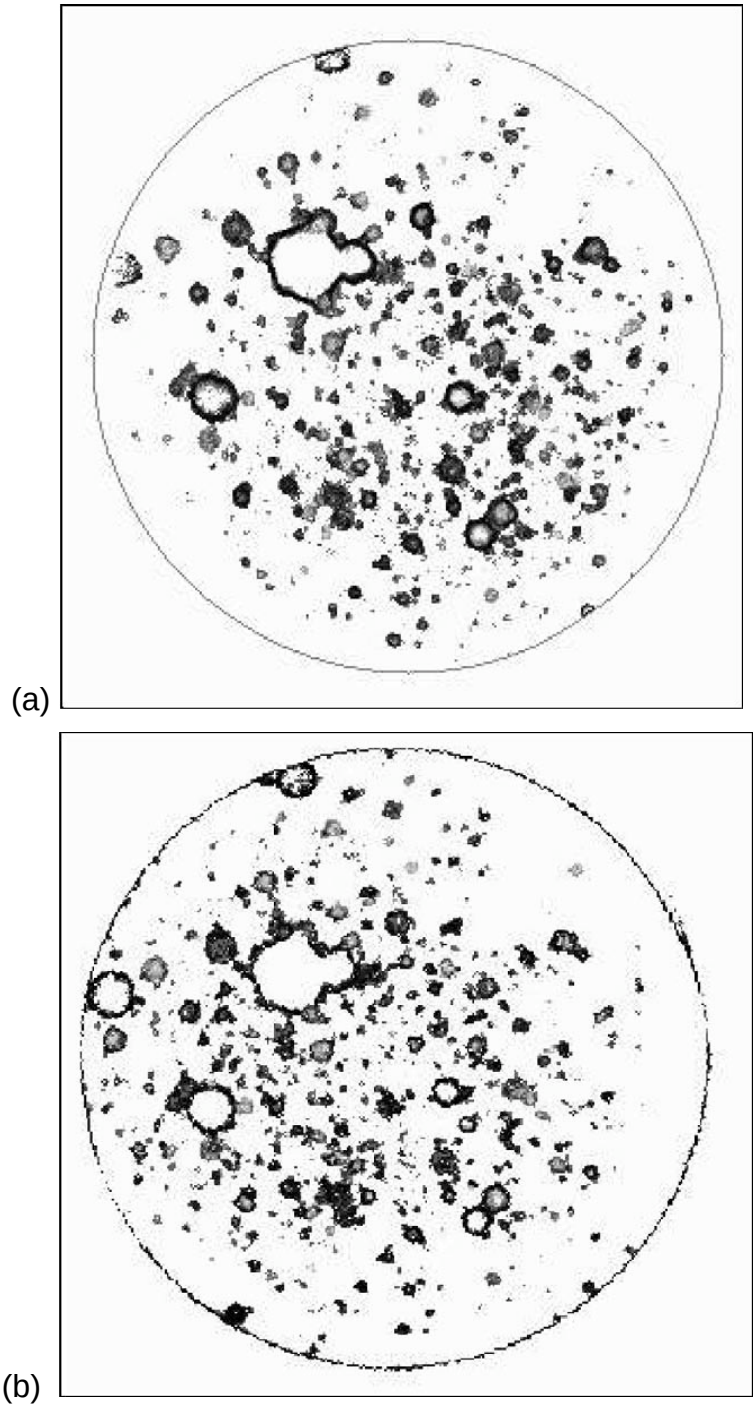

Figure 5-75. CT Images of mortar immediately after mixing (a) and after hardening (b).

Table 5-12. Results of CT scanning of samples from mixes P and R (10 samples from each) using the Skyscan CT-Analyzer and CT-Volume Software.

Sample	No. of slices	3-D Analysis				2-D analysis				
		Sample vol. (mm^3)	VOI (mm^3)	VOI (%)	S/V (mm^{-1})	Sample area (mm^2)	AOI (mm^2)	AOI (%)	No. of objects	Avg. size (mm)
R1	801	751	27.20	3.62	53.3	72.0	2.61	3.62	450	0.086
R2	801	786	9.89	1.26	82.8	75.4	0.94	1.25	210	0.078
R3	801	794	31.05	3.91	62.1	76.2	2.97	3.90	542	0.084
R4	801	790	22.37	2.83	61.5	75.8	2.14	2.82	395	0.083
R5	801	828	40.40	4.88	44.8	79.5	3.87	4.87	454	0.104
R6	801	811	26.50	3.27	52.4	77.8	2.54	3.26	396	0.090
R7	801	809	37.80	4.67	60.6	77.6	3.63	4.68	625	0.086
R8	801	799	28.20	3.53	61.1	76.6	2.70	3.52	472	0.085
R9	801	793	39.10	4.93	54.7	76.0	3.75	4.93	550	0.093
R10	801	789	26.20	3.32	54.3	75.6	2.51	3.32	409	0.088
Mean				3.62	58.8			3.62	450	0.088
S.D.				1.101	10.039			1.104	112.9	0.0070
CV (%)				30.4	17.1			30.5	25.1	8.0
P1	771	174	0.95	0.56	43.9	69.16	0.51	0.74	32	0.153
P2	961	175	5.26	2.97	19.6	69.71	2.28	3.25	44	0.184
P3	961	172	1.73	1.02	30.5	68.38	0.72	1.05	32	0.160
P4	961	171	2.60	1.52	20.2	67.92	1.03	1.52	33	0.202
P5	961	175	1.72	0.98	35.3	69.46	0.69	0.99	54	0.127
P6	961	173	2.58	1.49	25.5	68.89	1.03	1.49	43	0.175
P7	961	171	1.26	0.75	34.5	68.19	0.51	0.75	33	0.139
P8	961	170	2.14	1.24	27.5	67.53	0.84	1.24	32	0.177
P9	961	246	3.85	1.48	25.89	69.25	1.03	1.48	50.13	0.16
P10	961	178	1.70	0.95	33.5	70.85	0.67	0.95	44	0.139
Mean				1.31	29.3			1.36	40	0.162
S.D.				0.673	7.445			0.731	8.4	0.0234
CV (%)				51.3	25.4			53.8	21.0	14.5

The 2-D analysis was conducted on every slice of the sample and the average values are shown in Table 5-12. For example, 801 slices of sample R1 were reconstructed and the average number of objects (with level-level values between 181-255) located in each slice was 450 and the average size of the objects was 0.086 mm. The average total area occupied by the objects (AOI) was 2.61 mm^2 on each slice, which had a total area of 72.0 mm^2. In other words, the AOI occupied on average 3.62% of the total area of the slice. The 3-D analysis was performed on a "3-D model" constructed by stacking all of the slices together (see Figure 5-74 for an example of a 3-D model). For example, R1 has a total volume of 751

mm^3 when all 801 slices are stacked together. The total volume of interest (VOI), i.e. of low-density objects with gray levels in the range of 181-255, is 27.20 mm^3. In other words, the low-density objects represent 3.62% of the total volume of the sample. Using the threshold values chosen, the average air content of mixes P and R are 1.31 and 3.62 % (by volume), respectively. These compare with air contents of 2.7 and 9.45% determined by ASTM C 457. Selection of a lower level-level threshold would have resulted in an increased volume of air measured by CT, however, there currently is not a methodology for selecting the appropriate threshold values in any but an arbitrary fashion. This could possibly be done by calibrating the CT instrument (and software) using homogenous paste or mortar samples of known air contents.

Chapter 6 – Discussion

6.1 Mixture Design

For this research, concrete mixtures with varying amounts and types of AEA were produced. In general, the mixtures produced using a vinsol resin were prepared without problems. When preparing the mixtures using synthetic AEAs, it was found to be almost impossible to achieve an air content above 5-6% in the fresh concrete without using a water reducer. Upon investigation, it was shown that the hardened air content for at least one of the high dose mixtures was actually much higher than was measured by any of the fresh concrete testing methods. This seemed to indicate the fresh concrete tests for air content are not measuring all the air entrained in the concrete.

One explanation for the insensitivity of the fresh concrete air tests is that the types of air voids produced by synthetic AEAs, particularly the incremental bubbles produced by a high AEA dose, are small enough to not affect a volumetric or pressure test, or even a unit weight determination. However the same voids can be easily seen using a microscope and are therefore detected when doing a hardened air content determination. Figure 6-1 shows the void-size distributions measured on the high dose and low dose concrete mixtures prepared. It is clearly seen that the synthetic AEAs produced void size distributions that were finer relative to the distributions produced using vinsol resin. The specific nature of the air void size distribution produced from the various synthetic AEAs should be studied further. If fresh concrete tests are incapable of measuring the air content correctly, alternatives such as the flat bed scanner become more important.

6.2 ASTM C 666 Freeze-Thaw Testing

A number of interesting observations can be made from the ASTM C 666 Freeze-Thaw testing conducted as part of this research. First, in spite of the poor air-void system characteristics obtained in the low dose air-entraining admixture concrete mixtures, most all of the concrete mixtures prepared performed well in freeze-thaw testing. The notable exception is mixture P designated as VR-L, which means that the mix has a low dosage of a vinsol resin air-entraining admixture. The reported air content in the fresh concrete based upon ASTM C 231 and C 173 testing was 2.4% and 2.7%, respectively (see table 3-14). The hardened air content in mixture P based upon ASTM C 457 testing was 1.8% (see table 3-15). Mix P is the only mix with less than 3% air as determined by both fresh and hardened concrete tests. Mix D, designated as VR-LO, recorded an air content of 2.8% in the fresh concrete and 3.45% in the hardened concrete; all other mixes had air contents above 3% in both fresh and hardened concrete tests. As illustrated in Figure 6.2, the air-void system characteristics of mixtures A, D, J, M, and P, as determined and specified by ASTM C 457, were inadequate to provide freeze-thaw protection. That is, the measured spacing factor exceeds 0.200 mm. However, only mixture P performed poorly in freeze-thaw testing.

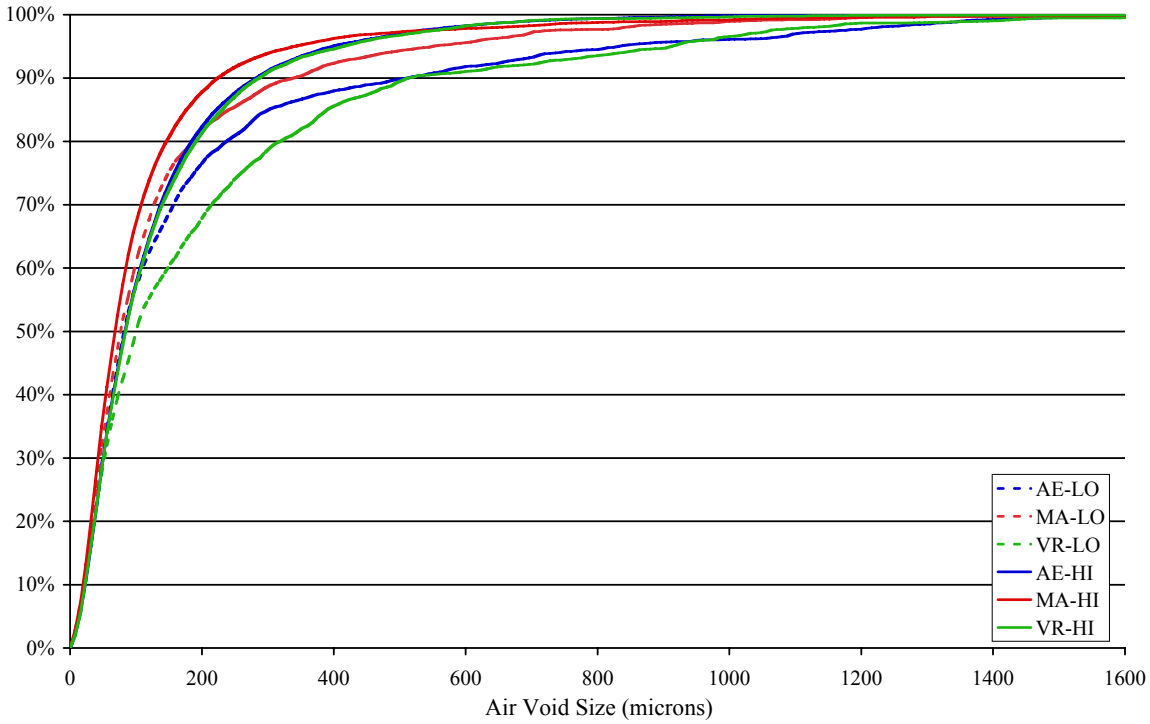

Figure 6-1. Cumulative distributions obtained from the various air-entraining admixtures used. Each curve represents the average of 10 separate ASTM C 457 analyses performed for each mixture type.

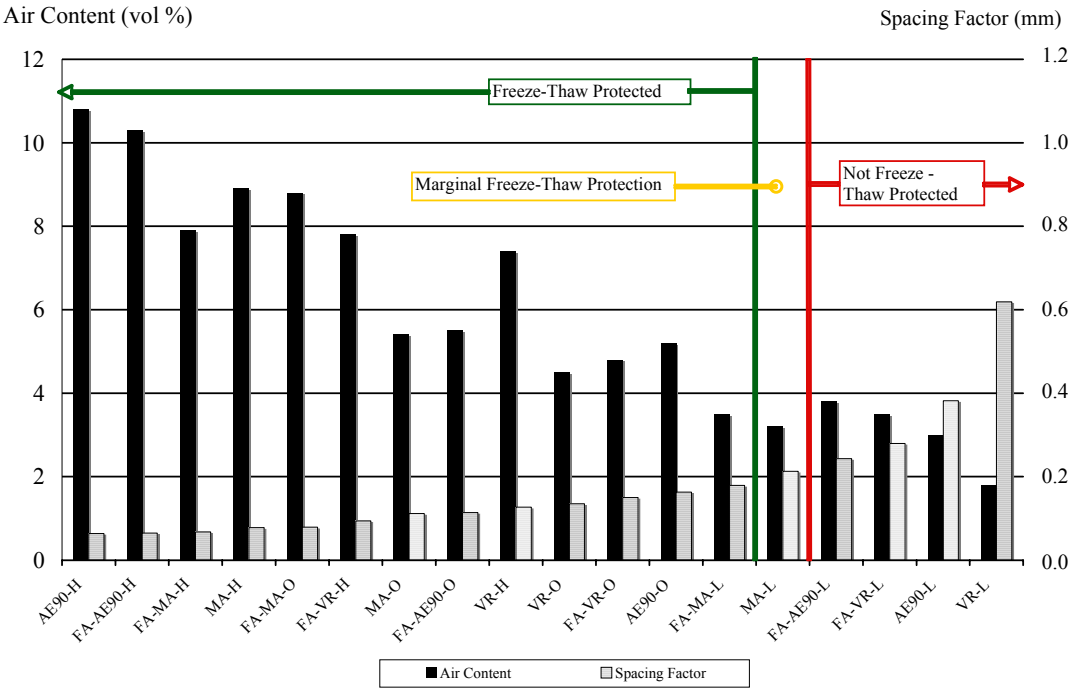

Figure 6.2 Summary table of air content and spacing factor for each mixture. Concrete with a spacing factor equal to or less than 0.200 mm is considered freeze-thaw durable.

The poor performance of mix P could be predicted from air-void characteristics of the VR-L concrete mixtures. Specifically, mixture P had an extremely large spacing factor (e.g. 0.619). However, mix D also had a large spacing factor (e.g. 0.382) but still gave satisfactory performance in the ASTM C 666 test. The better-than-predicted performance of mixtures A, D, J, and M probably results from the fact that this concrete has a lower water-to-cement ratio (higher strength) than the concretes used to develop the historical data presented in Figures 4-8 and 4-9.

The different AEAs resulted in slightly different types of air void distributions in the concrete mixtures prepared. As shown in Figure 6-1, the VR-L mixtures on average produced air-void systems that were coarser (i.e. a higher percentage of larger bubbles). The combination of fewer bubbles, and those present being relatively larger, certainly contributed to the poor F-T performance of the vinsol resin AEA at low doses.

There appeared to be no discernable change in F-T performance for mixtures prepared with fly ash. Additionally, the fly ash used in this project had no apparent effect on the entrained air obtained in each mixture. Admittedly, this is a limited study in terms of the evaluation of the effects fly ash may have on air entrainment. The main objective for including fly ash was to see if the bubbles in fly ash particles skew the measured hardened air content when automated methods are used. In general the fly ash did not affect the measured hardened air content.

The satisfactory F-T performance of the low synthetic AEA dose mixtures, coupled with the difficulties encountered in producing optimum and high synthetic AEA dose mixtures (Chapter 3), indicates that attention should be given to current specifications requiring 6-8% entrained air, or in some cases higher. Adequate F-T performance can be achieved with 4% air, as was the case in this study, and workability can be achieved through the use of water reducing admixtures. The historical 6-8% entrained air was determined empirically for vinsol resin based AEAs and this specification may no longer be appropriate for the synthetic admixtures used today, particularly when used in concrete with a relatively low *w/c*.

6.3 Air-Void System Analysis by Emerging Technologies

6.3.1 Flat Bed Scanner

A flat bed scanner based image analysis system was successfully developed and employed to perform ASTM C 457. The heart of this system is a Visual Basic script written to automate the analysis process and produce an off the shelf turnkey system for performing this analysis. The system requires contrast-enhanced concrete surfaces, the only additional sample preparation step required beyond that currently done for ASTM C 457 using microscopical methods. The most crucial factor in the accuracy of the calculated air void system parameters was the quality of the image collected by the flat-bed scanner which related directly to both the preparation of the sample and the ability of the flat-bed scanner to resolve the microscopic features of the concrete.

Methods described in this report were used to compare the capabilities of a high resolution flat-bed scanner to those of a conventional office flat-bed scanner. The accuracy assessment performed between the manual point count data and the scanner collected images suggested that the conventional office flat-bed scanner can perform on the same level as the high-

resolution scanner, at a fraction of the cost. Direct comparisons between the air void system parameters obtained from a motorized stage manual point count and those from the automated script program were made. Accuracy assessments comparing individual pixels from the motorized stage manual point count to equivalent pixels in the scanned images confirmed the correlations made in this research, again tying the final arbitration on performance to the human measurement.

A comparison of results obtained from the flat-bed scanner analyses to those obtained by an existing automated system was made. The existing system, known as RapidAir 457, is used across Europe and North America in various public and private research laboratories to perform automated air void system analyses. Analyses performed by the RapidAir 457 system upon polished samples previously analyzed via the automated flat-bed scanner method resulted in air void parameters with high correlations to those obtained by the flat-bed scanner method. The results show potential for an ASTM C 457 test procedure to be implemented using a flat-bed scanner based technique.

As a result of revisiting the sample preparation used in this research, it is clear that proper sample preparation is critical to obtaining the correct estimate of hardened air content by any automated method. It is equally important for manual point counting but in this case, the operator is able to make judgments that a computer has great difficulty in accomplishing. Although establishing the correct threshold is also important for accurately interpreting the images obtained, it is sample preparation that is most critical to the automated process.

In addition to sample preparation, the most critical step in an automated approach for determining air-void system parameters is establishing the correct threshold for converting the B/W contrast image to a true binary image. Four different approaches for establishing the correct threshold were evaluated. From Figures 5-63 through 5-68, it is clear that the minimum deviation from unity, the maximum Kappa statistic, and the error cross-over methods all provided similar results, and the maximum R square method yielded a higher threshold level than the other three methods. The higher threshold resulted in a slight underestimation of air content, but a pronounced underestimation of void frequency. None of the threshold methods showed a relationship in perfect agreement with the manual results. The three methods with similar results all performed well in terms of void frequency.

At the resolution of 8 x 8 micrometer pixels, a relatively low threshold level was necessary in order to include the smallest air voids. When the size of an air void approaches the same size as a pixel, but the position of the air void occurs between two or more neighboring pixels, the intensities of those pixels becomes a combination of the bright air void and the surrounding dark non-air. The same phenomenon occurs along the edges of larger air voids. A low threshold level is necessary in order to detect these smallest of air voids. However, at the same time, a low threshold also includes more of the neighboring pixels around the larger air voids. This effect is reflected in the consistent overestimation of total air content for the three threshold determination methods that utilized a relatively low threshold. There are numerous image analysis approaches to solving this problem. Future work developing the script will address these issues.

Ultimately, a threshold choice should yield air void parameters that most closely approximate unity. Therefore, the minimum deviation from unity method was selected as the best method for threshold optimization, although threshold levels determined by the maximum Kappa

statistic and the error cross-over methods did not differ significantly. Table 5-11 contains a summary of the air void parameters determined by both the manual procedure and by the automated procedure according to threshold levels set by the minimum deviation from unity method.

6.3.2 CT Scanner Method

CT scanning is a promising emerging technique for measuring the air-void characteristics of concrete. It has the advantage of traditional techniques in that it can be used to detect air in both hardened and fresh concrete (see Figure 5-75). Recent high-resolution micro-CT scanners are capable of detecting air voids below the size that can be detected by optical microscopy. However, a number of difficulties were encountered in this study, these being:

- High-resolution scanning can only be carried out on small samples
- The paste and aggregate phases cannot be fully differentiated
- The technique is highly sensitive to the selection of threshold values
- Cost of hardware and software
- Level of expertise required
- Duration required for scanning and, particularly, reconstruction

Although these drawbacks present considerable barriers to the wider application of this technique to the measurement of air-void parameters at this time, the technology (both hardware and software) is advancing at a sufficiently rapid rate that many of the problems will be overcome in the near future.

The air contents, as measured by CT, show considerable variation between samples from the same concrete specimen. This is undoubtedly due to the small sample size and resulting variation in the paste content between samples. There are two approaches for compensating for this deficiency, one is to increase the sample size and the second is to express the air contents as a proportion of the paste content. As the size of the sample increases, the resolution of the technique decreases. At this time, it is not possible to increase the sample size without loss of resolution. However, as CT technology advances it is possible that scanners will be produced in the not-too-distant future that are capable of testing larger samples at the required resolution. In the meantime, data for a representative sample volume must be collected by measurements made on multiple (smaller) samples. Determining the paste content of the concrete samples by CT requires that the technique be capable of differentiating between the cement paste and the aggregate. The images shown in this report show that coarse aggregate particles, and some of the larger sand particles, can be detected. However, due to the similarities between the chemical and physical properties (e.g. density) of the paste and the aggregates, it is not possible to differentiate between the finer aggregate particles and the cement paste. It is possible that this may be accomplished by dual-energy scanning techniques, but this was not explored as part of this study.

Although the software analysis did not produce a value for the average size of the voids in three dimensions, it did determine the average surface-area-to-volume ratio (S/V) for the 3-D model. This is a useful parameter as it gives an indication of the size and thus the number of voids. If the paste could be differentiated from the aggregates it would be possible to determine other characteristics of the air-void system such as the average distance between

the bubbles (i.e. similar to the spacing factor currently used). The threshold techniques tested in this research for the flat bed scanner may have applicability for processing CT images.

Chapter 7 - Conclusions and Recommendations

7.1 Mix Design/Fresh Concrete Testing

- The problems encountered in preparing the necessary concrete mixtures show that it is very possible to overdose a mixture with AEA when conventional field air tests indicate a low air content. A vicious cycle could result with failing tests requiring higher dosages of AEA resulting in increasingly reduced quality concrete.
- Fresh concret tests for air content seem to underestimate the hardened air content. This may be related to the nature of the air void size distribution produced by a synthetic AEA.
- High correlations were obtained between the results of the three fresh concrete tests (ASTM C 138, ASTM C 173 and ASTM C 231). No particular combination of AEA, air content or fly ash replacement resulted in better or worse correlations between the results.
- In all of the 18 mixtures the volumetric meter method (ASTM C 173) resulted in a higher air volume measurement than did the pressure meter method (ASTM C 231), but no statistically significant trends were observed in differences between the test results for the various mixture combinations. ASTM C 231 states the multi-operator precision of the pressure meter test to be 0.8% air. Therefore it is not possible to conclude that significant differences in the results obtained from the pressure meter and volumetric meter exist since 17 of the 18 sets of fresh concrete testing results differed by less than 0.8%.
- Good correlations exist between the results of the fresh concrete tests and the results obtained in performing manual point counts (ASTM C 457) of the hardened concrete specimens prepared from each of the 18 mixtures.

7.2 ASTM C 666 Freeze Thaw Testing

- ASTM C 666 testing was performed on 18 different mixtures with a constant cement and water content, but varying amounts of air entraining admixtures (AEAs).
- Using three different AEAs, mixtures were prepared with an optimal, high, and low dose of AEA resulting in air-void systems with optimal, high and low air contents, respectively. Fly ash was also used in some mixtures.
- In ASTM C 666 testing, all mixtures passed with 300 cycles and durability factors greater than 100%, except for mixture P prepared with a low dose of vinsol resin.
- The poor performance of mixture P was consistent with predictions of performance based on the measured spacing factors for each mixture. The good performance of mixtures A, D, J, and M with their marginal spacing factors indicates that the current specification for a maximum spacing factor of 0.200 mm may not be valid for concrete currently produced using a low *w/c* or synthetic AEAs.
- Fly ash did not affect the concrete performance or the determination of hardened air, by any method.

7.3 Emerging Technologies – Flat-Bed Scanner

- A flatbed scanner was clearly demonstrated to be a viable device for performing ASTM C 457.
- Two types of scanners were compared, a high-resolution flatbed scanner and a conventional office scanner. Both types of scanners were capable of performing ASTM C 457.
- The flatbed scanner method tends to report slightly higher air content values than those determined by manual point counting. Image processing approaches may eliminate this error. In general there was good agreement between the scanner, other automated methods, and manual point counting.
- The degree of correlation with manual results depends on the method used to establish thresholds for segmenting the gray scale image.
- Increased confidence in the automated systems can be achieved by refining the processes involved in the preparation of the sample surface. Improvements in surface preparation quality reduce the quantity of defects analyzed by the automated systems. Therefore, it is easy to appreciate the fact that most researchers dealing with these types of analyses identify the sample preparation as the key factor in obtaining quality results.
- The ability of the flat-bed scanners themselves to achieve increased resolution will only continue to improve as technology advances. Enhanced definition of features such as air void edges will be available for collection as flat-bed scanner resolutions continue to improve. Further research will explore these avenues while continuing to refine the application of the flat-bed scanner to ASTM C 457.

7.4 Emerging Technologies – CT Scanner

- CT scanning is a promising emerging technique for measuring the air-void characteristics of concrete. It has the advantage over traditional techniques in that it can be used to detect air in both fresh and hardened concrete.
- Recent high-resolution micro-CT scanners are capable of detecting air voids below the size that can be detected by optical microscopy. However, a number of difficulties were encountered. Although these drawbacks represent considerable barriers to the wider application of this technique to the measurement of air-void parameters at this time, the technology (both hardware and software) is advancing at a sufficiently rapid rate that many of the problems may be overcome in the near future.

7.5 Recommendations for Future Work

- Attention should be given to the current concrete mixture designs used in Wisconsin with regards to air entrainment requirements. With modern chemicals and procedures, it may be possible to reduce air contents without sacrificing durability. Adequate spacing factors seem achievable with 3-4% air by volume, depending upon the AEA used.
- Further development of the flatbed scanner should continue, addressing some of the systematic errors encountered by applying advanced image processing techniques

- The CT scanner is a promising device but is currently not capable of performing ASTM C 457 at a practical level. Further development of software and computing algorithms will result in this technique becoming viable. The ability of this technique to evaluate fresh concrete should be explored in more detail as it may provide a needed alternative for measuring air-void system parameters.

7.6 Implementation

Implementation of this research should begin with a close look at the existing mixture designs specified for paving concrete in Wisconsin. A detailed study focusing on the freeze-thaw performance relative to the amount of entrained air should be performed. Based on the research presented here, it would appear that lower target air contents could be used and still achieve an air-void system that provides adequate protection from freeze thaw cycling. By reducing the target air, it will be easier for ready mix producers to achieve the required air content without over dosing.

Because of the difficulties identified with accurately measuring the air content in fresh concrete when synthetic AEAs are used, QC/QA strategies for paving concrete should include measurement of hardened air content. In the near term, this will require continued use of manual point counts to perform ASTM C 457. The automated method detailed in this report, specifically the flat bed scanner approach, is very close to being ready to be implemented. The researchers are currently involved in a FHWA sponsored round robin study using various automated methods and as a result of this work, additional data will be available to help apply advanced image analysis techniques to correct problems still remaining. In general, image analysis can be applied easily. However, without knowing the "correct" answer, efforts to fine-tune the flat bed scanner will be useless. The round robin will provide measurements from multiple samples using multiple techniques to help bracket the true value of air-void system parameters. Once this is done, the flat bed scanner approach can be optimized as needed to provide reproducible, accurate results.

The remaining hurdle for implementing ASTM C 457 as a QC/QA tool will be sample preparation. Regardless of whether the air-void system is measured by manual or automated means, scanner or microscope, the preparation of the sample is the single most critical process. To implement this work, an automated sample preparation system should be used to eliminate sample preparation as a variable in the process. Numerous automated systems are available. Each must be thoroughly investigated to determine its applicability. Without a doubt, developing a "fool-proof" automated sample preparation approach will be key to the success of any QC/QA system relying on images to determine the hardened air content of the concrete.

The software developed for using the flat-bed scanner for performing ASTM C 457 is available for download at http://www.cee.mtu.edu/~krpeters/air_voids/.

References

AASHTO M 43 *Sizes of Aggregate for Road and Bridge Construction*, Standard Specifications for Transportation Materials and Methods of Sampling and Testing, 24th Edition, and the AASHTO Provisional Standards, 2004 Edition.

Ansari F., Zhang Z., Szary P., Mahler A., "Effects of Synthetic Air Entraining Agents on Compressive Strength of Portland Cement Concrete-Mechanism of Interaction and Remediation Strategy". Final Report. Report No. FHWA-NJ-2002-025. New Jersey Department of Transportation, 2002.

ASTM C 33-03, *Standard Specification for Concrete Aggregates*, American Society for Testing and Materials, West Conshohocken, Pennsylvania.

ASTM C 94/C 94M-04A, *Standard Specification for Ready-Mixed Concrete*, American Society for Testing and Materials, West Conshohocken, Pennsylvania.

ASTM C 125-03, *Standard Terminology Relating to Concrete and Concrete Aggregates*, American Society for Testing and Materials, West Conshohocken, Pennsylvania, 2000.

ASTM C 138/C 138M-01A, *Standard Test Method for Unit Weight, Yield, and Air Content (Gravimetric) of Concrete*, American Society for Testing and Materials, West Conshohocken, Pennsylvania.

ASTM C 143/C 143M-03, *Standard Test Method for Slump of Hydraulic Cement Concrete*, American Society for Testing and Materials, West Conshohocken, Pennsylvania.

ASTM C 150-04AE1, *Standard Specification for Portland Cement*, American Society for Testing and Materials, West Conshohocken, Pennsylvania.

ASTM C 173/C 173M-01E1, *Standard Test Method for Air Content of Freshly Mixed Concrete by the Volumetric Method*, American Society for Testing and Materials, West Conshohocken, Pennsylvania.

ASTM C 192/C 192M-02, *Standard Practice for Making and Curing Concrete Test Specimens in the Laboratory*, American Society for Testing and Materials, West Conshohocken, Pennsylvania.

ASTM C 231-04, *Standard Test Method for Air Content of Freshly Mixed Concrete by the Pressure Method*, American Society for Testing and Materials, West Conshohocken, Pennsylvania.

ASTM C 457-98, *Standard Test Method for Microscopical Determination of Parameters of the Air void System in Hardened Concrete*, American Society for Testing and Materials, West Conshohocken, Pennsylvania.

ASTM C 618-03, *Standard Specification for Coal Fly Ash and Raw or Calcined Natural Pozzolan for Use in Concrete*, American Society for Testing and Materials, West Conshohocken, Pennsylvania.

ASTM C 666-03, *Standard Test Method for Resistance of Concrete to Rapid Freezing and Thawing*, American Society for Testing and Materials, West Conshohocken, Pennsylvania.

ASTM C 1064/C 1064M-05, *Standard Test Method for Temperature of Freshly Mixed Hydraulic-Cement Concrete*, American Society for Testing and Materials, West Conshohocken, Pennsylvania.

Carlson J.M., Sutter L.L., Van Dam T., Peterson K. "Advancement on the Application of a Flat-Bed Scanner for Hardened Portland Cement Concrete Air-Void Analysis." Proceedings of the 27th International Conference on Cement Microscopy, Victoria, British Columbia, 2005.

Cohen, J., 1960, "A Coefficient of Agreement for Nominal Scales," *Educational and Psychological Measurement*, Vol. 20, No. 1, pp. 37-46.

Congalton, R. G., Green K., 1999, Assessing the Accuracy of Remotely Sensed Data: Principles and Practices, Lewis Publishers, New York, New York, USA, 137 p.

Congalton, R. G., Mead, R. A., 1983, "A Quantitative Method to Test for Consistency and Correctness in Photo-interpretation," *Photogrammetric Engineering and Remote Sensing*, Vol. 49, No. 1, pp. 69-74.

Cordon, W.A. 1966. "Freezing and thawing of concrete – mechanisms and control." *ACI Monograph No. 3,* American Concrete Institute, Farmington Hills, MI.

Cross, W., E. Duke, J. Keller, D. Johnston. Investigation of Low Compressive Strengths of Concrete Paving, Precast, and Structural Concrete. Final Report. Report No. SD98-03-F. South Dakota Department of Transportation, 2000.

Baumgart C.W., Linder K.D., Cave S.P., "An Automated Image Processing System for Concrete Evaluation." Intelligent Engineering Systems Through Artificial Neural Networks, Vol. 8, pp. 455-460, 1998.

Dewey G.R., Darwin D., "Image Analysis of Air Voids In Air-Entrained Concrete" Structural Engineering and Engineering Materials SM Report No. 29, University of Kansas Center for Research, August 1991.

European Standard, EN 480-11, "Admixtures for concrete, mortar and grout – test methods – Part 11: Determination of air void characteristics in hardened concrete".

Fagerlund, G. "On the Service Life of Concrete Exposed to Frost Action", *Freeze-Thaw Durability of Concrete*, E&FN Spon. ISBN: 0-419-20000-2, pp. 23-39, 1997

Fung, T., LeDrew, E., 1988, "The Determination of Optimal Threshold Levels for Change Detection Using Various Accuracy Indices," *Photogrammetric Engineering and Remote Sensing*, Vol. 54, No. 10, pp. 1449-1454.

Gay, F.T. A Factor Which May Affect Differences in the Determined Air Content of Plastic and Hardened Air-Entrained Concrete. International Conference on Cement Microscopy, pp. 276-292, 1982.

Gudmundsson H., Christensen P., 1978, "Luftporemaling i haerdnet beton," *Nordisk Betong*, No. 5.

Gonzales, R. C., Woods, R. E., 2002, Digital Image Processing - Second Edition, Prentice-Hall Inc., Upper Saddle River, New Jersey, USA, 793 p.

Hover, K. Analytical Investigation of the Influence of Air Bubble Size on the Determination of the Air Content of Freshly Mixed Concrete," Cement, Concrete and Aggregates, CCAGDP, Vol. 10, No. 1, Summer 1988, pp. 29-34.

Hover, K. Measuring Air in Fresh and Hardened Concrete, Part 3 of a 4-Part Series. Concrete Construction, April 1993, pp. 275-278.

Jakobsen U.H., Pade C., Thaulow N., Brown D., Sahu S., Magnusson O., De Buck S., De Schutter G., "The RapidAir System for Air Void Analysis of Hardened Concrete – A Round Robin Study" Proceedings of the 10th Euroseminar on Microscopy Applied to Building Materials. Paisley, Scotland. June, 2005.

Jensen, J. R., Introductory Digital Image Processing, A Remote Sensing Perspective - Second Edition, Prentice-Hall Inc., Upper Saddle River, New Jersey, USA, 316 p.
Gani M.S.J. Cement and Concrete. London: Chapman & Hall, 1997.

Klemens T., "Express Air Measurement" Concrete Construction - World of Concrete, v 48, n 8, August, 2003, p 31-32.

Kosmatka S., Kerkhoff B., Panarese W. Design and Control of Concrete Mixtures, 14th edition, Portland Cement Association, Skokie, Illinois, USA, 372 pages, 2002.

Litvan, G.G., "Freeze-Thaw Durability of Porous Materials", *Durability of Building Materials and Components: Proceedings of the First International Conference,* ASTM STP 691, pp. 455-463, 1978

Marchand, J., and E. J. Sellevold, and M. Pigeon. The Deicer Salt Scaling Deterioration of Concrete - An Overview. Durability of Concrete. Third International Conference, Nice, France. V.M. Malhotra. ACI SP-145. pp. 1-46, 1994.

Mehta, P. K. and P.J.M. Monteiro (1993). *Concrete: Structure, Properties, and Materials.* Second Edition. Prentice Hall. Englewoods Cliffs, NJ.

Mindess S., Young J.F., Darwin D. Concrete, 2nd edition, Upper Saddle River, NJ: Prentice Hall, 2002.

Moore O.L., "Pavement Scaling Successfully Checked." Engineering News Record, Vol. 125, No. 15, pp. 471-474, 1940.

Neville A.M. Properties of Concrete, 4th edition, New York: John Wiley & Sons, Inc., 1996.

Newlon and Mitchell, 1994. "Freezing and thawing." In *Significance of Tests and Properties of Concrete and Concrete-Making Materials,* ASTM STP 169C, American Society for Testing and Materials, Philadelphia, PA, pp. 153-163.

Pade C., Jakobsen U.H., Elsen J., "A New Automatic Analysis System for Analyzing the Air void system in Hardened Concrete." Proceedings of the 24th International Conference on Cement Microscopy, San Diego, California, pp. 204-213, 2002.

Peterson, K.R. Air Void Analysis of Hardened Concrete via Flat bed Scanner. M.S. Thesis, Michigan Technological University, May, 2001b.

Peterson K.R., Swartz R.A., Sutter L.L., Van Dam T.J., "Air Void Analysis of Hardened Concrete with a Flat bed Scanner" Proceedings of the 24th International Conference on Cement Microscopy, San Diego, California, pp. 304-316, 2002.

Pigeon M., and Pleau R. Durability of Concrete in Cold Climates. London: E & FN Spon, 1995.

Powers T.C., "A Working Hypothesis for Further Studies of Frost Resistance of Concrete". Journal of the American Concrete Institute, Vol 16, No 4, pgs 245-272, 1945.

Powers T.C., "A discussion of cement hydration in relation to the curing of concrete". Highway Research Board, Proceedings, Vol 27, pgs 6-14, 1947.

Powers T.C. and Helmuth R.A., "Theory of volume changes in hardened Portland cement pastes during freezing". Proceedings of the Highway Research Board, Vol 32, pgs 285-297, 1953.

Powers, T. C.. Resistance of Concrete to Frost at early Ages. Proceedings RILEM Symposium on Winter Concreting. Danish National Institute of Building Research, Copenhagen. pp. C1-C47, 1956.

Powers T.C.. Freezing Effects in Concrete. Durability of Concrete. ACI Special Publication SP-47-1. pp. 1-12, 1975.

Roberts, L. R. 1994. Air Content, Temperature, Unit Weight and Yield. *Significance of Tests and Properties of Concrete and Concrete-Making Materials* (Ed. P. Klieger and J.F. Lamond), ASTM STP 169C, American Society for Testing and Materials, Philadelphia, p. 65.

Russ, J. C., 1995, The Image Processing Handbook - Second Edition, CRC Press, Inc., Ann Arbor, Michigan, USA, 674 p.

Sutter L.L., "Macro Programming with NIH Image for Implementing ASTM C 457". Proceedings of the 20th International Conference on Cement Microscopy, Guadalajara, Mexico, pp. 382-384, 1998.

U.S. Bureau of Reclamation, 1956. "The air-void systems of Highway Research Board cooperative concretes." *Concrete Laboratory Report No. C-824*, Denver, Colorado, April.

Whiting, D.A. and M.A. Nagi. Manual on Control of Air Content in Concrete. EB116. Portland Cement Association, Skokie, Illinois. 42pp. ISBN-0-89312-179-7, 1998.

Wiese, D., Thomas, M.D.A., Thornton, M. and Peng, D. 2000. "A new method of air void analysis for structural concrete." *Proceedings of the 22nd International Conference on Cement Microscopy,* International Cement Microscopy Association, Metropolis, IL, pp. 389-398.

Zhang Z., Ansari F., Vitillo N., "Automated Determination of Entrained Air void Parameters in Hardened Concrete." ACI Materials Journal, V. 102, No. 1, January-February 2005.

Appendix A - Stereo-Microscope Images

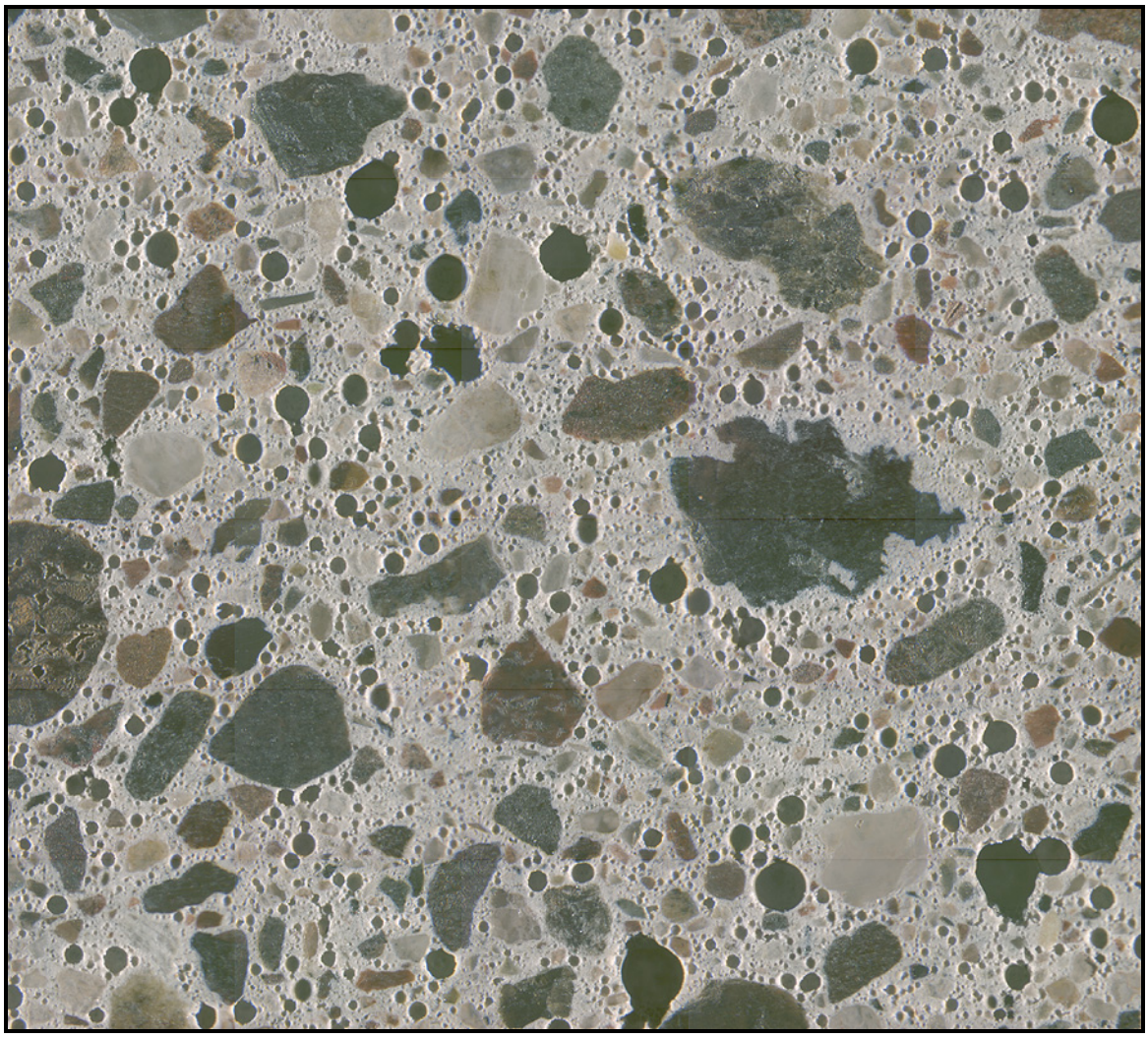

Figure A-1: A 5 x 6 mosaic of stereo microscope images collected during manual point count from sample AE-HI, image dimensions 13.060 x 11.754 mm (magnified here approximately 12x).

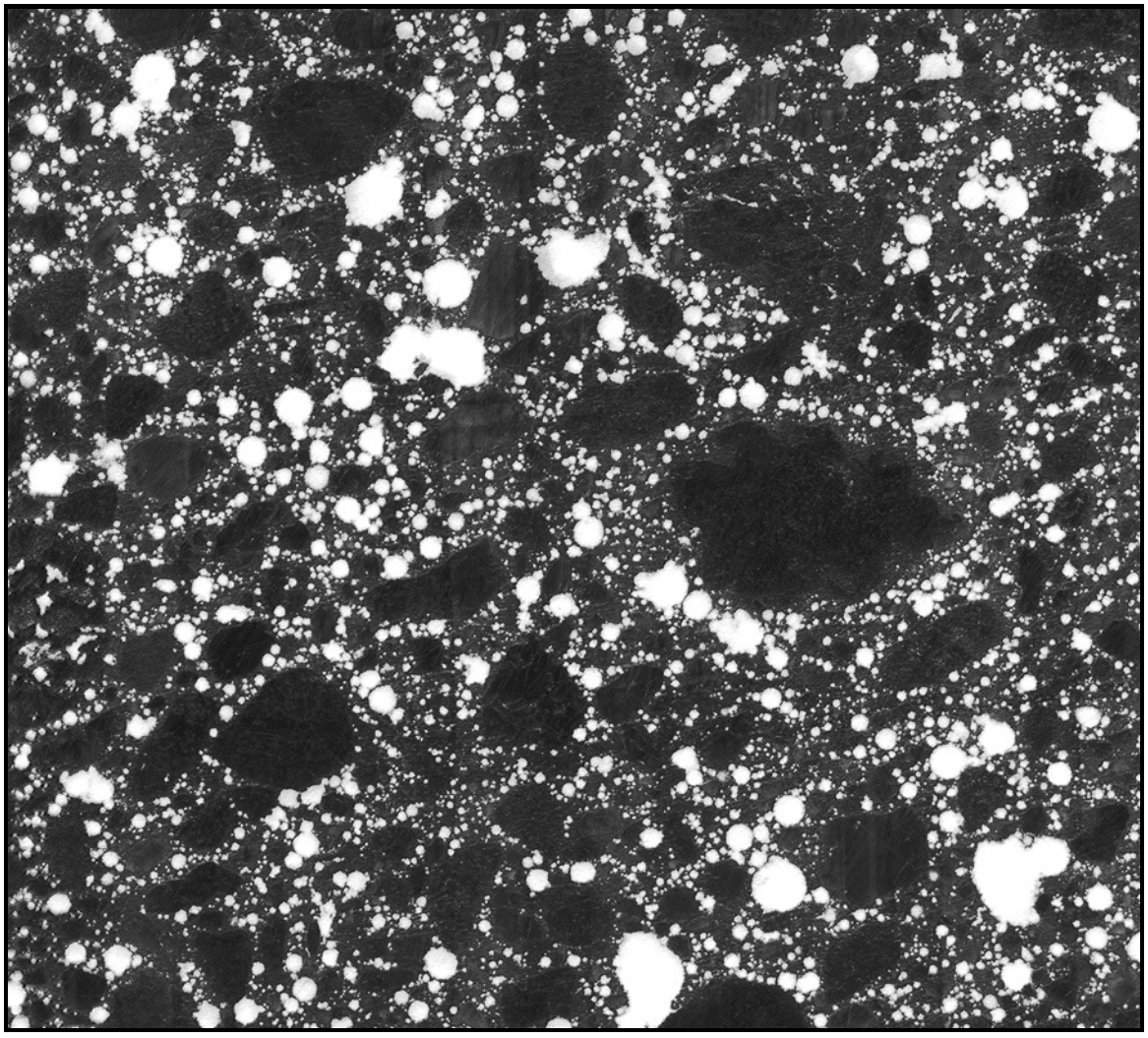

Figure A-2: High resolution scanner image of corresponding area from sample AE-HI after black and white treatment, image dimensions 13.060 x 11.754 mm (magnified here approximately 12x).

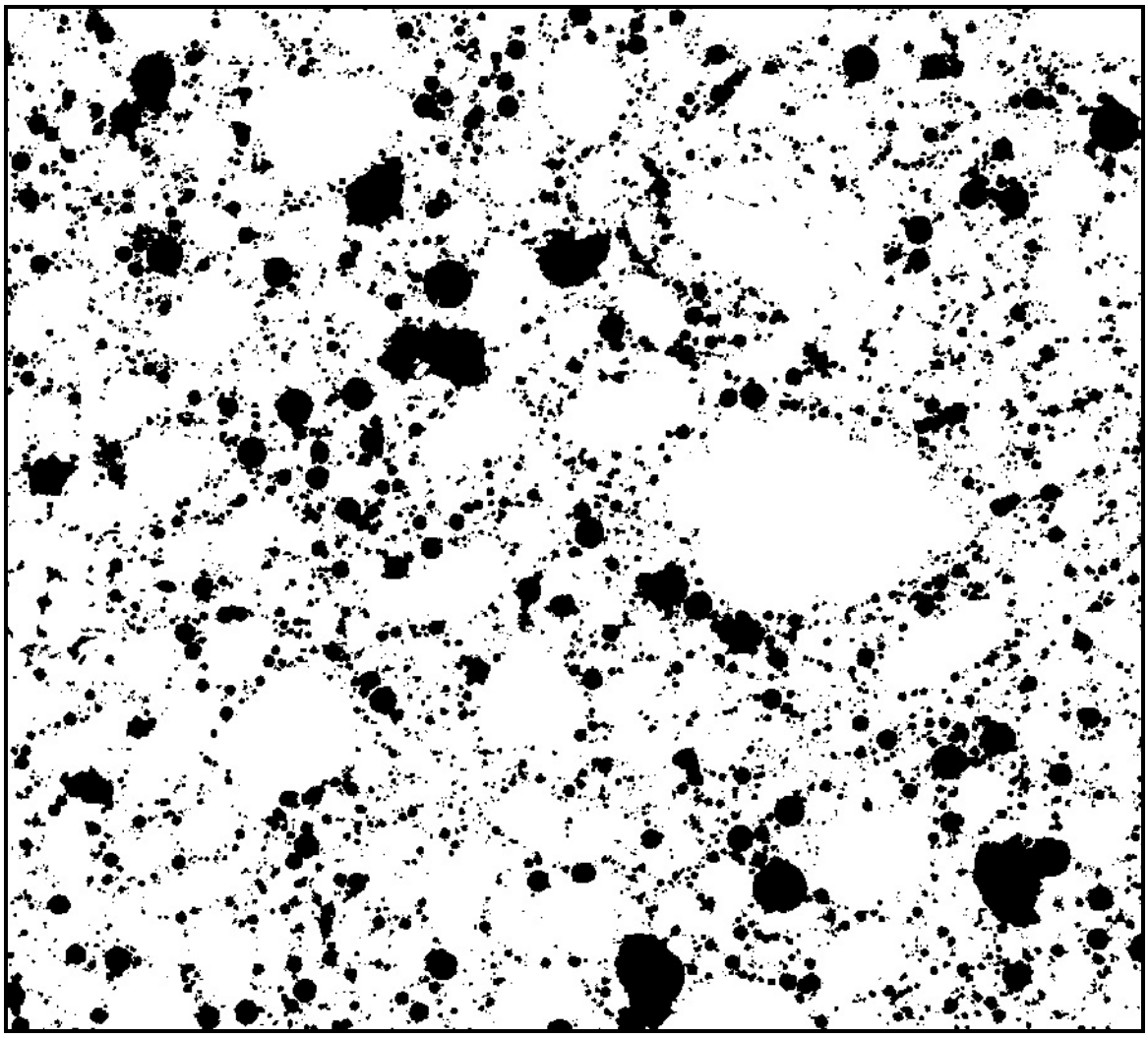

Figure A-3: High resolution scanner image of corresponding area from sample AE-HI after setting threshold to 160, and followed by an inversion (so that air voids appear black). Image dimensions 13.060 x 11.754 mm (magnified here approximately 12x).

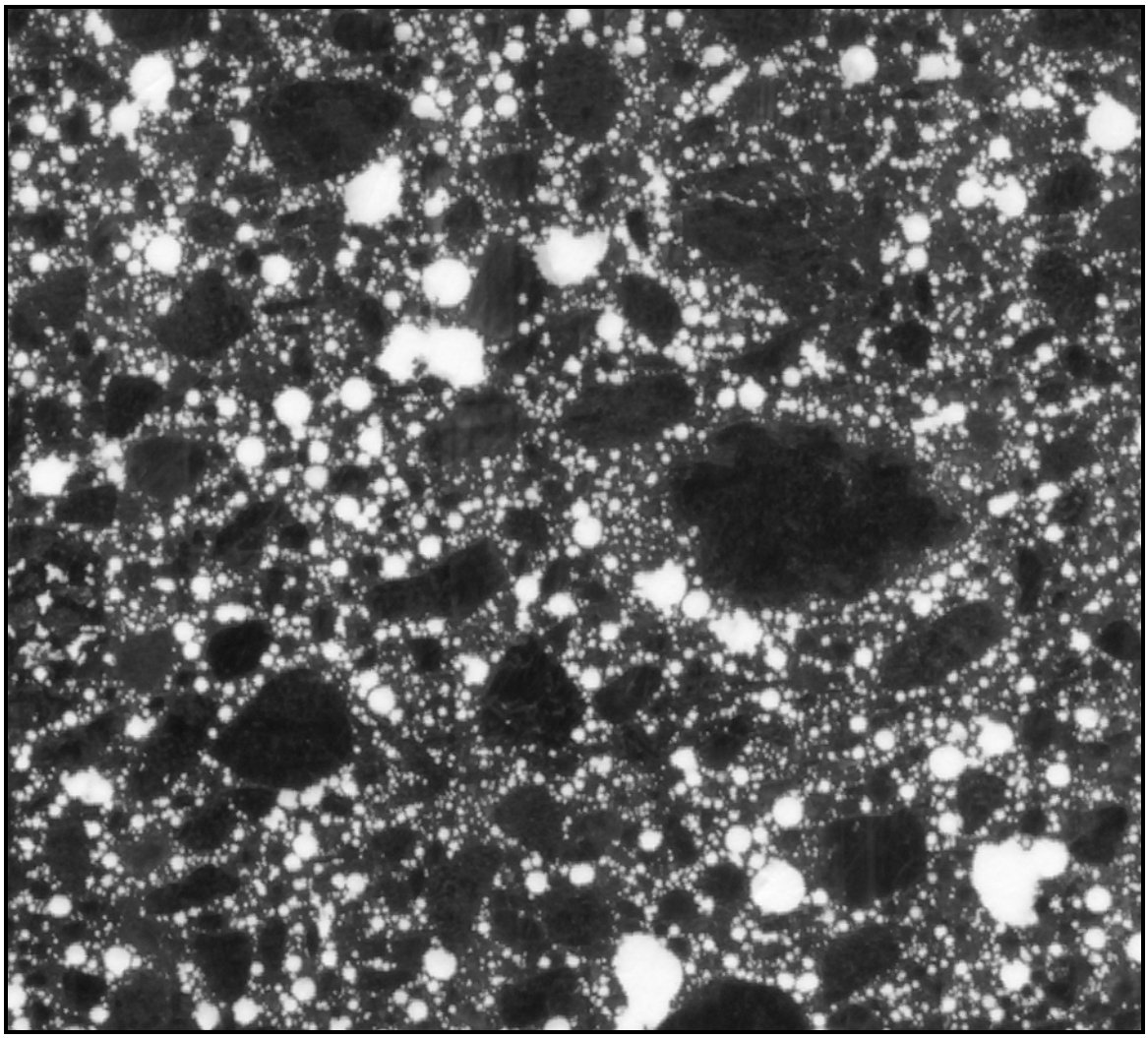

Figure A-4: Office desktop scanner image of corresponding area from sample AE-HI after black and white treatment, image dimensions 13.060 x 11.754 mm (magnified here approximately 12x).

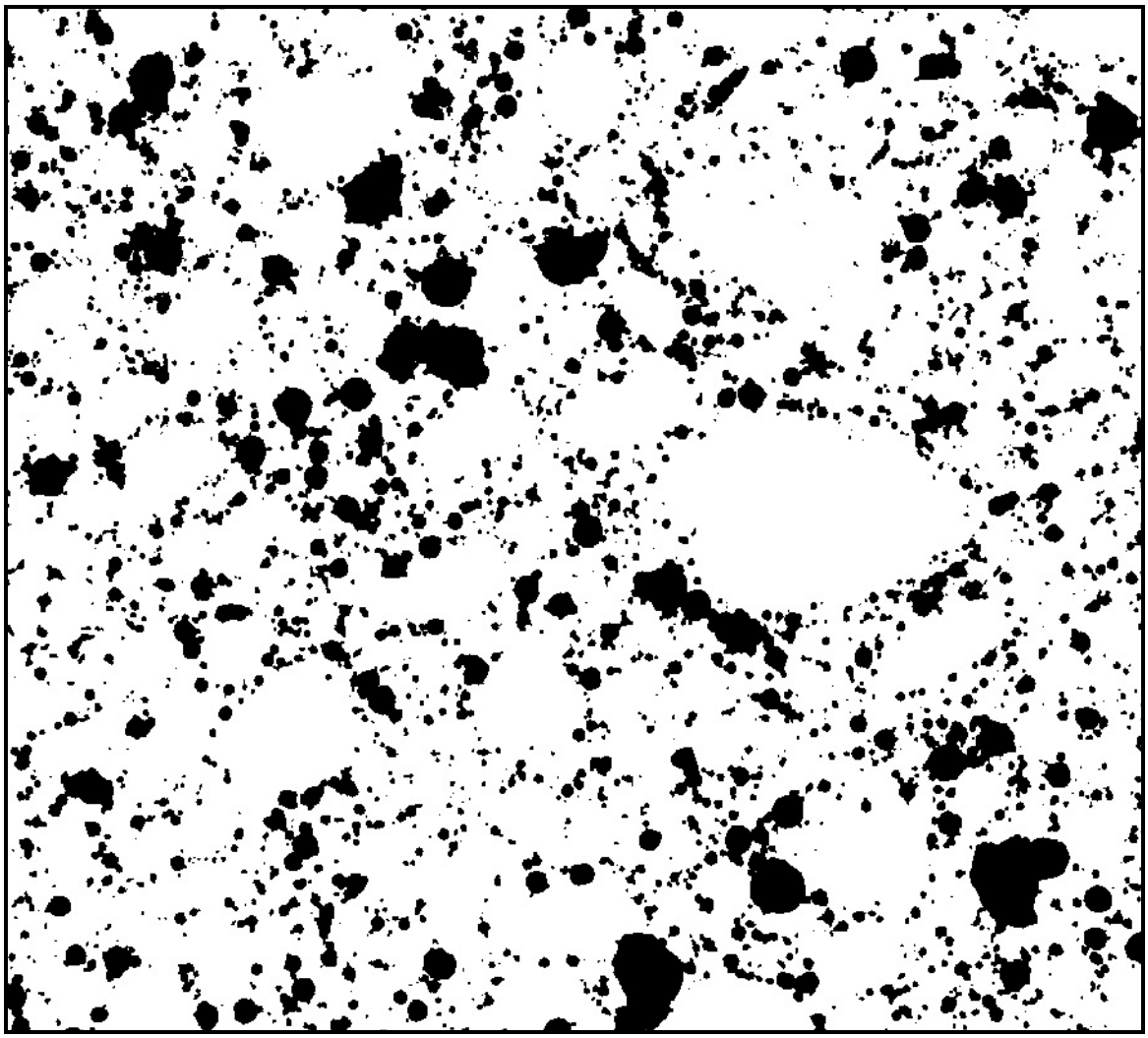

Figure A-5: Office desktop scanner image of corresponding area from sample AE-HI after setting threshold to 160, and followed by an inversion (so that air voids appear black). Image dimensions 13.060 x 11.754 mm (magnified here approximately 12x).

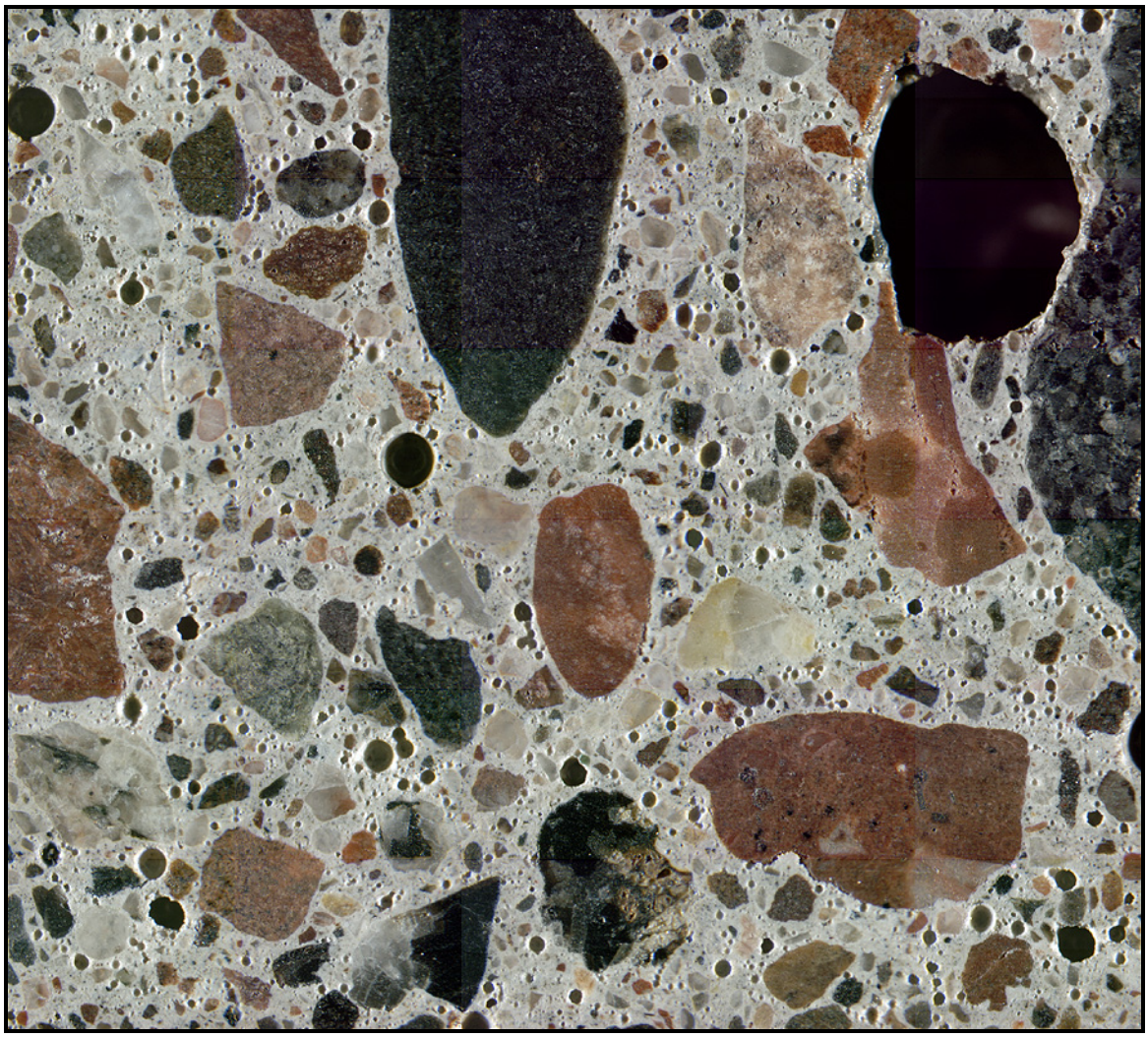

Figure A-6: A 5 x 6 mosaic of stereo microscope images collected during manual point count from sample AE-MED, image dimensions 13.060 x 11.754 mm (magnified here approximately 12x).

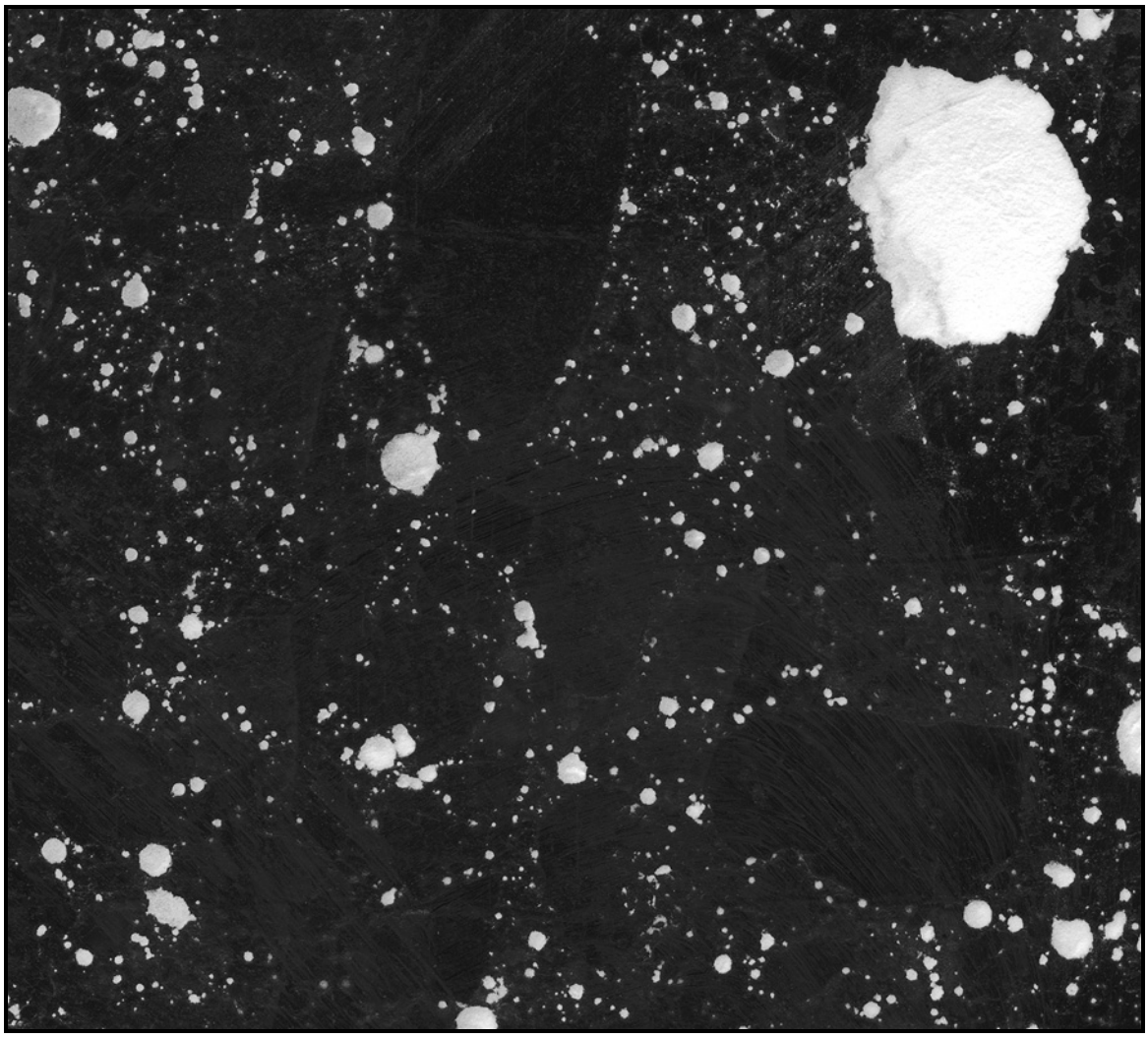

Figure A-7: High resolution scanner image of corresponding area from sample AE-MED after black and white treatment, image dimensions 13.060 x 11.754 mm (magnified here approximately 12x).

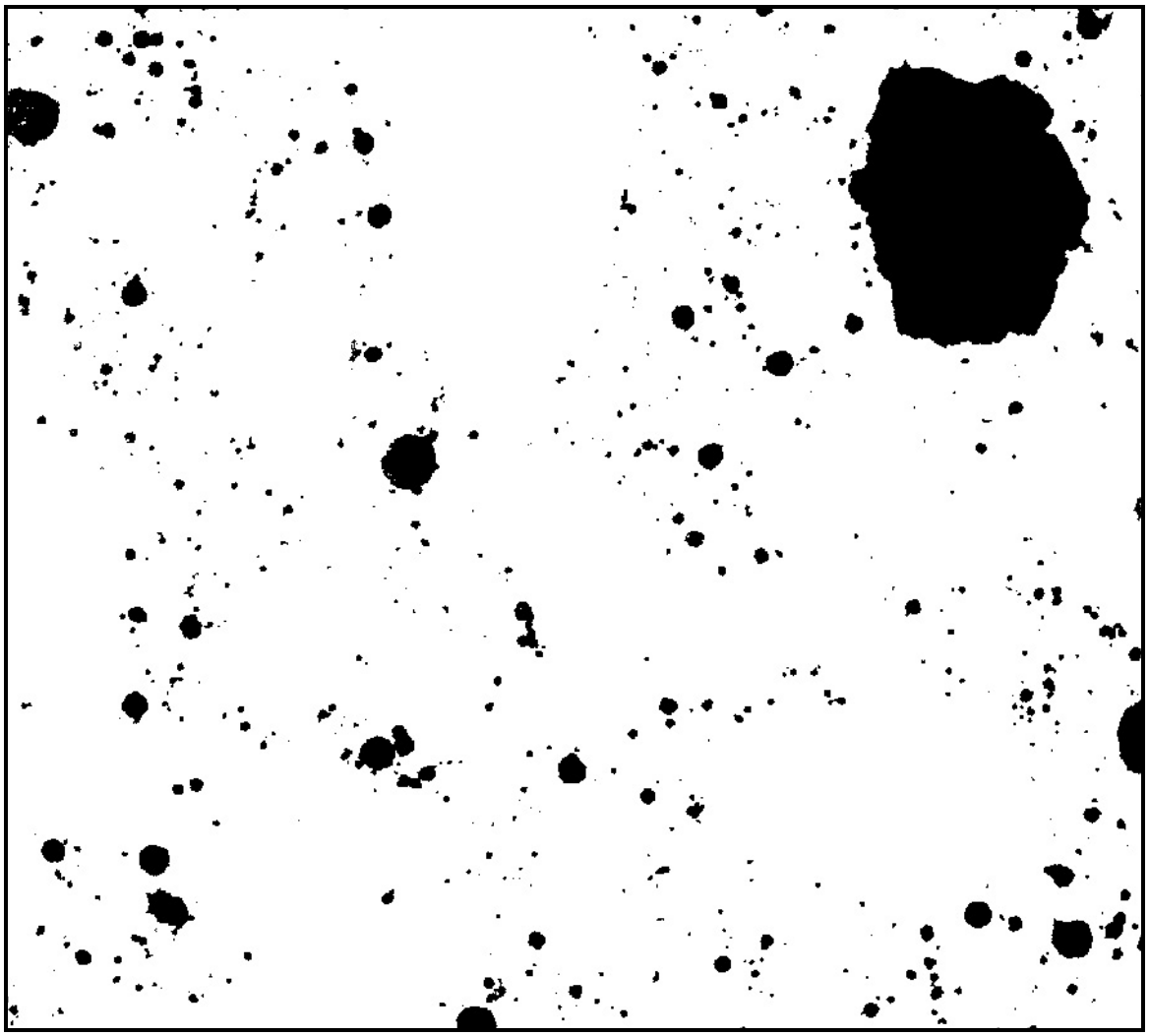

Figure A-8: High resolution scanner image of corresponding area from sample AE-MED after setting threshold to 160, and followed by an inversion (so that air voids appear black). Image dimensions 13.060 x 11.754 mm (magnified here approximately 12 x).

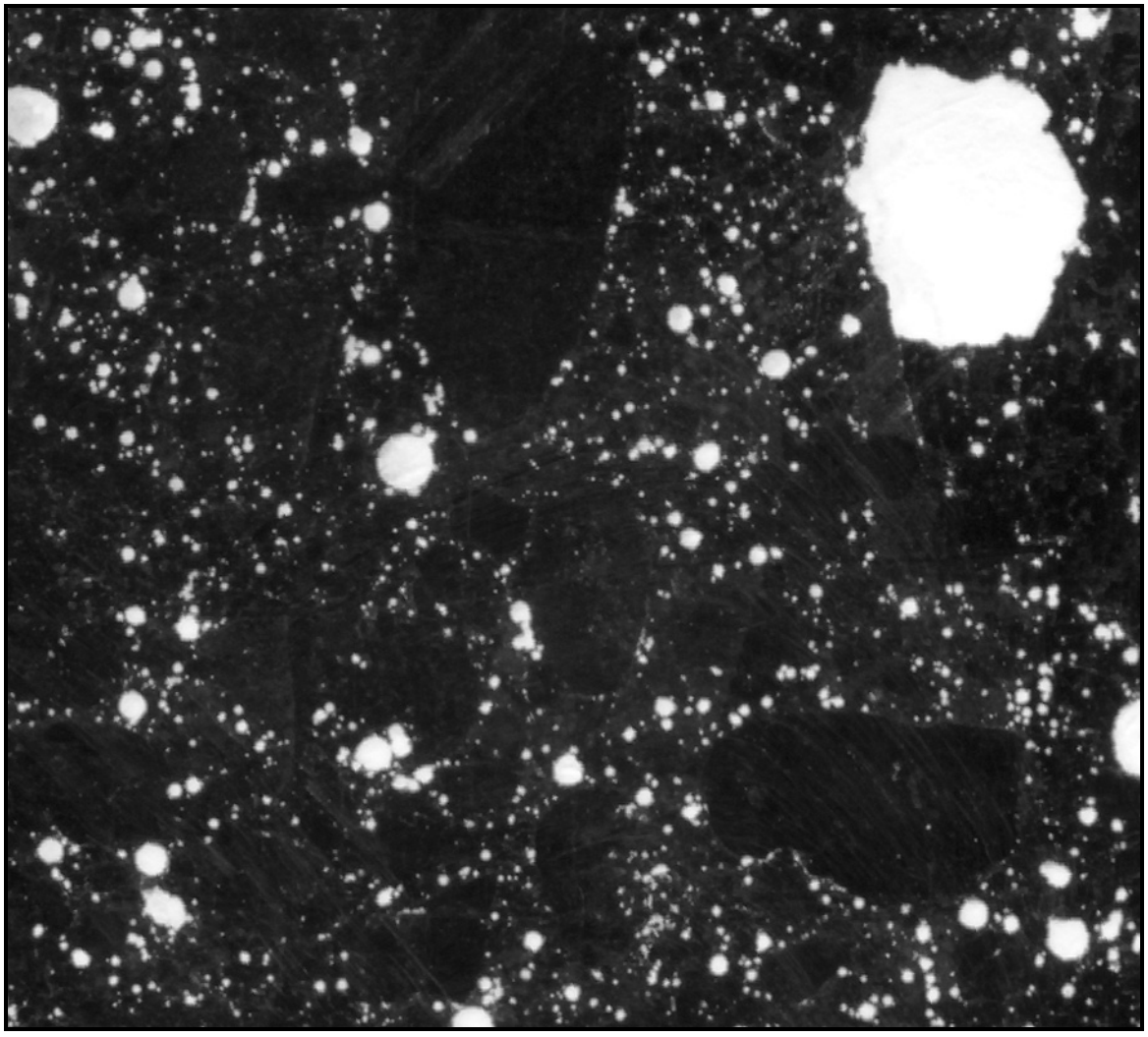

Figure A-9: Office desktop scanner image of corresponding area from sample AE-MED after black and white treatment, image dimensions 13.060 x 11.754 mm (magnified here approximately 12x).

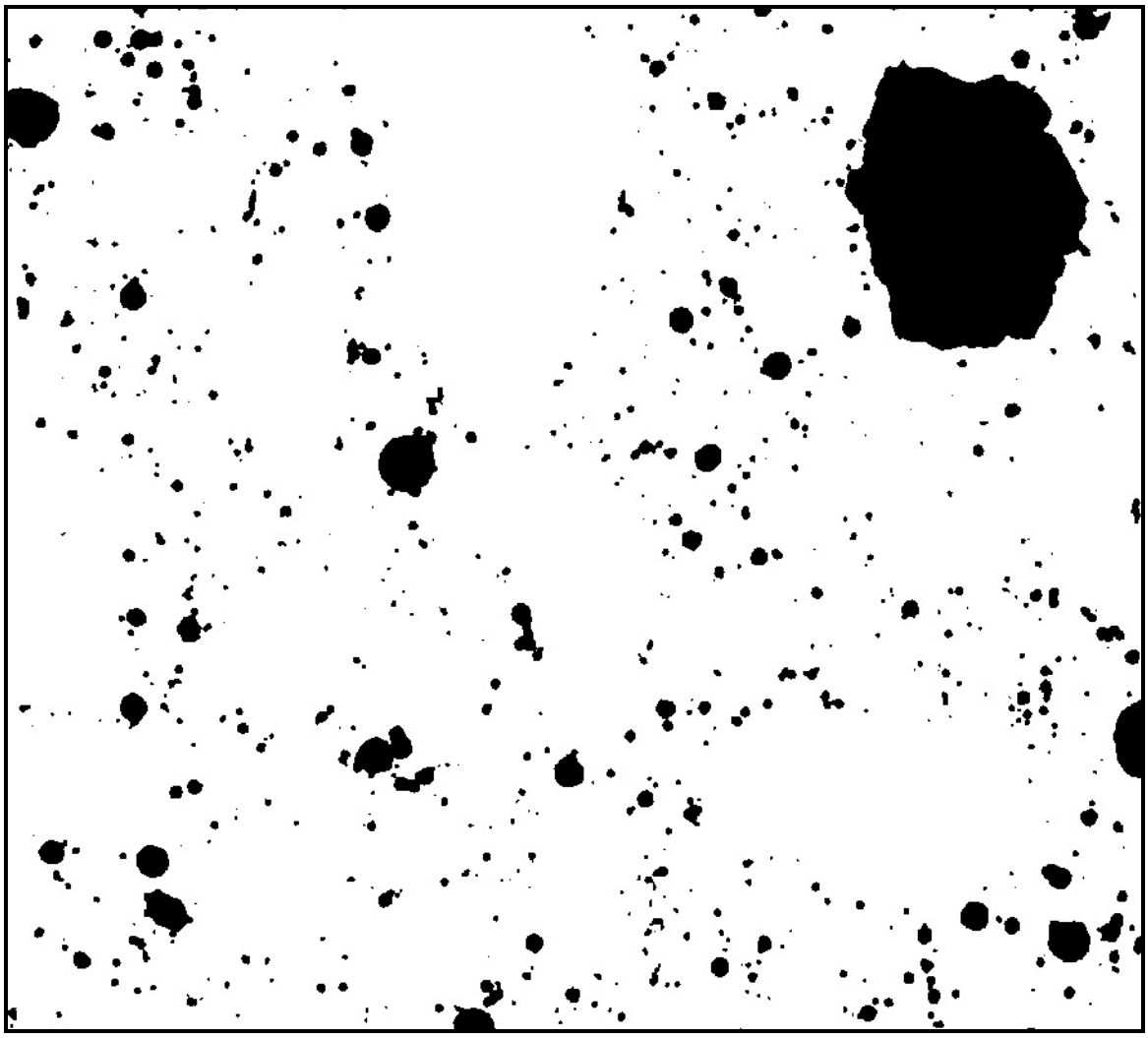

Figure A-10: Office desktop scanner image of corresponding area from sample AE-MED after setting threshold to 160, and followed by an inversion (so that air voids appear black). Image dimensions 13.060 x 11.754 mm (magnified here approximately 12x).

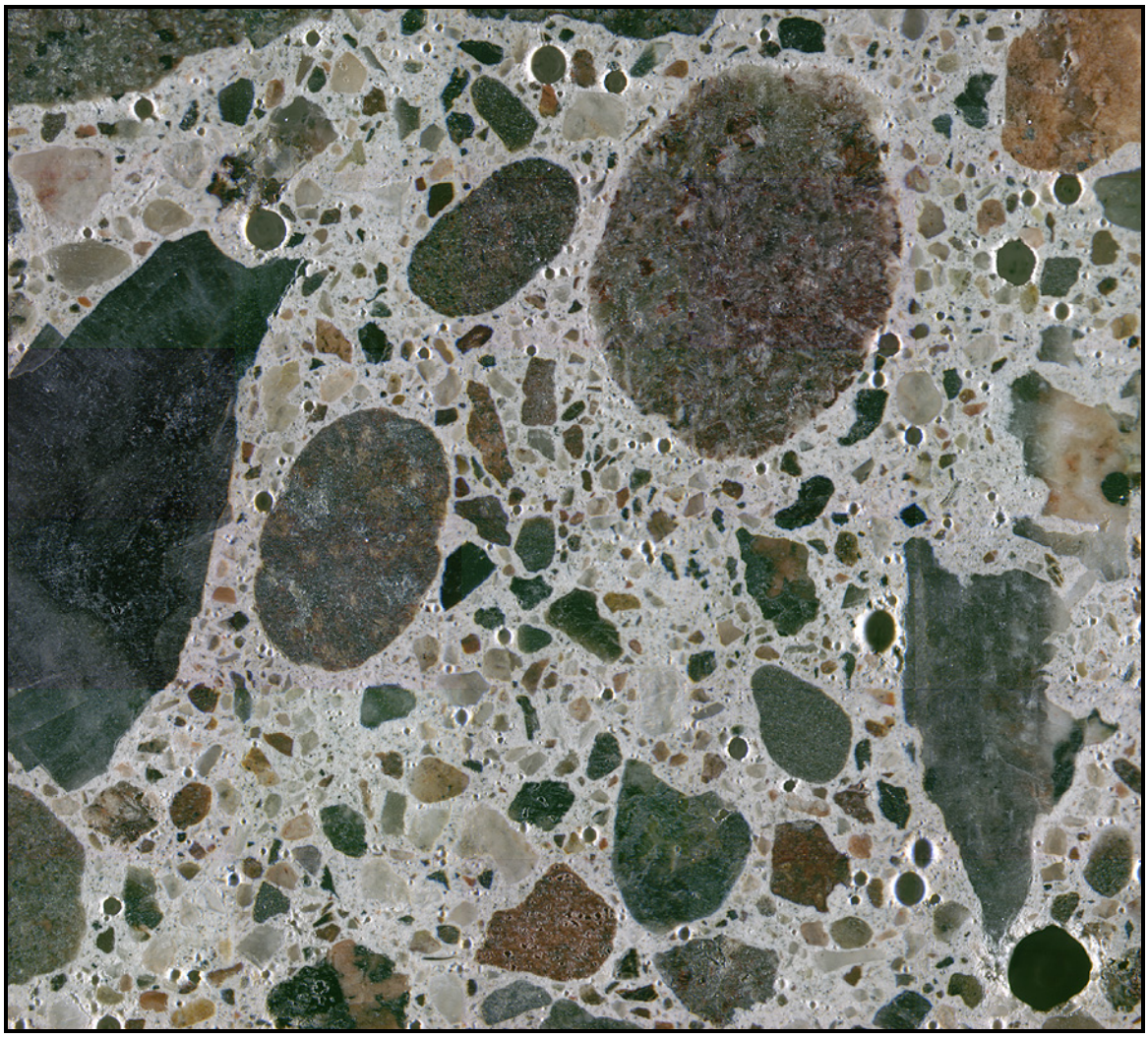

Figure A-11: A 5 x 6 mosaic of stereo microscope images collected during manual point count from sample AE-LO, image dimensions 13.060 x 11.754 mm (magnified here approximately 12x).

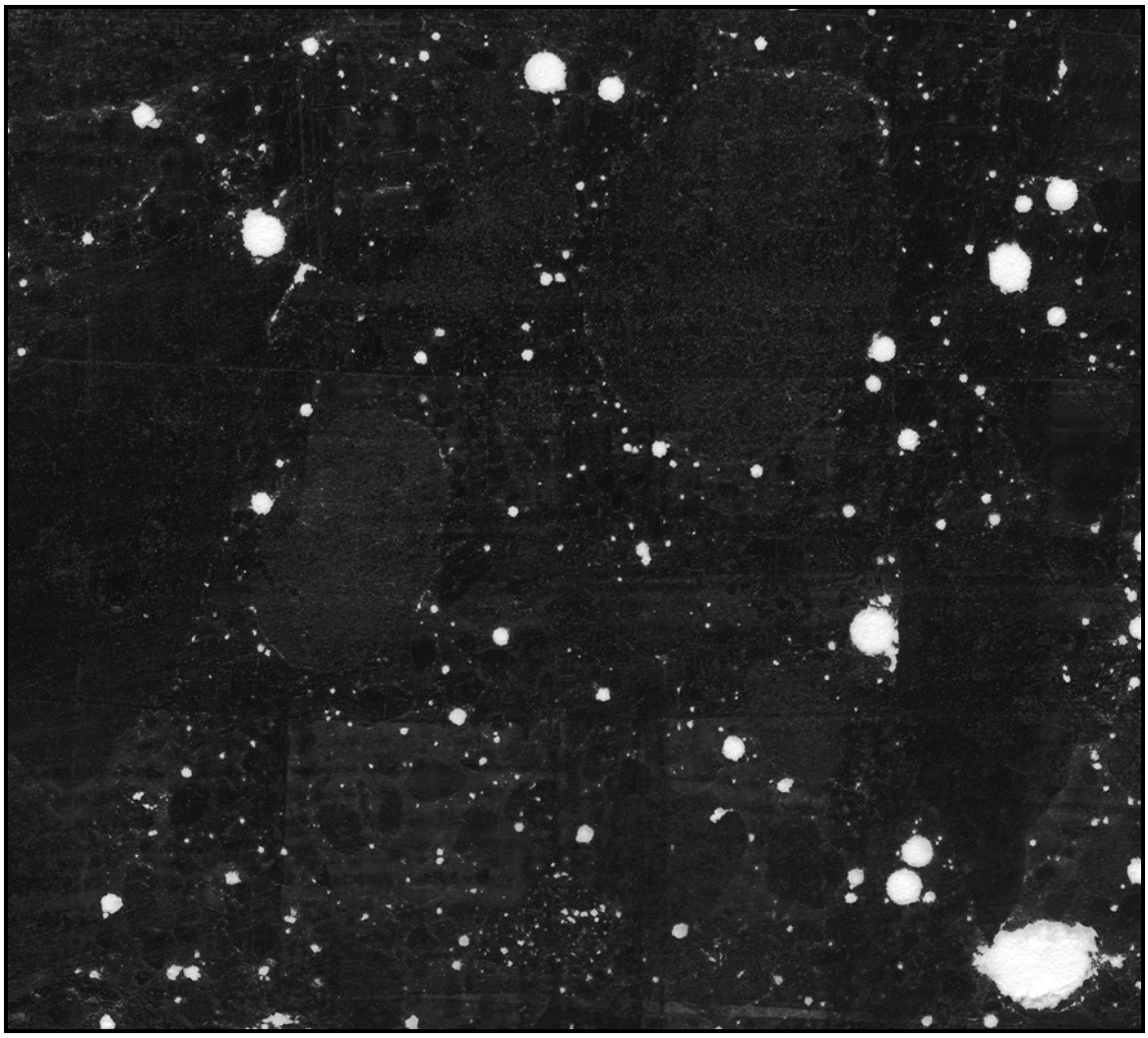

Figure A-12: High resolution scanner image of corresponding area from sample AE-LO after black and white treatment, image dimensions 13.060 x 11.754 mm (magnified here approximately 12x).

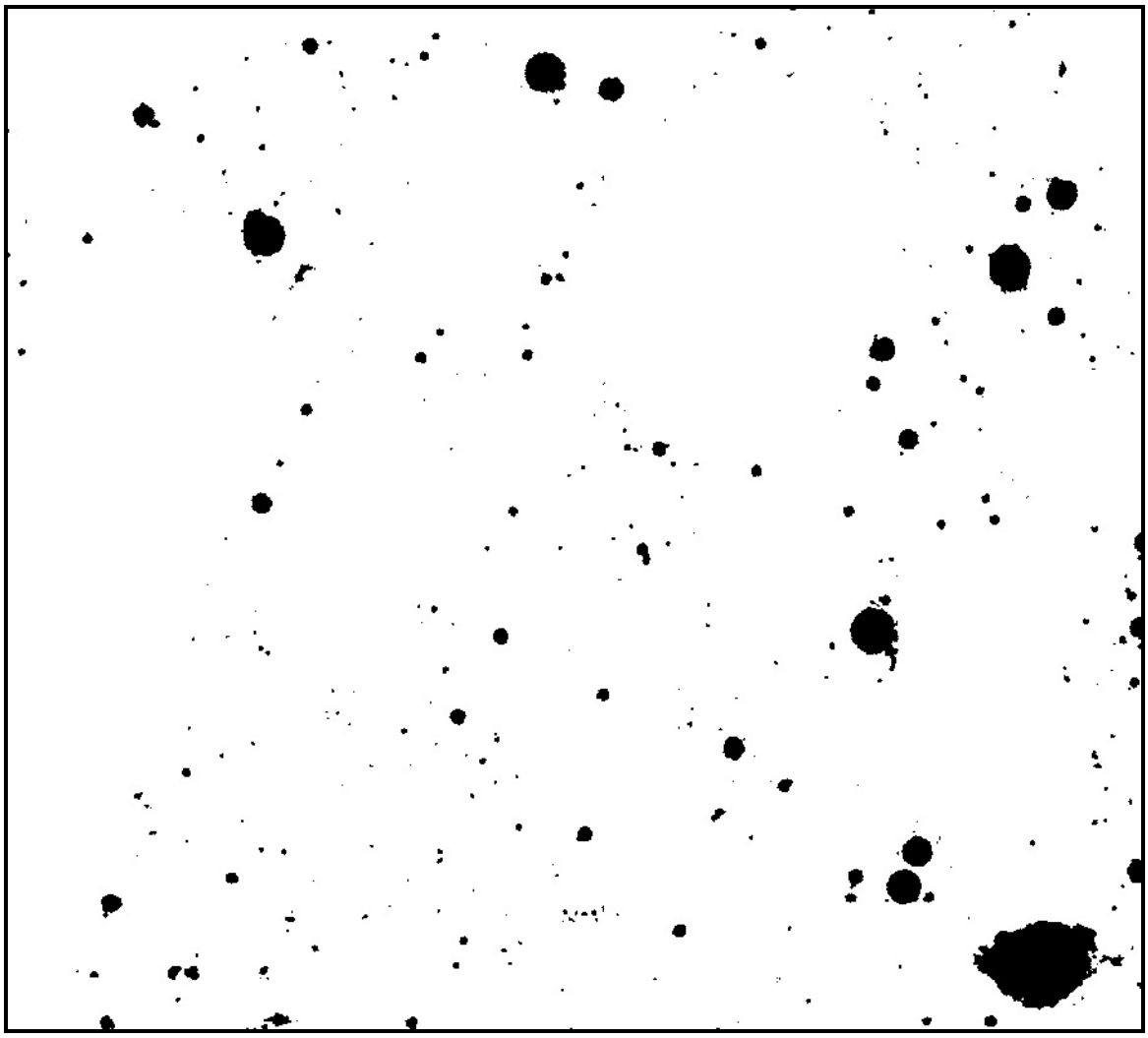

Figure A-13: High resolution scanner image of corresponding area from sample AE-LO after setting threshold to 160, and followed by an inversion (so that air voids appear black). Image dimensions 13.060 x 11.754 mm (magnified here approximately 12x).

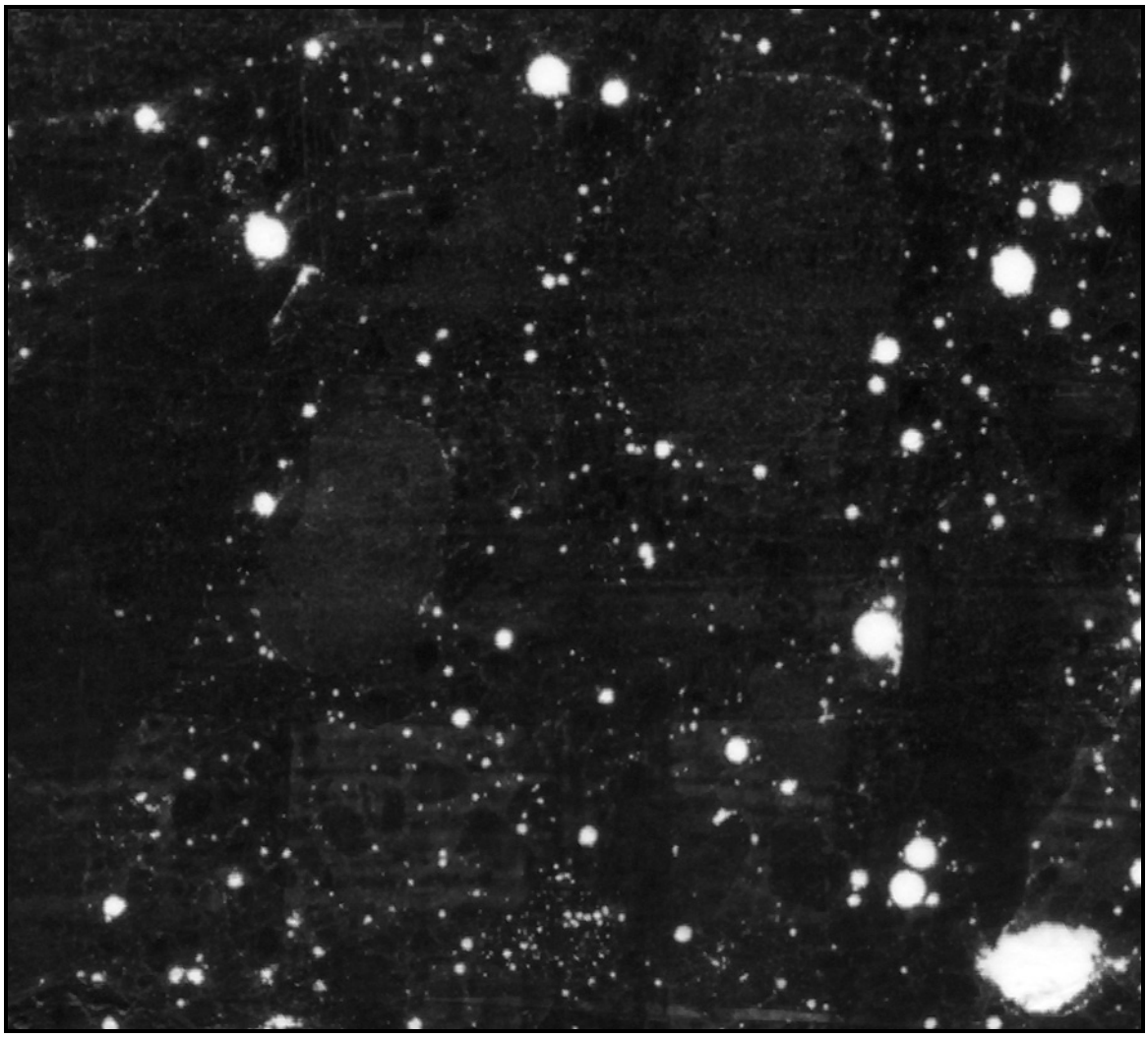

Figure A-14: Office desktop scanner image of corresponding area from sample AE-LO after black and white treatment, image dimensions 13.060 x 11.754 mm (magnified here approximately 12x).

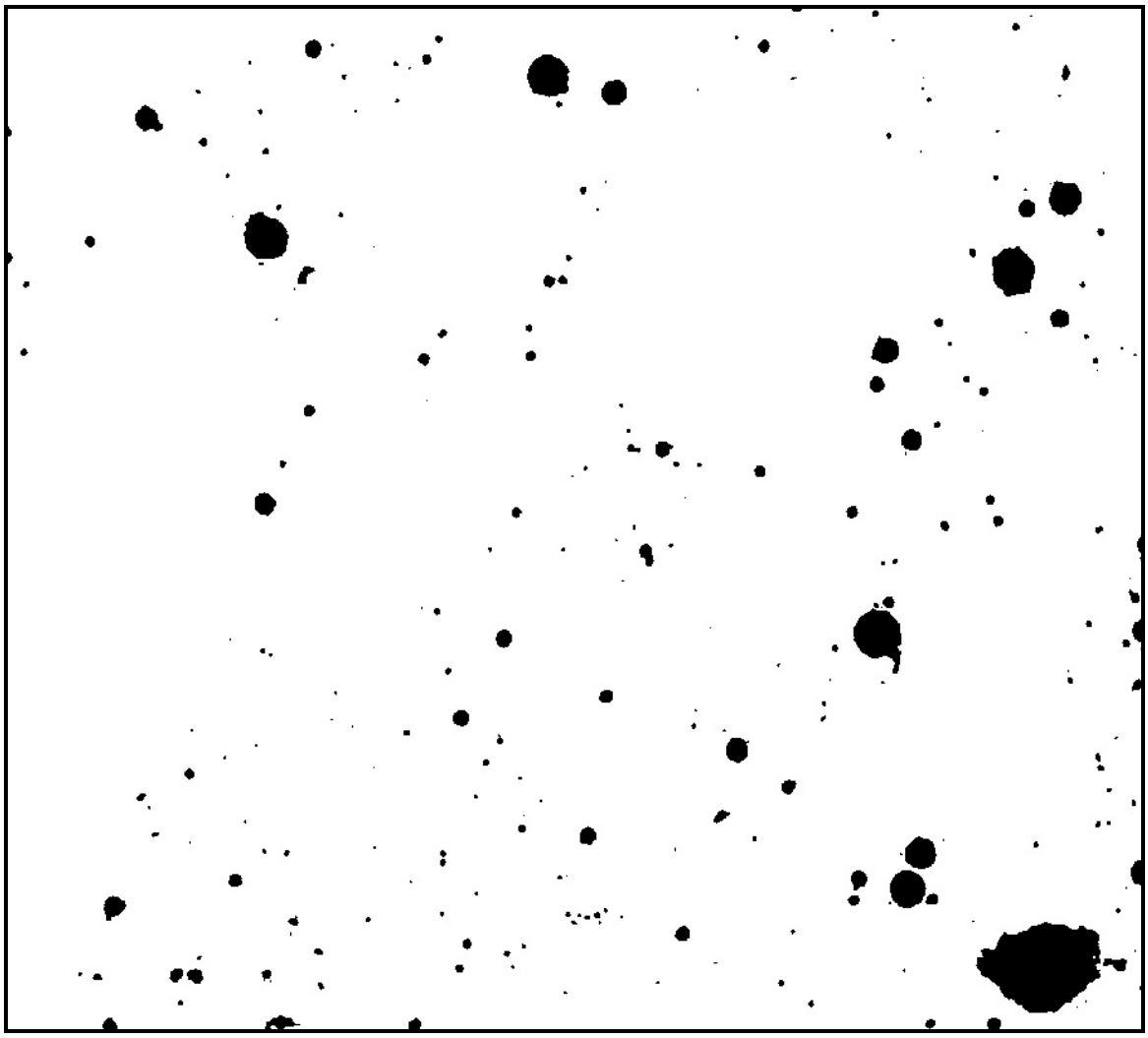

Figure A-15: Office desktop scanner image of corresponding area from sample AE-LO after setting threshold to 160, and followed by an inversion (so that air voids appear black). Image dimensions 13.060 x 11.754 mm (magnified here approximately 12x).

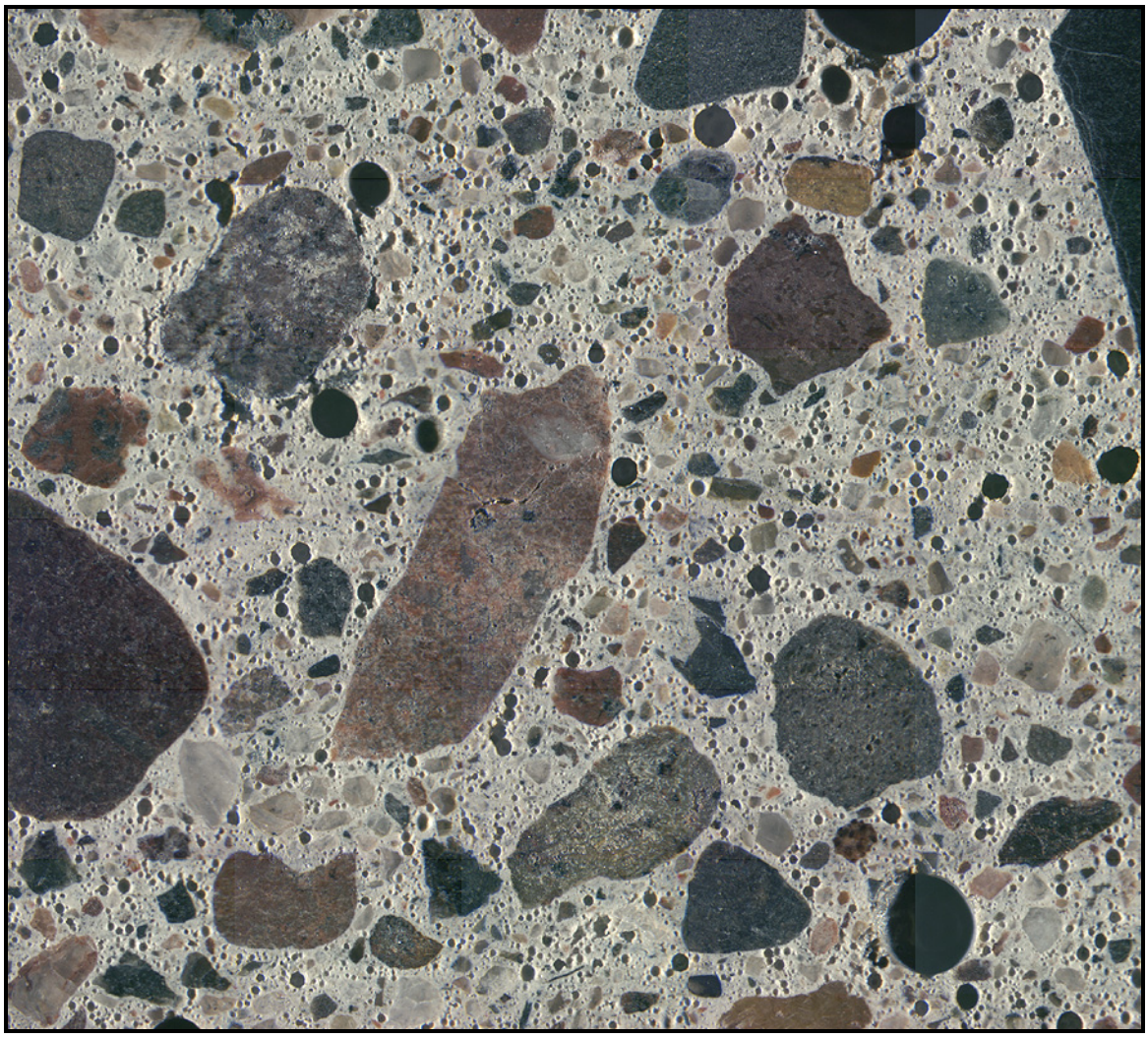

Figure A-16: A 5 x 6 mosaic of stereo microscope images collected during manual point count from sample MA-HI, image dimensions 13.060 x 11.754 mm (magnified here approximately 12x).

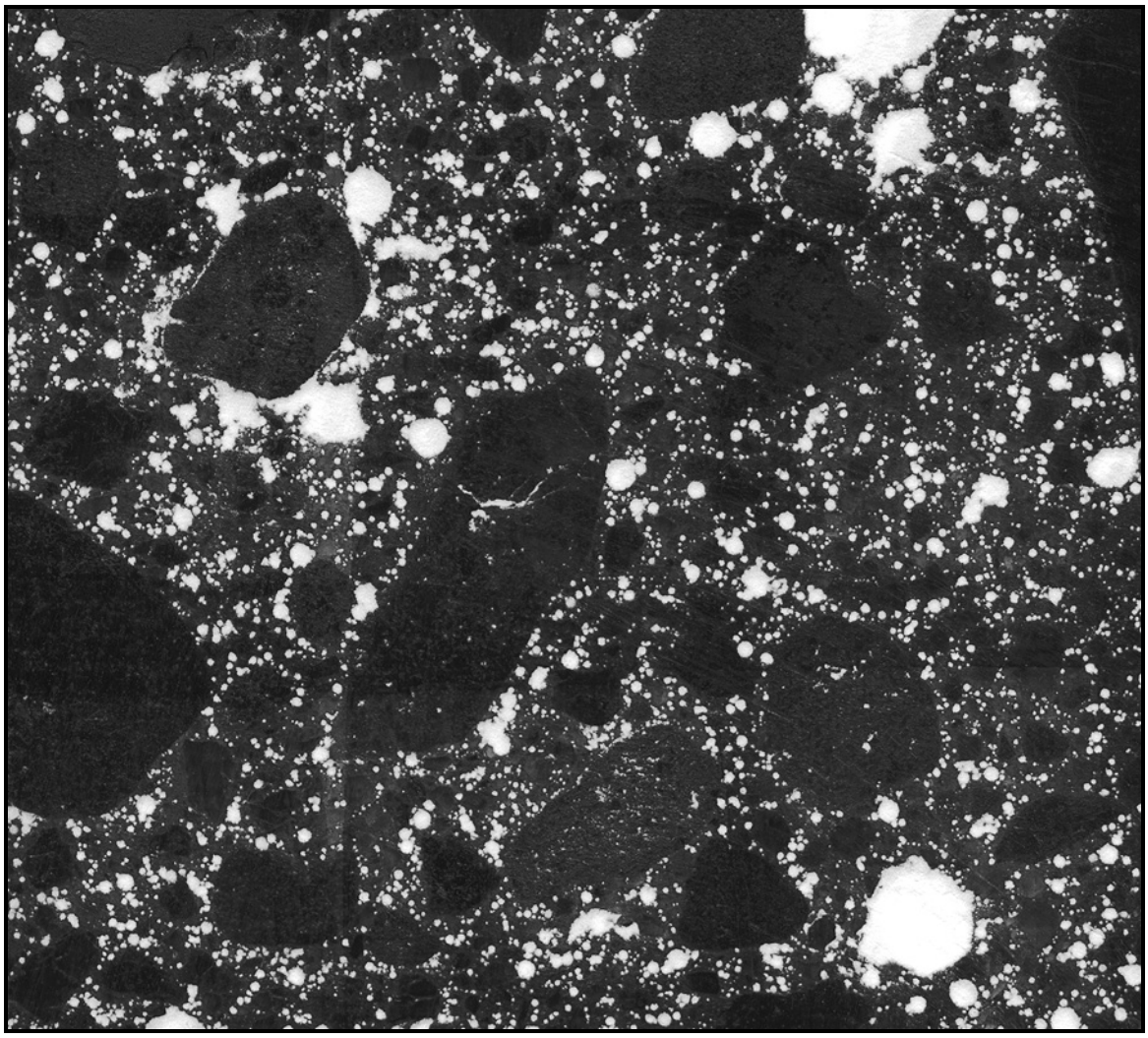

Figure A-17: High resolution scanner image of corresponding area from sample MA-HI after black and white treatment, image dimensions 13.060 x 11.754 mm (magnified here approximately 12x).

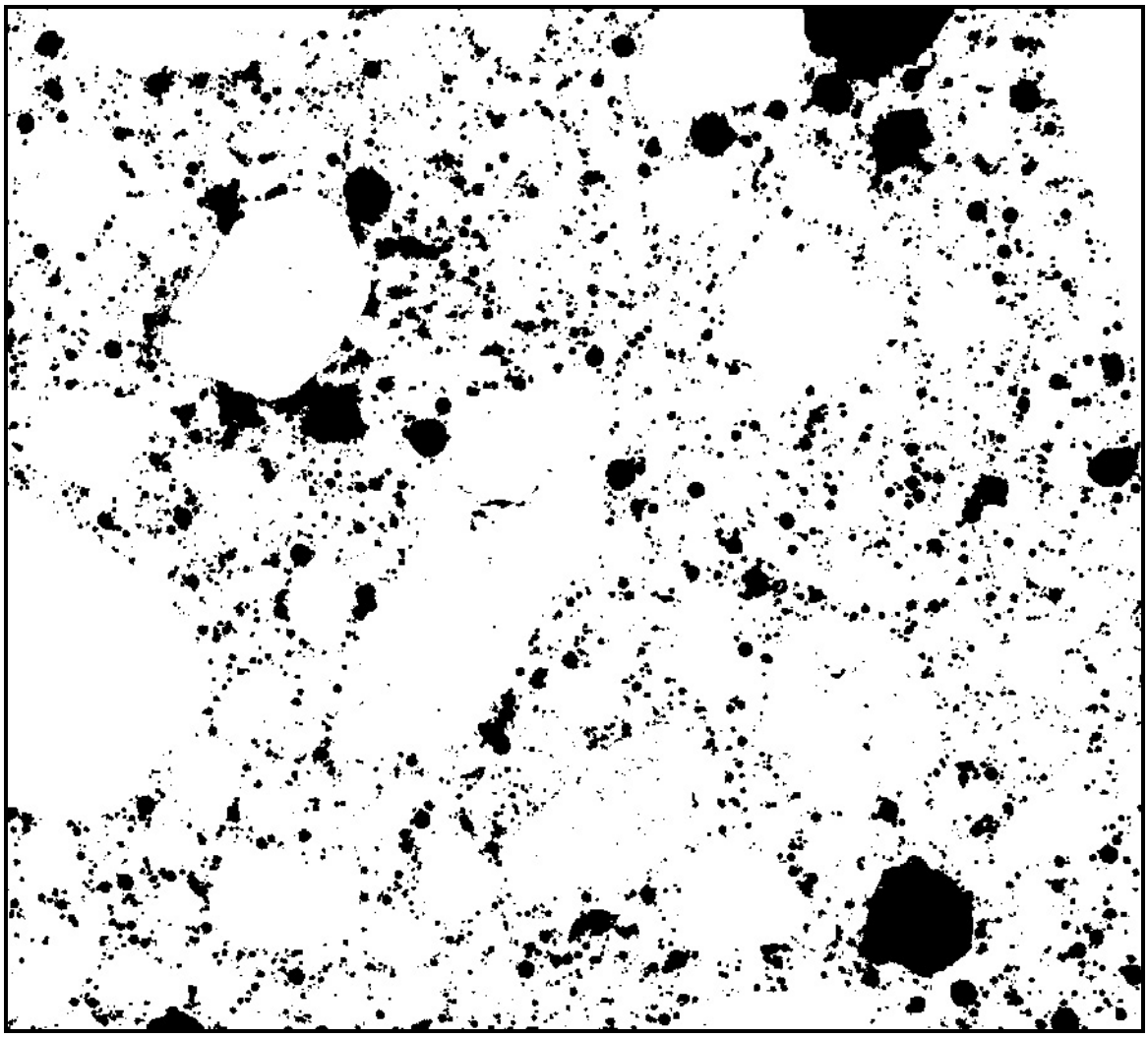

Figure A-18: High resolution scanner image of corresponding area from sample MA-HI after setting threshold to 160, and followed by an inversion (so that air voids appear black). Image dimensions 13.060 x 11.754 mm (magnified here approximately 12x).

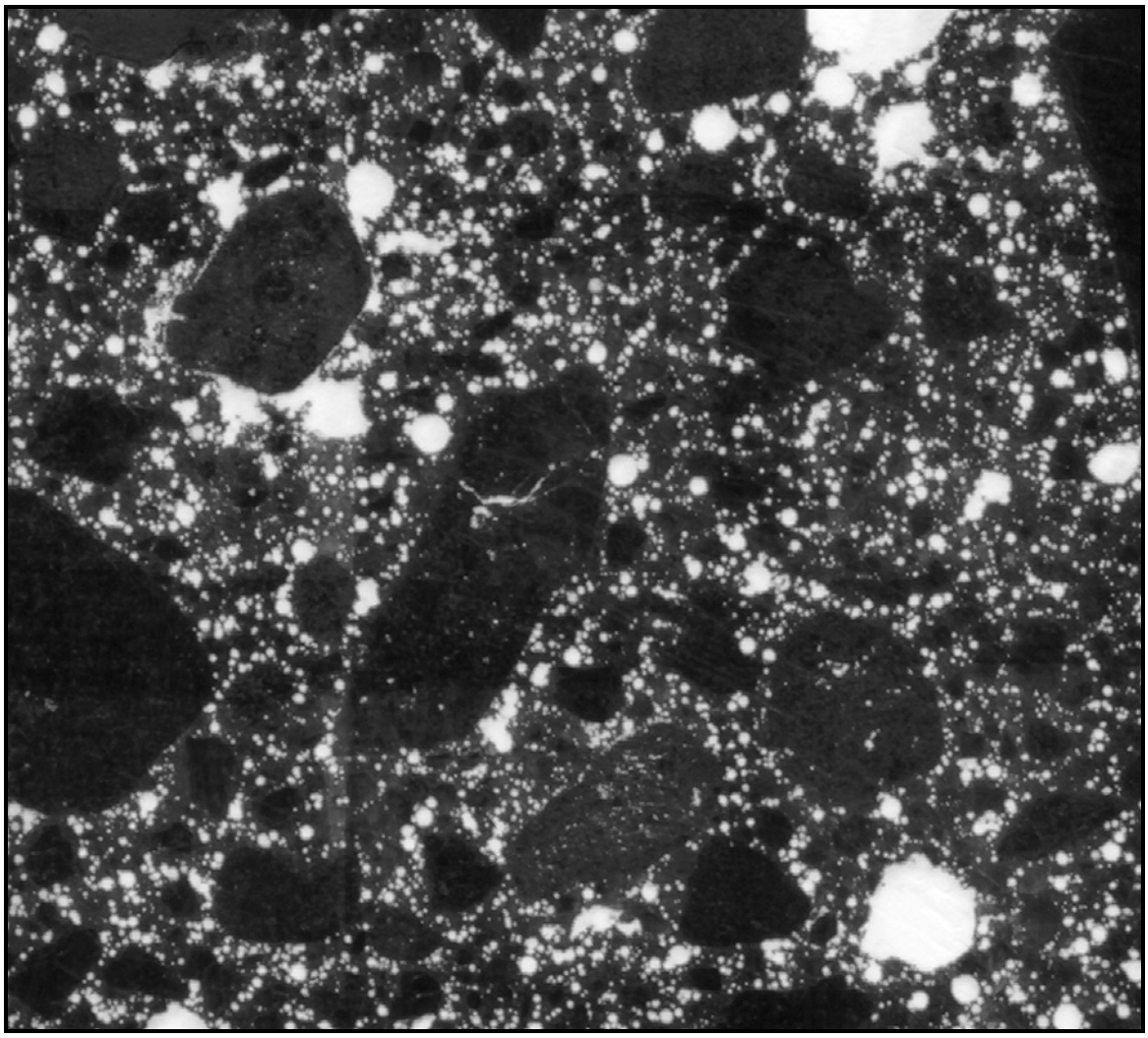

Figure A-19: Office desktop scanner image of corresponding area from sample MA-HI after black and white treatment, image dimensions 13.060 x 11.754 mm (magnified here approximately 12x).

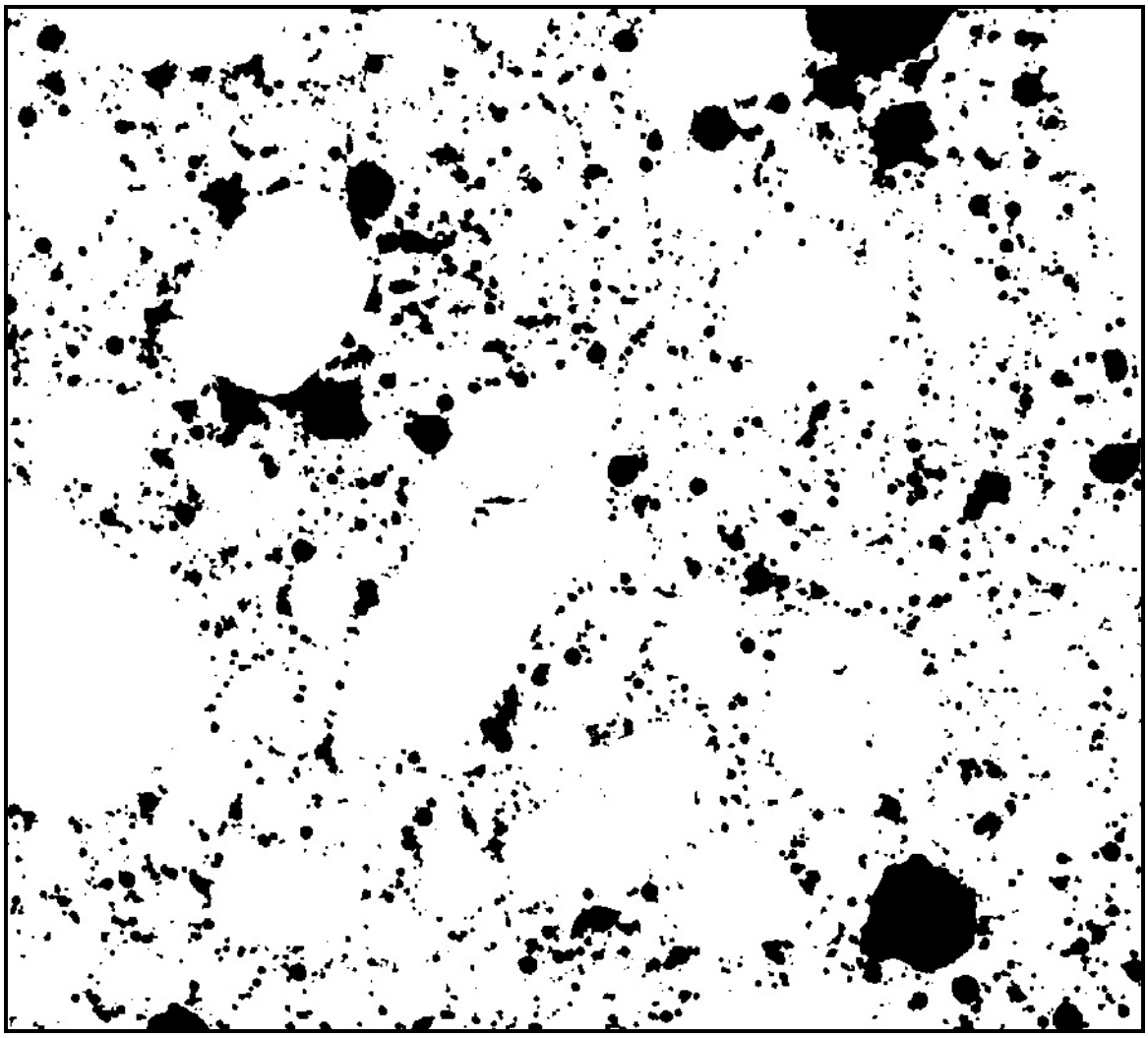

Figure A-20: Office desktop scanner image of corresponding area from sample MA-HI after setting threshold to 160, and followed by an inversion (so that air voids appear black). Image dimensions 13.060 x 11.754 mm (magnified here approximately 12x).

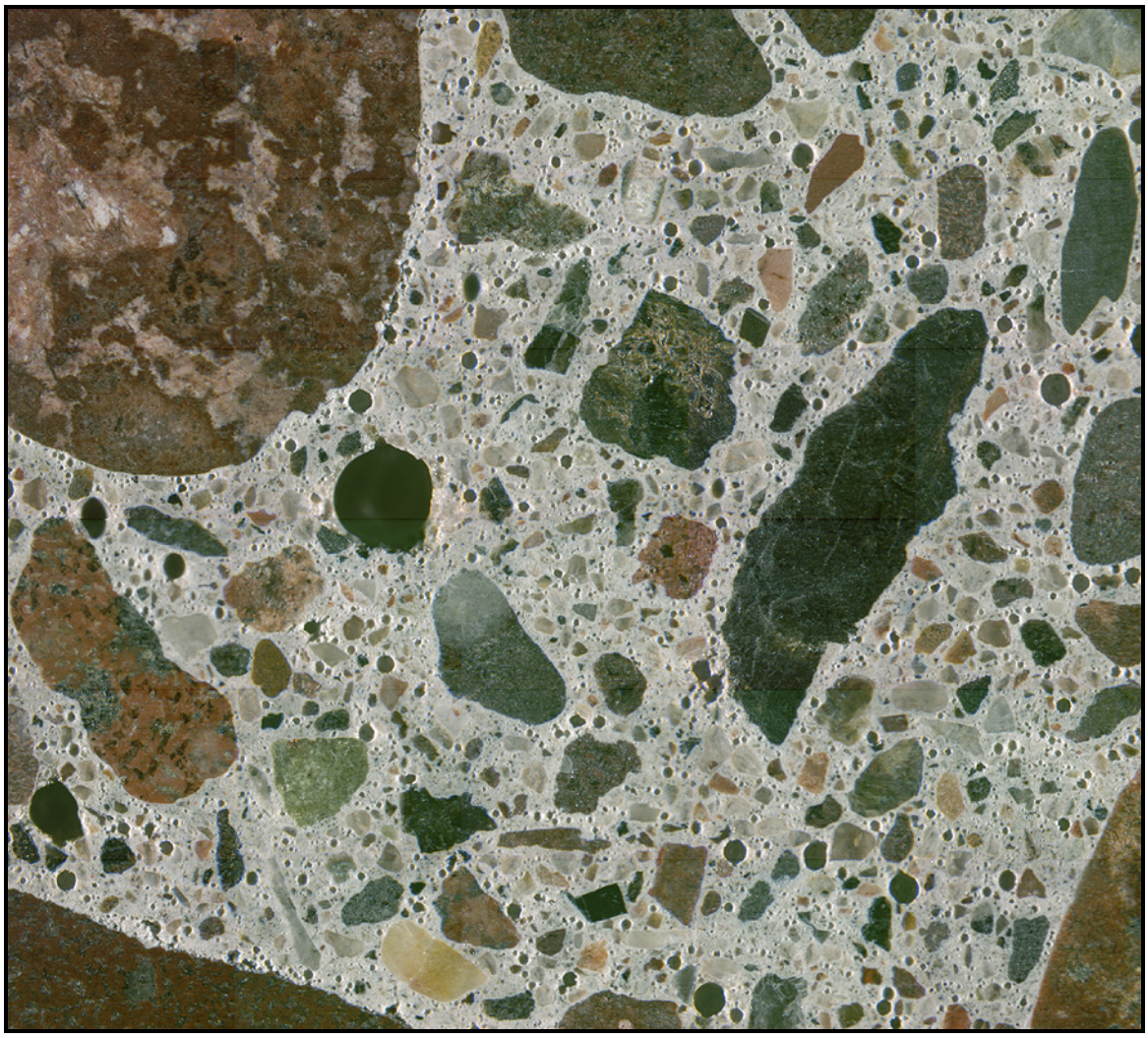

Figure A-21: A 5 x 6 mosaic of stereo microscope images collected during manual point count from sample MA-MED, image dimensions 13.060 x 11.754 mm (magnified here approximately 12x).

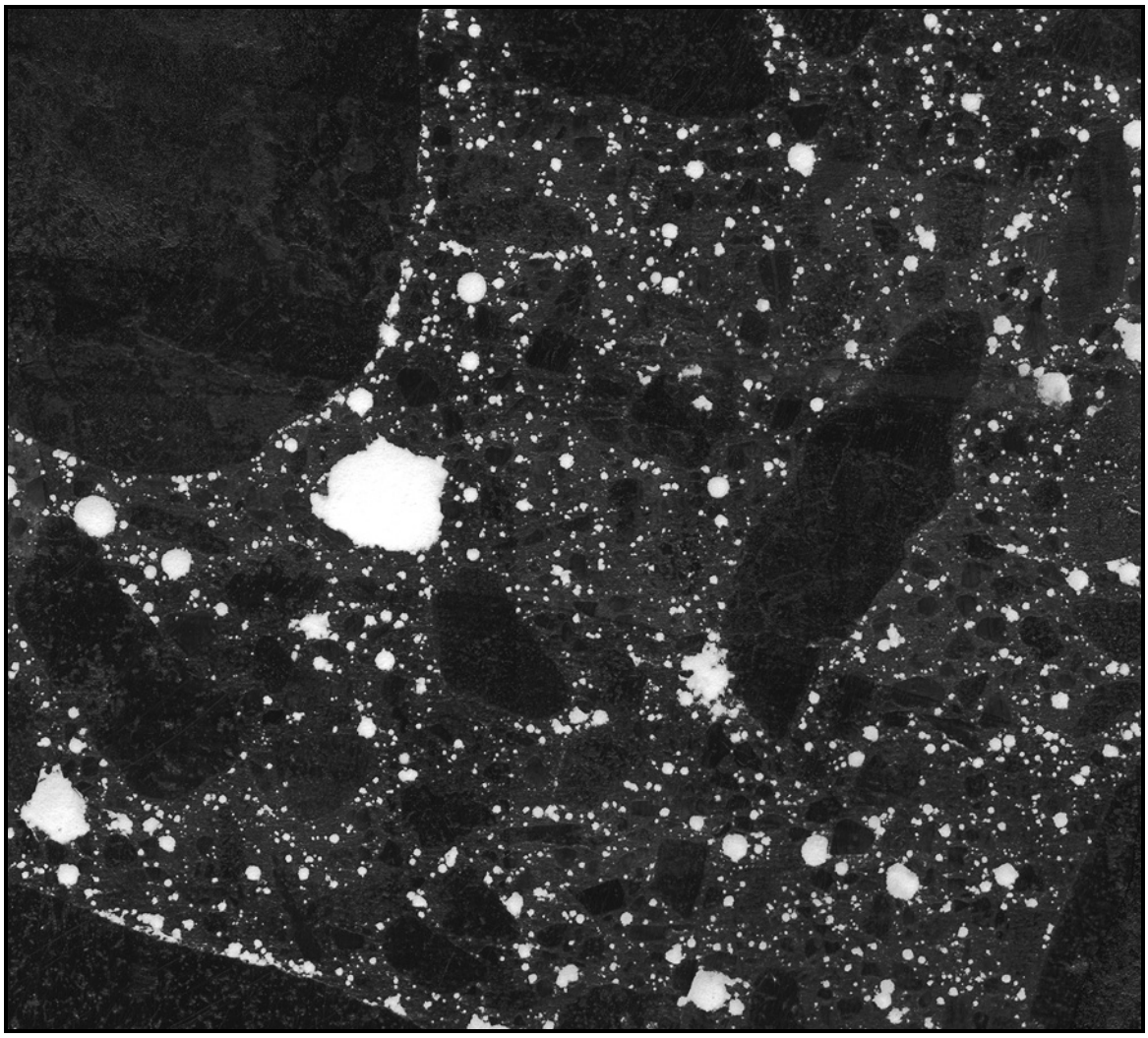

Figure A-22: High resolution scanner image of corresponding area from sample MA-MED after black and white treatment, image dimensions 13.060 x 11.754 mm (magnified here approximately 12x).

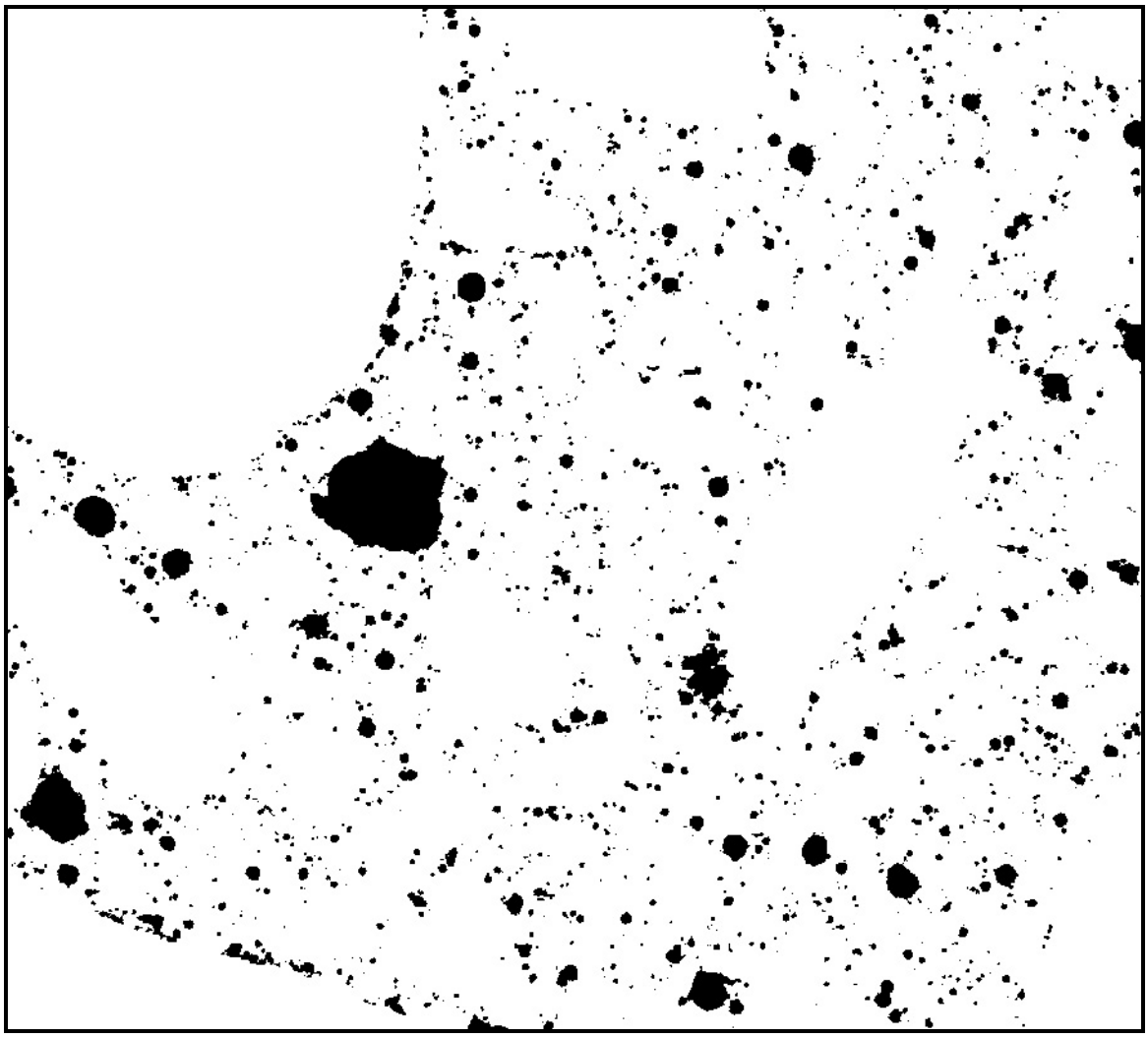

Figure A-23: High resolution scanner image of corresponding area from sample MA-MED after setting threshold to 160, and followed by an inversion (so that air voids appear black). Image dimensions 13.060 x 11.754 mm (magnified here approximately 12x).

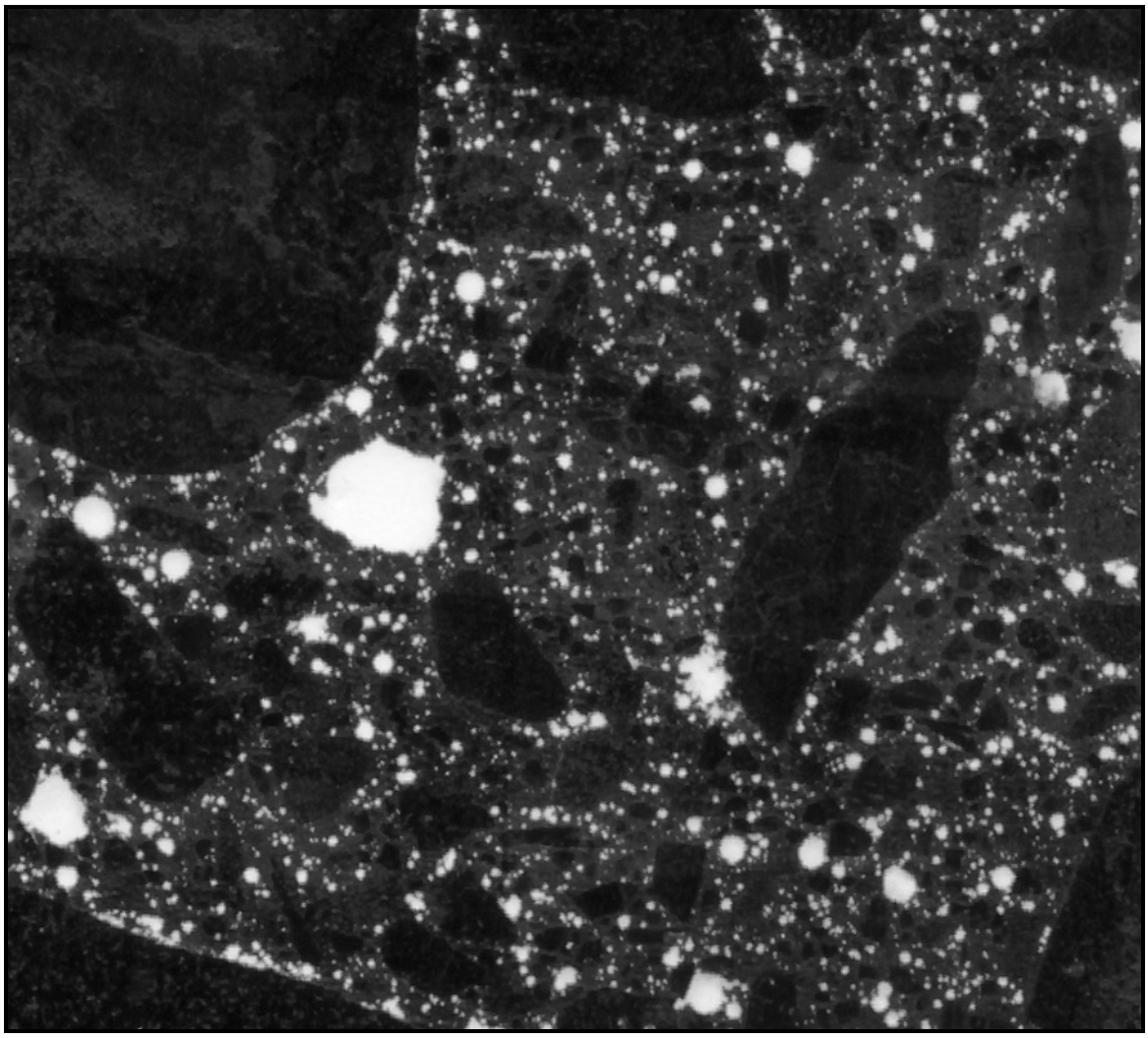

Figure A-24: Office desktop scanner image of corresponding area from sample MA-MED after black and white treatment, image dimensions 13.060 x 11.754 mm (magnified here approximately 12x).

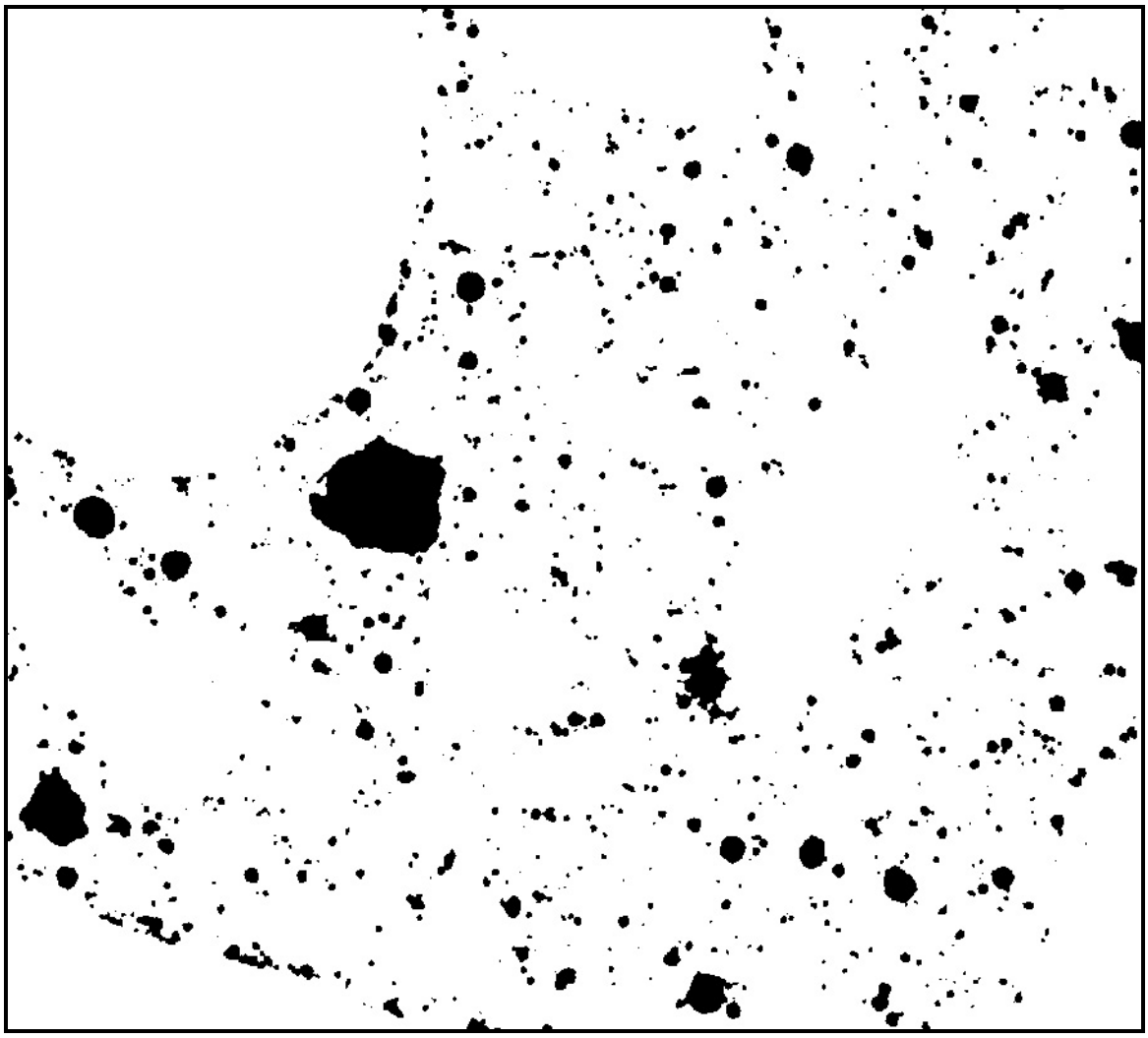

Figure A-25: Office desktop scanner image of corresponding area from sample MA-MED after setting threshold to 160, and followed by an inversion (so that air voids appear black). Image dimensions 13.060 x 11.754 mm (magnified here approximately 12x).

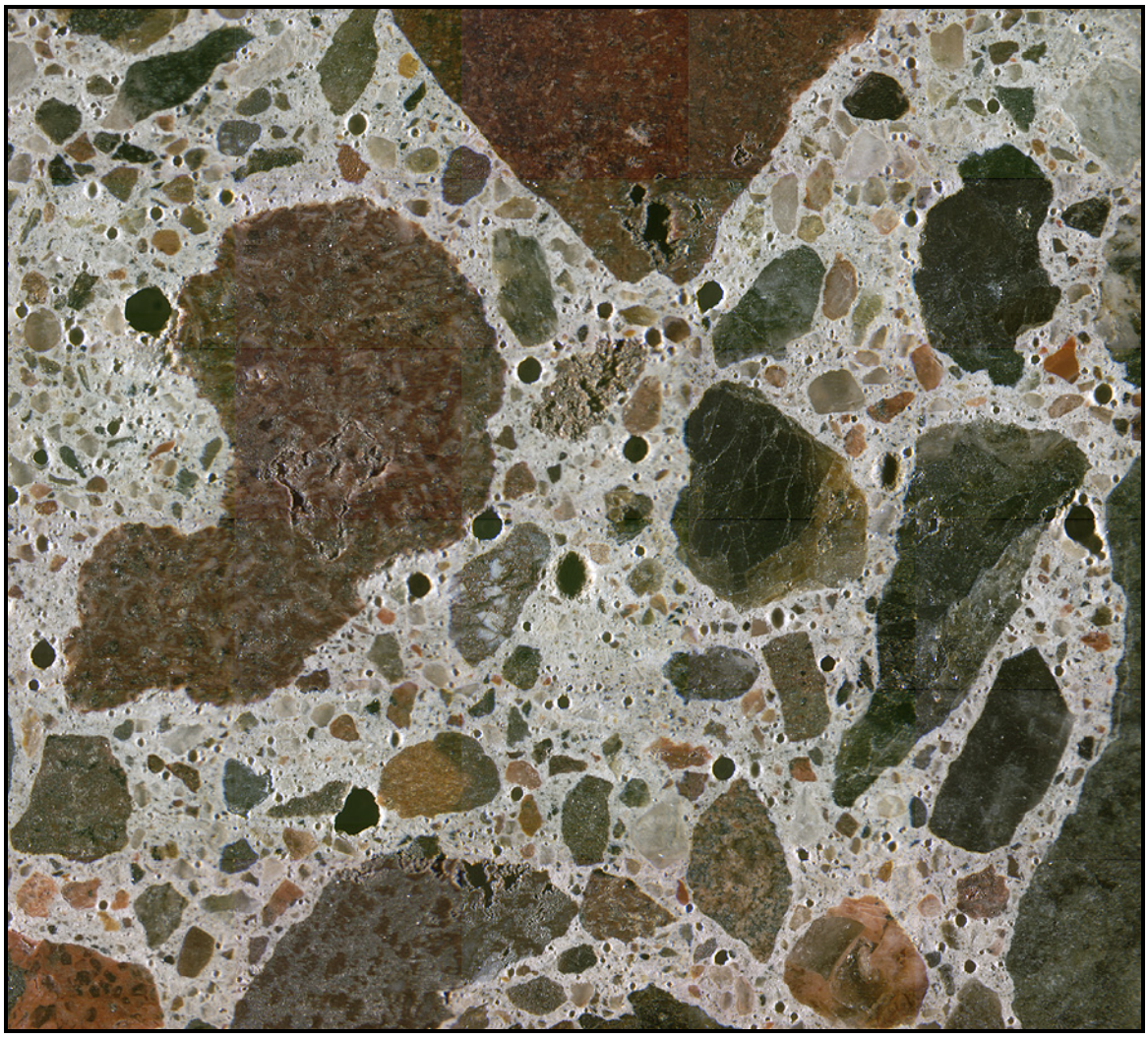

Figure A-26: A 5 x 6 mosaic of stereo microscope images collected during manual point count from sample MA-LO, image dimensions 13.060 x 11.754 mm (magnified here approximately 12x).

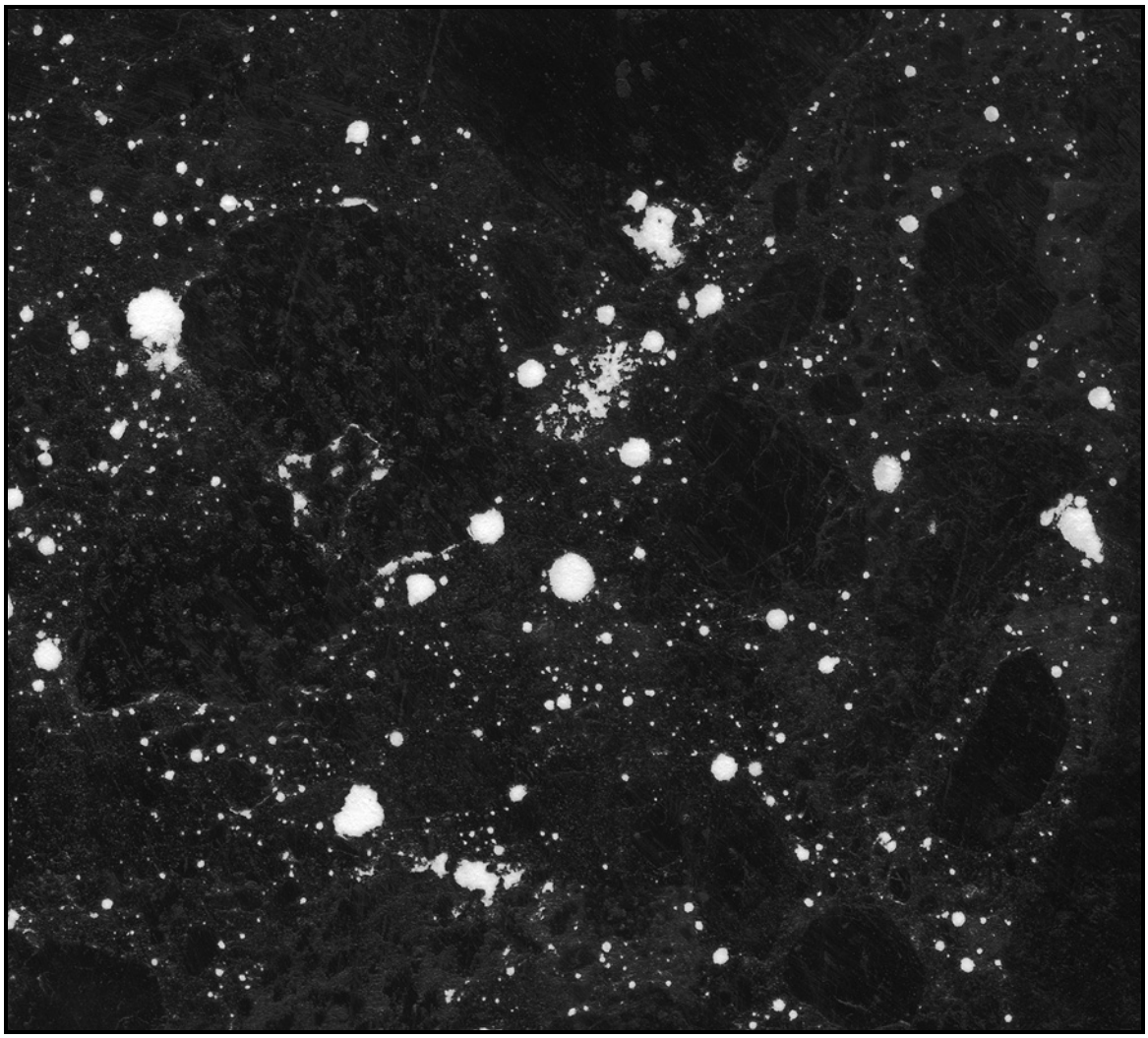

Figure A-27: High resolution scanner image of corresponding area from sample MA-LO after black and white treatment, image dimensions 13.060 x 11.754 mm (magnified here approximately 12x).

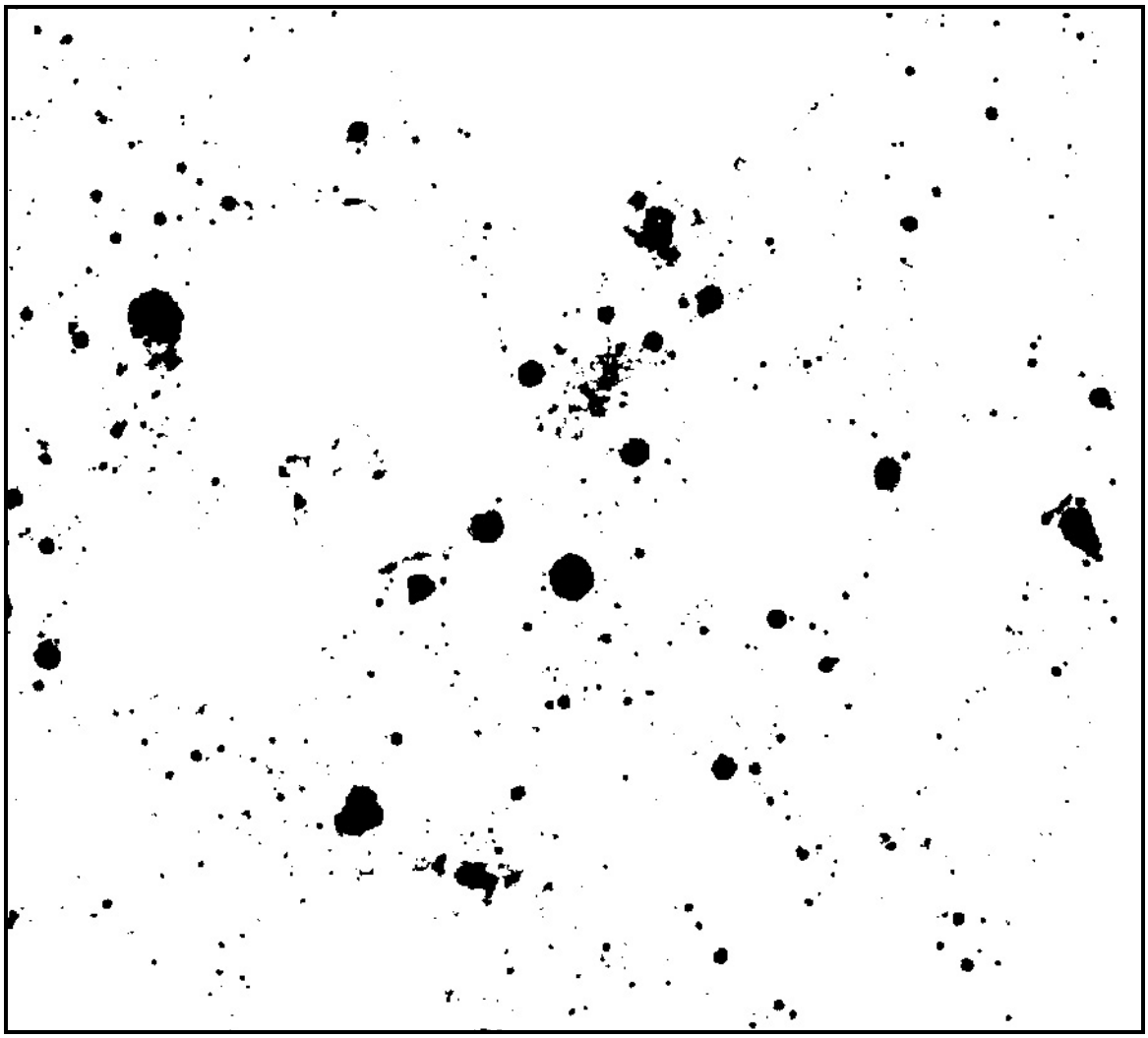

Figure A-28: High resolution scanner image of corresponding area from sample MA-LO after setting threshold to 160, and followed by an inversion (so that air voids appear black). Image dimensions 13.060 x 11.754 mm (magnified here approximately 12x).

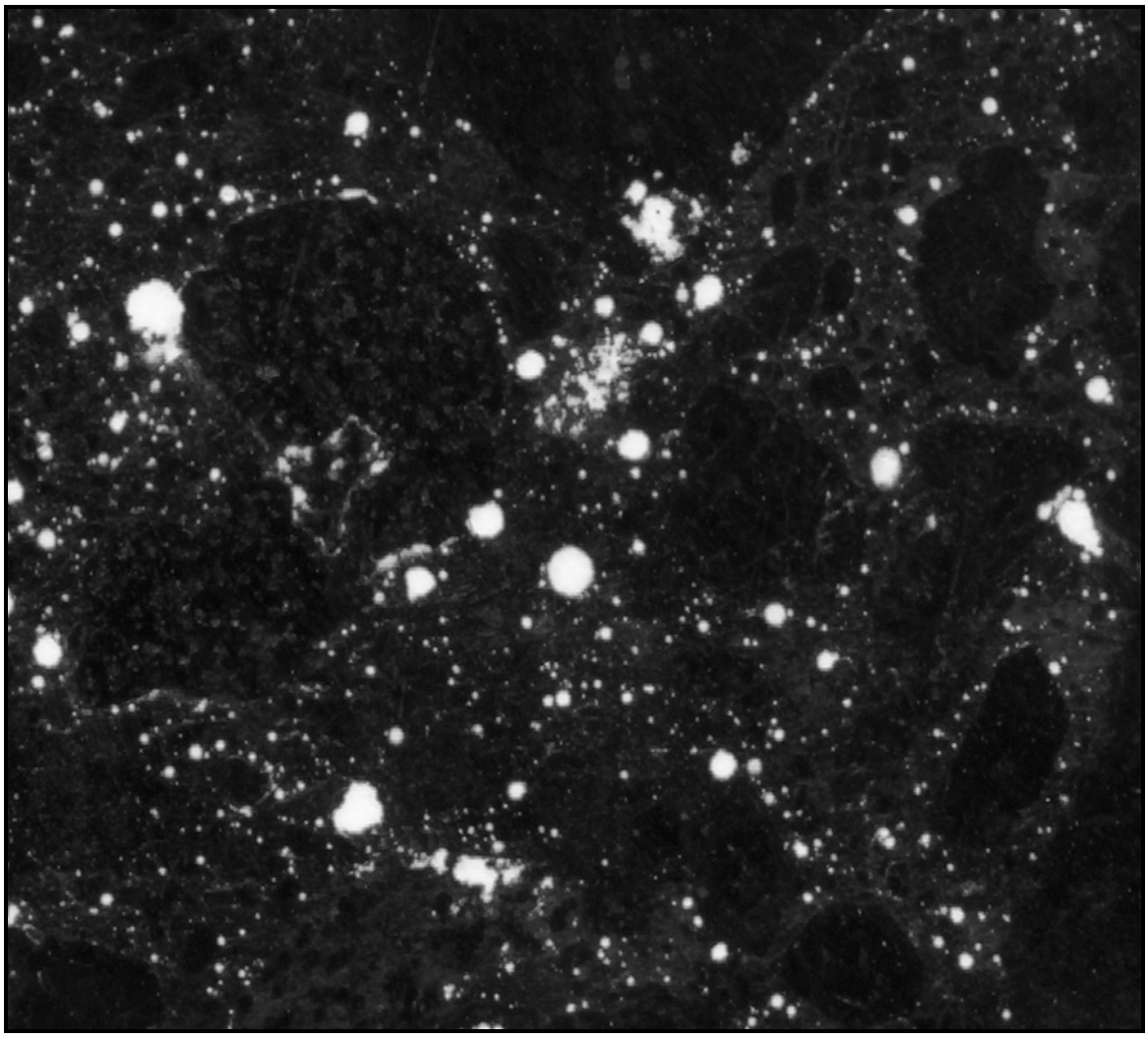

Figure A-29: Office desktop scanner image of corresponding area from sample MA-LO after black and white treatment, image dimensions 13.060 x 11.754 mm (magnified here approximately 12x).

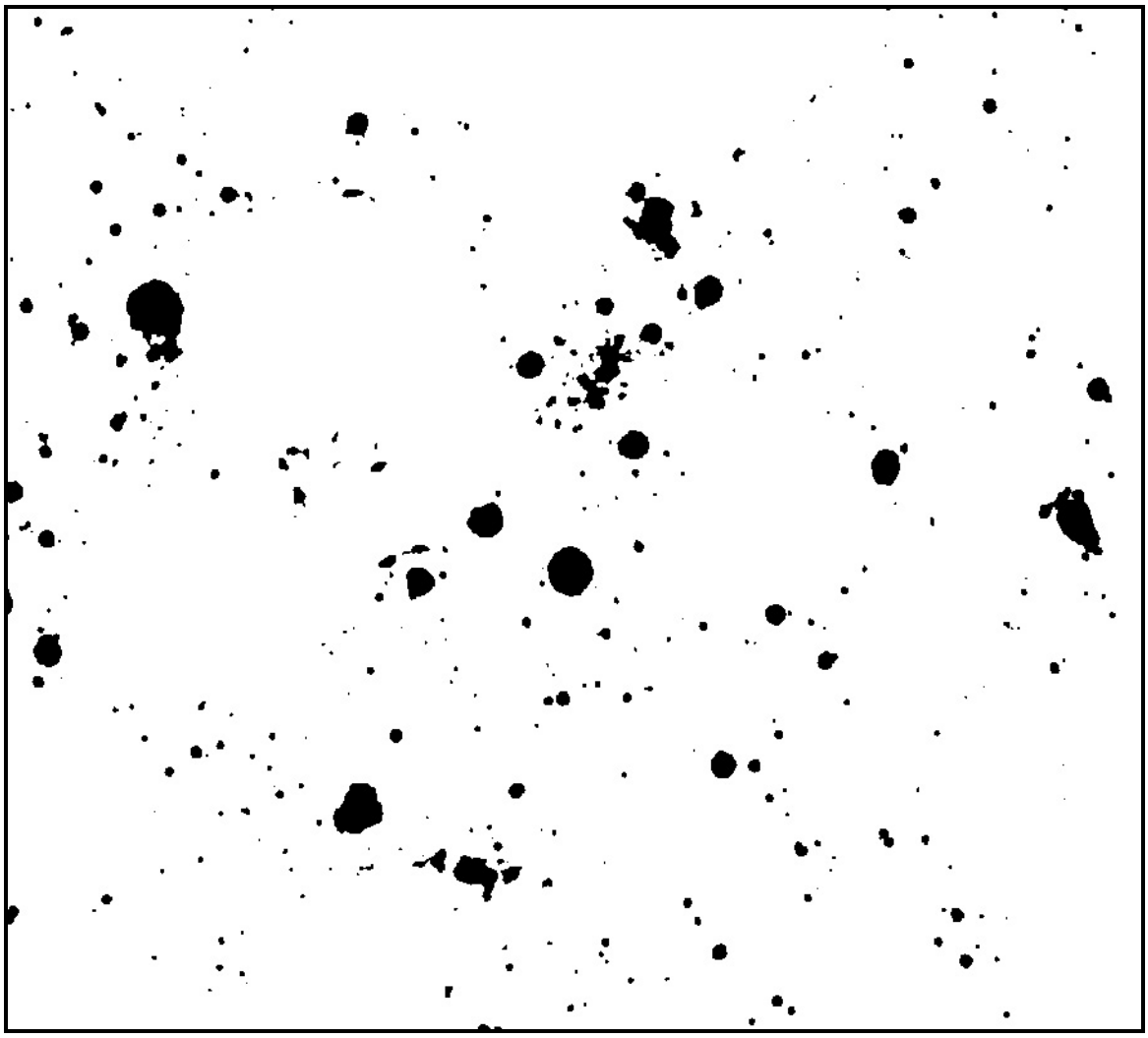

Figure A-30: Office desktop scanner image of corresponding area from sample MA-LO after setting threshold to 160, and followed by an inversion (so that air voids appear black). Image dimensions 13.060 x 11.754 mm (magnified here approximately 12x).

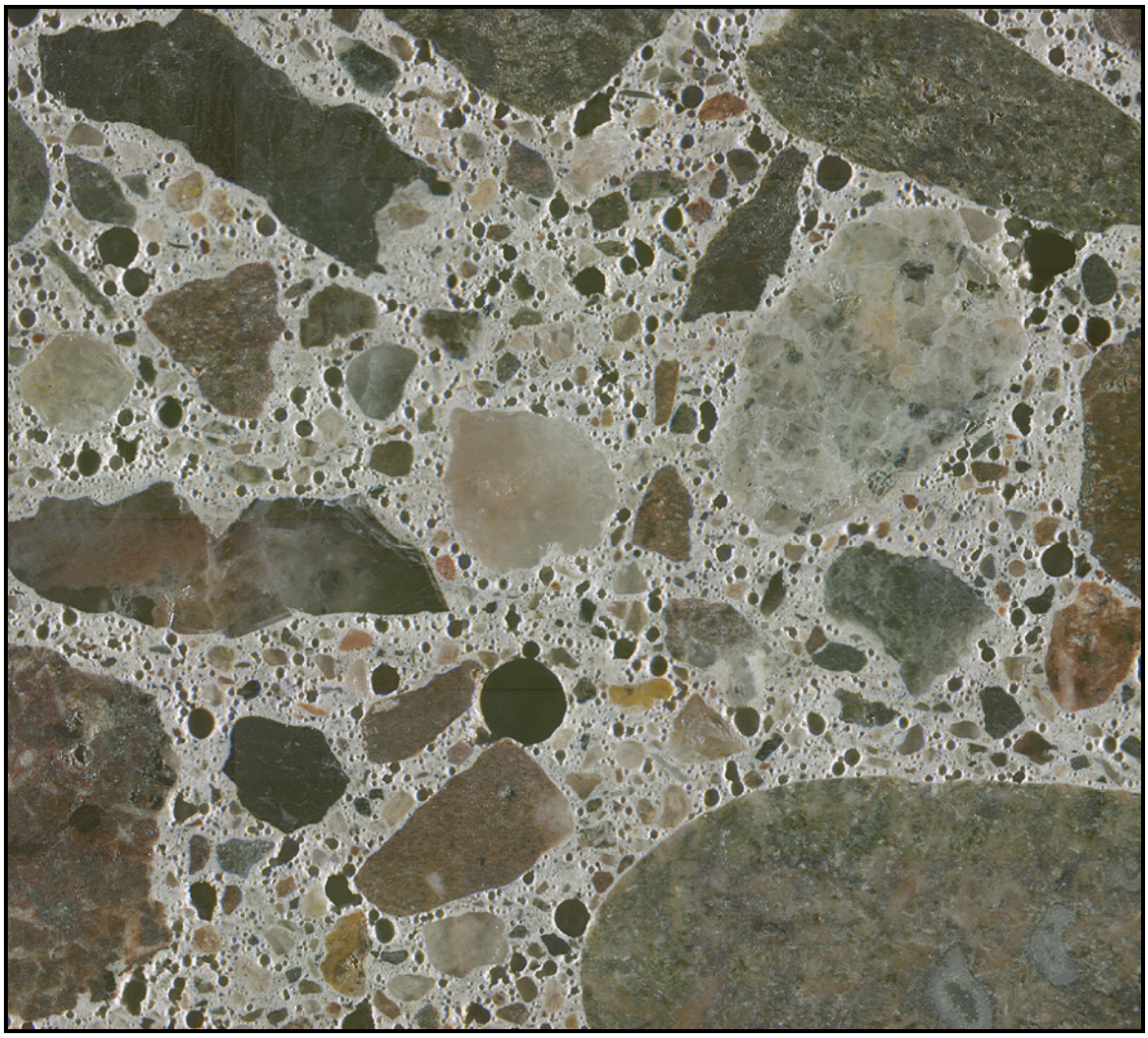

Figure A-31: A 5 x 6 mosaic of stereo microscope images collected during manual point count from sample VR-HI, image dimensions 13.060 x 11.754 mm (magnified here approximately 12x).

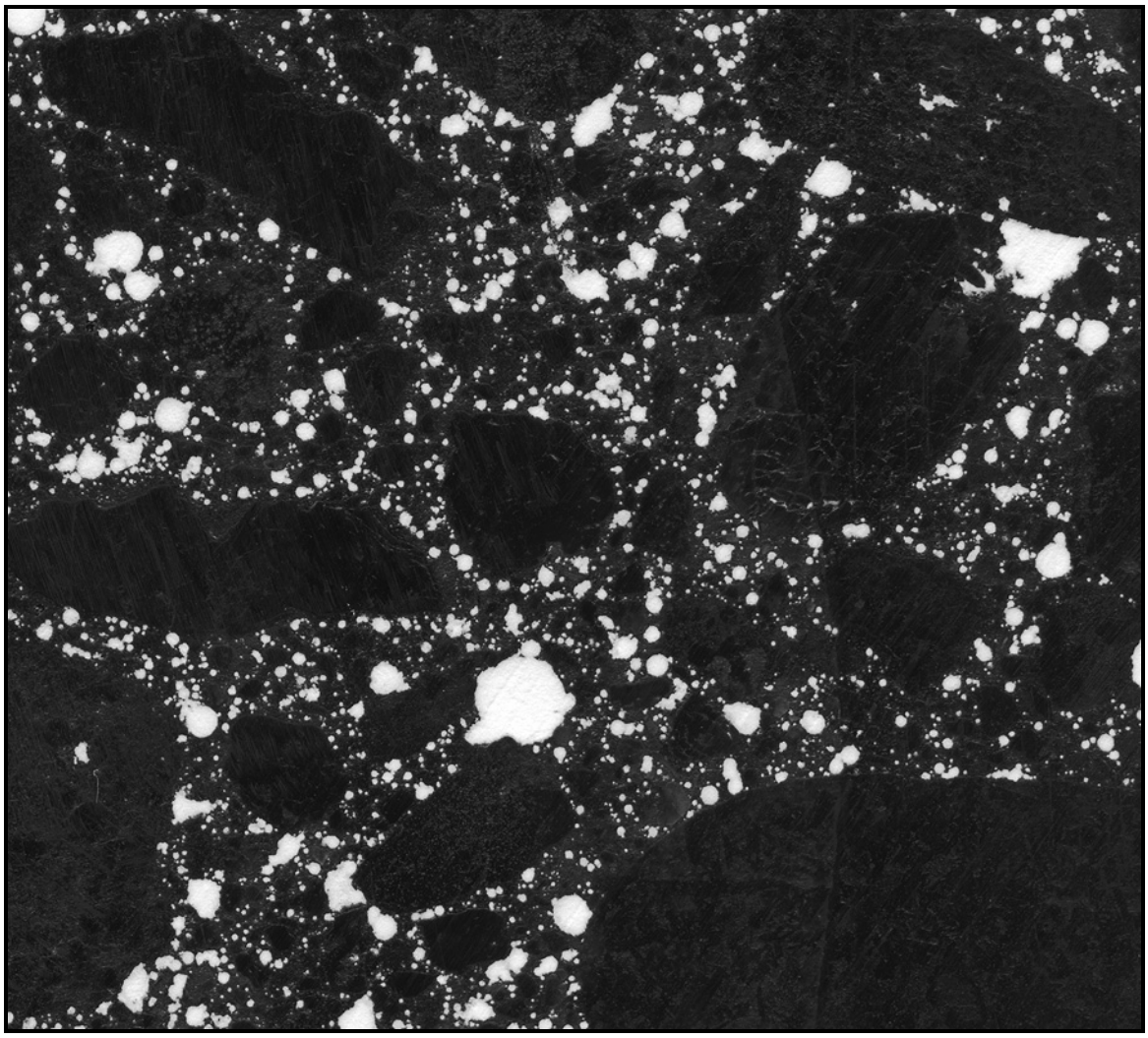

Figure A-32: High resolution scanner image of corresponding area from sample VR-HI after black and white treatment, image dimensions 13.060 x 11.754 mm (magnified here approximately 12x).

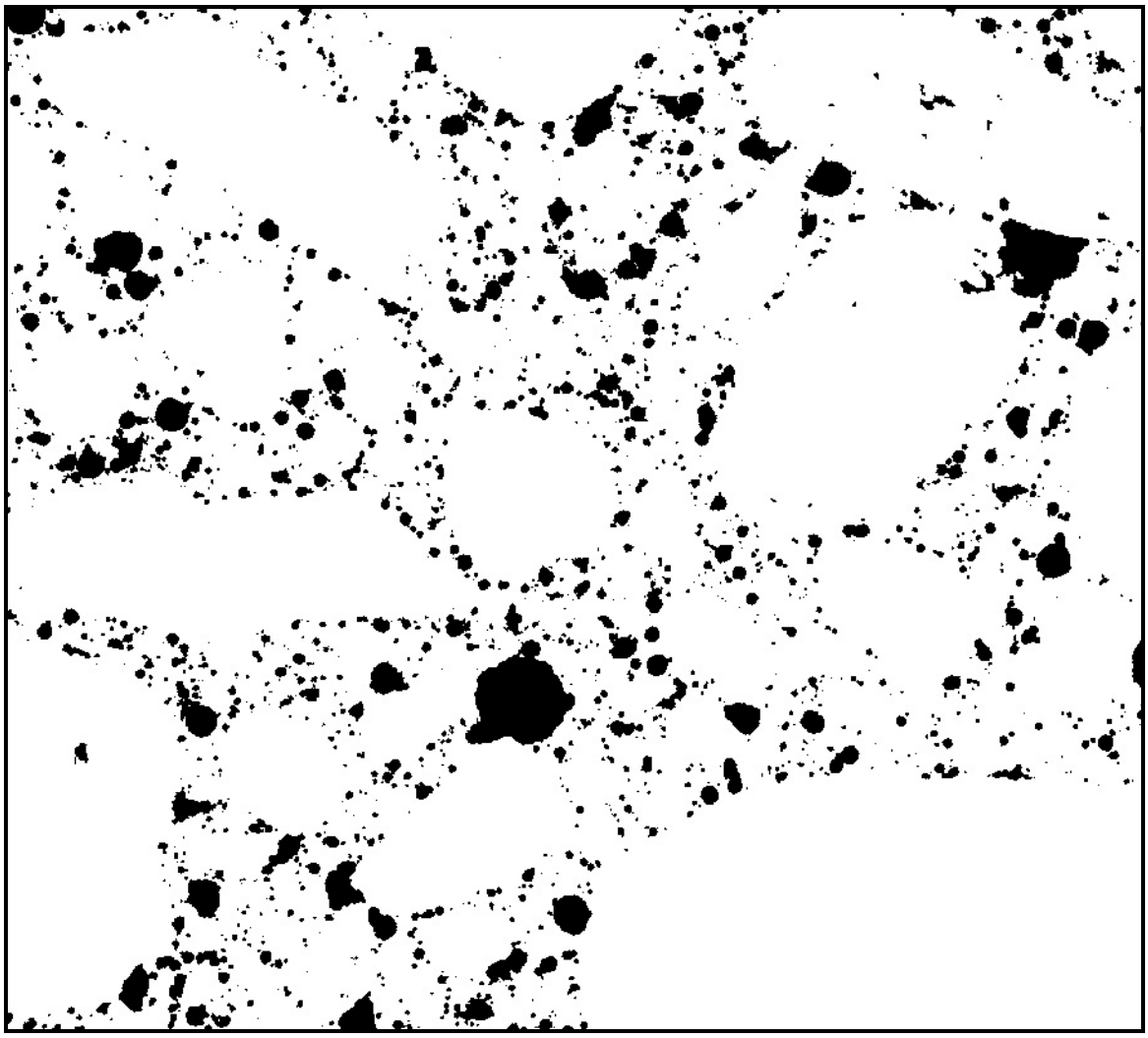

Figure A-33: High resolution scanner image of corresponding area from sample VR-HI after setting threshold to 160, and followed by an inversion (so that air voids appear black). Image dimensions 13.060 x 11.754 mm (magnified here approximately 12x).

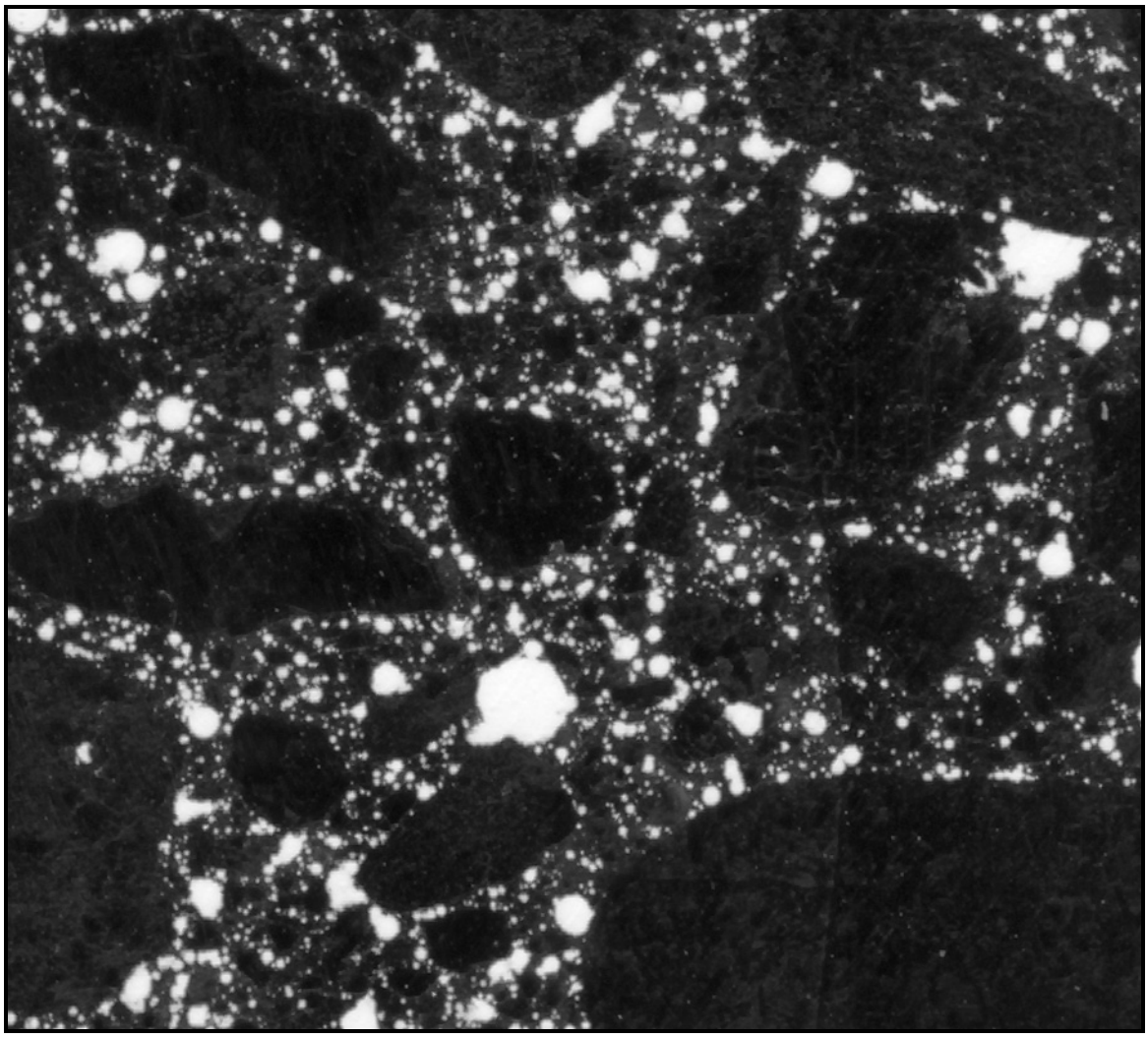

Figure A-34: Office desktop scanner image of corresponding area from sample VR-HI after black and white treatment, image dimensions 13.060 x 11.754 mm (magnified here approximately 12x).

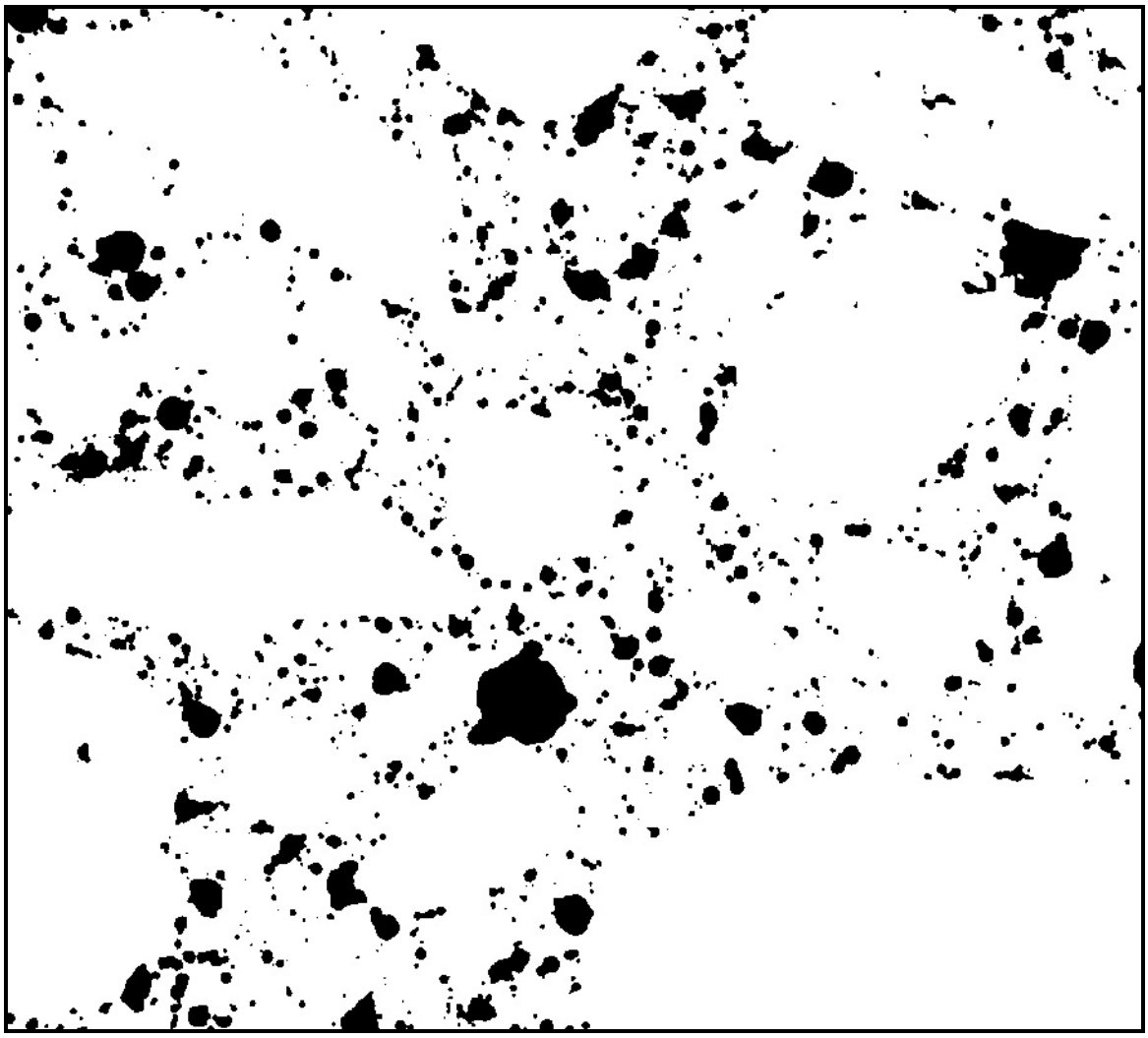

Figure A-35: Office desktop scanner image of corresponding area from sample VR-HI after setting threshold to 160, and followed by an inversion (so that air voids appear black). Image dimensions 13.060 x 11.754 mm (magnified here approximately 12x).

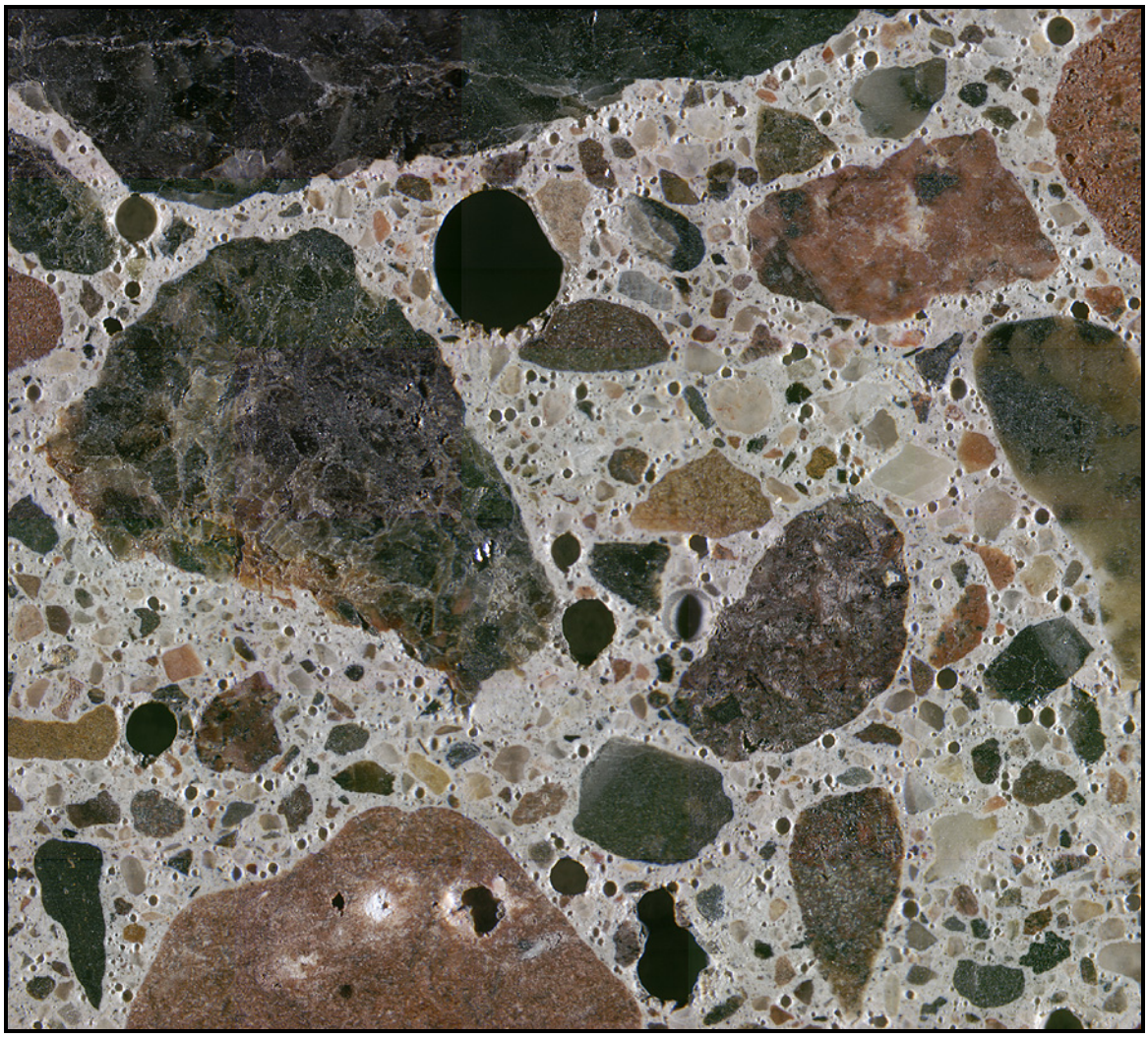

Figure A-36: A 5 x 6 mosaic of stereo microscope images collected during manual point count from sample VR-MED, image dimensions 13.060 x 11.754 mm (magnified here approximately 12x).

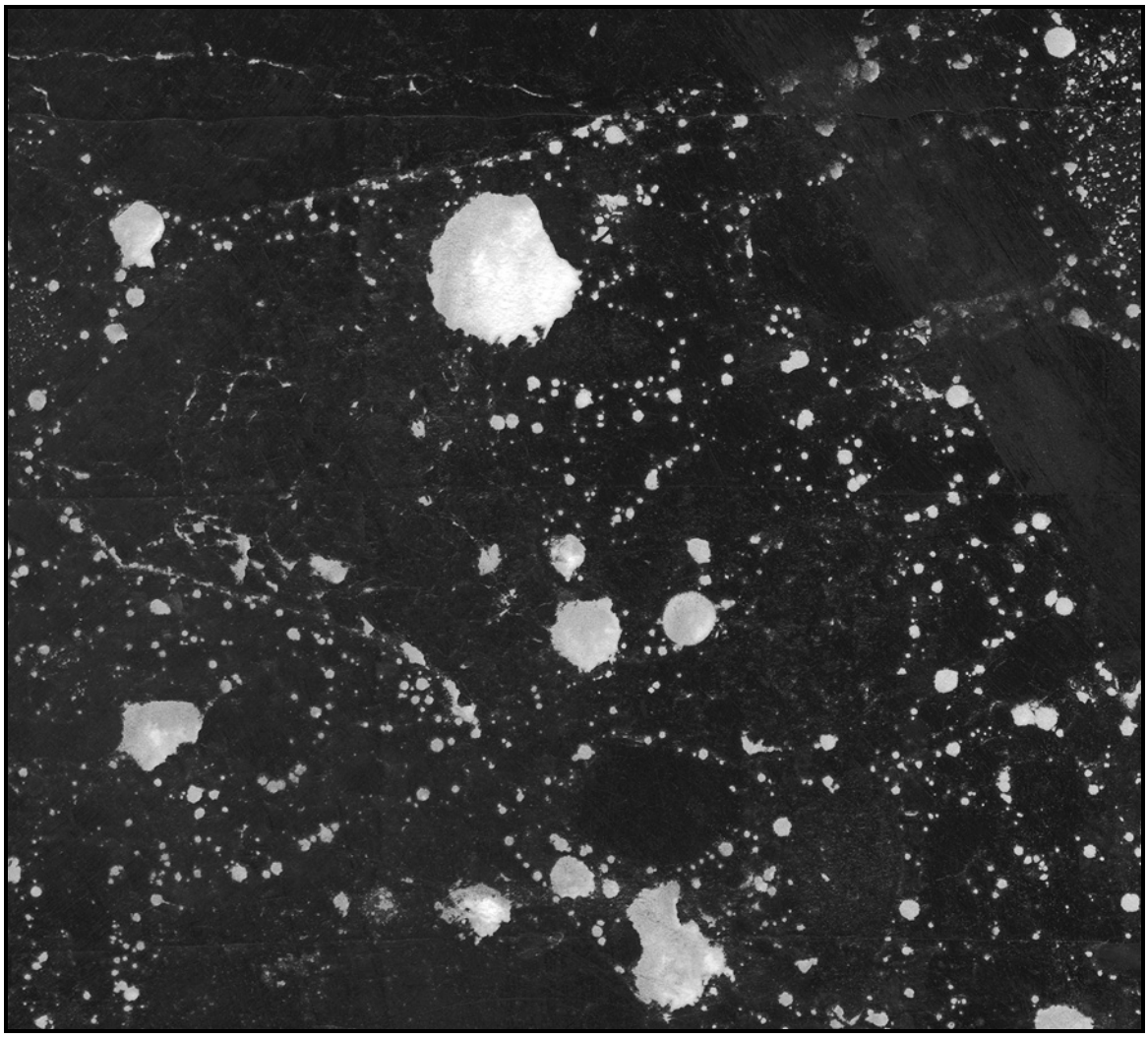

Figure A-37: High resolution scanner image of corresponding area from sample VR-MED after black and white treatment, image dimensions 13.060 x 11.754 mm (magnified here approximately 12x).

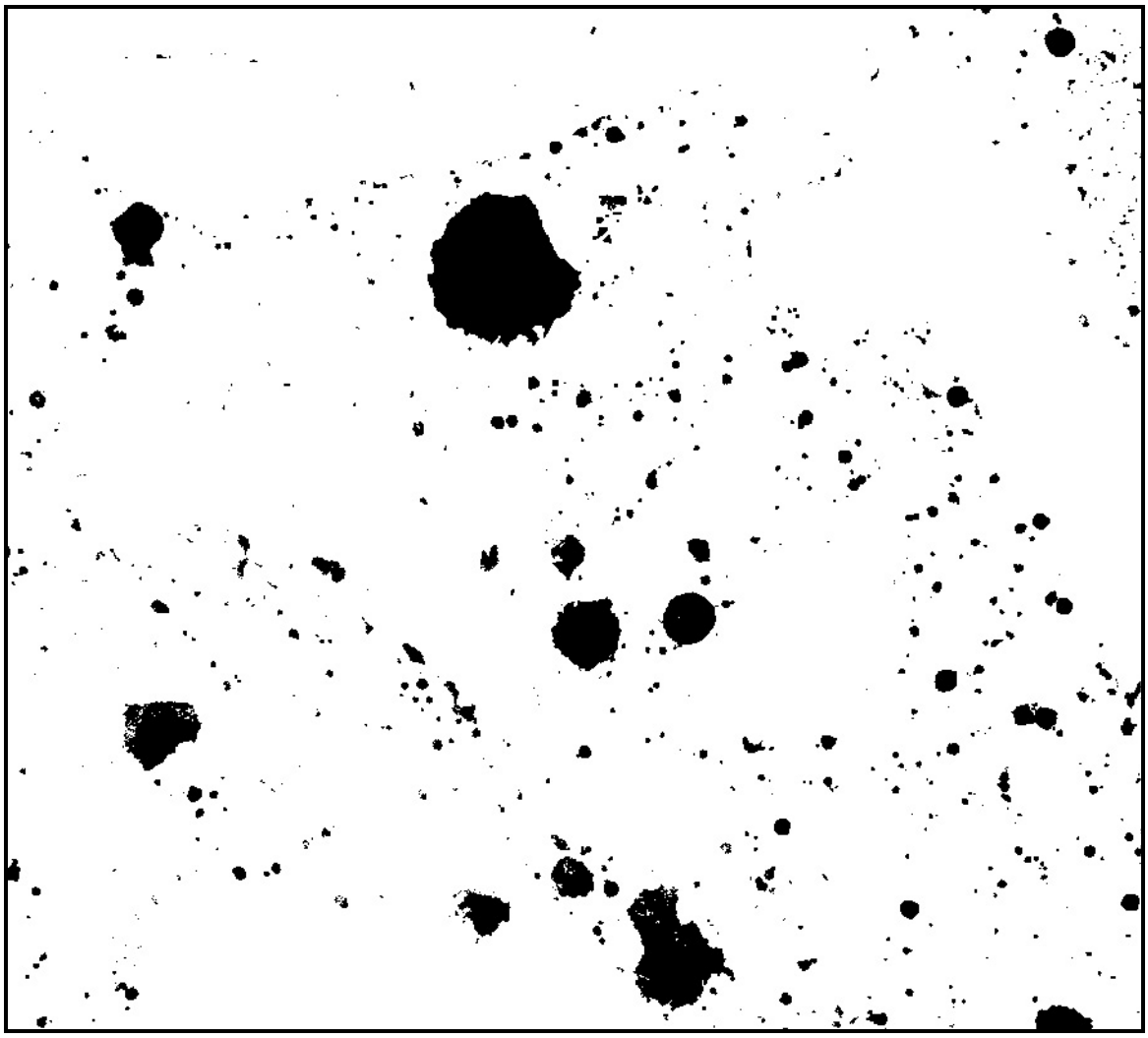

Figure A-38: High resolution scanner image of corresponding area from sample VR-MED after setting threshold to 160, and followed by an inversion (so that air voids appear black). Image dimensions 13.060 x 11.754 mm (magnified here approximately 12x).

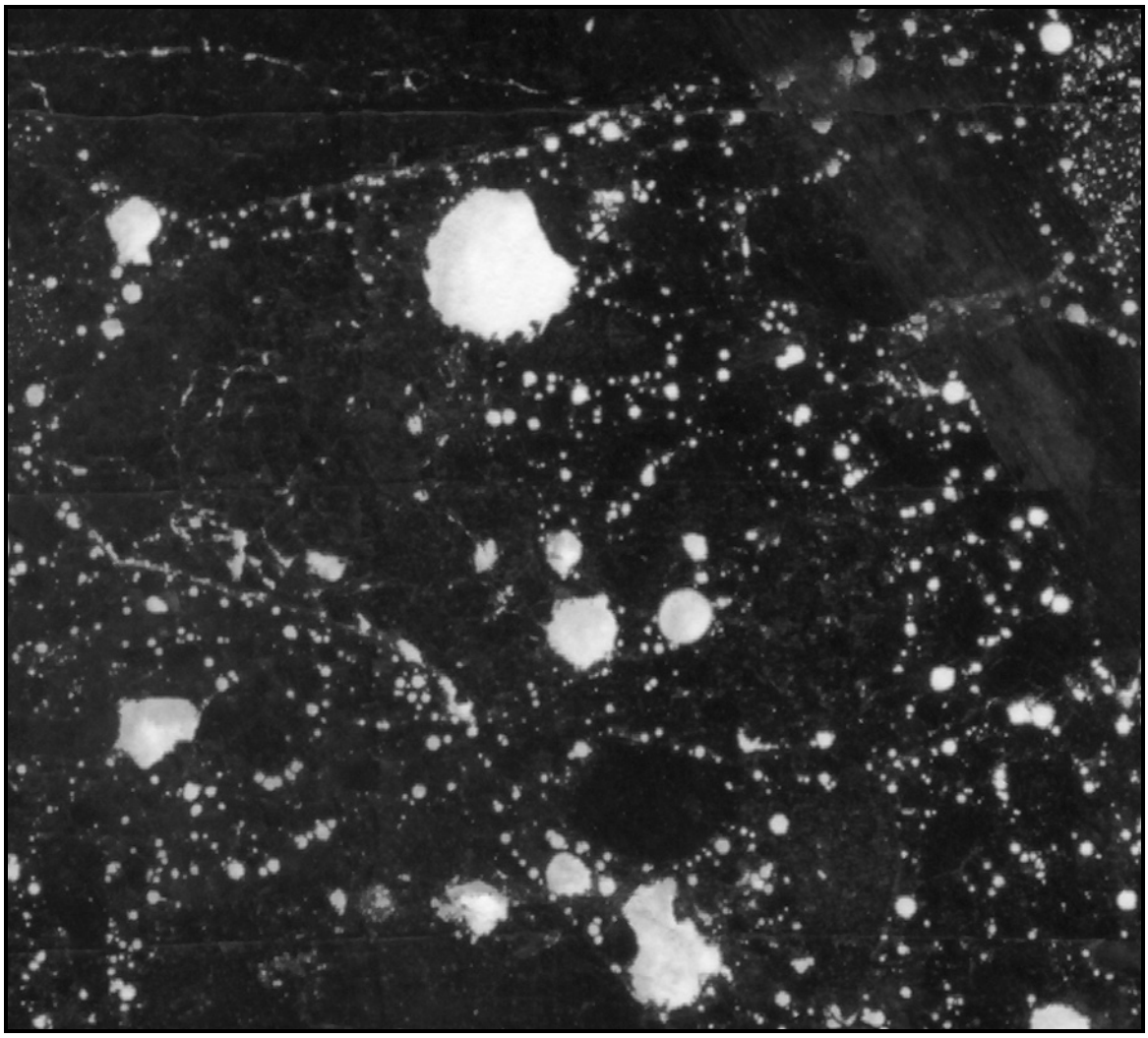

Figure A-39: Office desktop scanner image of corresponding area from sample VR-MED after black and white treatment, image dimensions 13.060 x 11.754 mm (magnified here approximately 12x).

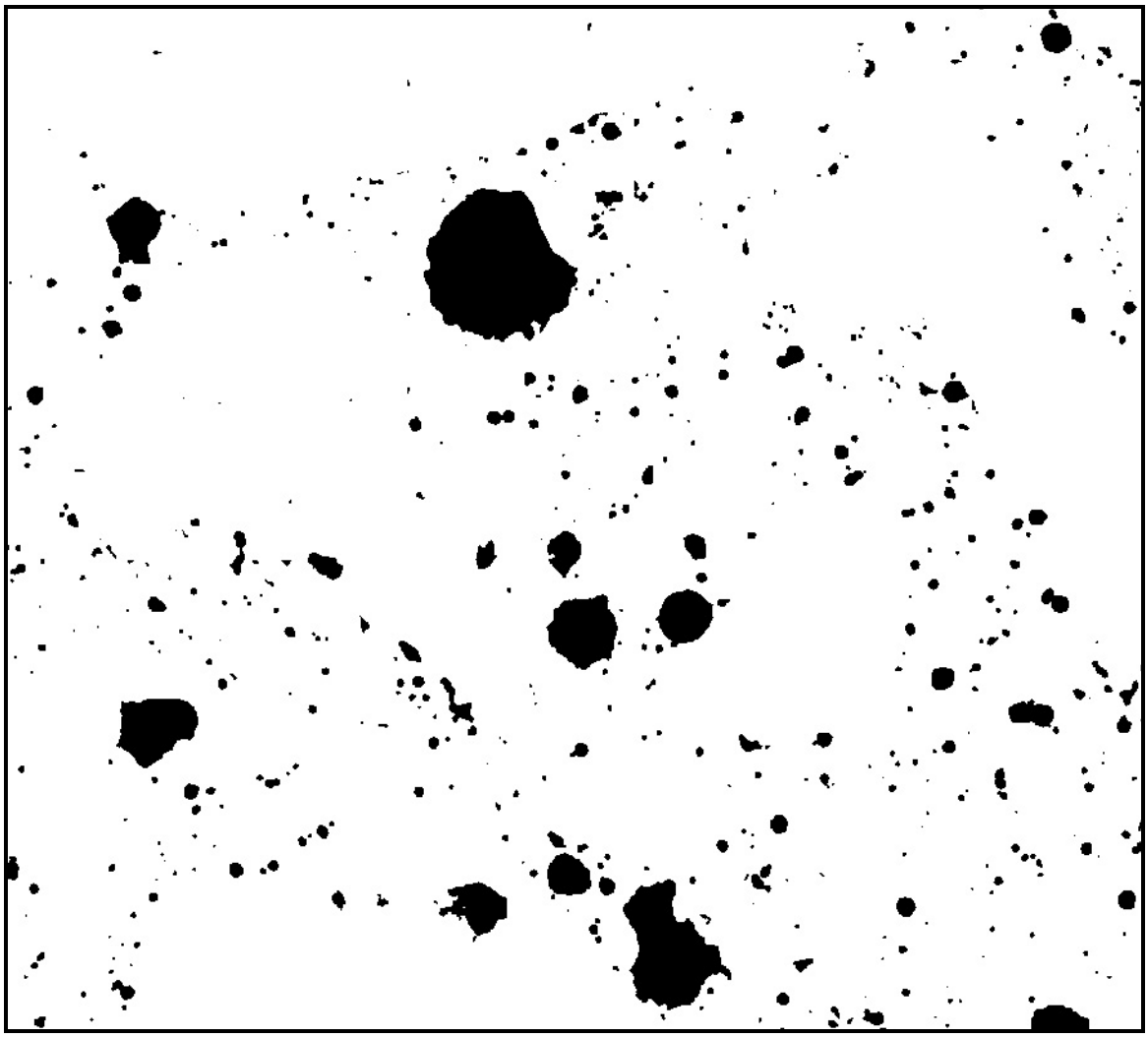

Figure A-40: Office desktop scanner image of corresponding area from sample VR-MED after setting threshold to 160, and followed by an inversion (so that air voids appear black). Image dimensions 13.060 x 11.754 mm (magnified here approximately 12x).

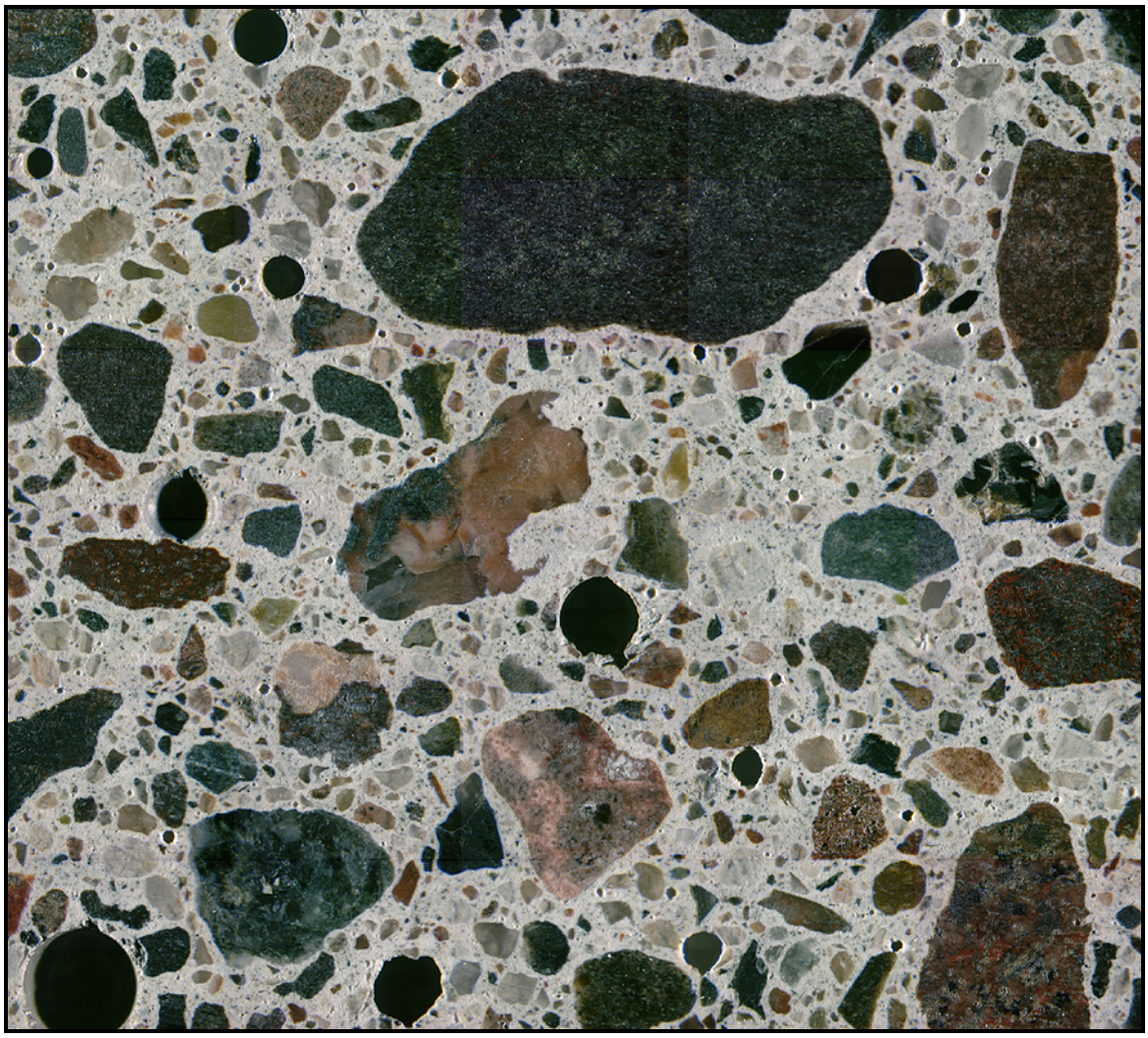

Figure A-41: A 5 x 6 mosaic of stereo microscope images collected during manual point count from sample VR-LO, image dimensions 13.060 x 11.754 mm (magnified here approximately 12x).

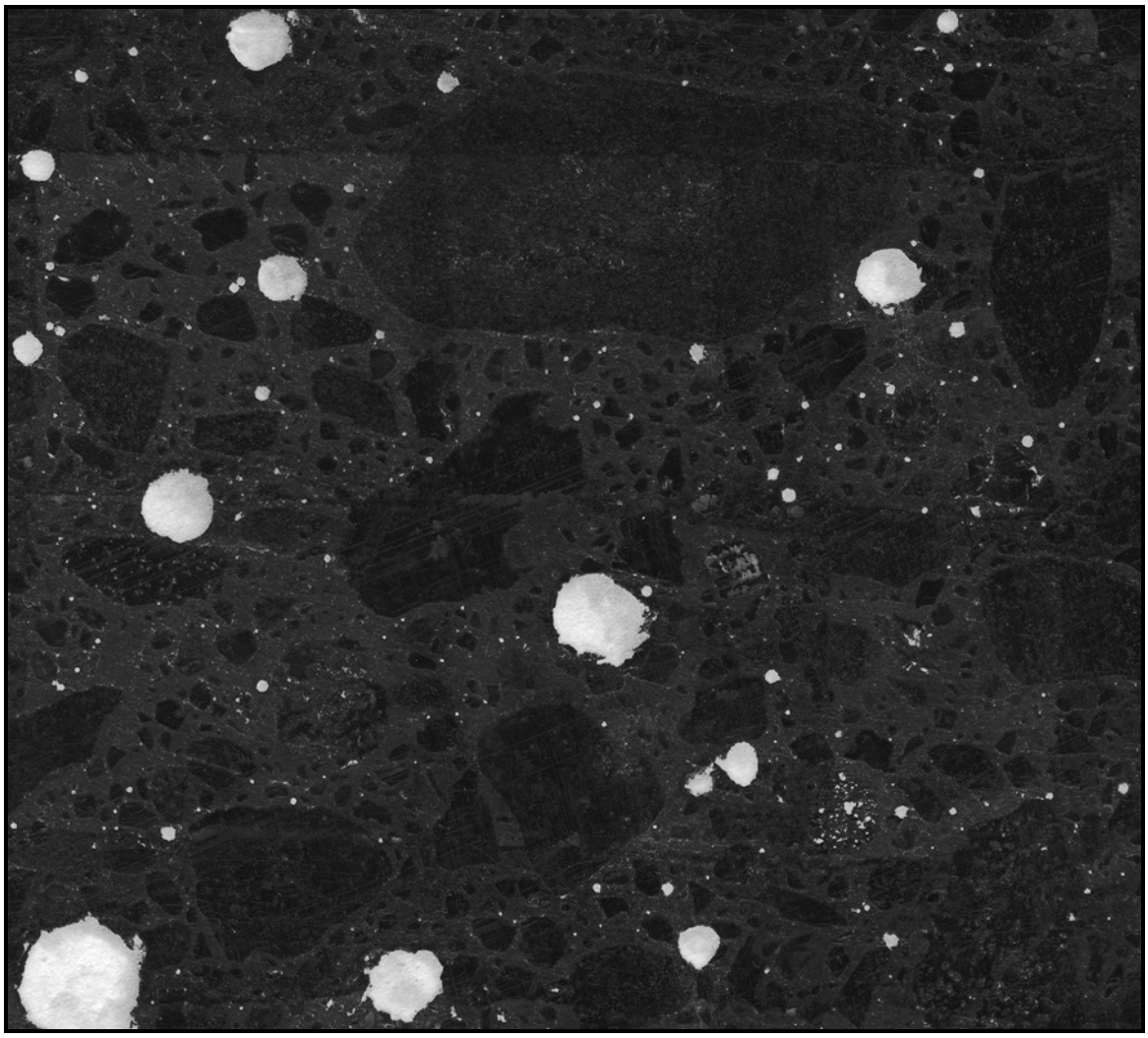

Figure A-42: High resolution scanner image of corresponding area from sample VR-LO after black and white treatment, image dimensions 13.060 x 11.754 mm (magnified here approximately 12x).

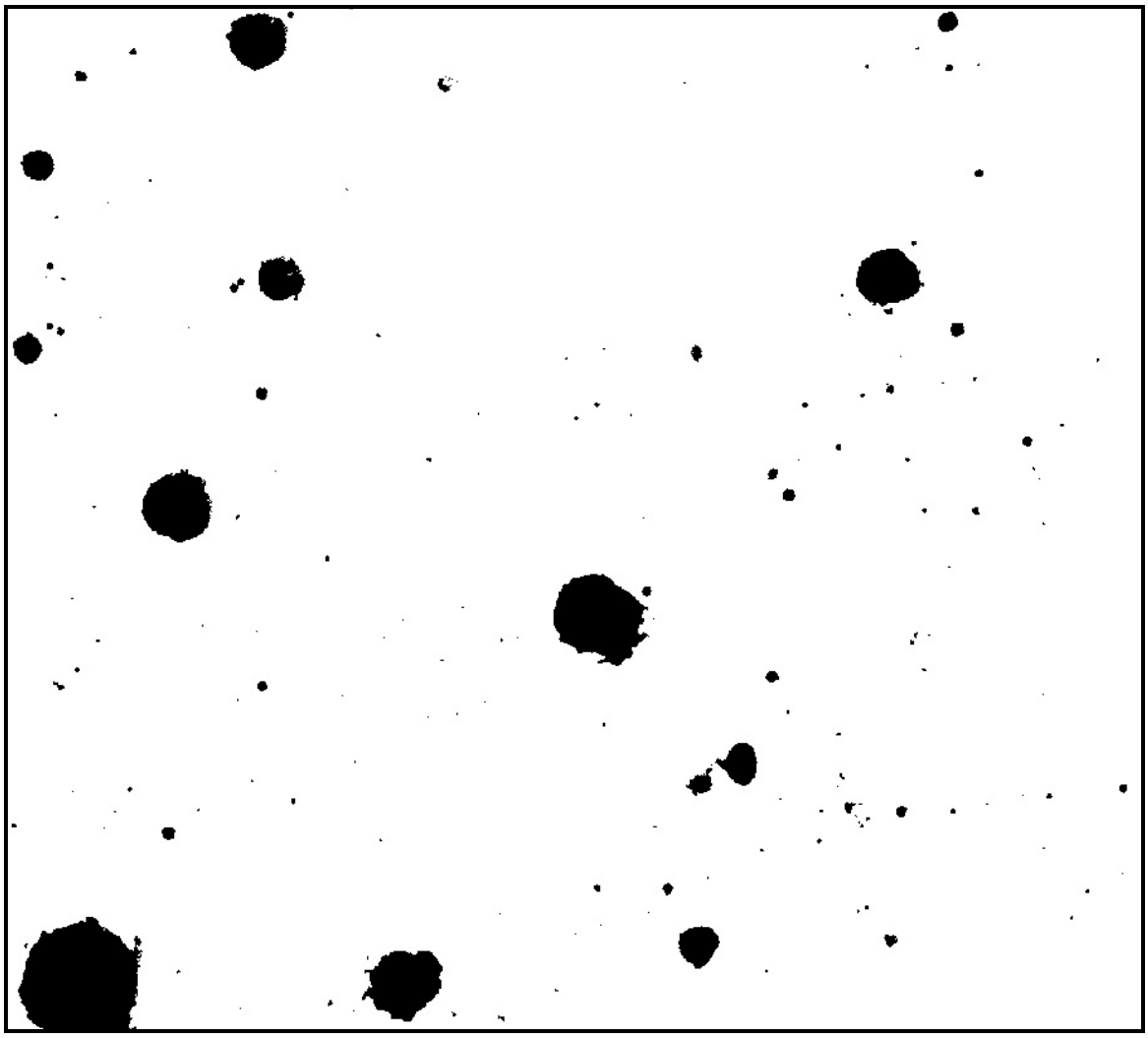

Figure A-43: High resolution scanner image of corresponding area from sample VR-LO after setting threshold to 160, and followed by an inversion (so that air voids appear black). Image dimensions 13.060 x 11.754 mm (magnified here approximately 12x).

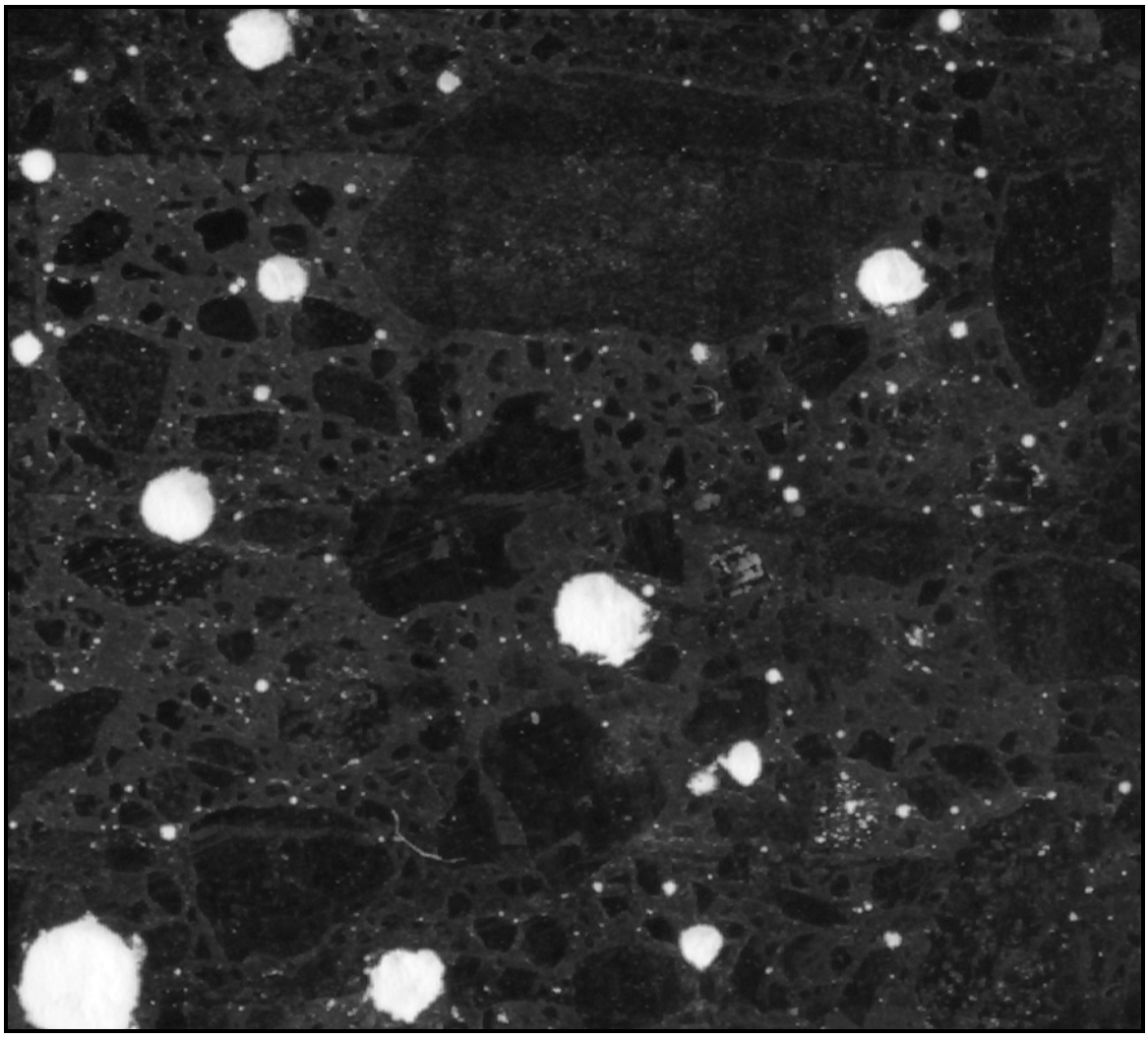

Figure A-44: Office desktop scanner image of corresponding area from sample VR-LO after black and white treatment, image dimensions 13.060 x 11.754 mm (magnified here approximately 12x).

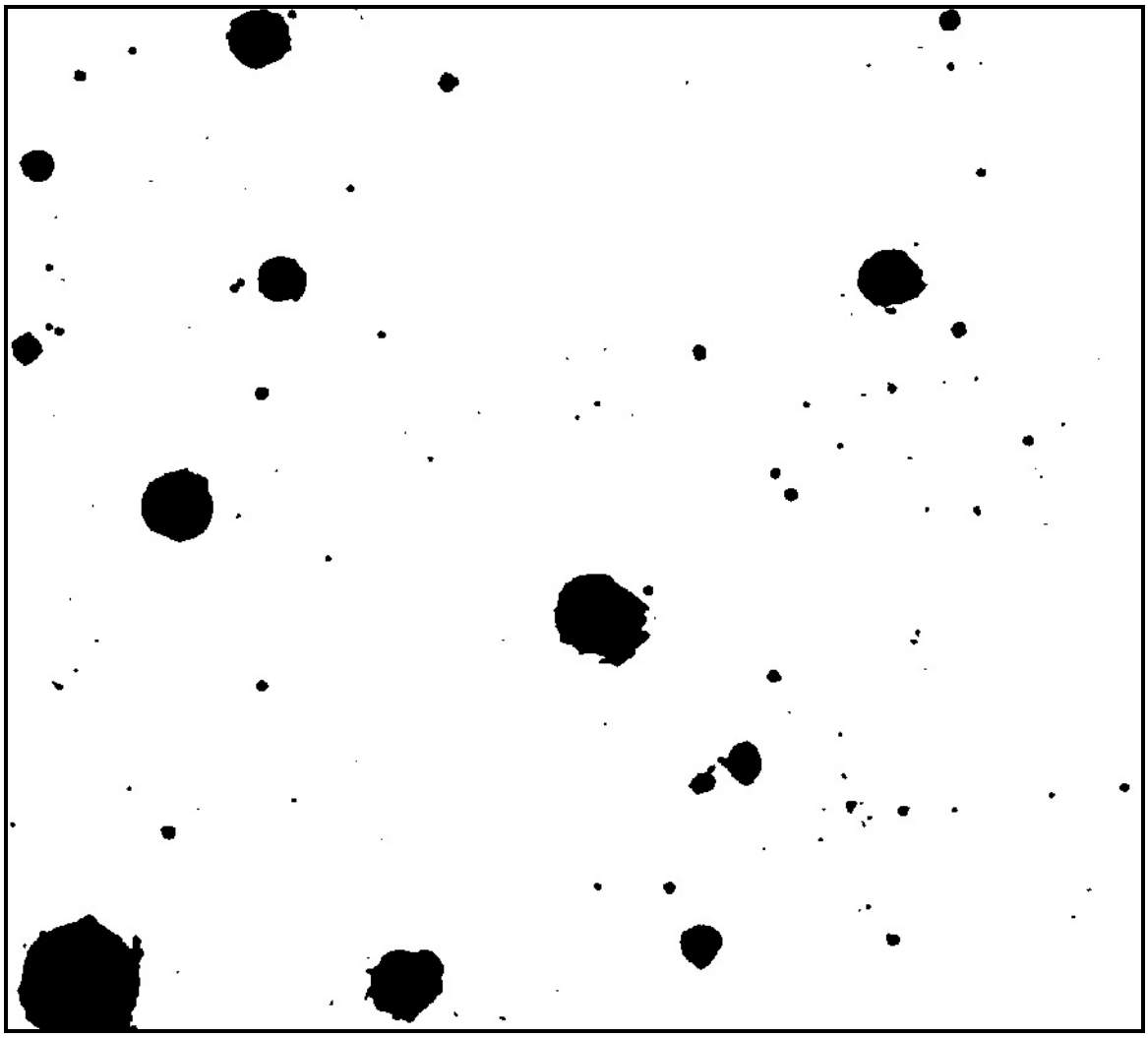

Figure A-45: Office desktop scanner image of corresponding area from sample VR-LO after setting threshold to 160, and followed by an inversion (so that air voids appear black). Image dimensions 13.060 x 11.754 mm (magnified here approximately 12x).

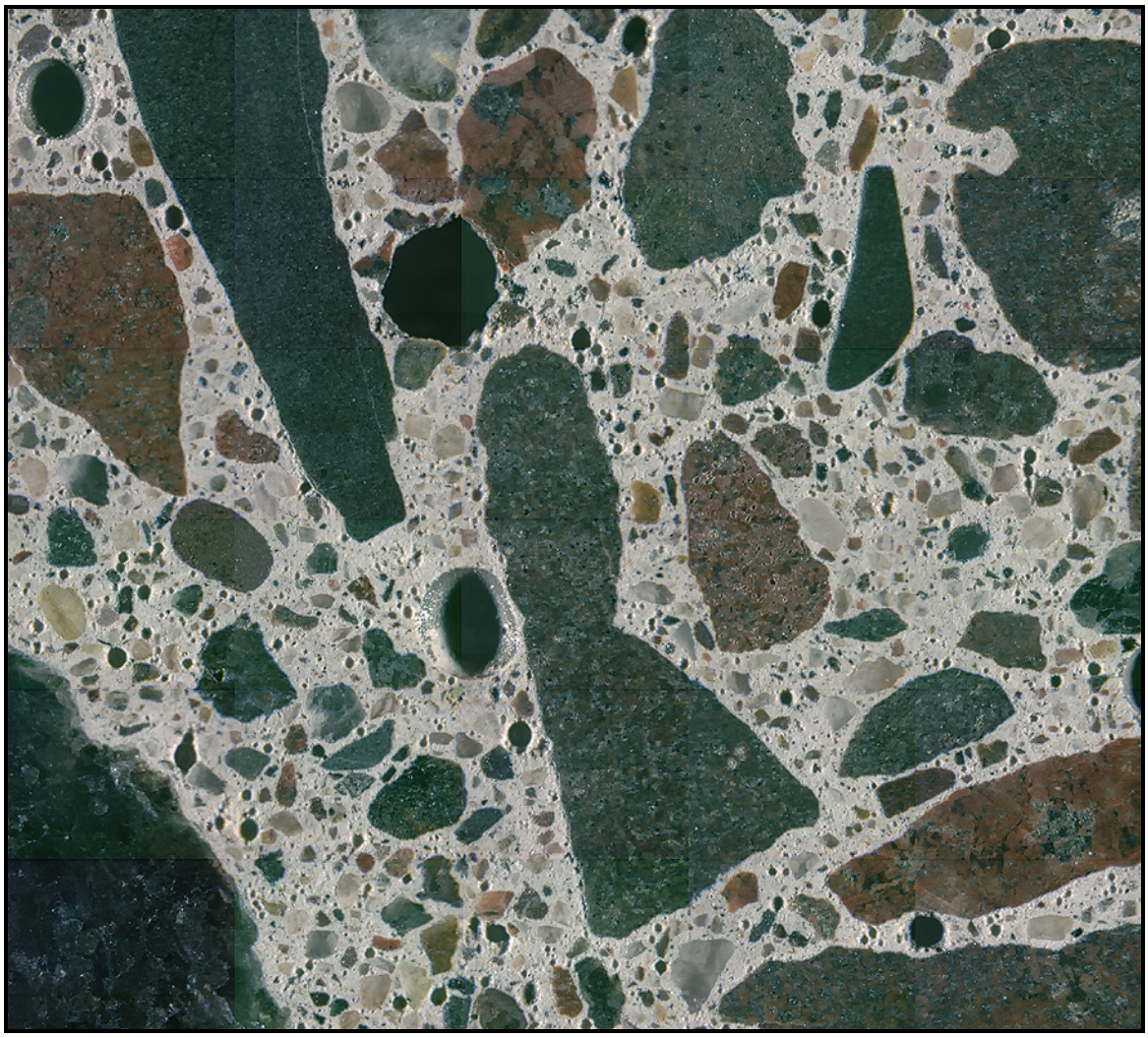

Figure A-46: A 5 x 6 mosaic of stereo microscope images collected during manual point count from sample VRFA-LO, image dimensions 13.060 x 11.754 mm (magnified here approximately 12x).

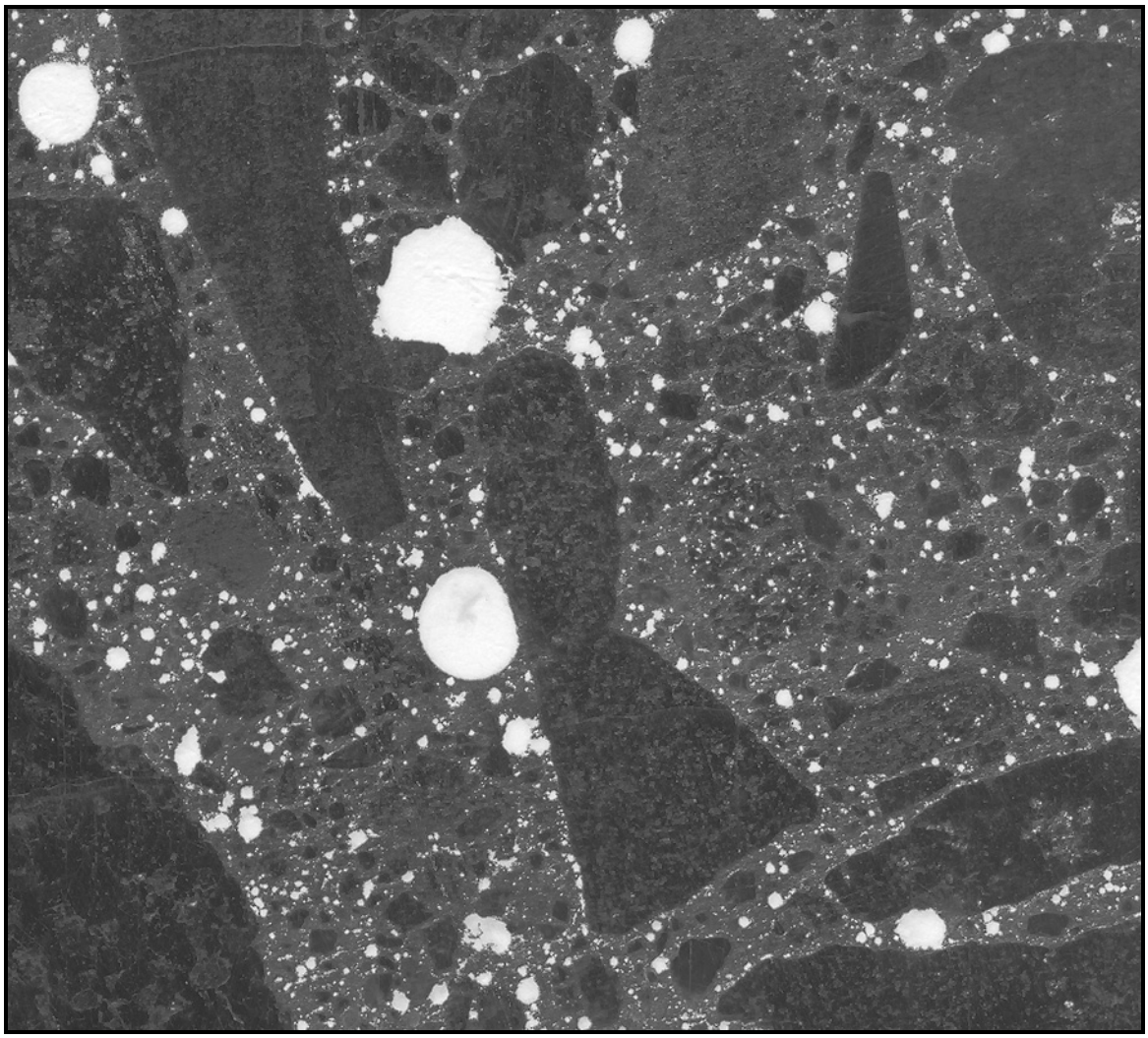

Figure A-47: High resolution scanner image of corresponding area from sample VRFA-LO after black and white treatment, image dimensions 13.060 x 11.754 mm (magnified here approximately 12x).

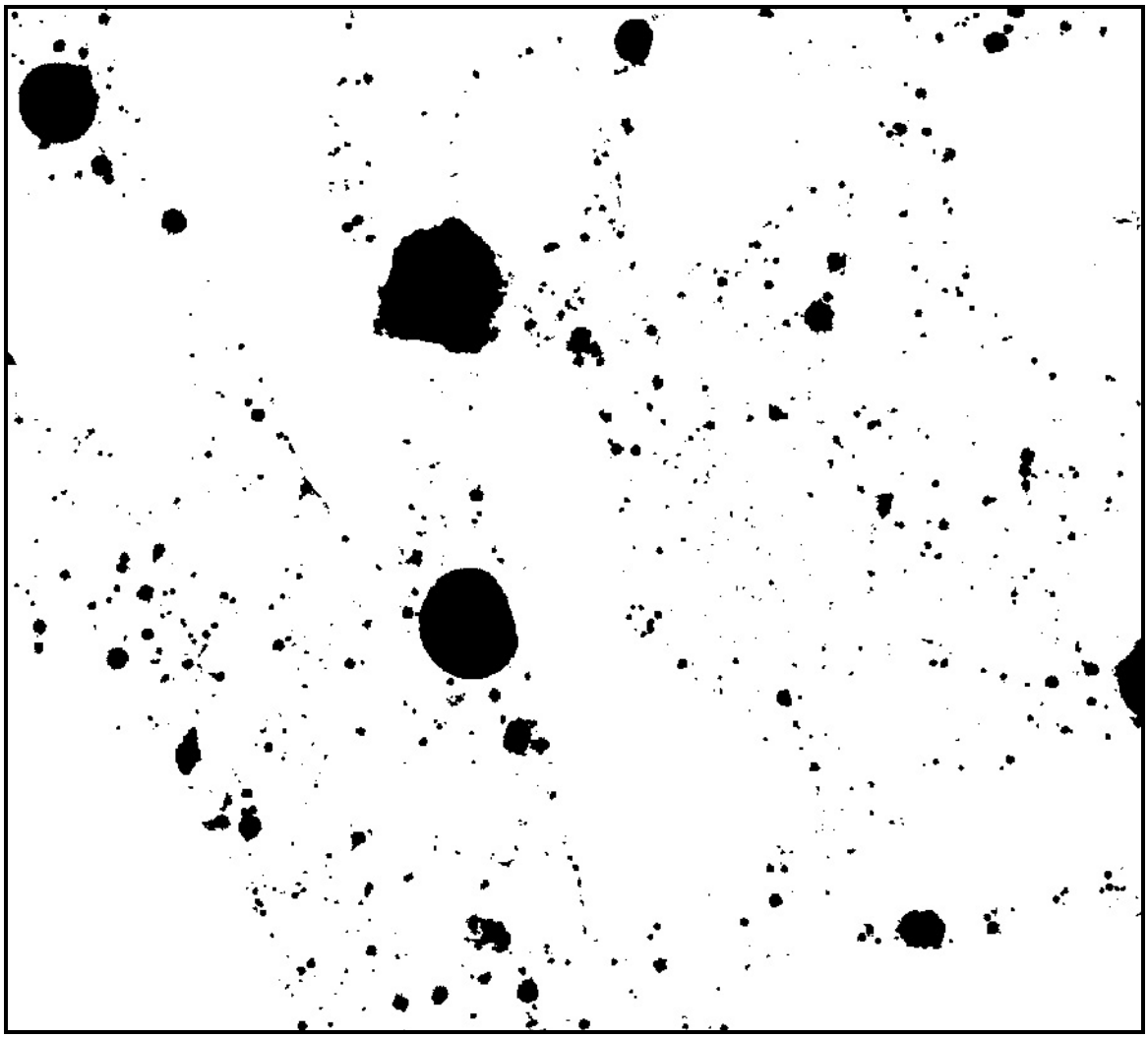

Figure A-48: High resolution scanner image of corresponding area from sample VRFA-LO after setting threshold to 160, and followed by an inversion (so that air voids appear black). Image dimensions 13.060 x 11.754 mm (magnified here approximately 12x).

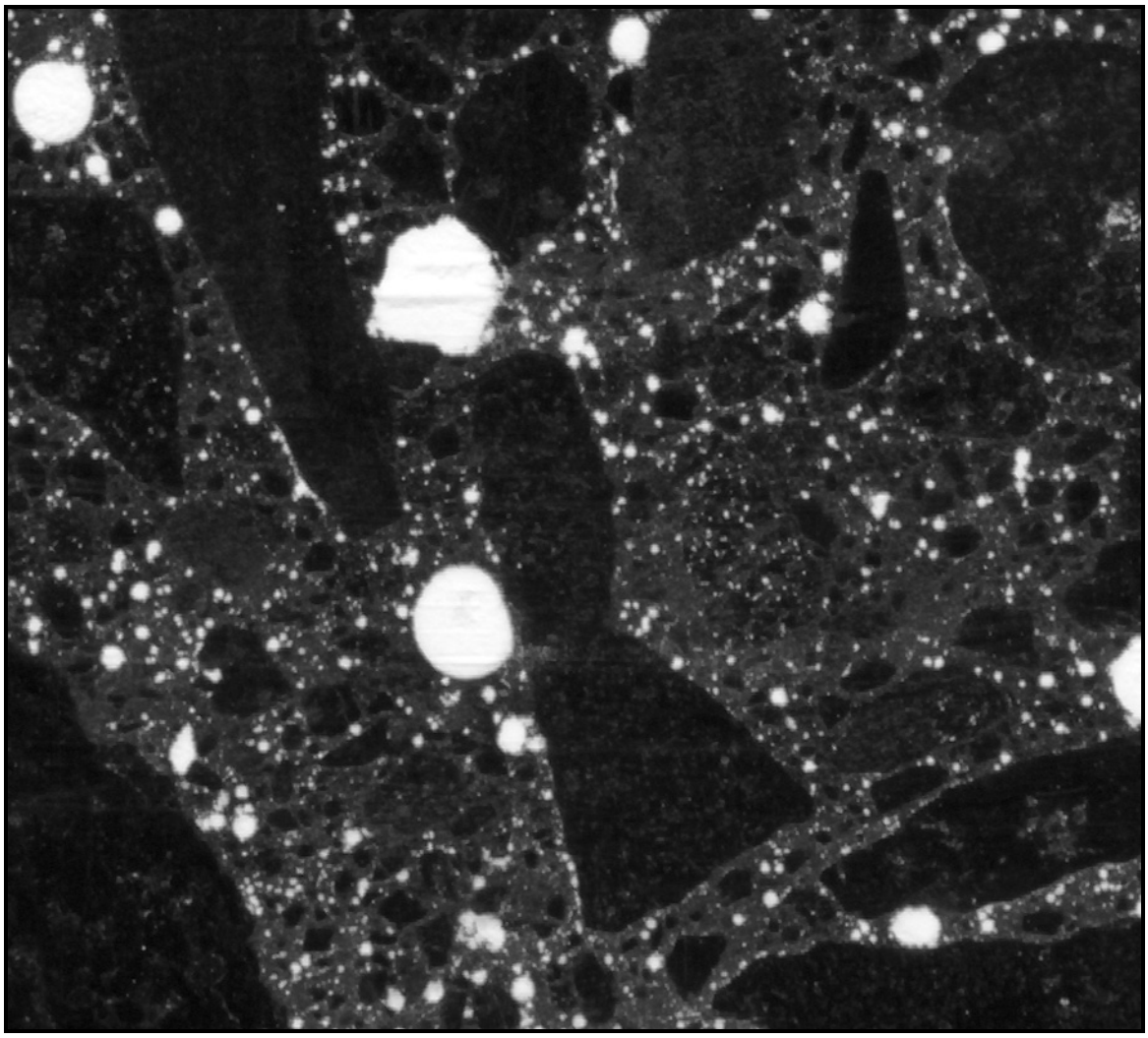

Figure A-49: Office desktop scanner image of corresponding area from sample VRFA-LO after black and white treatment, image dimensions 13.060 x 11.754 mm (magnified here approximately 12x).

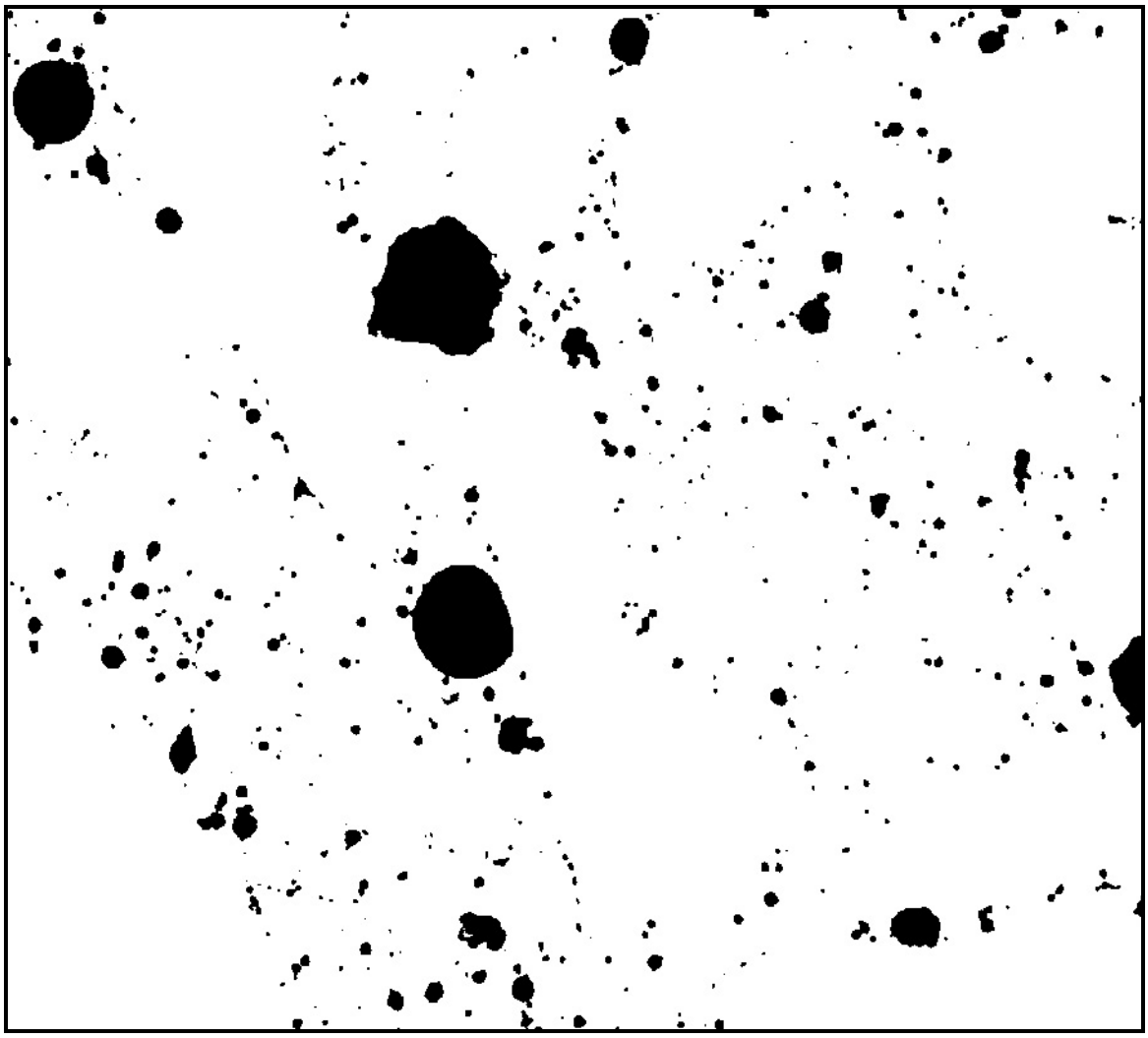

Figure A-50: Office desktop scanner image of corresponding area from sample VRFA-LO after setting threshold to 160, and followed by an inversion (so that air voids appear black). Image dimensions 13.060 x 11.754 mm (magnified here approximately 12x).